



**UNDERSTANDING SUB-CRITICAL WATER
HYDROLYSIS OF PROTEINS BY MASS
SPECTROMETRY:
APPLICATIONS IN PROTEOMICS AND BIO-
REFINING**

By

Thomas Powell

A thesis submitted to the University of Birmingham for the degree of DOCTOR OF PHILOSOPHY

The School Of Biosciences

College of Life and Environmental Sciences

University of Birmingham

March 2018

UNIVERSITY OF
BIRMINGHAM

University of Birmingham Research Archive

e-theses repository

This unpublished thesis/dissertation is copyright of the author and/or third parties. The intellectual property rights of the author or third parties in respect of this work are as defined by The Copyright Designs and Patents Act 1988 or as modified by any successor legislation.

Any use made of information contained in this thesis/dissertation must be in accordance with that legislation and must be properly acknowledged. Further distribution or reproduction in any format is prohibited without the permission of the copyright holder.

Abstract

Sub-critical water (SCW) hydrolysis has previously been used in the extraction of antioxidant compounds from a variety of food wastes, in-particular those which are rich in protein. The brewing industry generates high volumes of waste. The most abundant component, brewers' spent grain (BSG), is high in protein content. The work presented in this thesis aimed to investigate the SCW extraction of antioxidant compounds from BSG.

Whilst SCW hydrolysis has proved effective in the extraction of antioxidants from a wide range of compounds its mechanism of action has not been thoroughly investigated. High performance liquid chromatography (HPLC) coupled to tandem mass spectrometry (MS/MS) was used to analyse peptide production from the SCW hydrolysis of proteins. Sites of cleavage were identified and a mechanism of action of SCW on proteins was postulated. The results from this analysis also raised the possibility of using SCW as an alternative proteolytic reagent in proteomics experiments. Approaches for SCW-based proteomics were further explored by investigating SCW induced amino acid side chain modifications to aid peptide identification. Additionally, HPLC, MS/MS and search parameters were also carefully optimised to provide maximum peptide identifications.

To assess the antioxidant capacity of mixtures generated via SCW hydrolysis oxygen radical absorbance capacity (ORAC), reducing power (RP) and comet assays were used. The decomposition products responsible for antioxidant capacity were characterised using MS/MS.

The work presented in this thesis (Chapters 3 and 4) resulted in the publication of two articles in peer-reviewed journals on which I am first author and texts may be similar. The work in these papers was carried out by me and the articles were written by me in consultation with my co-authors.

- 1) Powell, T., S. Bowra, and H.J. Cooper. 'Subcritical Water Processing of Proteins: An Alternative to Enzymatic Digestion?' *Analytical Chemistry*, 2016. 88(12): p. 6425-32.
- 2) Powell, T., S. Bowra, and H.J. Cooper. 'Subcritical Water Hydrolysis of Peptides: Amino Acid Side-Chain Modifications' *Journal of the American Society for Mass Spectrometry*, 2017. 28(9): p. 1775-1786.

Thomas Powell - First Author

Helen J Cooper - Senior Corresponding Author

Acknowledgements

There are a great many people I would like to acknowledge and thank for their help and guidance whilst writing this thesis. First and foremost my supervisor Helen Cooper, who has been a brilliant mentor and has offered me amazing support both academically and otherwise. To my industrial supervisor, Steve Bowra, I thank for discussions and guidance from a different standpoint. His knowledgebase provided invaluable whilst completing this project.

I would like to thank my great friend Rian Griffiths for allowing me to pester her every day with an infinite amount of questions and even more jokes. Without her help I would not have achieved half as much as I have in the last three years and her help and kindness will never be forgotten. I would also like to thank Andrew Creese for his daily lab advice during my first 18 months. His input was responsible for most of the good data that went into this thesis. There are too many to thank by name - but in particular - Buffy Randall, Alex Dexter, Emma Sisley, Anna Simmonds, Klaudia Kocurek I have enormous gratitude for making me laugh when the going occasionally got tough.

For scientific advice it would be remiss of me not to mention Shabana Beagum, Fabio Aruntas, Neeraj Jumbu, Alessio Perotti and Rachel Akpiriri who were so generous with their time and training.

To my parents, I owe a particular debt, who has always been supportive of my career as well as the financial support they have provided over most of my life. It would also be remiss of me to fail to mention Simon King and Kazuo Kashio for endless laughs.

Contents

Chapter 1: Introduction.....	1
1.1 Overview.....	1
1.2 Mass spectrometry.....	2
1.2.1 Introduction to mass spectrometry.....	2
1.2.2 Ionization	2
1.2.3 Mass Spectrometers	8
1.2.4 Tandem Mass Spectrometry	15
1.3 Subcritical water.....	21
1.3.2 Physical-chemical properties of SCW	22
1.3.3 Subcritical water extraction.....	23
1.3.4 SCW Processing Models.....	24
1.3.5 The influence of SCW parameters	26
1.4 Brewers' waste	28
1.4.1 The brewing process.....	28
1.4.2 Brewers' spent grain (BSG) characterisation	30
1.5 Oxidative stress	32
1.5.1 Pro-oxidants.....	32
1.5.2 Antioxidants.....	33
1.5.4 Antioxidant assays.....	35
1.6 Proteomics.....	42
1.6.1 Sample preparation	42
1.6.2 Liquid chromatography.....	44
1.6.3 Analysis	46
1.7 Aims and objectives.....	48
Chapter 2: Methods	49
2.1 Samples.....	49
2.2 SCW Mediated Hydrolysis	49
2.2.1 Additional experiments in Chapter 3.....	50
2.2.1 Additional experiments in Chapter 4.....	51

2.3 Enzymatic digestion.....	51
2.4 Sodium dodecyl sulphate polyacrylamide gel electrophoresis (SDS PAGE).....	52
2.4.1 In gel digestion.....	52
2.5 Peptide Purification	53
2.6 Direct infusion Mass Spectrometry	53
2.7.1 Additional experiments in Chapter 5	54
2.7.2 Orbitrap Elite.....	55
2.7.3 Q-Exactive	56
2.8 Database Search Parameters	56
2.9 Antioxidant analysis.....	57
2.9.1 ORAC assay	57
2.9.2 Comet assay.....	58
2.9.3 Reducing power assay	59
Chapter 3: Sub-critical water hydrolysis of proteins: specificity and post translational modifications.....	60
3.1 Overview	60
3.2 Specificity of SCW Mediated Hydrolysis of Model Proteins.....	61
3.3 Protein sequence coverage: SCW hydrolysis as an alternative proteolytic reagent?.....	69
3.3.1 Peptides identified from the SCW hydrolysis of haemoglobin.....	69
3.3.2 Peptides identified from the SCW hydrolysis of BSA.....	71
3.3.3 Peptides identified from the SCW hydrolysis of β -casein	72
3.3.4 SCW hydrolysis of haemoglobin using a smaller protein: solvent ratio	73
3.4 SCW Mediated Hydrolysis and Phosphorylation.....	75
3.5 Analysis of Peptide Spectrum Matches	82
3.6 Conclusion	84
Chapter 4: Sub-critical water hydrolysis of peptides: amino acid modifications and conjugation	85
4.1 Overview.....	85
4.2 SCW hydrolysis of model peptide VQSIKCADFLHYMENPTWGR.....	86
4.3 SCW hydrolysis of model peptide VCFQYMDRGDR	98

4.4 SCW hydrolysis of model peptide VQSIKADFLHYENPTWGR	105
4.5 SCW hydrolysis of model peptide VQSIKCADFLHYMENPTWGR pre-treated with IAM	110
4.6 Conjugation reactions using SCW.....	116
4.7 Conclusion	126
Chapter 5: Sub-critical antioxidant extraction from protein	127
5.1 Overview.....	127
5.2 Characterisation of hordein extract	128
5.3 Preparation of hydrolysates	129
5.4 Antioxidant Potential of SCW hydrolysates	133
5.4.1 ORAC assay	133
5.4.2 Reducing Power assay	136
5.4.3 Comet assay	138
5.3.4 Identification of the molecular origin of the antioxidant activity	142
5.5 Small molecule analysis.....	144
5.5.1 BSA hydrolysate analysis.....	145
5.5.2 NTG hydrolysate analysis.....	166
5.5.3 BSG hydrolysate analysis	179
5.5.4 Amino acid hydrolysate analysis.....	191
5.6 Conclusion	209
Chapter 6: Sub-critical water applications in proteomics.....	210
6.1 Overview.....	210
6.2 Preparation of six protein mixture	211
6.3 LC MS/MS analysis using Orbitrap Elite	211
6.4 Optimisation of HPLC parameters.....	213
6.4.1 LC MS/MS analysis using Q-Exactive	216
6.4.2 Optimisation of search parameters.....	219
6.4.2 LC MS/MS analysis using longer column	222
6.4.3 LC MS/MS analysis using longer gradient.....	222
6.5 Conclusion	224
Chapter 7: Conclusion and Future Work.....	225

7.1 Sub-critical water hydrolysis of proteins: specificity and post translational modifications	225
7.2 Sub-critical water hydrolysis of peptides: amino acid modifications and conjugation	226
7.3 Sub-critical antioxidant extraction from protein	227
7.4 Sub-critical water applications in proteomics	228
Appendix	245

List of Figures

Figure 1. 1 - Schematic of electrospray ionisation demonstrating ion evaporation, charge residue and chain ejection models.	4
Figure 1. 2 - Schematic of LTQ-Orbitrap Elite. Adapted from [26].	8
Figure 1. 3 - Schematic of an ion trap. Figure adapted from [28].	9
Figure 1. 4 - Cross section of the Orbitrap mass analyser. Figure adapted from [32]. ..	11
Figure 1. 5 - Schematic of Q-Exactive HF mass spectrometer. Figure adapted from [34].	13
Figure 1. 6 - Schematic diagram and axis of motion of ions in a quadrupole.	14
Figure 1. 7 - The chemical structure of a peptide, together with the designation for fragment ions (the Roepstorff–Fohlmann–Biemann nomenclature) [39]. Adapted from [40].	16
Figure 1. 8 - Phase diagram of water with respect to pressure and temperature.	21
Figure 1. 9 - Apparatus used for SCW hydrolysis a) reaction tube, b) convection oven, c) thermocoupler.	25
Figure 1. 10 - Flow diagram of beer manufacturing.	29
Figure 1. 11 - Vitamin C mechanism of antioxidant action.....	34
Figure 1. 12 - Workflow of comet assay outlining key protocol stages.....	40
Figure 1. 13 - Workflow of reversed phase liquid chromatography.....	44
 Figure 3. 1 - Amino Acid sequences for a) α -globin, b) β -globin, c) BSA, d) β -casein.....	62
Figure 3. 2 - Specificity of SCW hydrolysis: Plots of the % of peptides identified against the amino acid residue immediately preceding the peptide N terminus for proteins haemoglobin, BSA, and β -casein under SCW treatment at 160 °C (0 min), 160 °C (20 min), and 207 °C (20 min). n = 3. Error bars represent one standard deviation.	65

Figure 3. 3 - Specificity of SCW hydrolysis: Plots of the % of peptides identified against the amino acid residue immediately preceding the peptide C terminus for proteins haemoglobin, BSA, and β -casein under SCW treatment at 160 °C (0 min), 160 °C (20 min), and 207 °C (20 min). n = 3. Error bars represent one standard deviation.	66
Figure 3. 4 - Mean sequence coverage obtained for trypsin digests and SCW hydrolysis at 160 °C for 0 min, 160 °C for 20 min, 207 °C for 20 min, 253 °C for 20 min, and 300 °C for 20 min for (A) α -globin and β -globin, (B) BSA, (C) β -casein, and (D) combined coverage for haemoglobin α -chain, haemoglobin β -chain, BSA, and β -casein at 160 °C for 20 min. * = p < 0.05 as determined by students' t test. n = 3. Error bars represent one standard deviation.	70
Figure 3. 5 - Summed survey scan mass spectra obtained following LC MS/MS analysis of SCW treated hemoglobin. (a) SCW treatment of 1 mg/ml Hb; (b) SCW treatment of 0.1 mg/ml Hb; (c) SCW treatment of 0.01 mg/ml Hb.	74
Figure 3. 6 - ETD MS/MS spectra of phosphopeptides produced following SCW hydrolysis or trypsin digestion of β casein.....	78
Figure 3. 7 - Percentage of peptide spectral matches following protein database search versus treatment conditions. n=3. Error bars represent one standard deviation.	83
 Figure 4. 1 - Direct infusion electrospray MS of a) untreated peptide VQSIKCADFLHYMENPTWGR, b) peptide VQSIKCADFLHYMENPTWGR treated with SCW at 140 °C for 10 min.	87
Figure 4. 2 a) ETD MS/MS spectrum of 3+ ions of [VQSIKCADFLHYMENPTWGR +2O], b) ETD MS/MS fragmentation of 3+ ions of [VQSIKCADFLHYMENPTWGR +3O]. Fragments shown in purple can belong to either species; fragments shown in red belong to the species with two oxidations on the cysteine and one on the methionine; fragments shown in blue belong to the species with three oxidations on the cysteine, c) CID MS/MS fragmentation of the quadruple oxidation product of VQSIKCADFLHYMENPTWGR.*Observed fragments are summarized on the peptide sequences, inset. Lower case denotes modified amino acid residues	91
Figure 4. 3 - Extracted ion chromatogram (m/z 815.0426, [VQSIKCADFLHYMENPTWGR+3O]) obtained following LC CID MS/MS and the two corresponding CID MS/MS spectra at retention times 16 minutes 45 seconds and 19 minutes. Observed fragments are summarised on the peptide sequences, inset. Lower case denotes modified amino acid residues.....	94
Figure 4. 4 - Direct infusion electrospray MS of peptide VQSIKCADFLHYMENPTWGR treated with SCW at a)160°C for 10 minutes; b) 180°C for 10 minutes and c) 200°C for 10 minutes.....	96

Figure 4. 5 - Direct infusion electrospray MS of 3+ ions of CID MS/MS spectrum of 2+ ions of [FLHYMENPT + O + C-term amidation].....	97
Figure 4. 6 - a) Direct infusion electrospray MS of a) untreated peptide VCFQYMDRGDR and b) peptide VCFQYMDRGDR treated with SCW at 140 °C for 10 min.	99
Figure 4. 7 - a) CID MS/MS spectrum of 3+ ions of [VCFQYMDRGDR +2O]; b) ETD MS/MS fragmentation of 3+ ions of [VCFQYMDRGDR +3O]. Fragments shown in purple belong to either species; fragments shown in red belong to the species with two oxidations on the cysteine and one on the methionine; fragments shown in blue belong to the species with three oxidations on the cysteine and c) ETD MS/MS spectrum of 2+ ions of [VCFQYMDRGDR +3O]. Observed fragments are summarized on the peptide sequences, inset. Lower case denotes modified amino acid residues.	101
Figure 4. 8 - a) - Extracted ion chromatogram (<i>m/z</i> 719.2973, [VCFQYMDRGDR +3O]) obtained following LC ETD MS/MS and the two corresponding ETD MS/MS spectra at retention times 11 min 30 s and 13 min 30 s. Observed fragments are summarized on the peptide sequences, inset. Lower case denotes modified amino acid residues....	103
Figure 4. 9 a - Direct infusion electrospray MS of a) untreated peptide VQSIKADFLHYENPTWGR; b) of peptide VQSIKADFLHYENPTWGR treated with SCW at 140 °C for 10 min.....	106
Figure 4. 10 -ETD MS/MS spectrum of 4+ ions of [VQSIKADFLHYENPTWGR+O].	108
Figure 4. 11 - CID MS/MS spectrum of 4+ ions of [VQSIKADFLHYENPTWGR+2O].	108
Figure 4. 12 - ETD MS/MS spectrum of 3+ ions of [VQSIKADFLHYENPTWGR- H ₂ O]. ...	109
Figure 4. 13 a) Direct infusion electrospray MS of a) peptide VQSIKADFLHYMENPTWGR treated with iodoacetamide; b) VQSIKADFLHYMENPTWGR following iodoacetamide treatment treated with SCW at 140 °C for 10 min	111
Figure 4. 14 - CID MS/MS spectrum of 3+ ions of [VQSIKADFLHYENPTWGR+C ₂ H ₅ ON].	112
Figure 4. 15 - ETD MS/MS spectrum of 3+ ions of [VQSIKADFLHYENPTWGR+C ₂ H ₅ ON+O].....	112
Figure 4. 16 - Direct infusion electrospray MS of peptide VQSICKADFLHYENPTWGR treated with iodoacetamide and DTT a) prior to SCW hydrolysis and b) hydrolysed at 140°C for 10 minutes.	115
Figure 4. 17 - Direct infusion electrospray MS of peptide VQSIKADFLHYENPTWGR incubated with benzyl bromide for a) 10 minutes at room temperature and b) 60 minutes at room temperature.	118
Figure 4. 18 - Direct infusion electrospray MS of peptide VQSIKADFLHYENPTWGR incubated with benzyl bromide hydrolysed at a) 140°C for 10 minutes; b) 140°C for 30 minutes and c) 140°C for 60 minutes.	122

Figure 5. 1 - SDS-PAGE analysis of the hordein fraction from the NTG and BSG extracts. The subgroups of hordeins (D-, C-, B-, γ - and A-hordein) are indicated. Lane 1 = NTG, lanes 2 = BSG. Markers with their molecular masses are shown in lane 3.	128
Figure 5. 2 - Number of Peptide identifications for LC MS/MS analyses from SCW hydrolysates and enzymatic digests for a) NTG and b) BSG. n=3. Error bars represent 1 S.D.	130
Figure 5. 3 - Example LC ion chromatogram for BSG hydrolysate.....	132
Figure 5. 4 - ORAC assay of NTG, BSG and BSA hydrolysates compared to commercial antioxidants at 0.05mg/ml. Absorbance was recorded at 700 nm. Data represent mean \pm SD of three replicates.....	134
Figure 5. 5 - Reducing power assay of NTG, BSG and BSA hydrolysates and commercial antioxidants at 0.05mg/ml. Absorbance was recorded at 700 nm. n=3. Data represent mean \pm SD of three replicates.....	137
Figure 5. 6 - Viability of HaCaT cells incubated in SCW hydrolysates and commercial antioxidants for 24h. n=3. Data represent mean values.	138
Figure 5. 7 - DNA strand breakage detected by the comet assay using a HaCaTs. Values represent the mean tail movement, where n = 2. Data represent mean \pm SD of two replicates.....	140
Figure 5. 8 - Example screenshot of comets visualised in the comet assay.	141
Figure 5. 9 - TE values obtained for enzymatic digests of NTG, BSG and BSA and equimolar amino acid mixture using the ORAC assay. n=3. Data represent mean \pm SD of three replicates.	143
Figure 5. 10 - Direct infusion ESI MS of BSA hydrolysed at a) 207°C for 20 min, b) 253 °C for 20 min and c) 300 °C for 20 min.	147
Figure 5. 11 - Direct infusion ESI MS of BSA hydrolysed at a) 207°C for 20 min, b) 253 °C for 20 min and c) 300 °C for 20 min.	168
Figure 5. 12 - Direct infusion ESI MS of BSG hydrolysed at a) 207 °C for 20 min, b) 253 °C for 20 min and c) 300 °C for 20 min.	181
Figure 5. 13 - Direct infusion ESI MS of 20 aa mixture at a) 207 °C for 20 min, b) 253 °C for 20 min and c) 300 °C for 20 min.	194
 Figure 6. 1 - Mean sequence coverage obtained for trypsin digests and SCW hydrolysis at 160 °C for 20 min for six protein mixture. n = 3. Error bars represent one standard deviation.....	212
Figure 6. 2 - Representative CID MS/MS spectrum from six protein mixture tryptic digest	214

Figure 6. 3 - Representative CID MS/MS spectrum from six protein mixture hydrolysate.....	215
Figure 6. 4 - Representative CID MS/MS spectrum from six protein mixture SCW hydrolysate using the Q Exactive.	218
Figure 6. 5 - Mean sequence coverage obtained for SCW hydrolysis at 160 °C for 20 min for six protein mixture using Q-exactive. n = 3. Error bars represent one standard deviation.....	223

List of Tables

Table 3. 1 - Summary of Phosphopeptides and Unmodified Peptides Containing Known Sites of Phosphorylation Observed Following SCW Hydrolysis or Trypsin Digestion of β -Casein.	76
Table 4. 1 - Ions identified following SCW hydrolysis of VQSIKADFLHYMENPTWGR.....	88
Table 4. 2 - Ions identified following SCW hydrolysis of VCFQYMDRGDR at 140 °C for 10 min.....	100
Table 4. 3 - Ions identified following SCW hydrolysis of VQSIKADFLHYENPTWGR at 140 °C for 10 min.	107
Table 4. 4 - Ions observed following SCW hydrolysis of iodoacetamide pre-treated VQSIKADFLHYMENPTWGR at 140 °C for 10 min.	113
Table 4. 5 - Ions Observed Following SCW hydrolysis of benzyl bromide pre-treated VQSIKADFLHYMENPTWGR at room temperature for 0 and 60 minutes and 140°C for 10, 30 and 60 minutes.....	120
Table 5. 1 - Ions Observed Following SCW Hydrolysis of BSA at 207 °C for 20 min...151	
Table 5. 2 - Ions Observed Following SCW Hydrolysis of BSA at 253 °C for 20 min...158	
Table 5. 3 - Ions Observed Following SCW Hydrolysis of BSA at 300 °C for 20 min...163	
Table 5. 4 - Ions Observed Following SCW Hydrolysis of NTG at 207 °C for 20 min. 171	
Table 5. 5 - Ions Observed Following SCW Hydrolysis of NTG at 253 °C for 20 min. .174	
Table 5. 6 - Ions Observed Following SCW Hydrolysis of NTG at 300 °C for 20 min...178	
Table 5. 7 - Ions Observed Following SCW Hydrolysis of BSG at 207 °C for 20 min...185	
Table 5. 8 - Ions Observed Following SCW Hydrolysis of BSG at 207 °C for 20 min...187	
Table 5. 9 - Ions Observed Following SCW Hydrolysis of BSG at 207 °C for 20 min...190	
Table 5. 10 - Ions Observed Following SCW Hydrolysis of AA at 207 °C for 20 min...198	
Table 5. 11 - Ions Observed Following SCW Hydrolysis of AA at 253 °C for 20 min...203	

Table 5. 12 - Ions Observed Following SCW Hydrolysis of AA at 300 °C for 20 min...208

Table 6. 1 - Percentage sequence coverage obtained for six protein mixture using different search parameters.220

List of Schemes

Scheme 1. 1 a) Cornell mechanism for N–Ca bond cleavage in ExD of peptides and proteins with charge solvation from a C-terminal donor amine group and **b)** the Utah–Washington mechanism for ExD. Scheme adapted from [57]..... 19

Scheme 3. 1 - Proposed mechanism for weak acid hydrolysis of the Asp-X bond.

Adapted from [192,

193].....

68

Scheme 5. 1 - Proposed mechanism for **a)** Deamination of glutamine and dehydration of glutamic acid, **b)** deamination of arginine, **c)** deamination of lysine and **d)**

dehydration of aspartic

acid.....152

List of Equations

Equation 1. 1 - Equation describing the electrostatic field of the orbitrap cell.	12
Equation 1. 2 - Equations describing the axial ion oscillations along the z axis of the orbitrap spindle electrode a) equation of motion, b) calculating the charge to mass ratio of an ion from frequency of oscillations.	12
Equation 1. 3 - Equation describing the quadrupolar field.	14
Equation 1. 4 - Equation describing the ionic product of water.	22
Equation 1. 5 - Equation for calculating the area under the curve for ORAC assays.	36

Appendix Figures

Appendix Figure 3. 1 - Summary of peptides identified following SCW hydrolysis of a) α -globin, b) β - globin, c)BSA and d) β -casein under conditions 160 °C for 0 minutes, 160 °C for 20 minutes, 207 °C for 20 minutes, 253 °C for 20 minutes and 300 °C for 20 minutes.246

Appendix Figure 4. 1 - ETD MS/MS spectrum of 4+ ions of [VQSIKADFLHYENPTWGR +O].....276

Appendix Figure 4. 2 - ETD MS/MS spectrum of 4+ ions of [VQSIKADFLHYENPTWGR +O].....277

Appendix Figure 4. 3 - ETD MS/MS spectrum of 3+ ions of [VCFQYMDRGDR +O]278

Appendix Figure 5.1 -HCD MS/MS of the ion observed at m/z 96.05.....279

Appendix Figure 5.2 -HCD MS/MS of the ion observed at m/z 97.08.....279

Appendix Figure 5.3 -HCD MS/MS of the ion observed at m/z 100.11.....279

Appendix Figure 5.4 -HCD MS/MS of the ion observed at m/z 101.06.....279

Appendix Figure 5.5 -HCD MS/MS of the ion observed at m/z 105.07.....280

Appendix Figure 5.6 -HCD MS/MS of the ion observed at m/z 106.05.....280

Appendix Figure 5.7 -HCD MS/MS of the ion observed at m/z 110.06.....280

Appendix Figure 5.8 -HCD MS/MS of the ion observed at m/z 111.06.....280

Appendix Figure 5.9 -HCD MS/MS of the ion observed at m/z 111.09.....281

Appendix Figure 5.10 -HCD MS/MS of the ion observed at m/z 112.09.....281

Appendix Figure 5.11 -HCD MS/MS of the ion observed at m/z 112.11.....281

Appendix Figure 5.12 -HCD MS/MS of the ion observed at m/z 114.13.....281

Appendix Figure 5.13 -HCD MS/MS of the ion observed at m/z 115.09.....	282
Appendix Figure 5.14 -HCD MS/MS of the ion observed at m/z 116.07.....	282
Appendix Figure 5.15 -HCD MS/MS of the ion observed at m/z 116.11.....	282
Appendix Figure 5.16 -HCD MS/MS of the ion observed at m/z 118.08.....	282
Appendix Figure 5.17 -HCD MS/MS of the ion observed at m/z 120.06.....	283
Appendix Figure 5.18 -HCD MS/MS of the ion observed at m/z 120.08.....	283
Appendix Figure 5.19 -HCD MS/MS of the ion observed at m/z 121.06.....	283
Appendix Figure 5.20 -HCD MS/MS of the ion observed at m/z 122.03.....	283
Appendix Figure 5.21 -HCD MS/MS of the ion observed at m/z 122.10.....	284
Appendix Figure 5.22 -HCD MS/MS of the ion observed at m/z 123.09.....	284
Appendix Figure 5.23 -HCD MS/MS of the ion observed at m/z 125.07.....	285
Appendix Figure 5.24 -HCD MS/MS of the ion observed at m/z 125.11.....	285
Appendix Figure 5.25 -HCD MS/MS of the ion observed at m/z 128.14.....	285
Appendix Figure 5.26 -HCD MS/MS of the ion observed at m/z 129.10.....	285
Appendix Figure 5.27 -HCD MS/MS of the ion observed at m/z 130.05.....	286
Appendix Figure 5.28 -HCD MS/MS of the ion observed at m/z 130.09.....	286
Appendix Figure 5.29 -HCD MS/MS of the ion observed at m/z 132.10.....	286
Appendix Figure 5.30 -HCD MS/MS of the ion observed at m/z 133.06.....	286
Appendix Figure 5.31 -HCD MS/MS of the ion observed at m/z 133.11.....	287
Appendix Figure 5.32 -HCD MS/MS of the ion observed at m/z 134.04.....	287
Appendix Figure 5.33 -HCD MS/MS of the ion observed at m/z 138.09.....	287

Appendix Figure 5.34 -HCD MS/MS of the ion observed at m/z 138.10.....	287
Appendix Figure 5.35 -HCD MS/MS of the ion observed at m/z 139.12.....	288
Appendix Figure 5.36 -HCD MS/MS of the ion observed at m/z 142.16.....	288
Appendix Figure 5.37 -HCD MS/MS of the ion observed at m/z 146.06.....	288
Appendix Figure 5.38 -HCD MS/MS of the ion observed at m/z 147.08.....	288
Appendix Figure 5.39 -HCD MS/MS of the ion observed at m/z 147.11.....	289
Appendix Figure 5.40 -HCD MS/MS of the ion observed at m/z 148.06.....	289
Appendix Figure 5.41 -HCD MS/MS of the ion observed at m/z 150.06.....	289
Appendix Figure 5.42 -HCD MS/MS of the ion observed at m/z 153.14.....	289
Appendix Figure 5.43 -HCD MS/MS of the ion observed at m/z 155.08.....	290
Appendix Figure 5.44 -HCD MS/MS of the ion observed at m/z 156.08.....	290
Appendix Figure 5.45 -HCD MS/MS of the ion observed at m/z 156.17.....	290
Appendix Figure 5.46 -HCD MS/MS of the ion observed at m/z 157.11.....	290
Appendix Figure 5.47 -HCD MS/MS of the ion observed at m/z 157.13.....	291
Appendix Figure 5.48 -HCD MS/MS of the ion observed at m/z 158.09.....	291
Appendix Figure 5.49 -HCD MS/MS of the ion observed at m/z 158.12.....	291
Appendix Figure 5.50 -HCD MS/MS of the ion observed at m/z 159.09.....	291
Appendix Figure 5.51 -HCD MS/MS of the ion observed at m/z 166.08.....	292
Appendix Figure 5.52 -HCD MS/MS of the ion observed at m/z 166.12.....	292
Appendix Figure 5.53 -HCD MS/MS of the ion observed at m/z 171.11.....	292
Appendix Figure 5.54 -HCD MS/MS of the ion observed at m/z 173.11.....	292

Appendix Figure 5.55 -HCD MS/MS of the ion observed at m/z 175.12.....	293
Appendix Figure 5.56 -HCD MS/MS of the ion observed at m/z 176.14.....	293
Appendix Figure 5.57 -HCD MS/MS of the ion observed at m/z 181.10.....	293
Appendix Figure 5.58 -HCD MS/MS of the ion observed at m/z 182.08.....	293
Appendix Figure 5.59 -HCD MS/MS of the ion observed at m/z 192.14.....	294
Appendix Figure 5.60 -HCD MS/MS of the ion observed at m/z 205.10.....	294
Appendix Figure 5.61 -Direct infusion ESI - MS of BSA hydrolysed at 160 °C for 0 min.....	294
Appendix Figure 5.62 - Direct infusion ESI - MS of BSA hydrolysed at 160 °C for 20 min.....	294
Appendix Figure 5.63 - Direct infusion ESI - MS of NTG hydrolysed at 160 °C for 0 min.....	295
Appendix Figure 5.64 - Direct infusion ESI - MS of NTG hydrolysed at 160 °C for 20 min.	295
Appendix Figure 5.65 - Direct infusion ESI - MS of BSG hydrolysed at 160 °C for 0 min.....	296
Appendix Figure 5.66 - Direct infusion ESI -MS of BSG hydrolysed at 160 °C for 20 min.....	296
Appendix Figure 5.67 - Direct infusion ESI - MS of an equimolar AA mixture hydrolysed at 160 °C for 0 min.....	297
Appendix Figure 5.68 - Direct infusion ESI - MS of an equimolar AA mixture hydrolysed at 160 °C for 20 min.	297

Appendix Tables

Appendix Table 4. 1 - Ions identified from the direct infusion electrospray MS of untreated VQSIKADFHYPHENPTWGR.....	300
Appendix Table 4. 2 - Peak assignments following ETD MS/MS of m/z 809.7136.....	301
Appendix Table 4. 3 - Peak assignments following ETD MS/MS of m/z 815.0426.....	302
Appendix Table 4. 4 a - Peak assignments following LC CID MS/MS of m/z 815.0457 at RT ~16 min 45 s and b) 19 mins.....	304
Appendix Table 4. 5 - Peak assignments following ETD MS/MS of m/z 820.3787.....	306
Appendix Table 4. 6 - Peak assignments following ETD MS/MS of m/z 517.5779.....	307
Appendix Table 4. 7 - Peak assignments following ETD MS/MS of m/z 522.9105.....	308
Appendix Table 4. 8 - Peak assignments following CID MS/MS of m/z 583.7703.....	309
Appendix Table 4. 9 - Ions identified from the direct infusion electrospray MS of iodoacetamide treated VQSIKADFHYPHENPTWGR.....	310
Appendix Table 4. 10 - Peak assignments following ETD MS/MS of m/z 469.2041.....	311
Appendix Table 4. 11 - Peak assignments following CID MS/MS of m/z 474.5359.....	312
Appendix Table 4. 12 - Peak assignments following LC ETD MS/MS of m/z 719.2973 at a) RT ~9min 30s and b) ~ 11 min 30s.....	313
Appendix Table 4. 13 - Peak assignments following ETD MS/MS of m/z 727.2950....	315
Appendix Table 4. 14 - Peak assignments following ETD MS/MS of m/z 468.2838.....	316
Appendix Table 4. 15 - Peak assignments following ETD MS/MS of m/z 710.2924.....	320
Appendix Table 4. 16 - Ions identified from the direct infusion electrospray MS of untreated VQSIKADFHYPHENPTWGR.....	326
Appendix Table 4. 17 - Peak assignments following ETD MS/MS of m/z 545.0272.....	327
Appendix Table 4. 18 - Peak assignments following CID MS/MS of m/z 549.0260.....	328
Appendix Table 4. 19 - Peak assignments following CID MS/MS of m/z 715.0316.....	330
Appendix Table 4. 20 - Ions identified from the direct infusion electrospray MS of iodoacetamide treated VQSIKADFHYPHENPTWGR.....	331
Appendix Table 4. 21 - Peak assignments following ETD MS/MS of m/z 818.0553.....	332
Appendix Table 4. 22 - Peak assignments following ETD MS/MS of m/z 823.3905.....	333
Appendix Table 4. 23 - Peak assignments following CID MS/MS of m/z 837.0585.....	334

Appendix Table 4. 24 - Peak assignments following CID MS/MS of *m/z* 622.0462.....338

Appendix Table 5.1 - Peptides identified from the SCW hydrolysis of NTG at 160°C for 0 minutes (CD).

Appendix Table 5.2 - Peptides identified from the SCW hydrolysis of NTG at 160°C for 20 minutes (CD).

Appendix Table 5.3 - Peptides identified from the SCW hydrolysis of NTG at 207°C for 20 minutes (CD).

Appendix Table 5.4 - Peptides identified from the SCW hydrolysis of NTG at 253°C for 20 minutes (CD).

Appendix Table 5.5 - Peptides identified from the SCW hydrolysis of NTG at 300°C for 20 minutes (CD).

Appendix Table 5.6 - Peptides identified from the tryptic digest of NTG (CD).

Appendix Table 5.7 - Peptides identified from the Proteinase K digest of NTG (CD).

Appendix Table 5.8 - Peptides identified from the SCW hydrolysis of BSG at 160°C for 0 minutes (CD).

Appendix Table 5.9 - Peptides identified from the SCW hydrolysis of BSG at 160°C for 20 minutes (CD)

Appendix Table 5.10 - Peptides identified from the SCW hydrolysis of BSG at 207°C for 20 minutes (CD).

Appendix Table 5.11 - Peptides identified from the SCW hydrolysis of BSG at 253°C for 20 minutes (CD).

Appendix Table 5.12 - Peptides identified from the SCW hydrolysis of BSG at 300°C for 20 minutes (CD).

Appendix Table 5.13 - Peptides identified from the tryptic digest of NTG (CD).

Appendix Table 5.14 - Peptides identified from the Proteinase K digest of NTG (CD).

Appendix Table 5.15 - Ions observed following SCW hydrolysis of BSA at 160 °C for 0 min.....341

Appendix Table 5.16 - Ions observed following SCW hydrolysis of BSA at 160 °C for 20 min.....	342
Appendix Table 5.17 - Ions observed following SCW hydrolysis of NTG at 160 °C for 0 min.....	344
Appendix Table 5.18 - Ions observed following SCW hydrolysis of NTG at 160 °C for 20 min.	346
Appendix Table 5.19 - Ions observed following SCW hydrolysis of BSG at 160 °C for 0 min.....	348
Appendix Table 5.20 - Ions observed following SCW hydrolysis of BSG at 160 °C for 20 min.....	350
Appendix Table 5.21 - Ions observed of an equimolar AA mixture incubated at room temperature.....	352
Appendix Table 5.22 - Ions observed following SCW hydrolysis of an equimolar AA at 160 °C for 0 min.	355
Appendix Table 5.23 - Ions observed following SCW hydrolysis of an equimolar AA at 160 °C for 0 min.	358
Appendix Table 6.1 - Peptides identified from the tryptic digest of six proteins using the LTQ orbitrap (CD).	
Appendix Table 6.2 - Peptides identified from the SCW hydrolysis of six proteins using the LTQ orbitrap (CD).	
Appendix Table 6.3 - Peptides identified from the SCW hydrolysis of six proteins using the Q-Exactive (CD).	
Appendix Table 6.4 - Peptides identified from the tryptic digest of six proteins using the Q-Exactive (CD).	
Appendix Table 6.5 - Peptides identified from the SCW hydrolysis of six proteins using the Q-Exactive using new search parameters (CD).	

Appendix Table 6.6 - Peptides identified from the SCW hydrolysis of six proteins using the Q-Exactive using new search parameters and a longer LC column (CD).

Appendix Table 6.7 - Peptides identified from the SCW hydrolysis of six proteins using the Q-Exactive using new search parameters, a longer LC column and an increased gradient length (CD).

Abbreviations

2'-azino-bis(3-ethylbenzothiazoline-6-sulphonic acid - ABTS

6-hydroxy-2,5,7,8-tetramethylchroman-2-carboxylic acid - Trolox

Acetonitrile - ACN

Advanced Quadrupole Technology - AQT

Alanine - A

Amino acid - AA

Area under the curve - AUC

Aspartic acid - D

Arginine - R

Asparagine - N

Automatic gain control - AGC

Bovine serum albumin - BSA

Brewers' spent grain - BSG

Brewers' spent grain – BSG

Catalase - CAT

Cellular antioxidant activity - CAA

Charge ejection model - CEM

Charged residue model - CRM

Chemical ionization - CI

Collision induced dissociation - CID

Curved linear trap - C-trap

Cysteine - C

Data independent acquisition - DIA

Data-dependent acquisition - DDA

Dithiothreitol - DTT

Dulbecco's modified eagles medium - DMEM

Electron capture dissociation - ECD

Electron impact ionization - EI

Electron transfer dissociation - ETD

Electrospray ionisation - ESI
False discovery rate - FDR
Fast atom bombardment - FAB
Ferric ion reducing antioxidant power - FRAP
Folin-ciocalteu reagent - FCR
Formic acid - FA
Gas chromatography - GC
Glutamic acid - E
Glutamine - Q
Glycine - G
Glutathione peroxidase – GSHPx
High performance liquid chromatography - HPLC
Higher energy collisional dissociation – HCD
Histidine - H
Hydrogen atom transfer - HAT
Iodoacetamide - IAM
Ion evaporation model – IEM
Isoleucine – I
Leucine - L
Linear trap quadrupole - LTQ
Liquid chromatography - LC
Liquid secondary ion mass spectrometry - LSIMS
Low melting point agarose - LMPA
Low molecular point – LMP
Lysine - K
Mass spectrometry -MS
Mass-to-charge - m/z
Matrix assisted laser desorption ionisation – MALDI
Methionine - M
Molecular weight - MW

Nano-electrospray ionization - nano-ESI

Non-treated grains - NTG

One-dimensional electrophoresis - 2-DE

Oxygen radical absorbance capacity - ORAC

Oxygen radical absorbance capacity - ORAC

Peptide spectrum matches – PSM

Phenylalanine - F

Polyethersulfone - PES

Post translational modifications – PTMs

Proline - P

Reactive oxygen species - ROS

Reducing power - RP

Reversed phase chromatography – RPLC

Serine - S

Single electron transfer - SET

Sodium dodecyl sulfate polyacrylamide gel electrophoresis - SDS-PAGE

Strong cation exchange - SCX

Subcritical extraction - SCE

Subcritical extraction - SCE

Subcritical water - SCW

Superoxide dismutase - SOD

Supplemental activation -sa

Tandem mass spectrometry - MS/MS

Threonine - T

Total antioxidant capacity - TAC

Total radical trapping antioxidant parameter - TRAP

Trifluoroacetic acid - TFA

Trolox equivalence antioxidant capacity – TEAC

Tryptophan - W

Tyrosine - Y

Two-dimensional electrophoresis - 1-DE

Valine - V

Chapter 1: Introduction

1.1 Overview

Subcritical water (SCW) is a highly versatile solvent [1]. Under certain conditions, SCW can display synthetic and catalytic properties. Growing evidence suggests that SCW can be used as a tool in the treatment of food industrial waste to create mixtures of biological value, e.g. with antioxidant properties. Food industry wastes are often rich in proteins and SCW has been widely used to generate antioxidant mixtures from these wastes. In this thesis I aim to demonstrate the SCW extraction of antioxidant compounds from the major by-product of the brewing industry, brewers spent grain (BSG).

The mechanisms of SCW hydrolysis are not well established. In the work presented in Chapter 3, the specificity of subcritical water with respect to the production of peptides from three model proteins is investigated. Tandem mass spectrometry (MS/MS) coupled with high performance liquid chromatography (HPLC) is an effective method of identifying the components of a complex mixture. In the work presented in Chapter 4, modifications induced during SCW hydrolysis using a model peptide approach are investigated, with the aim of aiding peptide identification during automated searches. The work presented in Chapter 5 aimed at identifying the decomposition products responsible for antioxidant capacity generated during SCW hydrolysis. Antioxidant capacity of SCW hydrolysates was assessed using Oxygen Radical Absorbance Capacity (ORAC), comet and reducing power assays. The fractions with the most powerful antioxidant capacity were analysed using MS/MS.

In the course of this work, the possibility of using SCW as an alternative proteolytic reagent during a proteomic workflow was raised in Chapters 3 and 4. This aspect was further explored in Chapter 6 where HPLC, MS/MS and search parameters were investigated.

In this introduction an overview of mass spectrometry (MS) (section 1.1), SCW hydrolysis (section 1.2), brewer's waste production (section 1.3), a brief summary of

oxidative stress, antioxidant function and antioxidant assays (section 1.4) and existing strategies in proteomics (section 1.5) is provided.

1.2 Mass spectrometry

1.2.1 Introduction to mass spectrometry

Mass spectrometry is an analytical technique that is used to measure the mass-to-charge (m/z) ratio of molecules that have been converted to ions.

The first step in a typical MS analysis is the production of gas-phase ions. The charged ions are separated in accordance to their m/z ratio using electric and/or magnetic fields to control the motion of the ions before the final stage which is detection of the separated ions. These steps are performed under a high vacuum, as molecular collisions reduce instrument accuracy and sensitivity.

1.2.2 Ionization

Ionization enables molecules to gain charge through interaction with chemicals, light or electrons. Prior to the 1980s, the ionization of molecules in mass spectrometry was primarily dependent upon either electron impact ionization (EI) or chemical ionization (CI). In EI a heated filament provides a source of electrons, which collide with the gaseous molecules of the analysed sample injected into the source. Under sufficient energy, this causes an electron to be expelled from the analyte, resulting in a positively charged ion. In contrast, CI produces ions through collisions between the analyte and primary ions present in the source. These methods were unsuitable due to biomolecular degradation and fragmentation that occurs during gas phase transition [2].

The first move towards analysing biomolecules was the development of 'soft' ionization techniques. Fast atom bombardment (FAB) uses a beam of high energy atoms to desorb ions from a surface [3]. This method yields little fragmentation of molecular ions, therefore facilitating analysis of larger biomolecules. A modification on

this technique, using highly energetic ions instead of atoms, was developed termed liquid secondary ion mass spectrometry (LSIMS). [4]

The advent of novel ionisation techniques such as matrix assisted laser desorption ionisation (MALDI) [5] and electrospray ionisation (ESI) [6], has further enabled the measurement of high molecular weight (MW) compounds such as proteins, peptides and oligonucleotides.

Figure 1.1 depicts a schematic of ESI. This occurs in three broad steps a) formation of charged droplets at the capillary tip, b) disintegration into smaller highly charged droplets and c) the final conversion of droplets into the gas phase.

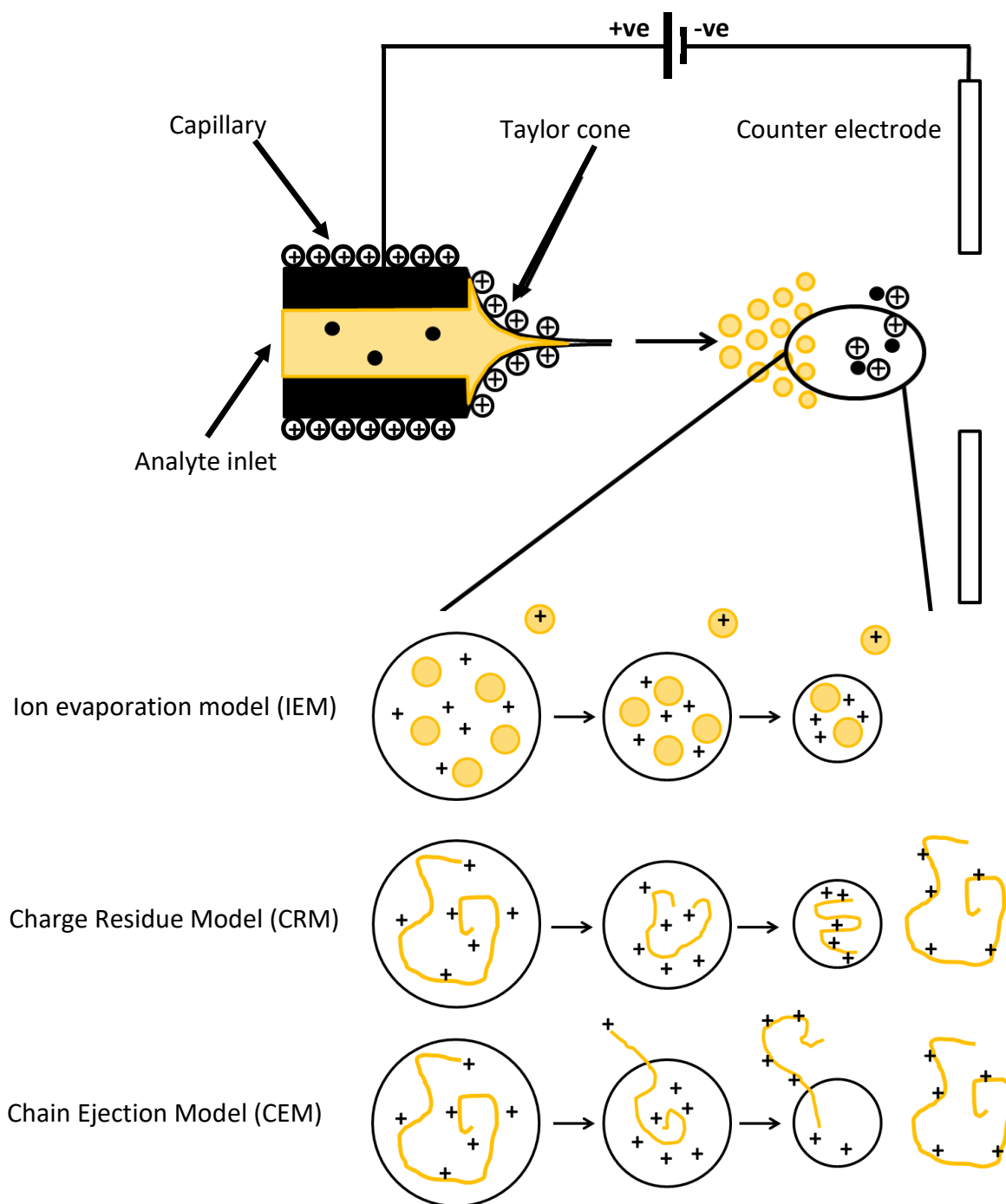


Figure 1. 1 - Schematic of electrospray ionisation demonstrating ion evaporation, charge residue and chain ejection models.

In the first step the sample is dissolved in an appropriate solvent, which typically consists of a combination of organic solvent and water with <1% acid/base to enhance protonation/ deprotonation. The omission is the protein analysis of native states. Here organic solvents are not used as they cause the protein to lose its tertiary structure [7]. The solution is passed through a capillary tube at a flow rate of $\sim 1\text{-}10\ \mu\text{L min}^{-1}$. A potential difference is applied between the capillary and the counter electrode which creates an electric field. This field induces an accumulation of charge at the capillary tip liquid surface. The repulsive forces created at the capillary push the liquid away whilst being counteracted by the surface tension at the liquid air boundary which pulls the droplet back. The droplet at the end of the tip becomes distorted. This phenomenon was described by Taylor in 1964 [8], and was hence termed the Taylor cone.

The emerging solution exits as a fine mist of charged droplets. These droplets are attracted to the counter electrode of the mass spectrometer, which is held at a negative potential, generating a small current [9]. The reduction in droplet size causes an increase in surface charge density. The organic component of the solvent evaporates at a faster rate, causing an increase in water percentage [10-12]. The increase in surface charge density is counteracted by Coulombic repulsion. The point where these two forces are equal is referred to as the Rayleigh limit. Once this limit is reached droplets burst via jet fission to produce smaller droplets. The process repeats until the droplet reaches a critical point where it is thermodynamically favourable for the ions at the surface to enter the gaseous phase.

Species are transferred into the gas phase through different mechanisms. Low MW species are hypothesised to be transferred into the gas phase via the ion evaporation model (IEM) [13, 14], whilst it is widely accepted that large globular species, of high MW, are thought to be transferred into the gas phase via the charged residue model (CRM) [15]. More recently a third model has been proposed, the charge ejection model (CEM) [16, 17].

The IEM model was originally conceived by Iribarne and Thomson in the late 1970s [13, 14]. The ion evaporation model assumes that the charged droplets shrink by evaporation until the charge density becomes so great that the repulsive forces are sufficiently large to expel solvated ions from the droplet.

The charge residue model (CRM) was originally proposed by Dole and co-workers in 1968 [15]. This model is applicable to higher molecular weight species, such as proteins. Since proteins are likely to contain multiple protonation sites (from basic amino acids), proteins often have multiple charge states. This model assumes that droplets contain one single analyte ion, and the solvent evaporates until the charge is retained on the non-volatile solute molecule [18].

The chain ejection model (CEM) has recently been proposed by Konermann and co-workers [16, 17]. In solution, proteins typically adopt a compact globular field where polar and charged residues are positioned on the outside of proteins, maximising favourable water interactions, whereas hydrophobic residues are positioned in the interior of proteins. This model assumes proteins become partially unfolded in the liquid phase by e.g. exposure to an acidic LC mobile phase. The core hydrophobic residues are now exposed, making it unfavourable for proteins to reside within the droplet interior. Instead, unfolded proteins migrate to the surface of droplets and one chain terminus gets expelled from the droplet to the vapour phase and the rest of the protein soon follows.

In this thesis the Advion TriVersa Nano Mate was used as an ionisation source. This technology utilises nano-electrospray ionization (nano-ESI). This follows the same fundamental principles outlined above, however the flow rates at which the samples are introduced are in the region of nLmin^{-1} rather than mLmin^{-1} used for standard ESI [19]. Nano-ESI has been favourably compared against conventional electrospray in protein analysis. Juraschek *et al.* showed analytes were better detected in nano-ESI in samples with salt contamination [20]. This was attributed to the reduced droplet size in nano-ESI compared with electrospray at higher flow rates. Furthermore, the lower flow rates used in nano-ESI allow for smaller quantities of sample to be analysed.

The Triversa Nanomate infuses samples using a small conductive pipette tip via a microfabricated chip composed of monolithic silicon, comprising 400 nozzles. The pipette tip is controlled by a robot which aspirates the solution and is sealed against the chip. A gas and voltage are then applied which electrospray the solution through the nozzles. This chip based approach produces highly stable ESI currents [21, 22].

The increasing mass range and mass accuracy of modern mass analysers has also been instrumental in the application of MS to biological samples. Mass analysers can either be used individually or in tandem within a mass spectrometer.

1.2.3 Mass Spectrometers

Two mass spectrometers were used in the work carried out in this thesis. These were the Orbitrap Elite and the Q-Exactive HF mass spectrometers.

1.2.3.1 Orbitrap Elite Mass Spectrometer

The Orbitrap Elite mass spectrometer is a hybrid mass spectrometer that consists of a dual-pressure linear ion trap (the linear trap quadrupole) (LTQ)) and an Orbitrap mass analyser. The LTQ-Orbitrap offers high resolving power (240,000) and excellent mass accuracy (specified as 2-5 ppm) [23]. These parameters are vital in providing de novo identifications of MS/MS spectra [24, 25], as well as excellent identification of fragment ions and localisation of post translational modifications (PTMs).

Figure 1.2 displays a detailed cross section of the Orbitrap Elite. Here, ions are injected into the mass spectrometer via a nano-ESI source, focused by a stacked ring ion guide (S-lens) and transferred to a dual-pressure ion trap mass analyser.

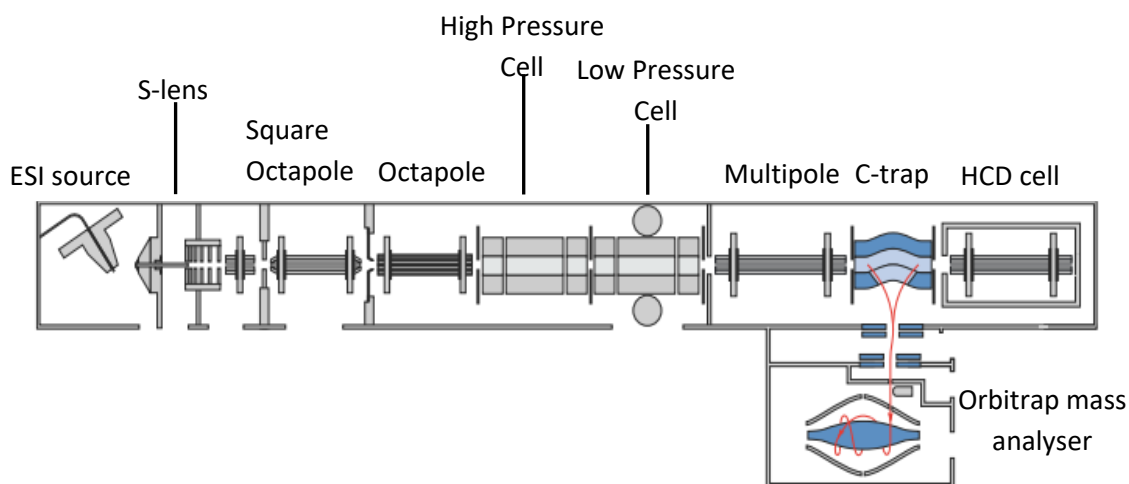


Figure 1. 2 - Schematic of LTQ-Orbitrap Elite. Adapted from [26].

Figure 1.3 shows a cross section of a typical 2-d ion trap. Upon entering the trap, collisions with an inert gas cause ions to cool as they progress along the z axis, whilst the application of an RF –only potential causes them to simultaneously oscillate along the xy plane. The rods are commonly divided into three segments. The application of a DC voltage to the ends facilitates ion trapping in the z direction.

The RF voltage applied allows the ions to be destabilised sequentially. Ions leave the trap in increasing m/z ratio, via axial ejection between two of the planar rods. This method of separation is referred to as the “mass-selective axial instability mode” as developed by Stratford *et al.* in the 1980s [27].

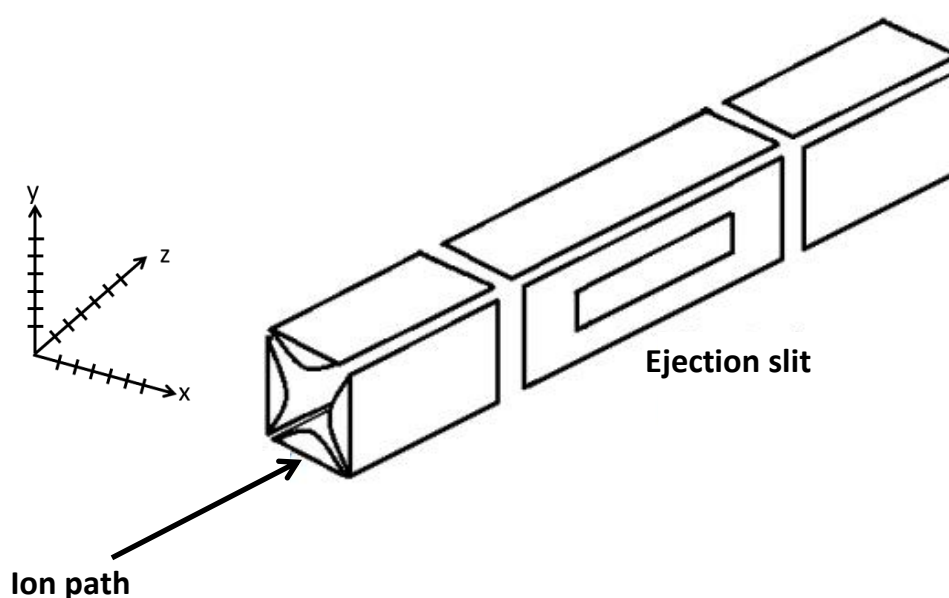


Figure 1. 3 - Schematic of an ion trap. Figure adapted from [28].

The Orbitrap Elite makes use of a dual pressure ion trap. A single aperture lens is used to separate two linear cells to allow differential pumping between the two portions. Helium is introduced into the high pressure cell (5.0×10^{-3} torr), whilst some portion leaks into the low pressure cell via the lens (3.5×10^{-4} torr). The high pressures in the first cell facilitate improved ion trapping as well as better isolation of precursor ions and subsequent fragmentation efficiencies. Furthermore, the presence of ejection

slots in all four rods facilitates ion ejection to occur at higher voltages, whilst also applying isolation waveforms. This means only ions of a specified m/z fill the trap, which vastly improves detection of low-abundant species. The low pressure cell is used as a mass analyser, which facilitates faster scan rates and higher resolution compared to less advanced versions of the Orbitrap Elite [29].

Ions are then transferred to a curved linear trap (C-trap) via a gas-free RF- only octapole. Upon entering the C-trap, ions collide with a nitrogen bath gas, lose kinetic energy and form a long, thin thread across the curved axis of the trap. The thread is compressed axially by apertures at the entrance and exit of the C-trap which have an rf voltage to provide a potential difference across the trap axis [23].

Ions are extracted by switching off the rf voltage of the C-trap and instead applying extracting dc pulses across the electrodes. Ions are ejected orthogonally to the axis of the C-trap via a slot in the pull out electrode. The ion beam then converges on the entrance of the orbitrap mass analyser [23].

Figure 1.4 shows the face view of the orbitrap. The device consists a coaxial, barrel-like, outer electrode, with an axial central electrode that is run through [30]. The outer electrode consists of two halves with a small interval. The maximum diameter of the inner electrode is 8mm and the outer electrodes 20 mm [31]. Ions are injected laterally between the two parts of the outer electrode. An appropriate voltage is applied to the central electrode, which is held at an opposite potential to the mode of ionization, and the outer electrode is held at ground potential. This creates a centrifugal force facilitating ion trapping.

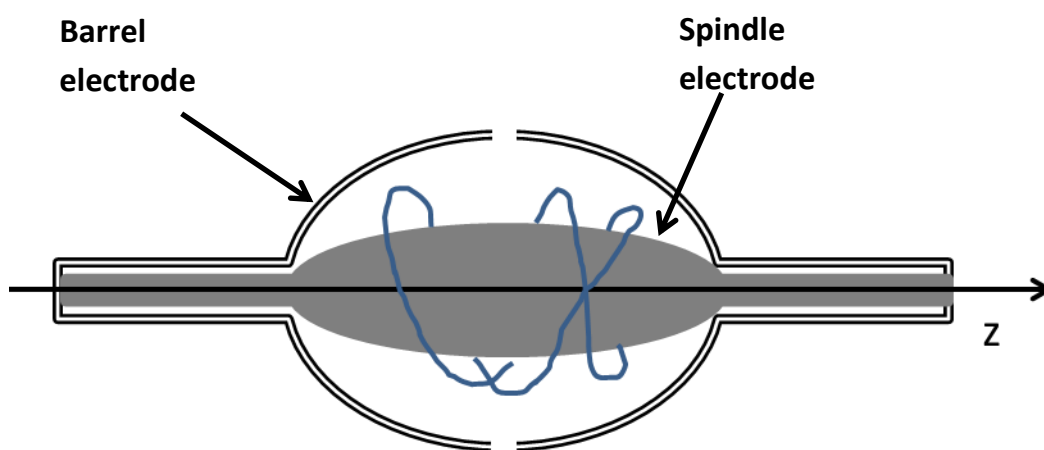


Figure 1. 4 - Cross section of the Orbitrap mass analyser. Figure adapted from [32].

The electrostatic field between the two electrodes creates a static electrical field which is described in **Equation 1.1**, where U is the electrostatic potential; r and z are the cylindrical co-ordinates; C is a constant, k is the field curvature and R_m is the characteristic radius.

$$U_{(r,z)} = \frac{k}{2} \left(z^2 - \frac{r^2}{2} \right) + \frac{k}{2} (R_m)^2 \ln \left[\frac{r}{R_m} \right] + C$$

Equation 1. 1 - Equation describing the electrostatic field of the orbitrap cell.

As ions orbit the spindle, they are free to move independently along the z-axis, such that the orbit around the central electrode becomes a series of complicated spirals. Each ion has a characteristic oscillation frequency that is dependent on its m/z . The motion along the z axis can be described as a simple harmonic oscillator, like a pendulum. **Equation 1.2** explains this motion and **Equation 1.3** shows that the frequency is directly linked to the m/z ratio and is independent of the kinetic energy of the injected ions, where ω = the frequency of axial oscillations in radians/ per second, E_z = energy characteristic of ion motion along the z axis, k is the field curvature of the orbitrap cell, q = ion charge and m = ion mass [33].

$$a) z(t) = z_0 \cos \omega t + \sqrt{\left(\frac{2E_z}{k} \right)} \sin \omega t$$

$$b) \omega = \sqrt{\left(\frac{q}{m} \right) k}$$

Equation 1. 2 - Equations describing the axial ion oscillations along the z axis of the orbitrap spindle electrode a) equation of motion, b) calculating the charge to mass ratio of an ion from frequency of oscillations.

1.2.3.2 Q-Exactive HF

A second hybrid mass spectrometer that was used in this thesis was the Q-Exactive mass spectrometer. This is a hybrid quadrupole-orbitrap instrument. **Figure 1.5** depicts a schematic of the Q-Exactive HF. Briefly; ions are injected via a nano-ESI source and focused using a S-lens. Ions are then transferred via a bent flatpole that facilitates the ejection of solvent droplets and other neutral species, preventing them from entering further into the instrument. Ions then enter a segmented quadrupole (HyperQuad Mass Filter with Advanced Quadrupole Technology (AQT)), which acts as a mass filter.

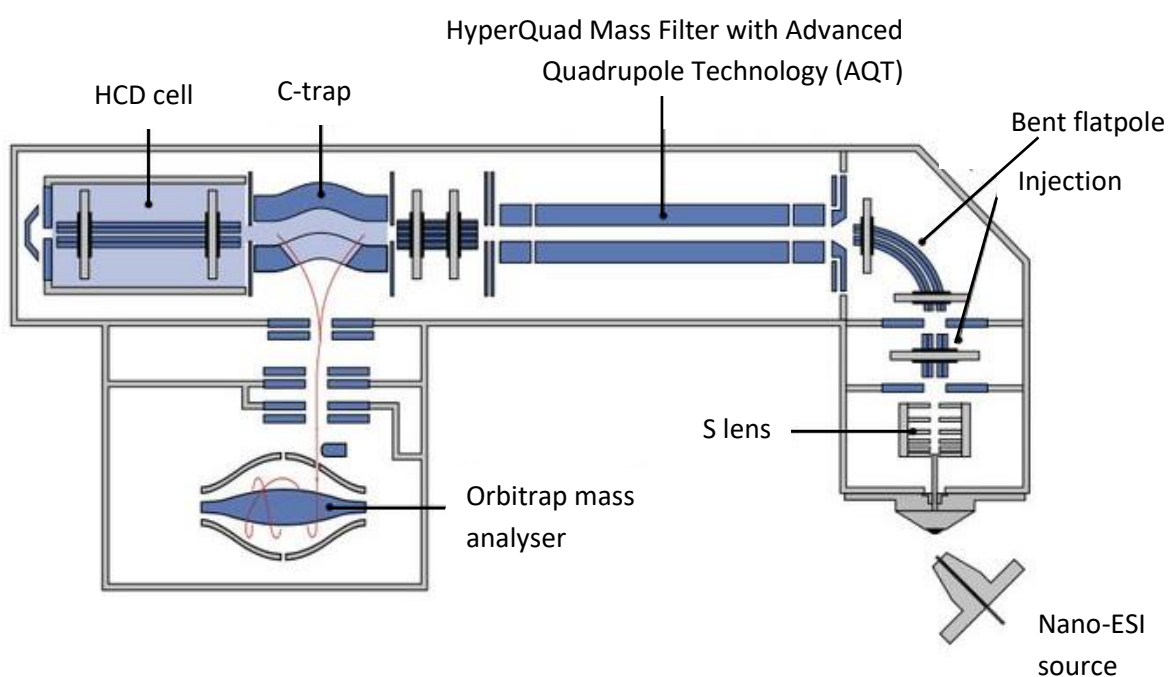


Figure 1. 5 - Schematic of Q-Exactive HF mass spectrometer. Figure adapted from [34].

Figure 1.6 shows a schematic of a quadrupole. Quadrupoles are devices which use the stability of the trajectories in oscillating fields to separate ions based on their m/z ratios. A quadrupole consists of four hyperbolic rods, each with an alternating radiofrequency applied to it [32].

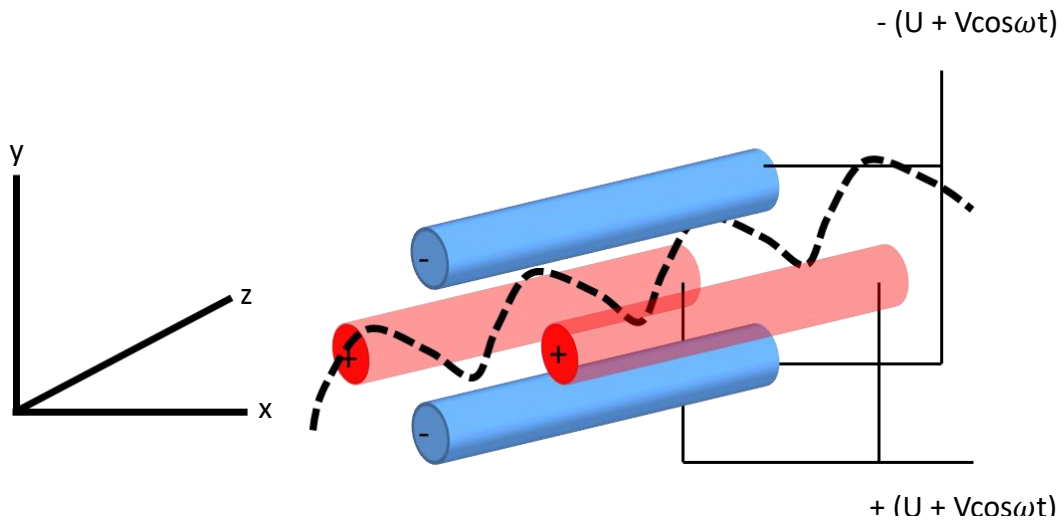


Figure 1. 6 - Schematic diagram and axis of motion of ions in a quadrupole.

Ions travelling along the z axis are subjected to a quadrupolar alternative field superposed on a constant field supplied via the four rods. These are described in **Equation 1.3**, where ϕ_0 is the potential of the rods, ω is the angular frequency of the field in radians per second, t is any time point, U is the DC voltage and V is the zero to peak amplitude of the RF voltage.

$$\Phi_0 = +(U - V \cos \omega t) \text{ and } -\Phi_0 = -(U - V \cos \omega t)$$

Equation 1. 3 - Equation describing the quadrupolar field.

A ion entering the space between the rods will be drawn towards rod of an opposite charge. If the potential of the rod changes sign before the ion is discharged, the ion will change trajectory. The trajectory of ions through the quadrupole is determined by their m/z , so ions can be selectively transmitted by adjusting the strength of the

electric and RF fields. Ions of differing m/z will have an unstable path and will be deflected towards one of the rods and be discharged [35].

The Q-Exactive offers the opportunity to select ions at a much faster rate due to the switching time of the quadrupole. This is advantageous compared to the orbitrap, where the LTQ system only allows a certain population of ions to remain stable within the trap [36].

1.2.4 Tandem Mass Spectrometry

Tandem mass spectrometry is conducted by performing two separate mass analysis events, in a single instrument. Through the fragmentation of an intact ion it is possible to predict its structure, based on predictable bond cleavages. This method of analysis is commonly used for the analysis of proteins, peptides and PTMs [36].

In MS based proteomic analyses, MS/MS can be used to peptide sequence as well as localise structural modifications. In the example of peptides, fragmentation most commonly occurs along the peptide backbone (**Figure 1.7**). The fragments observed depend on the fragmentation technique used. There are different fragmentation techniques available. These include collision induced dissociation (CID), electron transfer dissociation (ETD) and HCD [37]. CID and HCD fragmentation predominantly produce b and y product ions as well as occasional a ions. ETD fragmentation mostly forms c and z ions as well as occasional a, b or y ions [38].

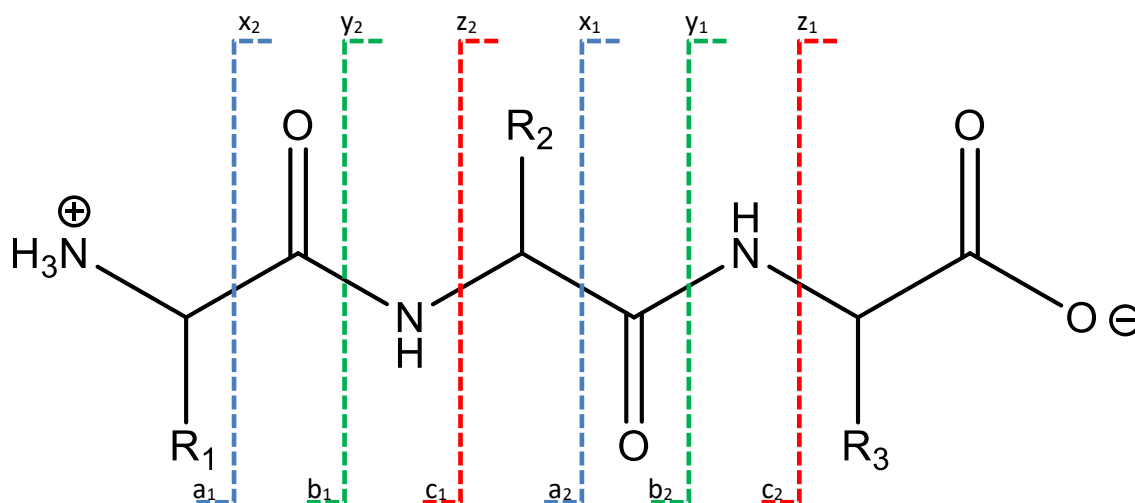


Figure 1. 7 - The chemical structure of a peptide, together with the designation for fragment ions (the Roepstorff–Fohlmann–Biemann nomenclature) [39]. Adapted from [40].

1.2.4.1 Collision induced dissociation (CID)

CID is achieved through collisions between the precursor ion and an inert gas. Some of the kinetic energy that is gained during the collision is converted into internal energy within the ion that results in bond dissociation, generating a fragment ion and a neutral loss molecule.

In proteomics, research is focused on peptide fragmentation. The mobile proton model describes the mechanisms of fragmentation in the CID of peptides [41]. The model assumes the energy imparted in the collision results in the transfer of a proton in a more basic region e.g. basic amino acid side chains or the N-terminus, can transfer to the amide nitrogen atoms, producing b_n and y_n ions. By finding the difference in mass between sequential b and y ions, it is possible to calculate the peptide sequence.

Whilst b and y fragments represent the most common fragmentation pathways, other possibilities do exist. Neutral losses from ions are common and include the removal of small molecules such as H_2O , NH_3 , and CO from peptides. Including these losses into criteria when searching for fragments can act as an additional source of information when assigning MS/MS spectra to peptide sequences [42].

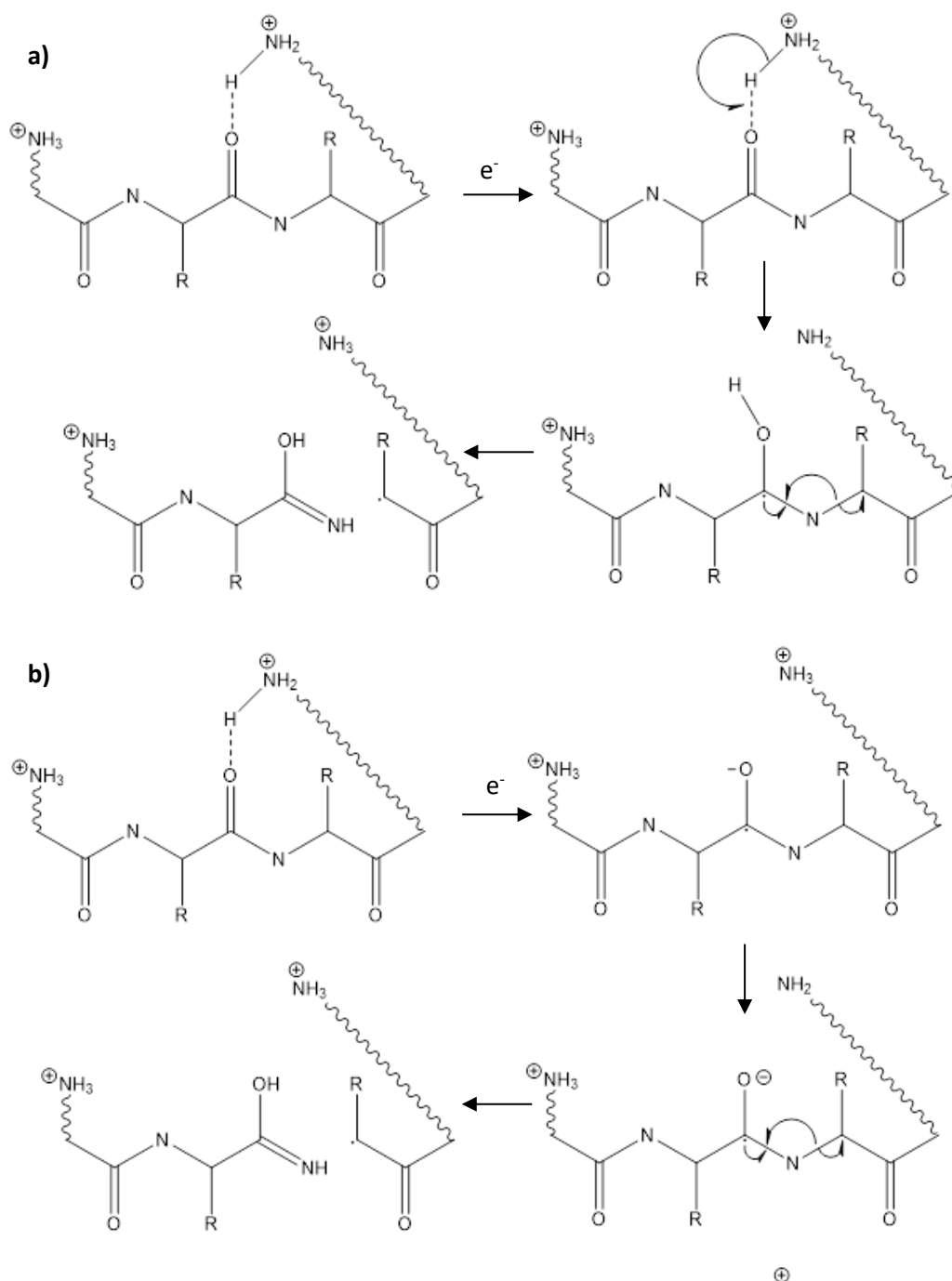
1.2.4.2 Electron Mediated Dissociation

Whilst CID is effective at producing sequence information, this mechanism of fragmentation results in the dissociation of the most labile bonds. Post translational modifications (PTMs) are often lost during this method of fragmentation and therefore prove impossible to localize during sequencing analysis. For example, in the case of phosphopeptides, the phosphate backbone competes with the peptide backbone as the preferred site of cleavage. Phosphoric acid is often displaced from the peptide, losing localisation information [43].

In 1998 electron capture dissociation (ECD) was reported as an alternative method to analyse peptide structures and was later found to be effective at retaining PTMs on fragments [44-46]. This technique is not without its limitations in that the precursor ions need to be completely immersed in near thermal electrons, effectively limiting this technique to analysis using a Fourier transform ion cyclotron resonance (FT-ICR) mass analyser [47, 48]. Six years later Syka and co-workers developed a methodology to enable peptide fragmentation, without the need for thermal electrons, termed electron transfer dissociation (ETD) [49]. ECD and ETD ions typically form c and z fragments (**Figure 1.7**). There are two major accepted theoretical mechanisms for the fragmentation of peptides using ECD/ETD: the Cornell mechanism [50] and the Utah-Washington mechanism [51] (**Scheme 1.1**).

The Cornell mechanism was developed by McLafferty and co-workers [50]. This mechanism suggests that initial electron capture will occur on a protonated amino acid side chain, typically that of a basic amino acid (lysine, arginine, histidine), forming a hypervalent radical N-species. Hydrogen atom ejection and transfer to the amide oxygen allows the formation of a carbon-centred amino-ketyl radical intermediate. Cleavage at the adjacent N-C α bond occurs and c and z fragments are subsequently formed. Whilst the Cornell mechanism explains the formation of these specific fragments where mobile hydrogen atoms are present, it fails to explain the observation of these fragments in examples where peptides do not carry fixed charge derivatives or metal adducts [52, 53].

The Utah-Washington mechanism was conceived by Simons *et al.* from the University of Utah [51], and then furthered by Turecek *et al.* from the University of Washington [54, 55]. This theory works on the principle that an electron is captured in a Coulomb-stabilised amide π orbital, forming an aminoketyl radical anion. This anion is superbasic with a proton affinity in the range of 1100–1400 kJ mol⁻¹ [54, 56]. The amide anion then abstracts a proton from an accessible site to become neutralized resulting in the formation of c and z fragments.



Scheme 1. 1 a) Cornell mechanism for N–Ca bond cleavage in ExD of peptides and proteins with charge solvation from a C-terminal donor amine group and **b)** the Utah–Washington mechanism for ExD. Scheme adapted from [57].

1.2.4.3 Higher energy collision dissociation (HCD)

HCD provides beam type CID MS/MS to effect vibronic dissociation. This approach differs from the collisional dissociation via resonant excitation of a trapped precursor population [58]. In the context of the Orbitrap mass analyser, ions are passed through the C-trap into an adjacent multipole, which acts as a collision cell. Fragments are passed back through the C-trap and into the orbitrap for high resolution analysis. HCD is advantageous to the ion-trap CID fragmentation described previously in that there is no low-mass cut off, the data is of higher resolution and increased ion fragments are transferred leading to a better signal-to-noise ratio [59].

Whilst these three fragmentation techniques are effective in the identification of peptides, they can also be used to aid the identification of small molecules such as drugs, toxins and metabolites [60-62].

1.3 Subcritical water

Figure 1.8 represents a phase diagram of water as a function of temperature and pressure. Under atmospheric pressure water melts at 0 °C and boils at 100 °C. In addition to the three phases of solid, liquid and gas, water can exist in a supercritical phase under conditions >373.9 °C and 220.6 bar [1]. Supercritical is defined as 'the state of a substance where there is no clear change between the liquid and gas phase' [63]. In this thesis, the focus is on the use of *subcritical* water. This refers to liquid water at temperatures between the atmospheric boiling point and the critical temperature of water.

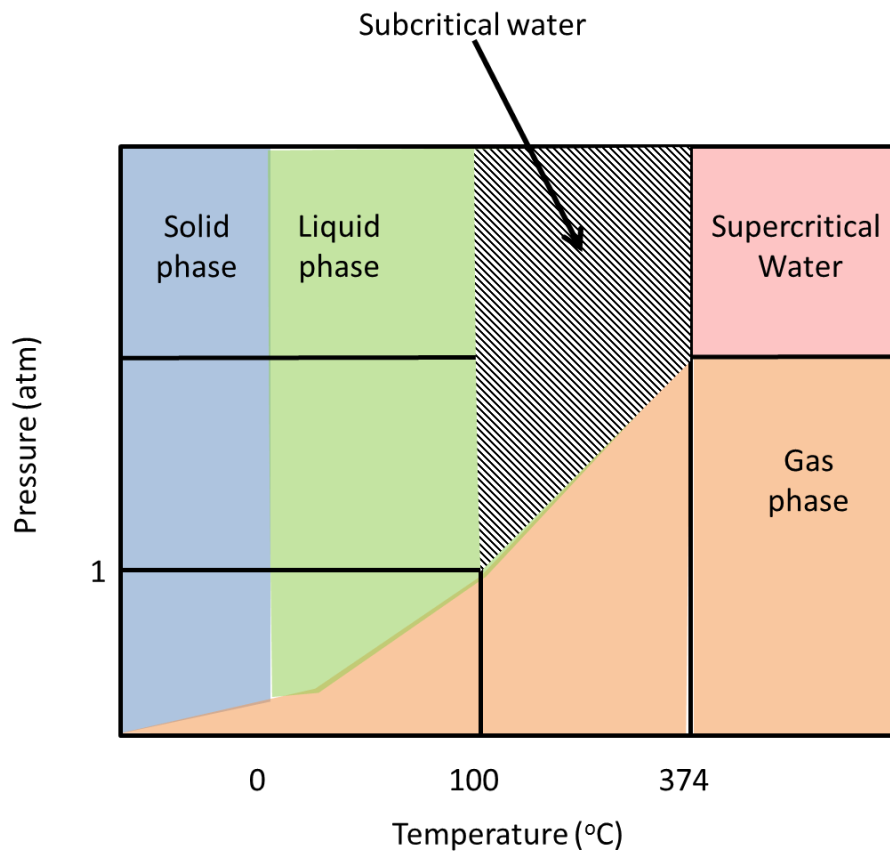


Figure 1. 8 - Phase diagram of water with respect to pressure and temperature.

1.3.2 Physical-chemical properties of SCW

Under ambient conditions water has an extremely high dielectric constant (ϵ_r) of $\sim 80 \text{ Fm}^{-1}$ at 20°C and 0.1 MPa . This property refers to water's ability to electrostatically bind to surrounding molecules. The dielectric constant of water decreases as it approaches the critical point (14.07 Fm^{-1} at 350°C and 20 MPa) [64]. Therefore there are reduced interactions between water molecules and surrounding ions as well as an increased movement of water molecules. Under these increased temperature and pressure conditions, where the hydrogen bonding network is disrupted, water is able to dissolve non-polar compounds. As a comparison, under subcritical conditions of $\sim 200 - 275^\circ\text{C}$, the dielectric constant of water is comparable to that of methanol and ethanol at 20°C (33.30 and 25.02 Fm^{-1}) [65].

Under ambient conditions water dissociates to form hydronium and hydroxide conditions. This is described in **Equation 1.4** where K_w = ionic product of water.

$$K_w = \frac{[\text{H}_3\text{O}^+][\text{OH}^-]}{[\text{H}_2\text{O}]}$$

Equation 1. 4 - Equation describing the ionic product of water.

Under subcritical conditions the ionic product of water (K_w) increases by ~ 100 orders of magnitude under subcritical conditions (from 10^{-14} to $10^{-12} \text{ mol.dm}^{-3}$). The increase in hydrogen and hydroxide ion concentration raises the reactivity of water and enables SCW to catalyse chemical reactions [66].

1.3.3 Subcritical water extraction

Over recent years an increasing amount of research has focused on the use of SCW for the recovery of valuable compounds from food waste [67]. The extraction of valuable compounds, from a sample traditionally discarded as waste, has significant economic potential. Food industry wastes are often rich in proteins and SCW has been widely used in the recovery of amino acids and peptides from these wastes [68, 69].

The fish industry is considered to be one of the most wasteful food industries, with ~40-50% of total weight contributing towards waste [70]. Tayokoli and Yoshida investigated the recovery of amino acids from scallop viscera [71]. The optimum yield of amino acids was observed at 240 °C, and temperatures above this showed degradation of amino acids into organic acids. Here, amino acids content was measured using an amino acid HPLC column with a post-column labelling method and amino acids quantity was analysed using a fluorescence detector.

Sereewatthanawut *et al.* demonstrated efficient recovery of amino acids and protein from deoiled rice bran [72]. Here, the protein and free amino acid content was analysed using spectrophotometric methods. The protein content was analysed by Lowry's assay, using bovine serum albumin (BSA) as a standard and amino acid content was analysed by Ninhydrin assays using L-glutamic acid as a standard. The yield of both protein and amino acids using SCW extraction from deoiled rice bran compared favourably to using alkali hydrolysis extraction, a more traditional method.

Additionally, in this study, the antioxidant capacity of the SCW hydrolysates was assessed using the 2'-azino-bis(3-ethylbenzothiazoline-6-sulphonic acid) (ABTS) assay. Hydrolysates showed a positive correlation between residency temperature and antioxidant capacity.

SCW has been reported as an excellent solvent in the recovery of other antioxidant compounds [73-76]. The recovery of these compounds is of great interest to cosmetic and food industries. Various extraction techniques have previously been applied in the withdrawal of bioactive compounds from biological mixtures, including Soxhlet extraction and maceration [77]. Whilst these techniques can offer effective recovery,

they do have many disadvantages, including exposure to hazardous and flammable liquid organic solvents [78]. Furthermore, they are not considered “green” procedures and may contribute towards pollution. Interestingly, Khajenoori *et al.* favourably compared subcritical extraction (SCE) against traditional approaches for the extraction of essential oils from the Iranian flower, *Zataria multiflora* Boiss [79].

Giray *et al.* investigated the products of the SCE of *Lavandula stoechas* flowers against those obtained following the more traditional extraction techniques of hydrodistillation and organic solvent extraction under ultrasonic irradiation [80]. Both heavy and light oxygenated compounds were shown to be extracted more efficiently using SCE. Here, both qualitative analysis of all mixtures as well as quantitative analysis of specified compounds was performed using gas chromatography (GC)-MS.

1.3.4 SCW Processing Models

Subcritical treatment has been carried out using both continuous [81] and batch [82] processing models. In the continuous flow model, water is passed through a pump and transferred into an extraction cell. The extraction cell is situated within a convection oven that contains the reactant. The resulting hydrolysate stream then exits through a cooling coil and the mixture is collected.

In the work presented in this thesis a batch mode SCW apparatus was used. In contrast to the continuous flow model, this set up is simpler in design. **Figure 1.9a** shows a typical processing tube. The pre-requisite volume of water and biomass are placed in the reactor and appropriately tightened (air tight). The mixture is heated up to temperature for the desired reaction time using a convection oven (**Figure 1.9b**). For reaction termination, the reactor is immersed into an ice bath. The temperature of the reaction can be monitored via a thermocouple where required, which can be injected into a reaction tube (**Figure 1.9c**).

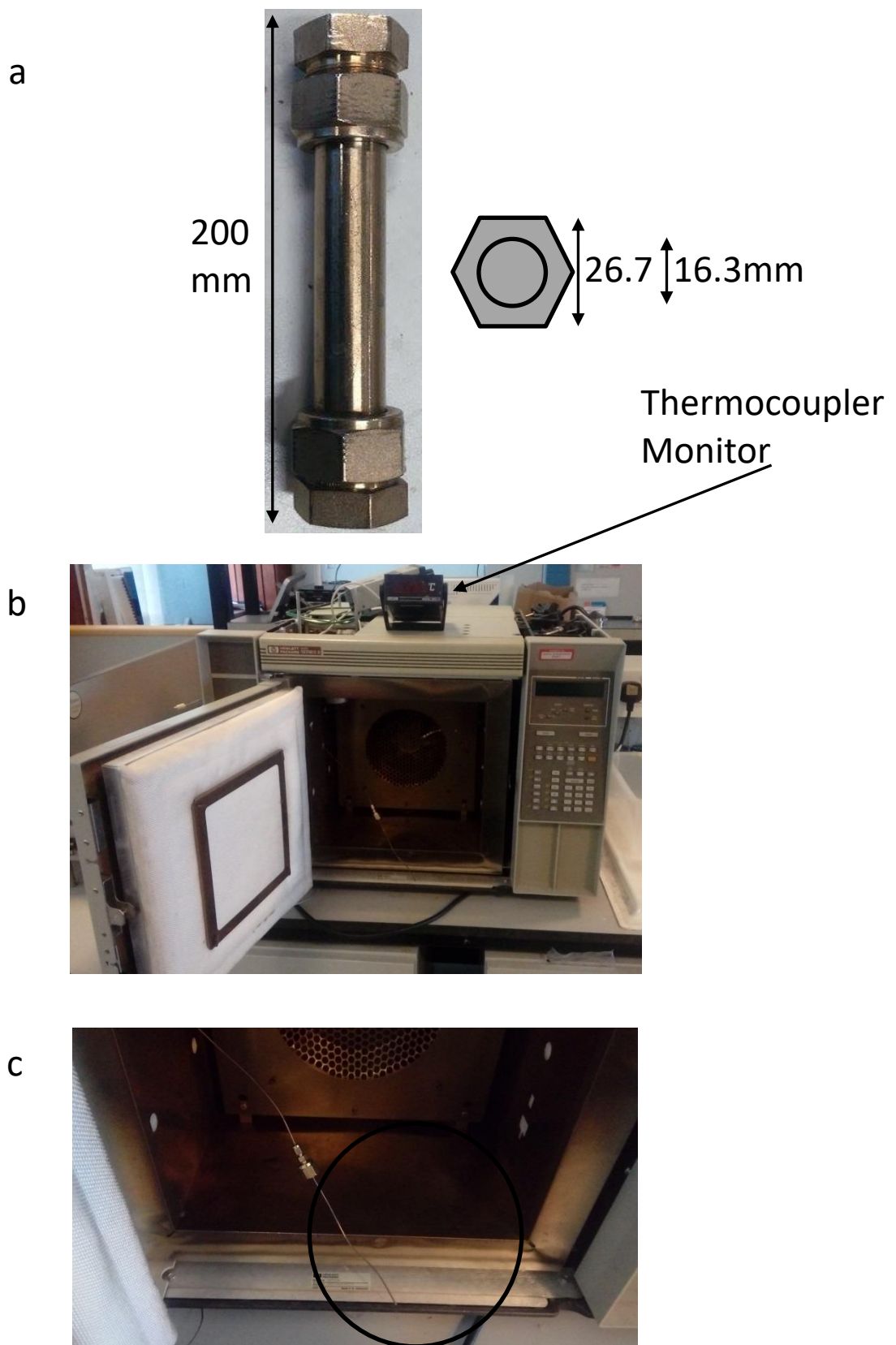


Figure 1. 9 - Apparatus used for SCW hydrolysis a) reaction tube, b) convection oven, c) thermocoupler.

1.3.5 The influence of SCW parameters

There are many parameters involved in the SCE of compounds. A subtle change in each one could result in a large shift in the extraction yield. Some of these parameters are discussed below.

1.3.5.1 Temperature

The residency temperature has a high degree of influence on the physiochemical properties of water and therefore choosing which temperature to use for extraction is of critical importance. A temperature too low will result in inefficient extraction, whilst using a temperature too high often risks its degradation [79]. Additional reactions may occur under these elevated temperatures i.e. the production of by-products or the decomposition of compounds. This was demonstrated by Vergara-Salinas *et al.* in the extraction of polyphenol from grape pomace extracts [83]. Here increasing the residency temperature above 150 °C resulted in the production of by-products and an overall decrease in yield due to polyphenol degradation.

1.3.5.2 Solid: water ratio

The importance of choosing an appropriate solid: water ratio in the efficient recovery of chosen compounds using subcritical water hydrolysis is disputed. Wang *et al.* studied the extraction of ursolic acid from the herb, *hedyotis diffusa* [84]. A sharp increase in yield was observed when 1g of sample was dissolved in 25 ml of water, compared to that obtained when dissolved in 20 ml water. A gradual decrease in yield was observed when the amount of water was increased incrementally to 40 ml.

Lei *et al.* investigated the recovery of resveratrol from grape seeds under a variety of conditions [85]. A surface response methodology was employed to identify the optimum extraction conditions for temperature, time, pressure and solid: water ratio. Here, the yield of resveratrol was constant under the different solid: water ratios employed.

1.3.5.3 Time

The residency time of the reaction is critical in extraction efficiency. Xu *et al.* investigated the effect of a variety of parameters on phenolic extraction from marigold flower residues [76]. The highest level of phenolic compounds could be obtained after 45 minutes of hydrolysis. An increase in extraction time beyond this resulted in a significant decrease in extraction efficiency. The authors speculated this may have been due to degradation of the phenolic compounds, or else polymerisation of the compounds under these extended residency times. Furthermore Awaluddin *et al.* studied the extraction of carbohydrates from *Chlorella vulgaris* [86]. Here, longer reaction times were shown to increase carbohydrate yield. In this study a maximum reaction time of 20 minutes is used.

1.3.5.4 Pressure

The influence of pressure on SCE efficiency has been disputed [87-89]. Under temperatures less than 300 °C an increasing pressure has little effect on the physical characteristics of water [1, 90]. Only under temperatures above this do the properties of water alter with respect to pressure [91]. Kartina *et al.* investigated hemicellulose extraction from oil palm (*Elaeis guineensis*) [92]. When the extraction pressure was increased from 500 psi to 800 psi the yield of hemicellulose showed a ~3 fold increase. This particular parameter is of little practical use as it is not one that can be directed using batch processing.

1.4 Brewers' waste

Barley is widely considered one of the world's most important cereals and is used as a raw material in the manufacturing of beer, one of the most consumed beverages globally. Beer brewing generates a variety of waste residues and by-products. SCW has previously been applied in the recovery of valuable compounds, such as antioxidant compounds, from industrial wastes [73-76]. In the work presented in this thesis, the aim is to develop SCE of antioxidant compounds from brewers' waste.

1.4.1 The brewing process

Figure 1.10 provides an overview of the brewing process. Whole barley grains consist of ~65% starch, 10-17% protein, 4-9% β -glucan and 2% lipids as well as small amounts of various minerals [93-95]. The barley grain consists of a germ (embryo), the endosperm and a grain coat. During the preparation of the barley feedstock it is cleaned and separated according to its size. The barley grain is then left for upwards of a month prior to malting.

The process of malting comprises three steps – 1) steeping, to allow absorption of water; 2) germination to initiate enzymatic breakdown; and 3) kilning, to ensure product stability.

In steeping, cleaned grains are incubated in 'steeping tanks' for 40-48 hours. The grains are held in water between 5-18°C. Over this period, the raw barley alternates between being submerged and drained until its moisture content increases from ~12% to ~44%. This hydration allows the initiation of germination [96, 97].

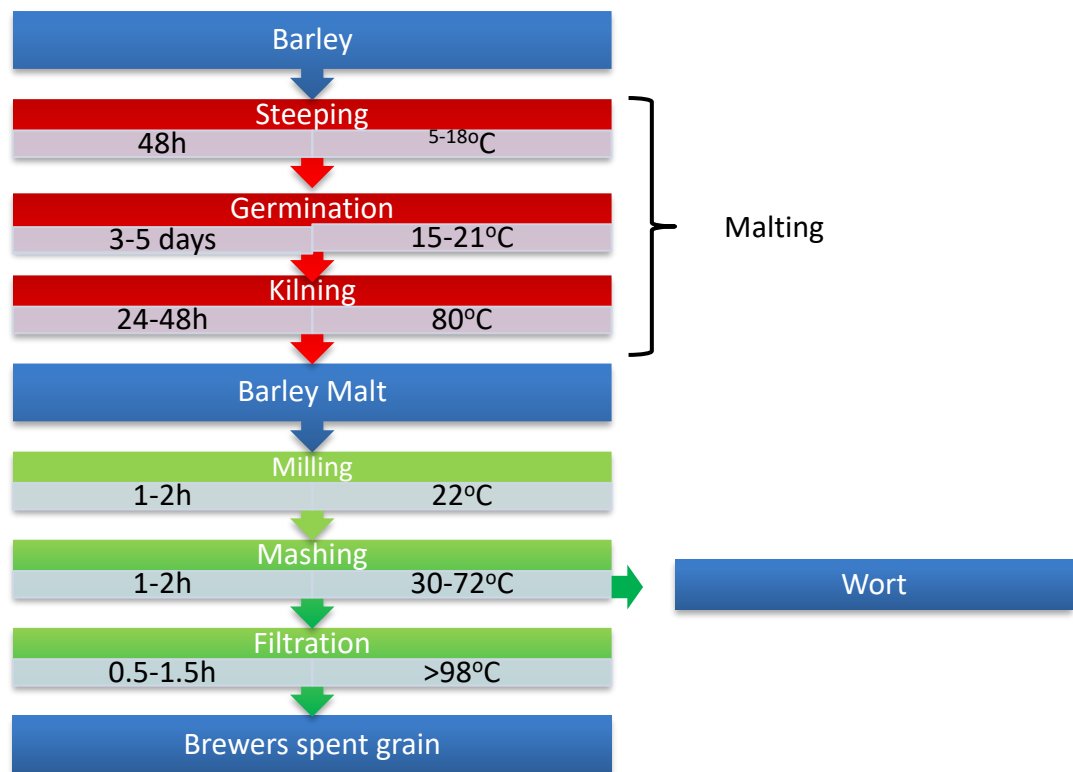


Figure 1. 10 - Flow diagram of beer manufacturing.

Steeped grains are transferred to a germination vessel which is maintained at 15 - 21°C with humid air. Germination results in the degradation of protein and carbohydrates, resulting in the opening up of starch reserves and activation of enzymes that are present in the barley endosperm. The grains are kiln dried with a finish heat of ~80 °C [97]. The changing of the kiln time, temperature and humidity allows different flavours to develop. Kilning is also efficient at removing microbial contamination [98, 99]. Dried malt is then stored for a period prior to the second half of the brewing process.

Barley malt is crushed in a process referred to as 'milling'. This step occurs over 1-2h at 22°C. This step is important in exposing the starch centre of the barley seed in such a way that the husk is left substantially intact whilst the rest becomes a coarse powder. This causes enzyme release and an increase in reaction surface area.

Beer is produced through careful mixing of crushed barley malt with hot water, in a process referred to as 'mashing'. In the brewery, the malted barley is periodically subjected to a range of temperatures, each one facilitating the activation of different malt enzyme. Enzymes primarily break down starch, but some breakdown of protein also occurs. The final step is the heating of the mixture to ~78 °C, which causes inactivation of the enzymes involved. Following mashing, a sweet liquid known as wort is produced. This fraction is removed and will go on to be fermented and conditioned before final filtration and bottling. There is also a residual, insoluble portion that is produced within the mash. This typically accounts for 25-30% of the mixture, and is removed immediately following mashing - this is referred to as 'brewers spent grain' (BSG) [97].

BSG is rich in cellulose, hemicellulose, lignin and proteins and therefore is of high nutritional value [100]. Despite the large amounts that are generated throughout the year, the use of spent grain is rather one dimensional, with 95% of all BSG being used as an animal feed [97]. Whilst this effectively reduces associated feeding costs as well as creating a suitable use for the material, rather than disposal [101, 102], there are several other characteristics of BSG which imply its potential in other fields.

1.4.2 Brewers' spent grain (BSG) characterisation

Around 12% of spent grain is made up of protein [103], where the prolamin family constitutes the main storage proteins. These are characterised by a high degree of glutamine and proline residues [104], as well as solubility in alcohol. The dominant protein present is the hordein family, of which four classes have been established, 1) D hordeins (100 kDa+), 2) C (sulfur-poor) (49-72 kDa), 3) B (sulfur rich) (28-45 kDa), and 4) γ -hordeins. A fifth class also exist, the A hordeins, but these are no longer considered true storage proteins. The B and C fractions account for 70-80% and 10-12%, respectively, of the total hordein, while the D and γ fractions are minor components [105, 106].

The production of antioxidants mixtures from protein based waste using SCW was discussed in Section 1.3.3.

As discussed in Chapter 1.2.3, SCW is effective at producing antioxidant mixtures from protein based mixtures. In the work presented in this thesis, SCW has been applied to BSG. Furthermore, peptides containing high levels of hydrophobic residues have been shown to have strong antioxidant activity, through the inactivation of reactive oxygen species (ROS) and scavenging of free radicals [107, 108]. Hordeins distinctively high levels of non-polar residues (Pro, Leu, Val); make them ideal candidates in the search for peptides with antioxidant activity. Bamdad and Chen have previously investigated the antioxidant effects of hordein hydrolysates [109]. In that study, a mixture of hordeins was digested using alcalase and the resulting peptides were analysed for antioxidant activity. Peptides with MW <1KDa were shown to have the highest antioxidant power.

1.5 Oxidative stress

Antioxidants role in homeostasis is to combat oxidative stress. Oxidative stress occurs when the body's normal homeostatic functions fail, and the balance between pro-oxidants and anti-oxidant systems are disrupted. Oxidative stress can result in damage to DNA, protein, lipids and mitochondrial function [110]. The effects of oxidative stress are variable. In the majority of instances a cell is able to combat the increased level of pro-oxidants and return to its original state [111]. In more severe cases, pro-oxidants can trigger apoptotic and necrotic pathways [112].

1.5.1 Pro-oxidants

Pro-oxidants include ROS, reactive nitrogen species (RNS) and reactive sulphur species (RSS) [113, 114]. ROS, such as hydrogen peroxide (H_2O_2), superoxide (O_2^-) and peroxy radicals ($\text{ROO}\cdot$), consist of both radical and non-radical species formed from the partial reduction of oxygen. ROS are primarily produced by mitochondria, cell membranes, the endoplasmic reticulum (ER) and peroxisomes [115], through both enzymatic and environmental stimuli. RNS derive from the metabolism of nitric oxide (NO) to generate molecules such as nitrogen monoxide ($\text{NO}\cdot$), nitrite (NO_2^-), nitrogen dioxide ($\text{NO}_2\cdot$), nitroxyl anion (NO^-) and peroxynitrate (O_2NOO^-). RSS arise from the metabolism of sulphur-containing molecules, particularly where sulphur atoms are in higher oxidation states [114, 116]. RSS include the thiyl radical ($\text{RS}\cdot$), glutathione (GSH), sulfenate (RSO^-), sulfinic acid (RSO_2^-), sulfonate (RSO_3^-) and hydrogen sulfide (H_2S).

The non-radical species that are generated above are prone to reacting with metal catalysts forming free radicals. For example, the Fenton Reaction (see below) describes hydroxyl radical formation from hydrogen peroxide [117].



If there is an excess of pro-oxidants, these can non-specifically attack biomolecules such as lipids, protein and DNA, leading to cell disorders including neurodegeneration and cancer [118-121].

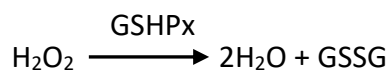
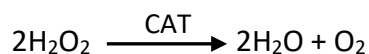
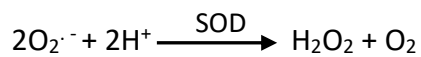
1.5.2 Antioxidants

Antioxidants are substances that retard the action of pro-oxidants. These molecules help prevent oxidative damage to important biological molecules such as proteins, lipids, carbohydrates or DNA.

1.5.2.1 Enzymatic antioxidants

The cell possesses enzymatic anti-oxidants to combat prooxidants in order to maintain cellular function. Examples include superoxide dismutase (SOD), catalase (CAT) and glutathione peroxidase (GSHPx) [122].

The reactions below describe the reactions catalysed by some of these enzymatic antioxidants. SOD is an enzyme with a generalized presence in the body that targets the superoxide anion by de-radicalising it to form the much less reactive hydrogen peroxide. H_2O_2 can be further detoxified to form water by either CAT, which is found in peroxisomes or GSHPx, which is present in the cytosol [123].



1.5.2.2 Non-enzymatic antioxidants

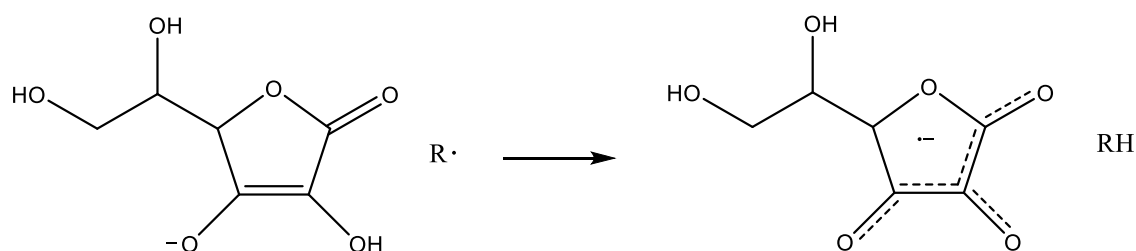


Figure 1. 11 - Vitamin C mechanism of antioxidant action.

As well as enzymatic antioxidants that are part of a healthy cells make-up, antioxidants can be introduced via dietary uptake. Common non-enzymatic antioxidants include Vitamin C, flavonoids and carotenoids.

Vitamin C (or ascorbic acid) is a water-soluble free radical scavenger and powerful antioxidant. Vitamin C functions by reducing free radicals via hydrogen donation and forming the stable compound dehydroascorbate. The electron is now shared within the ring structure of Vitamin C and is relatively stable (**Figure 1.11**) [124].

Flavonoids and carotenoids are common in fruits and vegetables and form a major part of dietary antioxidants. These compounds are effective in combatting ROS [125, 126]. Flavonoids and carotenoids actively bind free metal ions which otherwise can serve to catalyse hydroxyl radical formation. Furthermore, they have also shown to be effective at directly reducing free radicals via hydrogen atom donation.

An aim of this work presented in this thesis was to produce synthetic antioxidant compounds using SCW treatment of proteins. To evaluate the anti-oxidant activity of a various compounds a number of anti-oxidant assays have been implemented.

1.5.4 Antioxidant assays

To assess the antioxidant potential of mixtures, numerous antioxidant assays can be applied. There are two main mechanisms by which *in vitro* antioxidant assays work to assess the global antioxidant power of a substance. These are hydrogen atom transfer (HAT) – where a free radical is quenched via hydrogen donation and single electron transfer (SET) - where target compounds are reduced via electron transfer [127]. HAT based assays involve an antioxidant and substrate competing for degradation via peroxy radicals (often generated by azo compounds) [127]. Oxygen Radical Absorbance Capacity (ORAC) [128], Total Radical Trapping Antioxidant Parameter (TRAP) [129], and crocin bleaching assays [130] are common HAT based assays. SET-based assays are commonly monitored by a colour change. Folin-Ciocalteu Reagent (FCR) [131], Trolox Equivalence Antioxidant Capacity (TEAC) [132], Ferric ion Reducing Antioxidant Power (FRAP)[133] and reducing power (RP) [134]assays are common SET-based assays. Antioxidant assays can also be performed by directly measuring oxidative damage to cells that have been incubated with a test substance and a free radical generator. These include the cellular antioxidant activity (CAA) [135] and the comet assay [136].

1.5.4.1 ORAC assay

The ORAC assay was initially developed by Glazer and Ghiselli [128, 129]. In the original form of the assay β - phycoerythrin was used as a fluorescent probe and AAPH as a free radical generator. The amount of fluorescence detected via absorbance was proportional to the degradation of the probe. Cao and co-workers quantitated the total antioxidant capacity (TAC) of a substance by calculating the area under the fluorescence decay curve (AUC) of the sample compared to a negative control which did not contain any antioxidant [137]. These are described in **Equation 1.5**, where AUC is the area under the curve and f_x is the frequency at a given time point. β - phycoerythrin was later replaced as a probe by fluorescein, which was much more stable [138] and the process was subsequently automated [139].

$$AUC = 0.5 + \frac{f_1}{f_0} + \dots \frac{f_i}{f_0} + \dots \frac{f_{59}}{f_0} + 0.5 \left(\frac{f_{60}}{f_0} \right)$$

Equation 1. 5 - Equation for calculating the area under the curve for ORAC assays.

Cao *et al.* introduced the Vitamin E analogue, 6-hydroxy-2,5,7,8-tetramethylchroman-2-carboxylic acid (Trolox) into the ORAC assay. The antioxidant capacity of Trolox is monitored over a range of concentrations using the ORAC assay and used to generate a calibration curve. The ORAC values obtained for the test substances are given relative to Trolox concentration. This has allowed test substances to be directly compared to the ORAC values obtained for commercial standards [137]. The ORAC assay has previously been applied to microalgae [140], plasma [141] and vegetables [142].

The assay is not without its drawbacks, reaction rates of various antioxidants can significantly differ [143, 144]. Reaction measurements are incomparable if the reaction is not completed within the reaction time specified. Moreover, the ORAC assay is performed in an aqueous solution, which means antioxidant components that are insoluble will not be measured using this assay.

1.5.4.2 Reducing Power assay

The reducing power assay is a spectrophotometry based assay where antioxidant activity is monitored via absorbance. The assay was developed by Oyaizu in 1986 [134]. This is an example of a SET-based assay. Here, a Fe^{3+} /ferricyanide complex $[\text{FeCl}_3/\text{K}_3\text{Fe}(\text{CN})_6]$ is mixed with a test substance. A substance exhibiting reducing power will cause the complex to be reduced to the ferrous (Fe^{2+}) form. An overall colour change of yellow to green is noted. An increasing correlation between substances of high reducing power and overall colour change is observed. This is monitored by measuring absorbance at 700nm. This assay has previously been used to assess the antioxidant power of plant extracts from *M. serratum* and *Eichhornia crassipes* [145, 146].

1.5.4.3 Comet assay

The comet assay is a widely used assay for quantifying DNA damage and repair at a single cell level [136]. Briefly, the amount of damage that the DNA of a cell has undergone will affect its migration pattern under gel electrophoresis. The concept of using electrophoresis to measure DNA damage was first conceived by Ostling and Johnson in 1984 [147]. The authors showed that migration was more pronounced in radiation damaged DNA compared to control cells. This method was an improvement on the previously established methods of quantifying DNA damage due to the small number of cells that are required in the assay as well as no radiolabelling being required, thus allowing the use of any nucleated cell. A few years later, a modified protocol was introduced by Singh *et al.* who completed the protocol under alkaline conditions [148].

Both the neutral and alkaline variations of this assay have potential to differentiate between types of DNA damage. In the neutral comet assay, cellular DNA maintains its double stranded structure, which allows the detection of double stranded DNA breaks only. The more sensitive alkaline comet assay is the more widely used variant of the

assay [136]. This variant of the assay allows the detection of both single and double stranded DNA breaks, as well as alkali labile sites.

In contrast to the ORAC and reducing power assays outlined above the comet assay is performed on live cells. Cells can be extracted either from *in vitro* cell culture or directly from test subjects *in vivo* [149]. The *in vivo* comet assay is most commonly used as a method of supplementing and confirming results that were previously identified *in vitro*. The comet assay offers advantages over other *in vivo* tests due to its high sensitivity and that it can be applied to virtually any organ of interest.

Subsequently, it has been taken into account by health authorities in the development of drugs. For example, the genotoxicity of the drugs Cyanomethyl-carbamoylcyclohexyl-propylpiperazinyl-benzamide and Carbonyl-amino-indanylcabamic acid ester was assessed using the *in vitro* comet assay on V79 cells (Chinese hamster cell line) and then confirmed by the *in vivo* comet assay by European health authorities prior to further human testing [150].

Figure 1.12 shows the workflow followed to complete the comet assay in this thesis. a) Cells are allowed to grow in 6 or 12 well plates until ~70% confluent and then b) incubated with the test substance. Cells are then exposed to an oxidising agent, commonly via H₂O₂ addition or UV light [151]. In this thesis H₂O₂ treatment was used. c) Cells are detached from the well via trypsin and d) pelleted using centrifugation.

e) To ensure cells have not died as a result of trypsinisation or incubation with the test substance a cell viability assay is often employed [152]. In this assay a solution of trypan blue is added to a suspension of cells. Healthy cells maintain membrane integrity and do not uptake the dye, whereas dead cells do not have an intact membrane and take up the dye. Cells can be visualised using a standard light microscope and the live: dead cell ratio can be recorded. Most literature reports cell viability >90% prior to completing the comet assay [153, 154].

f) A sample of cells is then dissolved in low melting point (LMP) agarose at 37 °C and layered over a glass slide. The agarose is considered to be osmotic neutral, which

allows solutions to enter the gel and affect the DNA chemically without altering its position in the gel.

g) The slides are then submerged in a lysis solution that is either neutral or alkaline dependent on the variation of the assay being used. The lysis solution typically contains detergent to enable solubilisation of the cell membrane. All proteins, RNA and organelles freely diffuse into the agarose matrix. The lysis solution also uses a high salt concentration. This enables solubilisation of the nuclear histones.

h) Slides are subsequently immersed in either a neutral or alkaline electrophoresis buffer. The slides are incubated at 4 °C for a time period to allow the DNA supercoils to unwind and in the case of the alkaline comet assay - the nucleoid to become single stranded. Electrophoresis is performed where the amount of damage that a molecule of DNA has undergone, i.e. how many strand breaks have been induced, is proportional to the migration distance of the DNA. Strand breaks lead to increasingly relaxed DNA from its supercoiled structure and the electric current supplied allows DNA to extend from the nucleoid. The phosphate backbone of the DNA provides a negative charge which ensures net migration towards the anode. Slides are then neutralised, before dehydration with alcohol, which allows for long term storage.

i) The slides are then stained using a DNA-binding fluorescent dye. Common reagents include ethidium bromide, SYBR gold, SYBR green or alternatively by a non-fluorescing dye e.g. silver nitrate [155]. The comets are then visualised by fluorescent microscopy. The overall structure resembles a comet, with a circular 'head' of undamaged DNA followed by a 'tail' of damaged DNA. The brightness of the tail is measured relative to that of the head as an indication of overall DNA damage.

A major pitfall in the use of the comet assay is the lack of standardised inter-laboratory protocol. Although several guidelines have been published [156, 157], there are considerable differences between individual papers, making comparisons between results impossible.

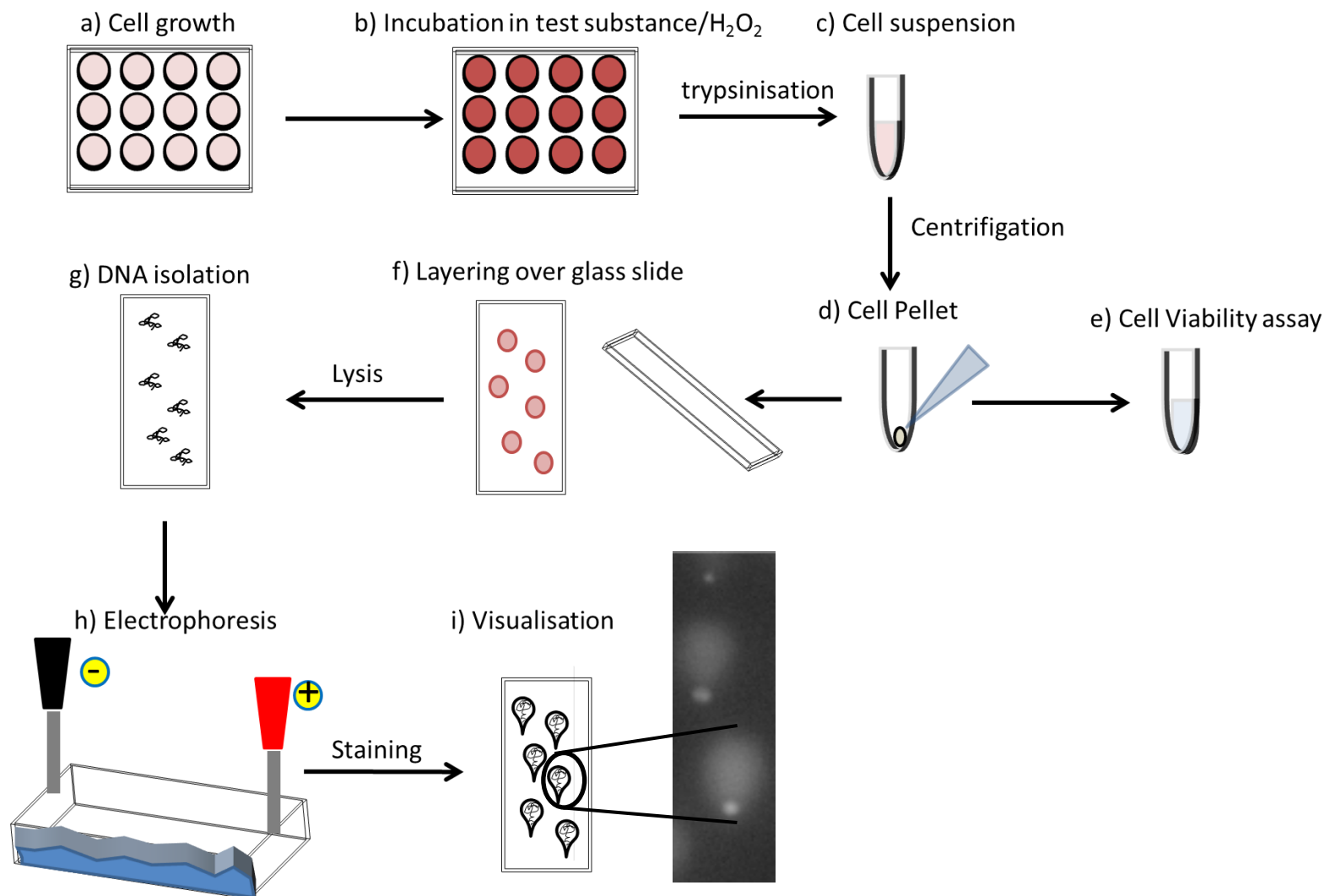


Figure 1. 12 - Workflow of comet assay outlining key protocol stages.

Many of the parameters used in the comet assay protocol are subject to change between different groups that have substantial effects on the eventual results. These include the density of the agarose gels, the strength of the alkaline used, incubation time and electrophoretic parameters. Furthermore, cells which have become necrotic or apoptotic during the incubation period may also be detected during the comet assay, resulting in comets with non-existent heads and large diffuse tails, resulting in so called 'hedgehog comets'. These are often excluded from scoring, although they can be regularly seen when treating cells with a non-lethal dose of an oxidising reagent. A particular point of variation in protocols is the electrophoretic step. Whilst most protocols employ a fixed voltage of 25 V and current of 300 mA, even a small change in the amount of buffer placed in the tank can have large effects on the voltage across the gel as well as the overall temperature [158].

1.6 Proteomics

Proteomics studies the protein component of cells, including interactions, modifications, quantification and localisation of proteins [159]. The progress of proteomics has been driven by development in technologies for protein/peptide separation[160], mass spectrometry analysis[23] as well as data analysis tools [161].

There are two main strategies in MS-based proteomics: top-down [162] and bottom-up [163]. The latter will be the focus of this thesis. Bottom up proteomics relies on complex mixtures of proteins being digested via enzymatic cleavage, most commonly using trypsin. Peptide identification is achieved by comparing theoretical MS/MS data generated from in silico digestion of a protein database against that of the experimental data. Whilst investigating the cleavage mechanisms of SCW on proteins in Chapter 3, the results suggested SCW could be used as an alternative reagent for proteolytic digestion. Proteolysis of standard proteins using SCW was shown to generate more peptides and greater sequence coverage than corresponding tryptic digests.

1.6.1 Sample preparation

Due to the complex nature of samples that are frequently required in proteomics, e.g. cell lysates, samples are often pre-fractionated prior to analysis. Proteins can be separated using sodium dodecyl sulphate-polyacrylamide gel electrophoresis (SDS-PAGE) via both one and two-dimensional electrophoresis (1-DE and 2-DE).

In SDS-PAGE samples are dissolved in SDS, an anionic detergent, which denatures a proteins secondary structure and applies a negative charge to each protein proportional to its mass (~ 1 negative charge to each 2 amino acids). An electric field is applied to the gel and the charged proteins migrate towards the positive electrode [164]. A proteins migration distance is proportional to the logarithm of its MW.

In 1-DE proteins are separated according to their MW only, however 2-DE offers separation by each proteins isoelectric point followed by MW separation. Proteins are

typically visualised using coomassie blue staining [165], although glutaraldehyde-free silver staining protocols and colloidal Coomassie staining have also been employed [166, 167].

Proteins are destained, reduced and alkylated in-gel, prior to enzymatic digestion, using a suitable protease. This is commonly trypsin, although in certain cases, for example where a protein lacks abundant arginine or lysine residues, other enzymes may be employed.

Gel-based approaches offer the advantage that low molecular impurities, including detergents and buffers, which often mask protein signal in downstream analyses, are removed during this approach.

Gel-free approaches are also used in pre-fractionation. In this approach samples are directly digested and subsequently fractionated at the peptide level. Many different off- and on-line peptide fractionation methods have been used.

Off-line fractionation methods have the advantages of being practically more simplistic to perform as well as the ability to use large amounts of starting material. Methods can be customarily selected. For example, charge based separation, such as strong cation exchange (SCX) is effective in enriching phosphopeptides due to the associate charge of the phosphate groups [168-172]. Whereas, fractionation based on hydrophobic interactions typically offers higher resolving power and provides a more effective separation of peptides, for example high-pH Reversed-Phase Fractionation [173].

The ultimate goal of both gel-based and gel-free approaches is to maximize the number of protein identifications, which greatly depends on how long the data acquisition is performed by the mass spectrometer.

1.6.2 Liquid chromatography

Peptides are eluted into the mass spectrometer via high-performance liquid chromatography (HPLC). Most HPLC separations are performed using reversed phase chromatography (RPLC) because of its compatibility with MS solvent systems. **Figure 1.13** shows the basic workflow of RPLC. The high resolution separation offered by this technology greatly reduces the number of co-eluting peptides, thereby reducing ion suppression.

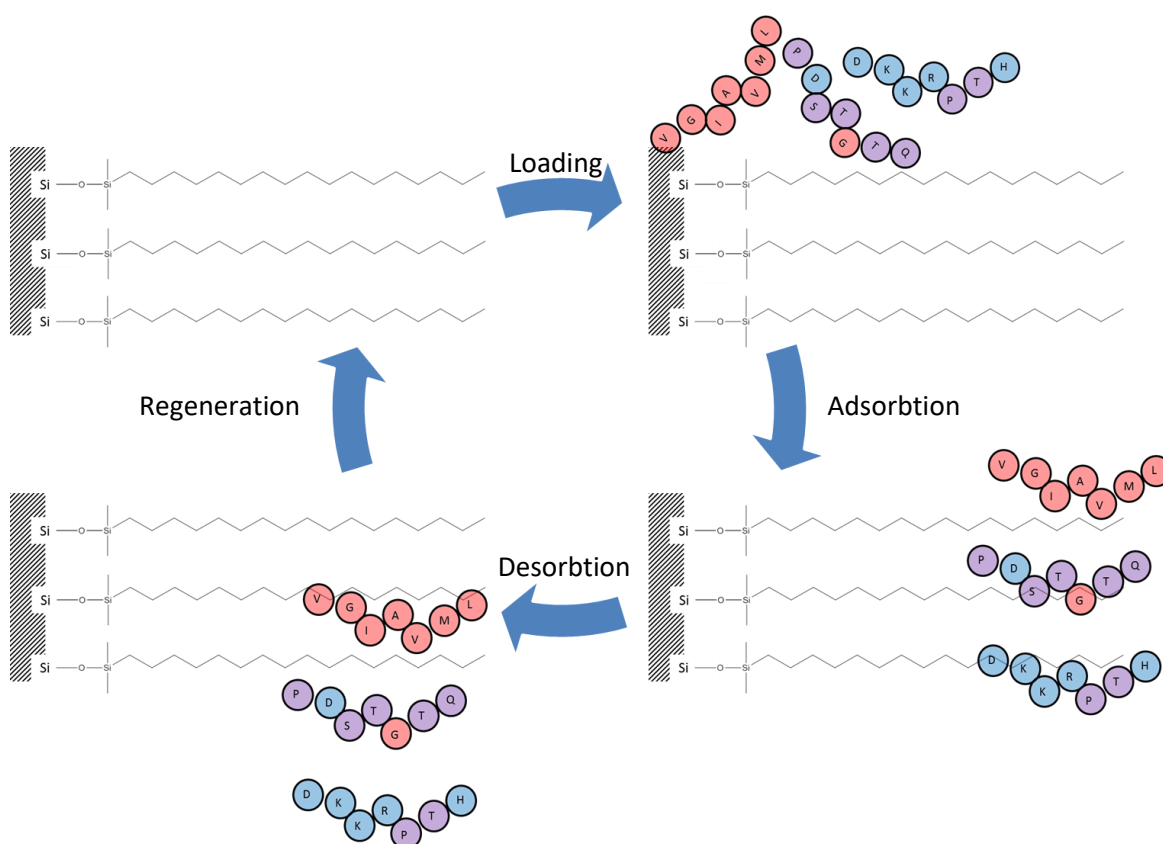


Figure 1. 13 - Workflow of reversed phase liquid chromatography.

The RPLC column consists of hydrophobic ligands linked to a beaded matrix. Silica is commonly used as a matrix due to its stability during the acidic and high organic conditions that are used for RPLC [174]. Silica-based matrices can be customised to effectively separate different types of molecules. The associated carbon chain lengths can be changed to facilitate effective separation of small molecules, peptides or proteins.

The mobile phase of RPLC contains a mixture of water and an organic solvent, typically acetonitrile or ethanol. A small amount of trifluoroacetic acid (TFA) is commonly added to protonate peptides.

The separation mechanism in HPLC depends on each peptide hydrophobically interacting with the stationary phase. The initial mobile phase conditions are predominantly aqueous, which favours adsorption between the solute and the stationary phase. The polarity of the initial mobile phase (mobile phase A) is controlled to dissolve hydrophobic solute as well as ensuring binding to the chromatographic matrix. The sample, dissolved in mobile phase A, is then loaded onto the column at an appropriate flow rate to ensure proper binding.

RPLC of the loaded biomolecules is performed using gradient elution. In this method an increasing amount of organic solvent (mobile phase B) is added to the mobile phase i.e. decreasing its polarity. The solutes are desorbed from the column according to their individual hydrophobicities. All samples are eventually eluted as the gradient is increased to 100% mobile phase B.

Despite this basic workflow facilitating the rapid analysis of peptide mixtures, a population of peptides are still not interrogated during analysis. Several studies have focused on optimising the parameters used in RPLC, including changing column and gradient lengths [175, 176].

MacCoss *et al.* investigated the effects of using both a longer column and longer gradient lengths on the number of peptides that could be identified from a *C. elegans* lysate [177]. The use of a longer gradient had a marked effect upon the amount of successful peptide IDs. The use of longer columns also showed increased peptide IDs, but only when longer gradients were also used. It is worth noting that the use of longer gradients will substantially decrease sample throughput, so these two factors need to be balanced when planning a proteomics experiment.

Recently, Kocher *et al.* demonstrated the use of very long 10 hour RPLC gradients for the identification of proteins from a HeLa lysate [178]. Whilst this gradient is

substantially longer than those typically used in proteomics the authors suggest that this method can remove the need for pre-fractionation, thereby making this a more efficient and easier method of peptide analysis overall.

1.6.3 Analysis

Following HPLC separation peptides are introduced into the mass spectrometer. The abundance and m/z of all ions eluting at a given time are measured (MS1 scan). Fragmentation data can be collected in either data-dependent or data independent acquisition modes (DDA or DIA). In DDA, (a preselected number of) the most abundant ions from each MS1 scan are isolated and subsequently fragmented [179]. Whilst this is efficient for the global identification of peptides, low abundant ions are often not detected. Alternatively, in DIA the fragmentation is independent of abundance. Instead of selecting the most abundant ions, these methods select only precursors and fragments with pre-specified m/z and elution profiles.

In the work presented in this thesis MS/MS data was acquired using data-dependent acquisition mode (DDA). In this methodology LC-MS/MS data are submitted to a protein database search algorithm, such as SEQUEST [180], Mascot [181], OMSSA [182], and X!Tandem [183]. Each protein is digested in-silico and the intact masses of the generated peptides are listed. The identity of a peptide is confirmed by comparing the peaks in the MS/MS experimental data against those of the in-silico digest.

Whilst many proteins that were present in sample prior to digestion will be assigned correctly, there will be inevitably some proteins that are incorrectly identified. A number of factors can lead to false PSMs, including low quality spectra and incomplete databases. The false discovery rate (FDR), is a statistical value that evaluates the number of false positive identifications.

A target-decoy method is widely used to calculate the FDR. In this method a decoy database is designed which contains proteins with non-genuine sequences. A common method of achieving this is to reverse all the protein sequences. Indeed, this is the

method using Proteome discoverer- the application used in this thesis. To calculate the FDR the number of peptides identified from the decoy database is given as a ratio against the real dataset. Commonly the FDR is set at 1% [184].

1.7 Aims and objectives

The overarching aim of the work in this thesis was to determine the products of SCW treatment of brewers' spent grain. To achieve that aim it was necessary to:

- 1) determine the specificity of SCW with respect to production of peptides from proteins (Chapter 3)
- 2) determine amino acid side chain modifications induced by SCW (Chapter 4)
- 3) determine the nature of small molecule products of SCW treatment of proteins and this antioxidant activity (Chapter 5).

In the course of this work, it became apparent that SCW may have a role to play in proteomic workflows and this aspect was further explored (Chapter 6).

Chapter 2: Methods

2.1 Samples

Protein

Protein standards human haemoglobin, bovine serum albumin (BSA), bovine β -casein, bovine cytochrome C, chicken lysozyme, *E. coli* β -galactosidase, bovine apo-transferrin and *S. cerevisiae* alcohol dehydrogenase were purchased from Sigma-Aldrich (Gillingham, UK) and used without further purification.

Non treated grains (NTG) and brewers' spent grain (BSG) hordein extracts were provided by Phytatec (UK). Briefly, extraction was performed by suspending the grain in 55% v/v 2-propanol, 1% v/v acetic acid, 2% v/v mercaptoethanol in water at 60 °C for 1 hour. The precipitates were recovered by centrifugation (2000 rpm), and lyophilized.

Peptide

Three lyophilized model peptides, VQSIKADFLHYMENPTWGR, VCFQYMDRGDR, and VQSIKADFLHYENPTWGR, were synthesized by Genic Bio Ltd. (Shanghai, China) and used without further purification.

Amino acid

Lyophilized amino acids were supplied by Phytatec (UK).

2.2 SCW Mediated Hydrolysis

Fifteen mg of protein (Chapters 3 and 5), 15 μ M peptide (Chapter 4) or 15 μ M total amino acid (Chapter 6) were dissolved in 15 mL of deionized water (J. T. Baker, Deventer, The Netherlands) and placed inside a reaction tube consisting of stainless steel metal piping, 200 mm \times 16.3 mm (internal diameter), total volume 42 cm³, capped using SS Tube Fitting, Reducing Union, 3/4 in. \times 1/4 in. (Swagelok, UK). SCW mediated hydrolysis was performed at temperatures of 160, 207, 253, and 300 °C on

proteins. SCW mediated hydrolysis was performed at temperatures of 140, 160, 180 and 200 °C on peptides.

Reaction tubes were placed in a gas chromatography (GC) oven pre-set to 30 °C and allowed to equilibrate for at least 10 min prior to increasing the temperature of the oven. The reaction temperature was monitored by use of a thermocouple attached to one of the reaction tubes. It took 5 min 10 s to reach 140 °C, 6 min 40 s to reach 160 °C, 7 min 0 s to reach 180 °C, 7 min 30 s to reach 200 °C, 7 min 40 s to reach 207 °C, 10 min 30 s to reach 253 °C and 16 min 45 s to reach 300 °C. The selected residency, i.e., 0 and 20 min, began after reaching the chosen temperature. Each experiment was performed in triplicate. The reaction was quenched by placing the reaction tubes into a bucket of ice for 5 min. One ml aliquots of the hydrolysate were then stored at -20 °C until analysis.

2.2.1 Additional experiments in Chapter 3

Smaller protein: solvent ratio - 1.5 and 0.15 mg of haemoglobin (Sigma-Aldrich) was dissolved in 15 mL of deionized water (J.T., Baker) and treated as above with SCW conditions of 160 °C for 20 min.

Reduction of BSA Pre-SCW Processing - Fifteen mg of BSA was added to 8.75 mL of 100 mM ammonium bicarbonate (Fisher Scientific, Loughborough, UK). 3.13 mL of 48 mM dithiothreitol (DTT) (Sigma-Aldrich) in 100 mM ammonium bicarbonate was added to the sample and incubated for 30 min at 56 °C. A further 3.13 mL of 264 mM iodoacetamide (IAM) (Sigma-Aldrich) in 100 mM ammonium bicarbonate was added to the sample and incubated for 20 min at room temperature in the dark. Samples were introduced into the SCW reaction vessel directly.

Reduction of BSA Post-SCW Processing - Fifty µL of hydrolyzed BSA was added to 50 µL of 10 mM dithiothreitol (Sigma-Aldrich, Gillingham, UK) in 100 mM ammonium bicarbonate (Fisher Scientific) and incubated for 30 min at 56 °C. Fifty µL of 55 mM

iodoacetamide (Sigma-Aldrich) in 100 mM ammonium bicarbonate was added to the sample and incubated for 20 min at room temperature in the dark.

2.2.1 Additional experiments in Chapter 4

Reduction of peptide Pre-SCW Processing - a 15 mL solution containing ~15 μ M peptide, ~14 mM iodoacetamide (Sigma-Aldrich), and 100 mM ammonium bicarbonate (Fisher Scientific) was incubated for 20 min at room temperature in the dark. In experiments where a thiol was introduced as a quenching agent, ~14 mM DTT (Sigma-Aldrich) was added following alkylation, and incubated in the dark at room temperature for 30 min.

Benzyl bromide conjugation - a 15 mL solution containing ~15 μ M peptide and ~15 μ M Benzyl bromide (Sigma-Aldrich) was incubated at room temperature for 10 and 60 minutes and 140 °C for 10, 30 and 60 minutes

2.3 Enzymatic digestion

Fifty μ g of protein was made up in 90 μ L of 100 mM ammonium bicarbonate (Fisher Scientific). Fifty μ L of 10 mM DTT (Sigma-Aldrich) in 100 mM ammonium bicarbonate was added and incubated for 30 min at 56 °C. Fifty μ L of 55 mM IAM (Sigma-Aldrich) in 100 mM ammonium bicarbonate was added to the sample and incubated for 20 min at room temperature in the dark. Samples were digested overnight with Trypsin Gold (Promega, Madison, WI) or for 2 hours with Proteinase K (Promega) in 50 mM ammonium bicarbonate (protein/enzyme 50:1) at 37 °C, pH 8. Proteolysis was quenched by addition of 0.5% TFA.

2.4 Sodium dodecyl sulphate polyacrylamide gel electrophoresis (SDS PAGE)

NTG and BSG solutions for SDS page were dissolved in an 8M urea solution. Twenty μ l of sample and 5 μ l of 4X LDS sample buffer (Expedon, Cambridge, UK) were mixed heated to 95°C for 5 minutes and centrifuged at 13,000 rpm for 1 minute, prior to loading onto a NuPAGE 10% Bis-Tris gel (Expedon). Gels were immersed in TrisHCl/tricine SDS running buffer with 60 mM TrisHCl, 80 mM tricine, 2.5mM sodium bisulphate and 0.1% SDS (Fisher Scientific). Samples were electrophoresed for 20 minutes at 100kV, followed by 50 minutes at 150kV.

2.4.1 In gel digestion

Briefly, each band in the gel was cut using a scalpel and the pieces were further excised into 1mm x 1mm x 1mm cubes. The pieces were washed with 100 mM ammonium bicarbonate (Fisher Scientific) for 5 min and then with 60 μ l acetonitrile (ACN) (J.T.,Baker) for a further 5 minutes. This solution was removed and the gel pieces were rehydrated with 50 μ l 100 mM NH_4HCO_3 for 5 min. An equal volume of ACN was added to the solution and it was incubated for 30 minutes. This washing solution was then removed and the gel pieces were dried using a vacuum centrifuge. 50 μ l of 10mM DTT (Sigma-Aldrich) in 100mM NH_4HCO_3 was then added and incubated at 56°C for 30 minutes. This liquid was then removed and replaced with 55mM IAM (Sigma-Aldrich) in 100mM NH_4HCO_3 and incubated at room temperature in the dark for 20 minutes. The bulk of the solution was removed via a pipette and the gel pieces were dried in a vacuum centrifuge. The gel pieces were rehydrated with 13 ng/ μ l of Proteinase K (Promega) and incubated at room temperature for 30 minutes. The samples were then diluted with 20 μ l 100mM NH_4HCO_3 , and then incubated for 2 hours at 37°C. Peptides were extracted with the addition of 30 μ l of 2% ACN and 1% formic acid (FA) (Sigma-Aldrich), and then with 30 μ l of 40% ACN and 1% FA. The pooled extracts were dried in a vacuum centrifuge and resuspended in 0.1% FA.

2.5 Peptide Purification

Both enzymatic and SCW generated peptides were desalted using ZipTip C18 pipette tips (Millipore, Bedford, MA, USA) according to manufacturers' instructions. The desalted samples were dried and resuspended in 10 μ L of FA (Thermo Fisher, Bremen, Germany) prior to MS analysis.

2.6 Direct infusion Mass Spectrometry

Samples were diluted to a concentration of ~ 3 μ M in 50:50 water: methanol (J.T., Baker), 0.1% formic acid (Fisher Scientific), and introduced to the mass spectrometer by electrospray ionisation.

All direct infusion ESI-MS experiments were performed on a Thermo Fisher Orbitrap Elite (Thermo Fisher). Data acquisition was controlled by Xcalibur 2.1 (Thermo Fisher). All mass spectra and tandem mass spectra were recorded in the Orbitrap at a resolution of 240,000 at m/z 400.

CID - The automatic gain control (AGC) target was 5×10^4 charges with maximum injection time of 300 ms. CID was performed in the ion trap using helium at normalized collision energy of 35% and the fragments were detected in the Orbitrap. The normalised collision energy sets the collision energy relative to the parent mass prior to fragmentation. Width of the precursor isolation window was 1.5 m/z .

ETD - The AGC target was 5×10^4 charges with maximum injection time 300 ms. Supplemental activation (sa) ETD was performed in the ion trap with fluoranthene reagent ions (AGC target for reagent ions was 1×10^5 charges with a maximum injection time of 100 ms) and a normalized collision energy of 25%. Width of the precursor isolation window was 1.5 m/z . Fragment ions were detected in the Orbitrap

HCD - Ions were transferred to the HCD cell and subjected to fragmentation with 75% normalized collision energy. The automatic gain control (AGC) target was 5×10^4

charges with maximum injection time of 300 ms. and the fragments were detected in the orbitrap. Width of the precursor isolation window was 1 m/z .

2.7 Liquid Chromatography Tandem Mass Spectrometry (LC MS/MS)

LC MS/MS experiments were performed on a Thermo Fisher Orbitrap Elite or the Q-Exactive (both Thermo Fisher). Data acquisition was controlled by Xcalibur 2.1 (Thermo Fisher). All direct infusion electrospray mass spectra and tandem mass spectra were recorded in the Orbitrap at a resolution of 240,000 at m/z 400.

Peptides were separated using online reversed phase LC (Dionex Ultimate 3000), using a binary solvent system consisting of mobile phase A (water (J.T., Baker)/0.1% formic acid (Fisher Scientific) and mobile phase B (acetonitrile (J.T., Baker)/ 0.1% formic acid (Fisher Scientific)). Peptides were loaded onto a PepMap C₁₈ column 75 μ m (diameter) x 150 mm (length) (LC Packings, Sunnyvale, CA), in mobile phase A. The percentage of mobile phase B increased in a linear gradient from 0 to 3.2% between 0 and 6 minutes and then to 44% between 6 and 30 minutes. The column was then washed with 90% mobile phase B between 30minutes and 40 minutes before re-equilibrating at 3.2% mobile phase B between 40 minutes and 56 minutes. A flow rate of 0.350 nL/min was applied.

Samples eluted directly via a Triversa Nanomate nanoelectrospray source (Advion Biosciences, Ithaca, NY) into the mass spectrometer.

2.7.1 Additional experiments in Chapter 5

Longer gradients - Peptides were loaded onto a C₁₈ column (LC Packings), in mobile phase A. The percentage of mobile phase B increased in a linear gradient from 0 to 3.2% between 0 and 6 minutes and then to 44% between 6 and 230 minutes. The column was then washed with 90% mobile phase B between 230minutes and 252

minutes before re-equilibrating at 3.2% mobile phase B until 270 minutes. A flow rate of 0.350 nL/min was applied.

Longer column- For specified experiments an Acclaim PepMap C₁₈ 75µm (diameter) x 500 mm (length) column was used (LC Packings).

2.7.2 Orbitrap Elite

CID - The mass spectrometer performed a full MS scan (m/z 380–1800) and subsequent MS/MS scans of the seven most abundant ions that had a charge state >1 . Survey scans were acquired in the Orbitrap with a resolution of 60,000 at m/z 400. The AGC target for the survey scans was 10^6 charges with maximum injection time of 1 s. CID was performed in the ion trap using helium at normalized collision energy of 35%, and the fragments were detected in the Orbitrap (resolution 60,000 at m/z 400). Width of the precursor isolation window was 2 m/z . AGC target for CID was 5×10^4 charges with a maximum injection time of 100 ms.

ETD - The mass spectrometer performed a full MS scan (m/z 380–1800) and subsequent MS/MS scans of the seven most abundant ions that had a charge state >1 . Survey scans were acquired in the Orbitrap with a resolution of 60,000 at m/z 400. The AGC target for the survey scans was 10^6 charges with maximum injection time of 1 s. ETD was performed in the linear ion trap with fluoranthene ions with a maximum fill time of 100 ms. The fragments were detected in the Orbitrap (resolution 60,000 at m/z 400). Width of the precursor isolation window was 2 m/z . Precursor ions were activated for 100 ms (charge-dependent activation time was enabled). The AGC target for ETD was 5×10^4 charges. Supplemental activation was used with normalized collision energy of 25%.

2.7.3 Q-Exactive

HCD - The mass spectrometer performed a full MS scan (m/z 380–1800) and subsequent MS/MS scans of the twenty most abundant ions that had a charge state >1 . Survey scans were acquired in the Orbitrap with a resolution of 120,000 at m/z 200. The AGC target for the survey scans was 3×10^6 charges with maximum injection time of 50 ms. HCD was performed in the HCD cell using HCD at normalized collision energy of 28%, and the fragments were detected in the Orbitrap (resolution 15,000 at m/z 200). Width of the precursor isolation window was 1.2 m/z . AGC target for HCD was 1×10^5 charges with a maximum injection time of 50 ms.

2.8 Database Search Parameters

Raw MS/MS data files from Xcalibur software (version 3.0.63; Thermo Fisher) were submitted to Proteome Discoverer software (version 1.4.1.14; Thermo Fisher) for SEQUEST searches against the relevant protein sequence as obtained from uniprot. Two missed cleavages were allowed for tryptic digests. Database searches for SCW hydrolysed samples were searched using “nonspecific enzyme”. Precursor mass tolerance was 10 ppm, and MS/MS tolerance was 0.5 Da. For trypsin digests of hemoglobin and BSA, carbamidomethylation of cysteines was set as a static modification, while deamidation and oxidation were set as variable modifications. For the trypsin digest of β -casein, phosphorylation was introduced as a further variable modification. For database searches of SCW hydrolyzed hemoglobin, deamidation and oxidation were set as variable modifications. For database searches of SCW hydrolyzed β -casein: deamidation, oxidation, and phosphorylation were set as variable modifications. For SCW hydrolysis of BSA, deamidation and oxidation were set as variable modifications. When BSA was treated with DTT and iodoacetamide (both prior to and following SCW hydrolysis), carbamidomethylation was included as a static modification. In subsequent searches (see text), database searches were performed with additional variable modifications: dehydration of Asp, Glu, Thr, and Ser and pyroglutamic acid formation. All other search parameters remained the same.

2.9 Antioxidant analysis

2.9.1 ORAC assay

The protocol used in this assay was based on the protocol developed by Huang *et al.*, [139]. Phosphate buffer stock solutions (100mM) were prepared by dissolving 2.75g monosodium phosphate (Fisher Scientific) and 21.5 g of dipotassium phosphate (Fisher Scientific) in 1L of water (J.T. Baker) and maintained at room temperature. Fluorescein stock solutions (6.6µM) (Sigma-Aldrich) in 100 mM phosphate buffer were maintained at 4 °C in the dark. Stock solutions of 100mM phosphate buffer were maintained at room temperature. Stock solutions of 20mM 6-hydroxy-2,5,7,8-tetramethylchroman-2-carboxylic acid (Trolox) (Sigma-Aldrich) in ethanol were maintained at -20 °C.

Prior to the ORAC assay the following were freshly prepared: 300 nm fluorescein solution 100 mM phosphate buffer. 50 µM Trolox, 300mM of 2,2'-Azobis(2-methylpropionamidine) dihydrochloride (AAPH) (Sigma-Aldrich) in 100 mM phosphate buffer.

Twenty five µL of antioxidant (Trolox or sample or phosphate buffer in control experiments), 150 µL of fluorescein (0.3 µM) and were placed in black 96-well microplates (Thermo Fisher). The mixture was incubated at 37 °C for 30 minutes. Thirty µl of AAPH (300mM) was added to each well using a multichannel pipette. Fluorescence was recorded every minute for 1 hour. Fluorescent values were determined in the Infinite F200 PRO Microplate reader (Tecan, Männedorf, Switzerland). Excitation and emission wavelengths were set as 485 (25) nm and 535 (25) nm. Each assay was repeated three times independently on different days. Within every assay each sample had a minimum of 3 replicates. Results are quoted relative to Trolox concentration.

2.9.2 Comet assay

SCW incubation solutions - All extracts were filter sterilised using a 0.2µm Polyethersulfone (PES) Filters (Milipore, Massachusetts, USA) prior to use in cell culture. Each solution was resuspended to a final concentration of 0.05 mg/ml in Dulbecco's Modified Eagles Medium (DMEM) (Lonza, Basel, Switzerland). 30% H₂O₂ (Sigma-Aldrich) was added to a final concentration of 50µM in DMEM with 4.5 g/L glucose with L-glutamine and supplemented with 10% fetal calf serum.

Cell culture - HaCaT keratinocyte cells from adult human skin were cultured in DMEM (Lonza). Cells were routinely split once per week and seeded at a density of 1 x 10⁴ cells/ml into 6 well tissue culture plates (Fisher Scientific). Following 24 hours of growth DMEM was replaced with incubation solutions and incubated for a further 24 hours. For the last 30 minutes of incubation time the incubation solutions were removed and replaced with 50 µM H₂O₂ (Sigma-Aldrich). A control was included where cells were not incubated in hydrolysates.

Comet assay - The comet assay was performed under alkaline conditions (pH > 13) according to the procedure of Singh et al [148]. Following the incubation period cells were twice washed with PBS and detached with trypsin. Cells were washed with PBS and then suspended in 200 µl fresh PBS. 15µl cells were resuspended in 150 µl 0.75% low melting point (LMP) agarose (Bioline, London, UK) in PBS (pH 7.4), and placed on microscope slides precoated with 0.8% normal melting point (NMP) agarose (Bioline). The slides were covered with a glass cover slip (22x64mm, VWR) avoiding bubbles formation, placed on a metallic tray over ice and left in the cold room (at 4 °C) for approximately 20min to allow the agarose to set. Cells were lysed overnight at 4 °C in the dark in a buffer containing 2.5 M NaCl, 100 mM Na₂-EDTA, 1% Triton X-100, 10 mM Tris-HCl (all Fisher Scientific). Later, the slides were incubated in an electrophoresis unit in a buffer containing 300mM NaOH (Fisher Scientific) and 1mM Na₂-EDTA, pH≥13 for 20 minutes to unwind the DNA and then electrophoresed for 30 minutes (32V, 300mA) using a Bio-Rad power pack 200 power supply (Bio-Rad Laboratories, Hercules,

USA). Slides were washed in a buffer containing 400 mM Tris base before fixing with -20 °C ethanol.

Slides were then stained with 50µl DNA-specific SYBR gold (1:1000 in dH₂O, Invitrogen, Paisley, UK) before placing new glass cover slips and storing slides in the cold room in a foil-wrapped moist box for analysis (within 24h).

Visualisation - Slides were visualised using a fluorescence microscope with a xenon arc lamp (Zeiss Axio lab, (Cambridge, UK). Excitation and emission filters were set at 490 nm and 520 nm respectively. The images were analysed using Cometscore image analysis software (version 1.5) (Tritek corp, Virginia, USA). The % tail DNA was calculated as explained in Chapter 1. For the comet assay results, the mean was calculated using 50 separate comets from two independent slides.

2.9.3 Reducing power assay

This assay protocol was adapted from that reported by Oyazi [185]. Phosphate buffer stock solutions (0.2 M) were prepared by dissolving 16.84 g monosodium phosphate (Fisher Scientific) and 20.88 g of dipotassium phosphate (Fisher Scientific) in 1l of water (J.T. Baker) and maintained at room temperature. Test solutions were suspended in 0.2 M phosphate buffer containing 0.17 M NaCl and 3.35 mM KCl at a concentration of 0.05 mg/ml. 1 ml of each was added to a further 2.5 ml of 0.2 M phosphate buffer and 2.5 ml potassium ferricyanide (5%) (Sigma-Aldrich). The mixture was incubated at 50 °C for 30 minutes. The reaction was stopped by the addition of 2.5 ml 10% trichloroacetic acid (TCA) (Fisher Scientific) followed by centrifugation at 3000 rpm for 10 minutes. The upper supernatant (2.5 ml) was mixed with distilled water (2.5 ml) and 0.1% ferric chloride (0.5 ml) and incubated at room temperature for 10 minutes. The absorbance was measured at 700 nm. Increased absorbance reflects increased reducing power.

Chapter 3: Sub-critical water hydrolysis of proteins: specificity and post translational modifications

The work presented in this chapter has been published in part as an article in Analytical Chemistry on which I am first author [186].

3.1 Overview

The aim of the work presented in this chapter was to investigate the mechanism by SCW hydrolysis of proteins occurs, through the identification of peptide hydrolysis products by liquid chromatography tandem mass spectrometry (LC MS/MS). The specificity of SCW with respect to the production of peptides from three model proteins, haemoglobin (molecular weight (MW) 15 117 Da α -globin; 15 857 Da β -globin), bovine serum albumin (BSA) (MW 66 389 Da), and β -casein (MW 23 568 Da) was explored. If the position of cleavage can be directed and SCW is efficient at generating peptides, the feasibility of using SCW hydrolysis as an alternative technique for proteolysis in proteomics studies was explored.

Trypsin is currently the protease of choice in the majority of these studies; however this approach has various limitations. In cases where Arg or Lys are inconveniently placed along the amino acid sequence i.e. too far apart or too close together, segments of the proteome can be missed. In these instances, this limited sequence information makes it impossible to localise PTMs in unmapped regions [187]. This is in addition to the lengthy time periods and high costs associated with enzymatic digestion [188]. Using SCW may overcome these difficulties. In order to achieve this goal, the sequence coverage and number of peptides generated from the enzymatic digestion of the three proteins with trypsin were compared with those obtained following SCW treatment.

Lastly, the effect of SCW treatment on two protein post-translational modifications, disulphide bonds (in BSA) and phosphorylation (in β -casein), was investigated.

3.2 Specificity of SCW Mediated Hydrolysis of Model Proteins

To investigate the specificity of SCW hydrolysis, experiments were performed on three purified model proteins, haemoglobin, BSA and β -casein. **Figure 3.1** shows the amino acid sequence of each protein. Disulphide bonds and phosphosites are highlighted. Hydrolysis was performed at 160 °C for 0 and 20 minutes, 207 °C for 20 minutes, 253 °C for 20 minutes and 300 °C for 20 minutes as described in Chapter 2.1. Peptides were desalted (as described in Chapter 2.5), analysed using LC MS/MS (as described in Chapter 2.7) and identified using an automated search (as described in Chapter 2.8).

Figure 3.2 shows plots of the percentage of peptides resulting from SCW treatment at 160 for 0 and 20 minutes and 207 °C for 20 minutes versus the amino acid residue in the protein sequence immediately preceding the N-terminus of the resulting peptide, i.e., the amino acid residue adjacent to the peptide's N-terminus. No specificity was observed in the amino acid residue adjacent to the peptide's C-terminus (**Figure 3.3**). Peptide summary maps are shown in **Appendix Figure 3.1**. SCW treatment at 160 °C for 0 min showed preferential cleavage toward the N-terminus of aspartic acid in α - and β -globin. The percentage of identified peptides which follow an aspartic acid residue was $30.9 \pm 9.4\%$ in the α -globin and $23.1 \pm 13.4\%$ in the β -globin, several fold higher than the natural abundance of aspartic acid residues in both α - and β -globins (5.7% in both cases). Similar results were seen for BSA where $31.5 \pm 6.5\%$ of peptides were preceded by an aspartic acid residue, significantly higher than the natural abundance of aspartic acid in the BSA sequence (6.9%). The percentage of SCW peptides which follow an aspartic acid residue in β -casein was $17.4 \pm 7.5\%$, again several fold greater than the natural abundance of the residue in the protein (1.9%). No favoured cleavage adjacent to the structurally similar glutamic acid residue was observed. At this temperature favoured cleavage toward arginine in BSA ($19.4 \pm 5.9\%$) and lysine in β -casein ($17.4 \pm 5.9\%$) was also observed.

Similar results were seen following treatment at 160 °C for 20 min. The percentage of peptides with N-terminus adjacent to an aspartic acid residue was $31.1 \pm 5.0\%$ (α -

globin), $42.4 \pm 4.2\%$ (β -globin), $44.3 \pm 3.7\%$ (BSA), and $23.4 \pm 2.6\%$ (β -casein). For β -casein, there appears to be some preferential cleavage adjacent to glutamic acid.

a

VLSPADKTNVKAAWGKVGAHAGEYGAEALERMFLSFPTTKTYFPHFDLSHGSAQV
KGHGKKVADALTNAVAHVDDMPNALSALSDLHAHKLRVDPVNFKLLSHCLLVTLA
AHLPAEFTPAVHASLDKFLASVSTVLTSKYR

b

VHLTPEEKSAVTALWGKVNVDEVGGEALGRLLVVYPWTQRFFESFGDLSTPDAVM
GNPKVKAHGKKVLGAFSDGLAHLDNLKGTFATLELHCDKLHVDPENFRLLGNVLVC
VLAHHFGKEFTPPVQAAYQKVVAGVANALAHKYH

Figure 3. 1 - Amino Acid sequences for a) α -globin, b) β -globin, c) BSA, d) β -casein.

c)

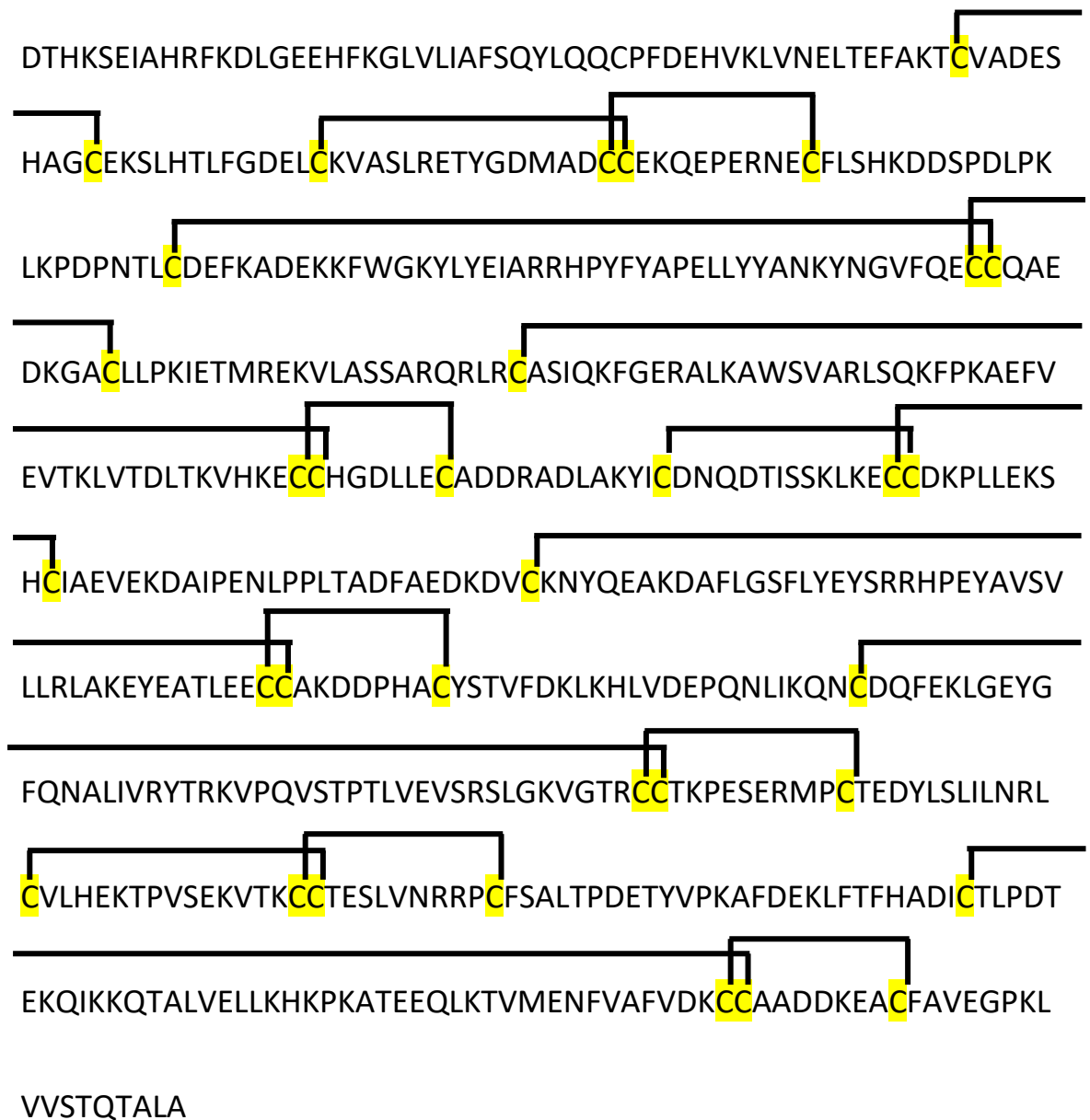


Figure 3. 1 (continued) - Amino Acid sequences for a) α -globin, b) β -globin, c) BSA, d) β -casein.

d)

RELEELNVPGEIVEpSLpSpSpSEESITRINKKIEKFQpSEEQQQTEDELQDKIHPFAQT
QSLVYPPFGPIPNSLPQNIPPLTQTPVVVPPFLQPEVMGVSKVKEAMAPKHKEMPF
PKYPVEPFTESQSLTLTDVENLHLPLLLQSWMHQPHQPLPPTVMFPPQSVLSLSQ
SKVLPVPQKAVPYPQRDMPIQAFLLYQEPVLGPVVRGPFPIIV

Figure 3. 1 (continued) - Amino Acid sequences for a) α -globin, b) γ -globin, c) BSA, d) β -casein.

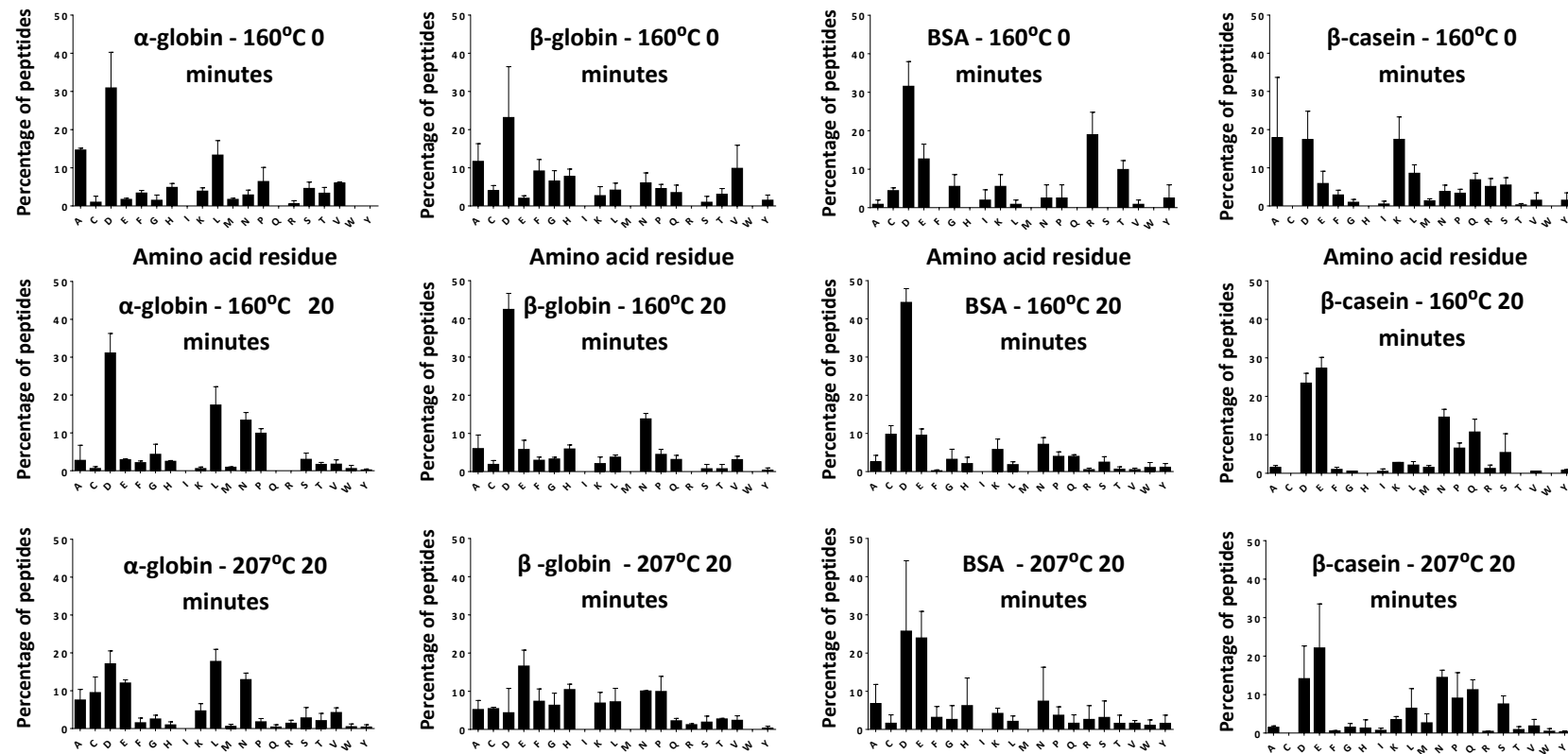


Figure 3. 2 - Specificity of SCW hydrolysis: Plots of the % of peptides identified against the amino acid residue immediately preceding the peptide N terminus for proteins haemoglobin, BSA, and β-casein under SCW treatment at 160 °C (0 min), 160 °C (20 min), and 207 °C (20 min). n = 3. Error bars represent one standard deviation.

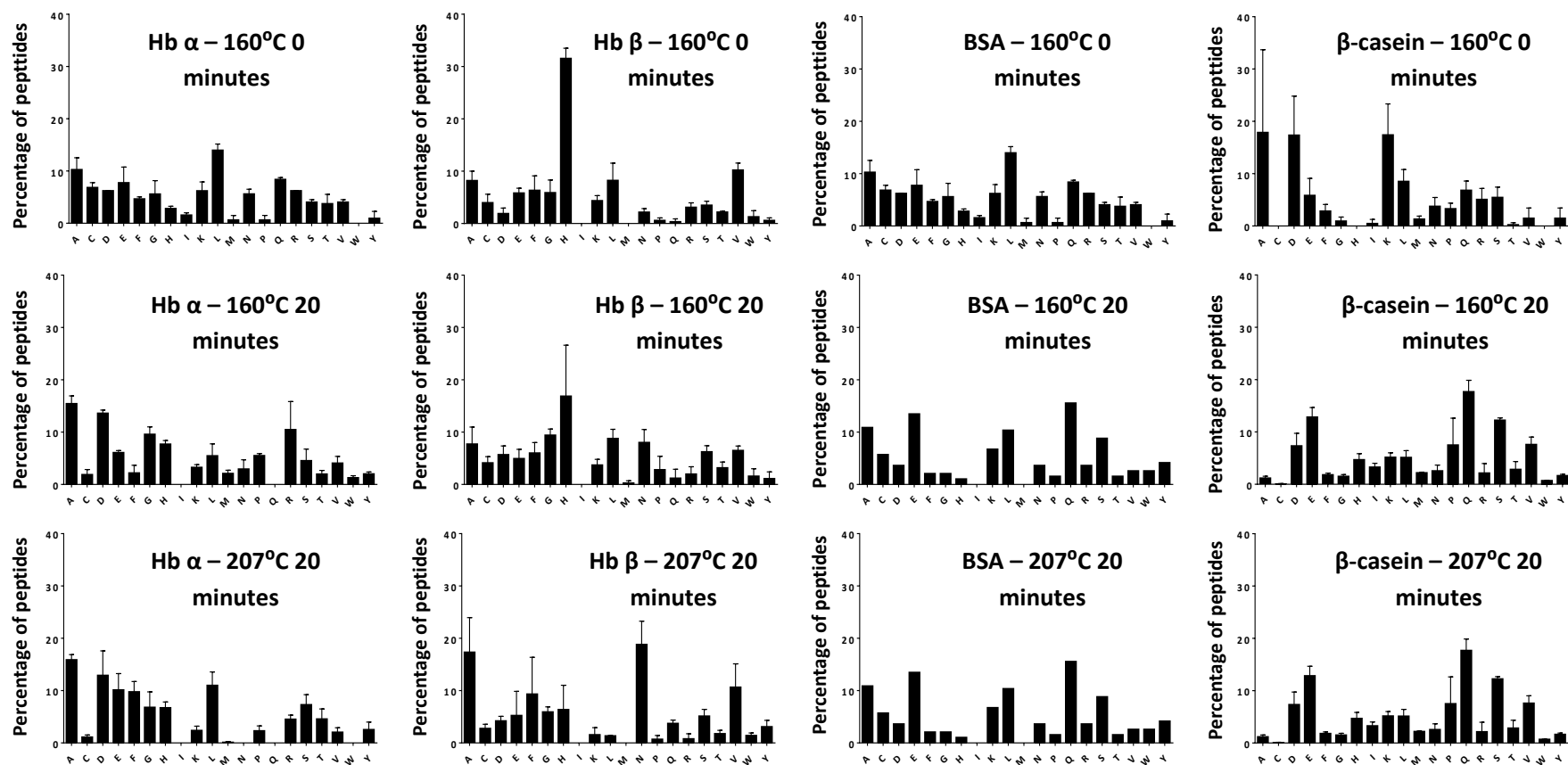


Figure 3.3 - Specificity of SCW hydrolysis: Plots of the % of peptides identified against the amino acid residue immediately preceding the peptide C terminus for proteins haemoglobin, BSA, and β -casein under SCW treatment at 160 °C (0 min), 160 °C (20 min), and 207 °C (20 min). $n = 3$. Error bars represent one standard deviation.

residue ($27.2 \pm 2.9\%$), much higher than the natural abundance of glutamic acid (9.1%). At this temperature, favoured cleavage toward arginine in BSA ($0.5 \pm 0.5\%$) or lysine in β -casein ($2.8 \pm 0.0\%$) was not observed. At 207°C , there appears to be a reduction in specificity toward the C-terminus of aspartic acid residues, and a more uniform distribution among the amino acid residues is observed. The percentages of peptides whose N-terminus was adjacent to aspartic acid in the full length protein are $17.1 \pm 3.4\%$ (α -globin), $4.3 \pm 6.3\%$ (β -globin), $25.7 \pm 19.1\%$ (BSA), and $14.1 \pm 8.6\%$ (β -casein). The large standard deviation seen in BSA is due to an outlier in the data: in one replicate, 7.2% of peptides were preceded by an aspartic acid. There also appears to be some specificity toward glutamic acid residues in β -globin ($16.5 \pm 4.2\%$), BSA ($23.9 \pm 7.0\%$), and β -casein ($22.1 \pm 11.5\%$), higher than the natural abundance of glutamic acid residues in β globin (5.5%), BSA (10.1%), and β -casein (9.1%).

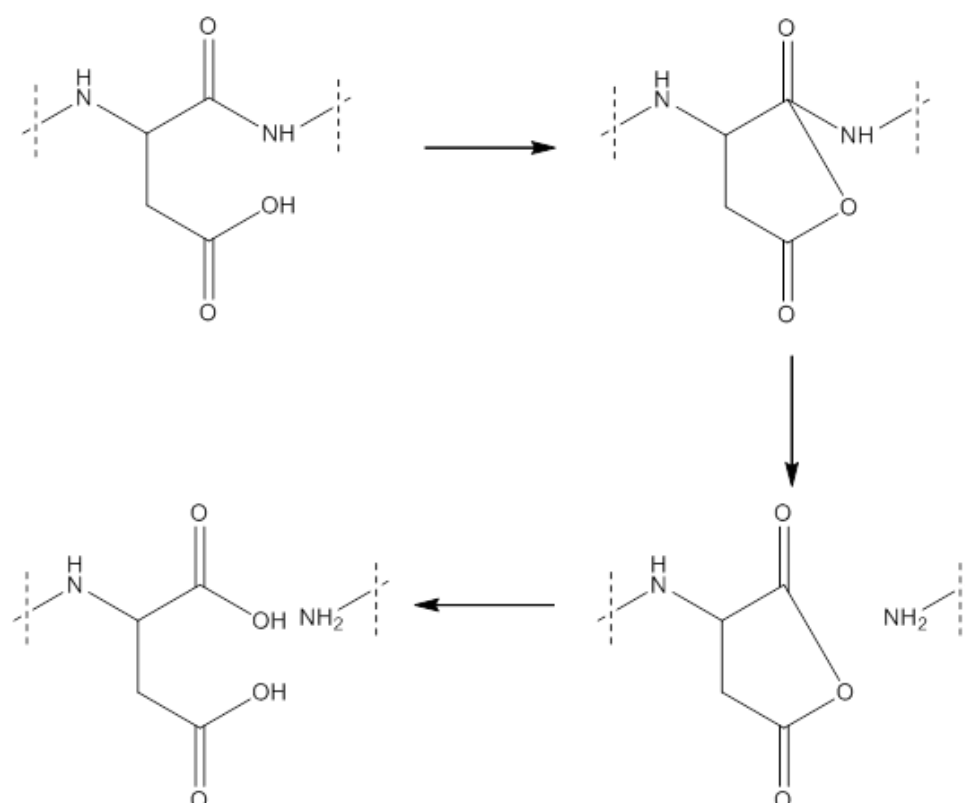
Above temperatures of 207°C there was a significant reduction in the number of peptides that were identified. This is discussed further in Chapter 3.3. SCW specificity was not assessed at these temperatures.

These results both support and contrast work by Kang and Chun which demonstrated that SCW treatment of fish waste at 200°C results in liberation of aspartic acid and serine in high quantities relative to the other amino acids, indicating that these residues are more susceptible to hydrolysis by SCW [189]. My results show favoured cleavage at aspartic acid residues but not serine residues.

Partridge and Davis showed that weak acid hydrolysis of proteins results in preferential release of aspartic acids [190]. In the presence of weak acids, neutral carboxyl groups in the aspartate side chain act as proton donors in the hydrolysis of the adjacent peptide bonds. The production of aspartic acid rather than glutamic acid was attributed to the lower pKa of aspartate. Similarly, Fisher and co-workers showed that chemical treatment of proteins with formic acid results in specific cleavage at aspartic acid residues [191]. The results described above suggest that weak acid hydrolysis of proteins occurs under SCW conditions. **Scheme 3.1** shows the proposed mechanism

for cleavage of the Asp-X bond [192, 193]. Weak acid hydrolysis of proteins has also been observed in studies employing microwave-assisted non-enzymatic digestion. Microwave assisted acid hydrolysis of proteins was first demonstrated by Li and co-workers using 6 M HCl [194] and subsequently trifluoroacetic acid [195]. Hua *et al.* showed that use of dilute formic acid resulted in specific cleavage C-terminal of aspartic acid residues [196], a finding echoed by Swatkoski *et al.* in their work using acetic acid [197].

The optimum pH for weak acid hydrolysis of Asp-X is ~2 [192, 197]. The pH of subcritical water is between 5.5 and 5.7 in the temperature range used in this work [198]. It may be possible therefore to mediate the reaction by addition of a weak acid to the protein solution prior to SCW treatment; however, that was not attempted here.



Scheme 3. 1 - Proposed mechanism for weak acid hydrolysis of the Asp-X bond. Adapted from [192, 193].

It is worth noting that the SCW peptide summary maps shown in **Appendix Figure 3.1** suggest that, following initial cleavage of the peptide bond, secondary cleavage of the peptide products occurs. That occurrence would explain the “blocklike” appearance of the summary map (which is not evident in the results obtained for trypsin).

3.3 Protein sequence coverage: SCW hydrolysis as an alternative proteolytic reagent?

In Section 3.2, the action of SCW hydrolysis was identified with regards to its specificity. SCW was efficient at generating peptides and in Section 3.3 I analyse its potential as an alternative proteolytic reagent, by comparing the peptides identified from the SCW hydrolysis of the three proteins against those obtained using a conventional tryptic digest. **Appendix Figure 3.1** shows the peptides identified for each protein under each hydrolysis condition.

The reliable identification of a protein is closely linked to the percentage of the protein sequence covered by identified peptides, or protein sequence coverage. **Figure 3.4** shows the effect of SCW reaction temperature and time on mean % protein sequence coverage from haemoglobin, BSA, and β -casein, compared with enzymatic digestion of the proteins with trypsin. SCW reaction conditions were 160 °C for 0 min, 160 °C for 20 min, 207 °C for 20 min, 253 °C for 20 min, and 300 °C for 20 min.

3.3.1 Peptides identified from the SCW hydrolysis of haemoglobin

The trypsin digestion of haemoglobin (**Figure 3.4 A**) gave high sequence coverage for both the α -globin ($88.9 \pm 3.6\%$) and β -globin ($92.7 \pm 4.0\%$). SCW hydrolysis at 160 °C for 0 min gave comparable protein coverage: $91.5 \pm 5.6\%$ for α -globin and $87.9 \pm 3.3\%$ for β -globin. Extending the SCW reaction time to 20 min resulted in increased sequence coverage: $97.4 \pm 3.9\%$ for α -globin and $96.2 \pm 0.8\%$ for β -globin. The sequence coverage obtained following SCW treatment at 207 °C was $82.3 \pm 11.2\%$ for α -globin and $76.7 \pm 9.9\%$ for β -globin. A sharp reduction in protein coverage was observed following SCW treatment at 253 °C ($33.6 \pm 0.8\%$ for α -globin and $41.2 \pm 16.1\%$ for β -globin), presumably due to decomposition of the peptides to component

amino acids. This is discussed further in Chapter 5 where lower MW compounds are identified.

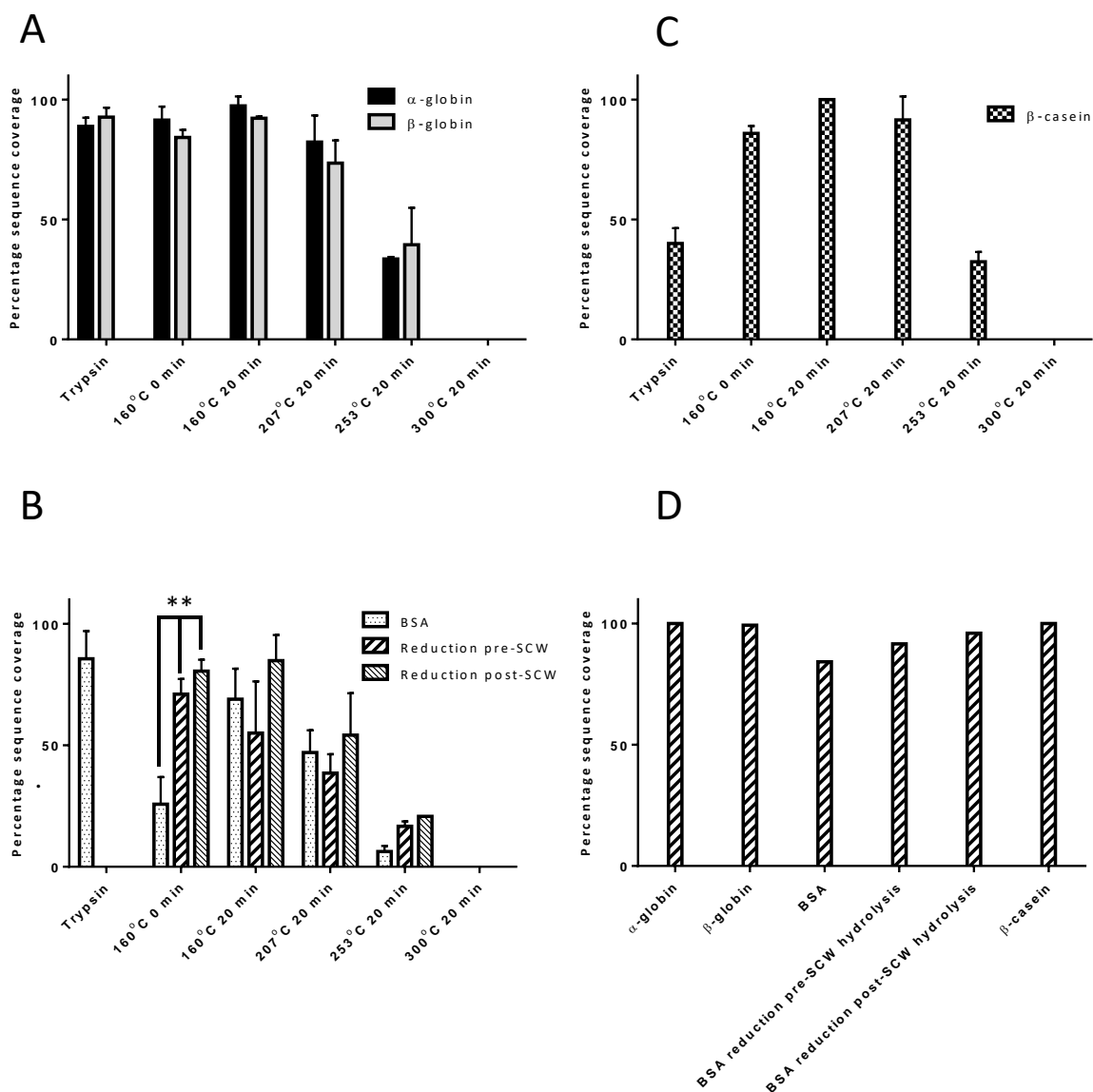


Figure 3. 4 - Mean sequence coverage obtained for trypsin digests and SCW hydrolysis at 160 °C for 0 min, 160 °C for 20 min, 207 °C for 20 min, 253 °C for 20 min, and 300 °C for 20 min for (A) α-globin and β-globin, (B) BSA, (C) β-casein, and (D) combined coverage for haemoglobin α-chain, haemoglobin β-chain, BSA, and β-casein at 160 °C for 20 min. * = $p < 0.05$ as determined by students' t test. $n = 3$. Error bars represent one standard deviation.

No peptides were identified following SCW treatment at 300 °C for 20 min. The decrease in protein coverage observed between 253 and 300 °C supports previous

work by Espinoza *et al.* which showed a decrease in the amount of peptides produced following SCW treatment of whey protein isolate above 220 °C due to conversion into amino acids [199].

3.3.2 Peptides identified from the SCW hydrolysis of BSA

The average protein coverage obtained following SCW mediated hydrolysis (160 °C, 0 min) of BSA (**Figure 3.4 B**) was $32.1 \pm 3.4\%$, significantly lower than the coverage seen for haemoglobin under the same conditions. Maximum sequence coverage was obtained following SCW treatment at 160 °C for 20 min ($69.0 \pm 12.5\%$). Nevertheless, this maximum coverage obtained following SCW treatment falls short of that obtained following trypsin digestion of reduced and alkylated BSA ($85.6 \pm 11.4\%$). The protein coverage obtained following SCW treatment at 207 °C (20 min) and 253 °C (20 min) was $47.0 \pm 9.2\%$ and $6.3 \pm 2.3\%$, respectively. No peptides were observed following treatment at 300 °C.

BSA contains 16 disulphide bonds. These PTMs are highlighted in **Figure 3.1c**. The reduced sequence coverage observed for BSA suggests that SCW treatment does not result in the cleavage of disulphide bonds. To test that hypothesis, BSA was treated with dithiothreitol (DTT) and iodoacetamide (IAM) both pre- and post-SCW treatment. When disulphide bonds were reduced post-SCW treatment, a significant increase ($p = 0.007$) in sequence coverage was observed for SCW conditions 160 °C for 0 min ($80.5 \pm 4.7\%$). At all other SCW conditions, the levels of sequence coverage were not significantly different to those obtained for non-reduced BSA. When disulphide bonds were reduced pre-SCW treatment, again, a significant increase ($p = 0.016$) in sequence coverage was observed for SCW conditions 160 °C for 0 min ($71.1 \pm 6.2\%$). As seen above, the coverages obtained following SCW treatment in all other conditions were not significantly different to those for non-reduced BSA.

Following SCW hydrolysis of untreated BSA at 160 °C (0 min), five cysteine-containing peptides (incorporating 4 cysteine residues) were identified of which the component cysteine residues are involved in three disulphide bonds. This observation suggests that SCW supports cleavage of disulphide bonds. Nevertheless, the cleavage is limited as demonstrated by the results following chemical reduction: reduction of BSA pre-SCW hydrolysis resulted in identification of 98 cysteine containing peptides (incorporating 26 cysteine residues involved in 16 disulphide bonds) and reduction of BSA post-SCW hydrolysis revealed 142 cysteine-containing peptides (incorporating 32 cysteine residues involved in 17 disulphide bonds). For the peptides identified from the SCW hydrolysate of untreated BSA at 160 °C for 20 min, 35 cysteine-containing peptides were identified. Reduction of BSA pre-SCW treatment revealed 175 cysteine-containing peptides, and reduction of BSA post-SCW mediated hydrolysis revealed 232 cysteine containing peptides. The overall protein sequence coverage was similar for the three conditions; therefore, the differences in observed cysteine-containing peptides suggest that only very limited disulphide bond cleavage occurs under SCW conditions of 160 °C for 20 min. These results suggest that proteins containing disulphide bonds should be reduced and alkylated either prior to or post-SCW treatment in order to maximize sequence coverage.

3.3.3 Peptides identified from the SCW hydrolysis of β -casein

Trypsin digestion of β -casein gave an average protein sequence coverage of $40.0 \pm 6.4\%$ (**Figure 3.4 C**). This low sequence coverage can be explained by the paucity of arginine and lysine residues in the protein sequence. In contrast, SCW hydrolysis at 160 °C, 0 min, gave high sequence coverage ($86.0 \pm 3.0\%$). Under SCW conditions of 160 °C for 20 min, protein sequence coverage of 100% was achieved in all replicates. A reduction in protein coverage was observed following SCW treatment at 207 °C for 20 min ($91.6 \pm 9.8\%$), and this trend continued following SCW treatment at 253 °C for 20 min ($32.4 \pm 4.1\%$). No peptides were identified at 300 °C for 20 min. The results obtained for β -casein illustrate the advantages of SCW hydrolysis over trypsin for identification of some proteins.

On the basis of the results above, the optimum SCW conditions in terms of protein sequence coverage were 160 °C for 20 min. **Figure 3.4 D** summarizes the total combined coverage for the three replicates obtained at these conditions for each protein. The high protein coverages obtained suggest that these SCW hydrolysis conditions may be used as an alternative to trypsin in bottom-up proteomics.

3.3.4 SCW hydrolysis of haemoglobin using a smaller protein: solvent ratio

In the SCW experiments described above, 15 mg/15 mL of protein was used in each reaction tube. Twenty µL of hydrolysis product (equivalent to 20 µg of starting protein) was desalted using ZipTip C18 pipet tips and loaded onto the LC column. In the tryptic digestion experiments, 50 µg of protein was digested and analysed. Although comparable amounts of starting protein are ultimately analysed by LC MS/MS in the two experiments, the amount of protein in the SCW reaction is much higher. The suitability of the SCW setup for lower protein concentration was therefore investigated for haemoglobin solutions of concentration 0.1 and 0.01 mg/mL (160 °C for 20 min). SCW hydrolysis using 0.1 mg/mL of haemoglobin gave comparable sequence coverage to that described above for both α-globin ($97.2 \pm 2.6\%$) and β-globin ($94.3 \pm 1.6\%$). Sequence coverage remained high when using 0.01 mg/mL of haemoglobin (i.e., 150 µg of starting product) for both α-globin ($99.5 \pm 0.4\%$) and β-globin ($91.7 \pm 3.4\%$).

Figure 3.5 shows the summed survey scan mass spectra at each of the three concentrations. The base peak in these mass spectra corresponds to 3+ ions of [VHLTPEEKSAVTALWGKVNVND-H₂O]. The signal intensities are 8.5×10^6 , 1.3×10^6 , and 2.6×10^6 , i.e., within an order of magnitude, across the concentration range. (Note that the automatic gain control was used in each experiment to control the number of ions entering the orbitrap.) These results suggest that the SCW hydrolysis would be suitable as a proteomics sample preparation method.

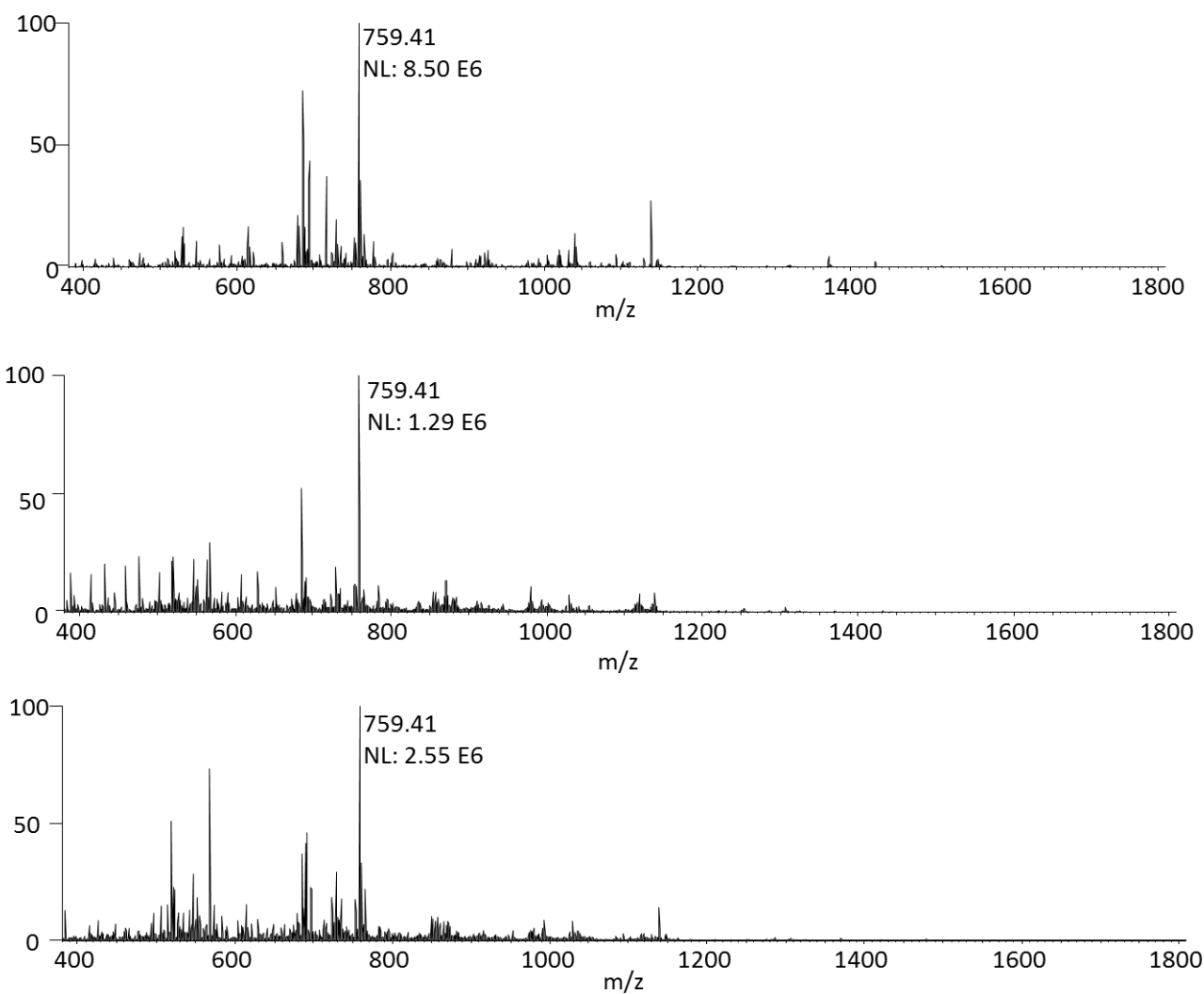


Figure 3. 5 - Summed survey scan mass spectra obtained following LC MS/MS analysis of SCW treated hemoglobin. (a) SCW treatment of 1 mg/ml Hb; (b) SCW treatment of 0.1 mg/ml Hb; (c) SCW treatment of 0.01 mg/ml Hb.

3.4 SCW Mediated Hydrolysis and Phosphorylation

PTMs are of paramount importance in a protein's function. Protein phosphorylation is a particularly key PTM which plays a crucial role in virtually all cellular signalling pathways. Retaining sites of phosphorylation during proteolysis is of paramount importance for phosphosite identification or ultimately quantification.

β -casein is phosphorylated at serine residues at positions 15, 17, 18, 19, and 35 (**Figure 3.1**). SCW treated samples of β -casein were analysed by liquid chromatography electron transfer dissociation (ETD) tandem mass spectrometry (LC ETD MS/MS). ETD retains labile post-translational modifications on peptide backbone fragments, thereby enabling localization of sites of modification [200]. The results were compared with those obtained following trypsin digestion of β -casein and subsequent LC ETD MS/MS. Observed phosphopeptides (and observed unmodified counterparts) are summarized in **Table 3.1**, with annotated mass spectra of the phosphopeptides shown in **Figure 3.6**. No phosphopeptides were identified following SCW treatment at 160 °C for 20 min or at temperatures above 160 °C.

In the trypsin-digested β -casein sample, one phosphosite (Ser35) was identified, belonging to the peptide FQsEEQQTEDELQDK (s is phosphoserine). This phosphopeptide was observed in each of three repeats. The remaining phosphosites fall within the tryptic peptide ELEELNVPGEIVESLSSSEESITR; however, that peptide was not detected in any of the repeats. The peptide comprises a high number of glutamic acid residues, in addition to four acidic phosphate groups, and does not favour formation of positive ions.

In contrast, phosphopeptides containing all of the phosphosites (Ser15, Ser17, Ser18, Ser19, and Ser35) were identified following SCW treatment at 160 °C for 0 min. Seven phosphopeptides were identified across three repeats. Two peptides contained pSer35, and a further two contained pSer15. One peptide contained pSer15, pSer17, and pSer18. One peptide containing Ser 15 and Ser17 was identified but was observed to be modified at Ser17 only.

Peptide sequence	Theoretical Mass	Calculated Mass	PPM
Phosphopeptides identified in SCW hydrolysed β-casein at 160°C for 0 minutes			
IEKFQ ^s EEQQQTED	1817.7356	1817.7423	3.6474
KIEKFQ ^s EEQQQTED	1945.8306	1945.8395	4.5379
RELEELNVPGEIVE ^s	1791.8292	1791.8347	3.0304
RELEELNVPGEIVE ^s L	1904.9132	1904.9211	4.1104
RELEELNVPGEIVESL ^s	1991.9452	1991.9551	4.9349
RELEELNVPGEIVE ^s L ^{ss}	2238.9099	2238.9137	1.6660
RELEELNVPGEIVESL ^{ss} EESITRINK	3316.5477	3316.5649	5.1732
Non-phosphopeptides identified in SCW hydrolysed β-casein 160 °C for 0 minutes			
RELEELNVPGEIVES	1712.8701	1712.8694	0.4087
RELEELNVPGEIVESL	1825.9542	1825.9602	3.2859
RELEELNVPGEIVESLS	1912.9862	1912.9902	2.0910
Phosphopeptides identified in trypsin digest of β-casein			
FQ ^s EEQQQTEDELQDK	2061.8285	2061.82197	3.1671

Table 3. 1 - Summary of Phosphopeptides and Unmodified Peptides Containing Known Sites of Phosphorylation Observed Following SCW Hydrolysis or Trypsin Digestion of β -Casein.

Finally, a doubly phosphorylated peptide was observed which contained four potential modification sites (Ser15, Ser17, Ser18, and Ser19). The two phosphosites could be localized to Ser17, Ser18, and Ser19 but could not be unambiguously assigned due to lack of cleavage between the serine residues. The observation of phosphopeptides with under-occupancy of known modification sites, together with the observation of unmodified peptides, suggests that SCW treatment can result in removal of

phosphorylation. This process is exacerbated under harsher SCW conditions: No phosphopeptides were identified from samples treated for 20 min at 160, 207, 253, or 300 °C. Nevertheless, under milder conditions, sufficient phosphorylation is retained to identify all modification sites.

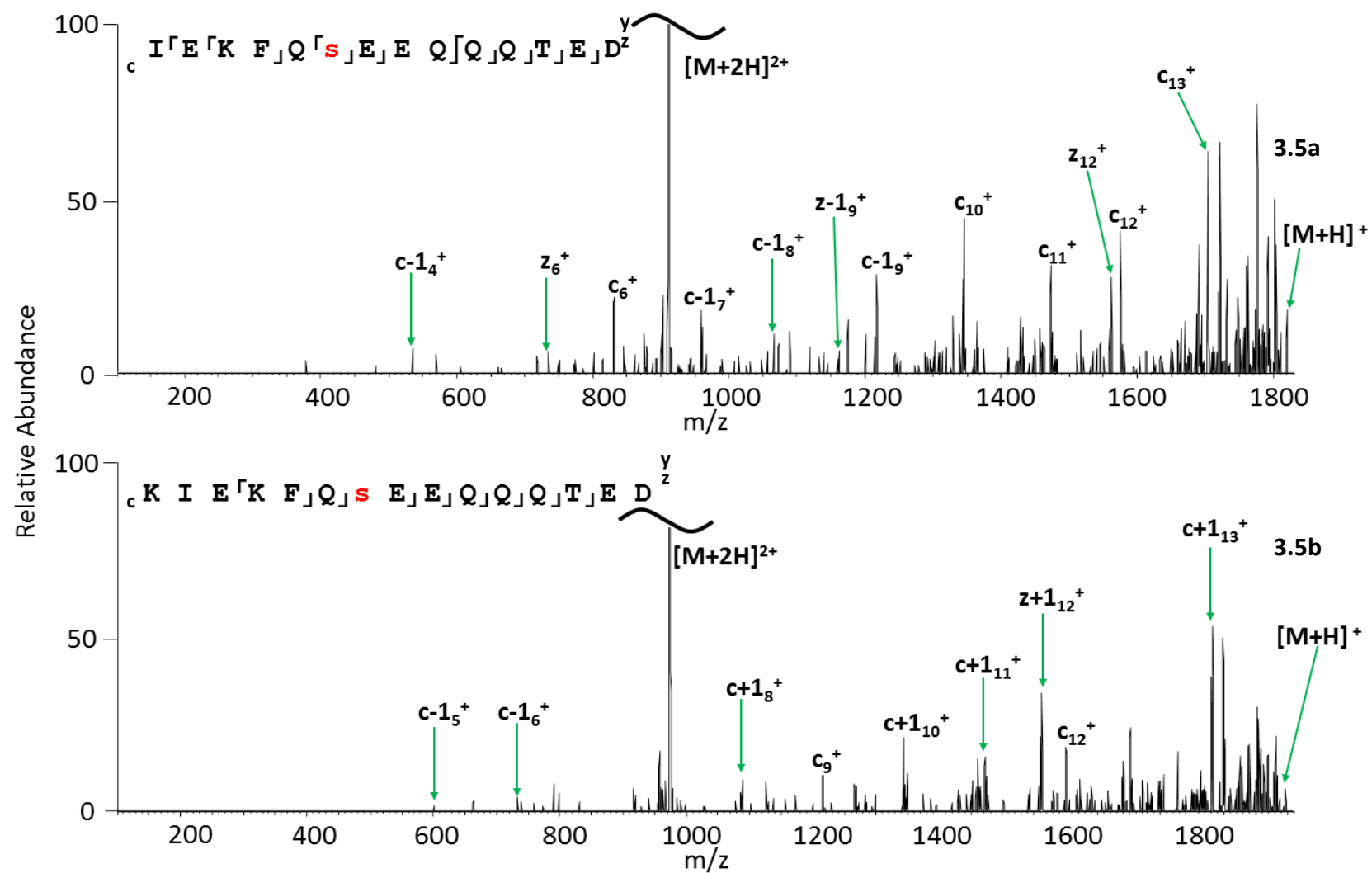


Figure 3. 6 - ETD MS/MS spectra of phosphopeptides produced following SCW hydrolysis or trypsin digestion of β casein.

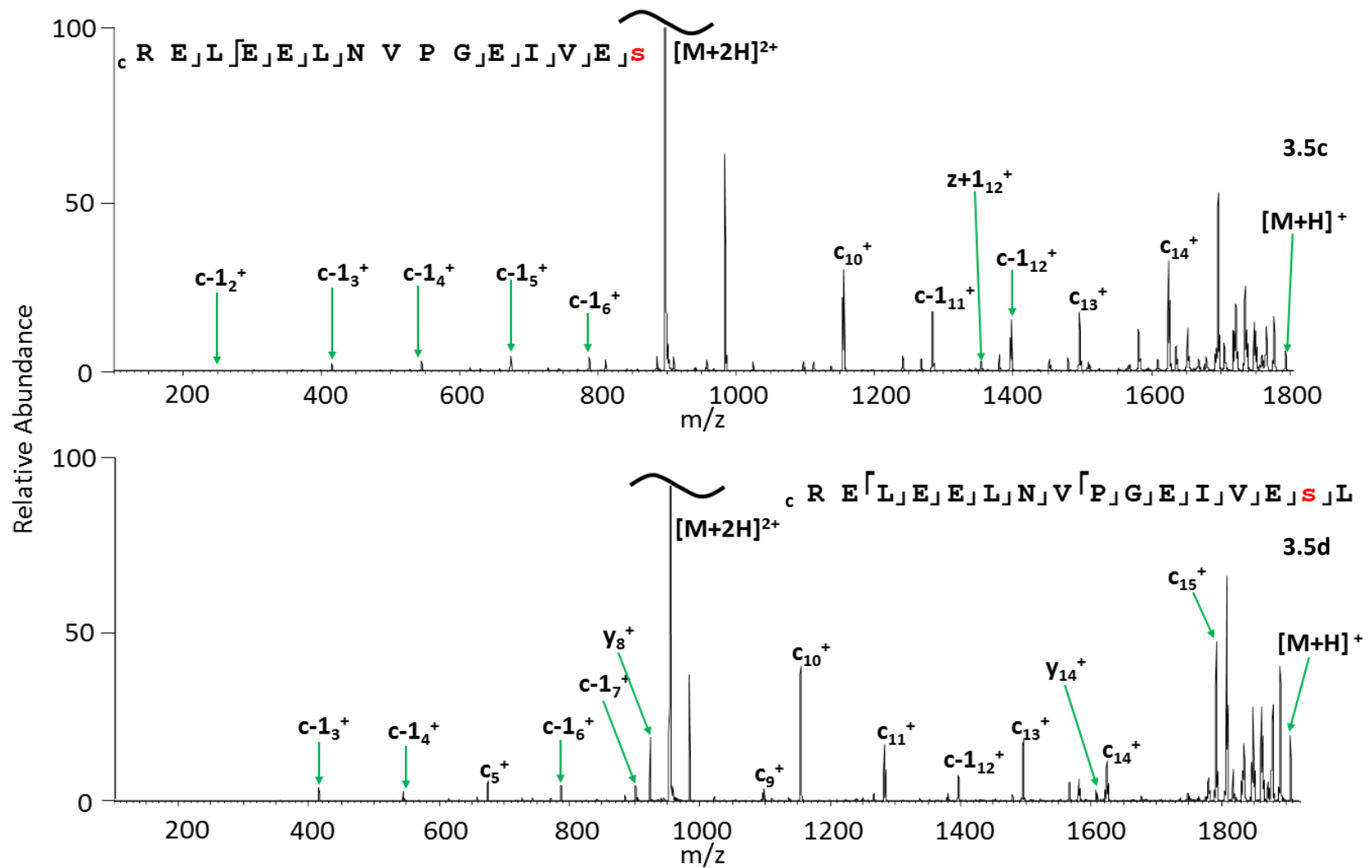


Figure 3. 6 (continued) - ETD MS/MS spectra of phosphopeptides produced following SCW hydrolysis or trypsin digestion of β casein.

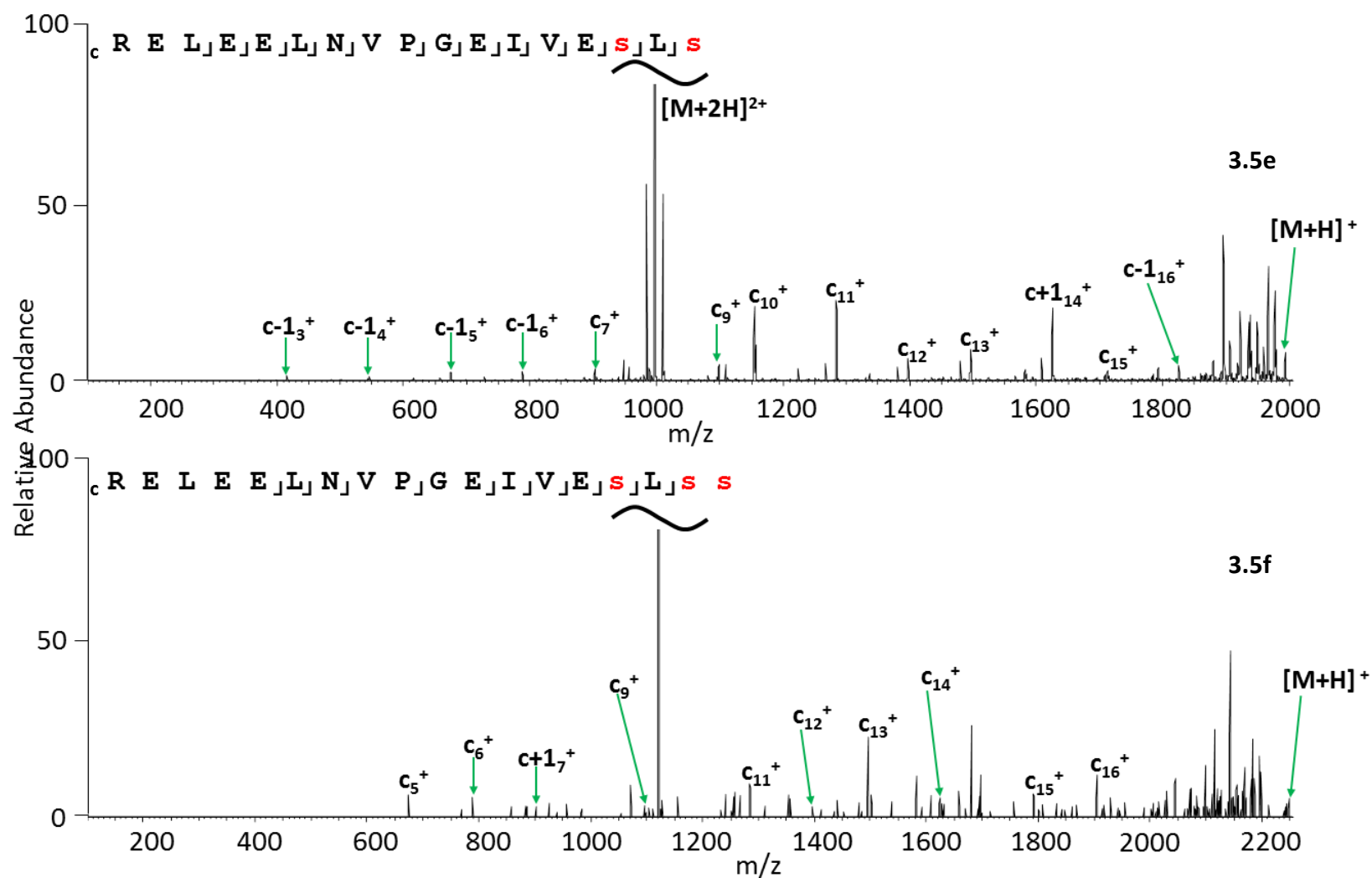


Figure 3. 6 (continued) - ETD MS/MS spectra of phosphopeptides produced following SCW hydrolysis or trypsin digestion of β casein.

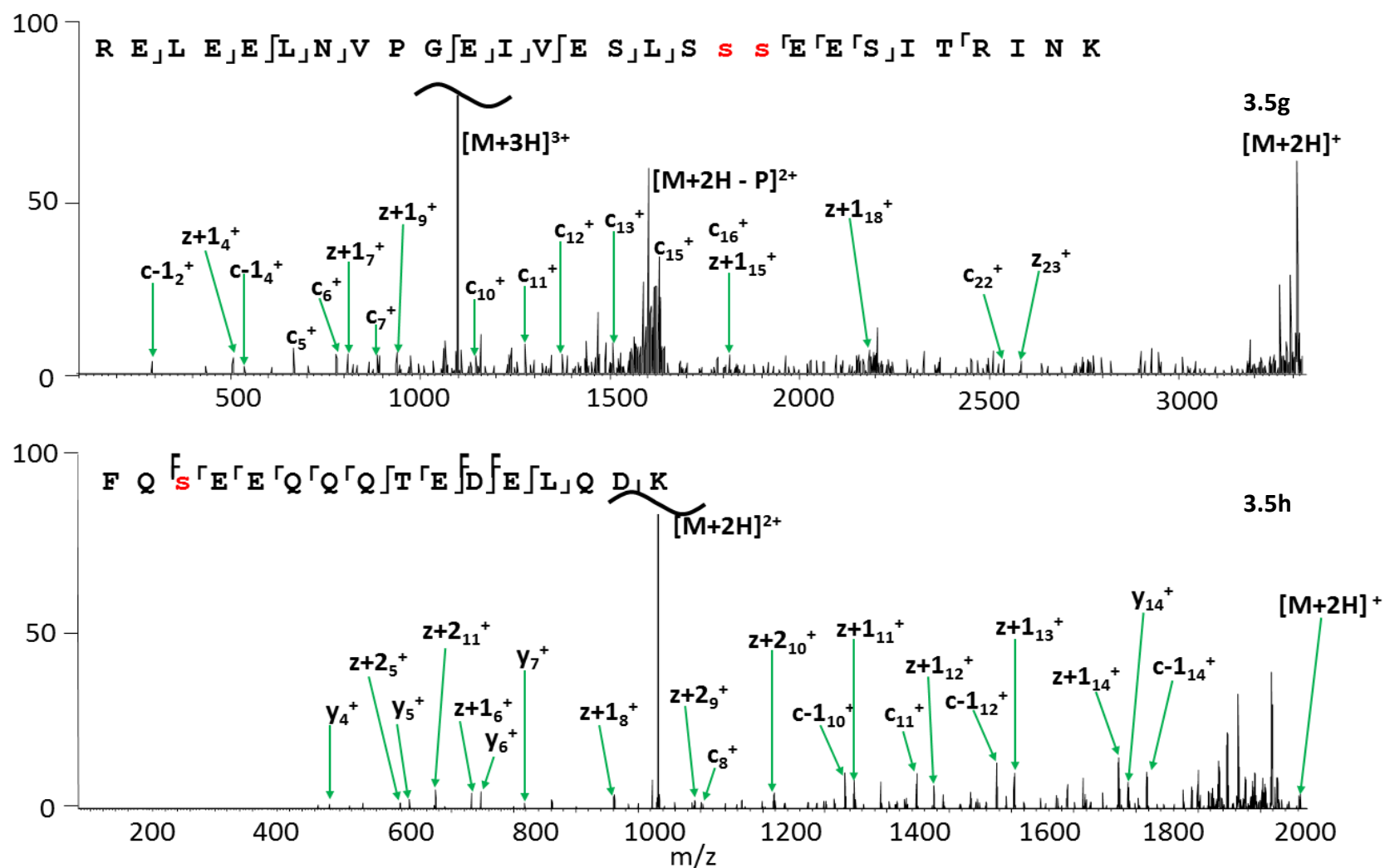


Figure 3. 6 (continued) - ETD MS/MS spectra of phosphopeptides produced following SCW hydrolysis or trypsin digestion of β casein.

3.5 Analysis of Peptide Spectrum Matches

In Section 3.2 and 3.3 SCWs effectiveness as a proteolytic agent was demonstrated by its ability to provide high sequence coverage of proteins, as well as its capability at maintaining post-translational modifications. Despite the high coverages obtained the percentage of peptide spectrum matches (PSM) was low. The PSM scoring function refers to MS/MS spectra which were confidently assigned to a peptide sequence in the protein database search.

Figure 3.7 shows a plot of the percentage of PSMs versus proteolysis conditions (either trypsin digestion or SCW hydrolysis). The percentage of PSM for the samples treated with trypsin were consistently greater ($23.2 \pm 4.7\%$ for haemoglobin, $89.8 \pm 10.5\%$ for BSA, and $31.9 \pm 4.3\%$ β -casein) than for those treated with SCW ($<7\%$ in all cases). This observation suggests that, in addition to cleavage of the peptide bond, SCW treatment results in other hydrolysis products, presumably due to degradation of the amino acid side chains.

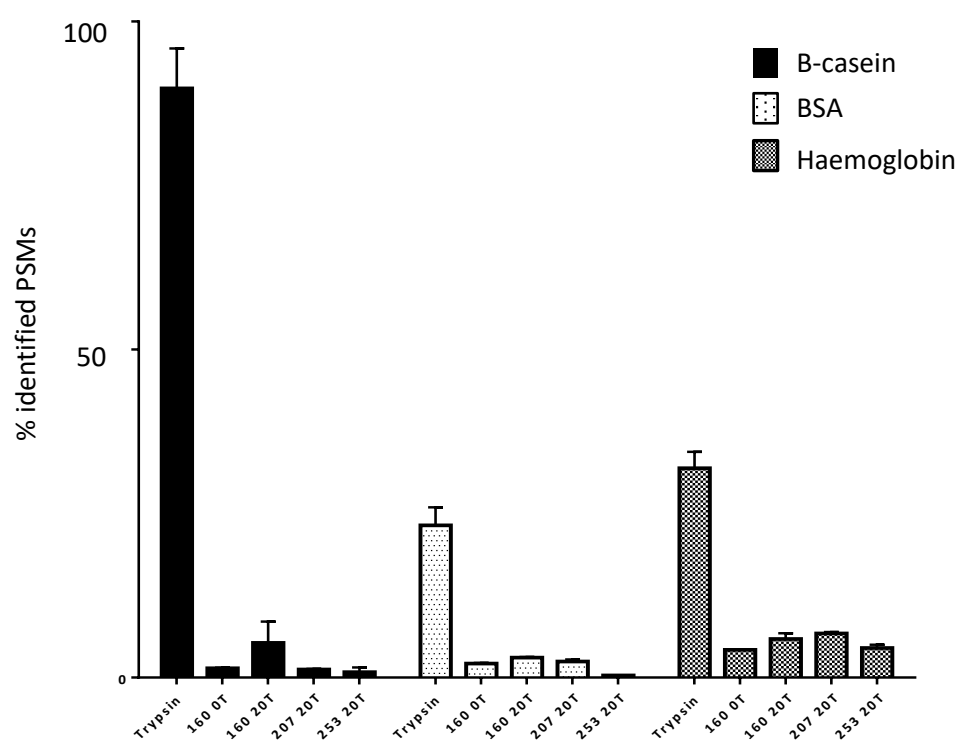


Figure 3. 7 - Percentage of peptide spectral matches following protein database search versus treatment conditions. n=3. Error bars represent one standard deviation.

3.6 Conclusion

The work presented in this chapter investigates the specificity of SCW hydrolysis of proteins and the feasibility of SCW as an alternative proteolytic reagent for proteomics. SCW was shown to display partial specificity towards aspartic and glutamic acid residues. Sequence coverages obtained were comparable to those obtained with trypsin. The majority of the experiments described here used 15 mg of starting protein (1 mg/mL); however, the results also showed that SCW treatment of 150 µg of protein (0.01 mg/mL) gave very high protein sequence coverage (>90%). Moreover, under mild SCW conditions, phosphorylation generally remains on the peptide hydrolysis products, and all known phosphorylation sites were identified in β -casein; however, there was some evidence for dephosphorylation.

Interestingly, despite the high sequence coverage, the percentage of peptide spectral matches, i.e., MS/MS spectra that were confidently assigned to a peptide sequence, was low. That suggests that in addition to hydrolysis of the peptide bond cleavage is occurring elsewhere in the protein, e.g., in the amino acid side chains. This possibility is explored in **Chapter 4**.

Chapter 4: Sub-critical water hydrolysis of peptides: amino acid modifications and conjugation

The work presented in this chapter has been published in part as an article in the Journal of the American Society for Mass Spectrometry on which I am first author [201].

4.1 Overview

In **Chapter 3** it was shown that SCW has the potential to be used as an alternative proteolytic technique during bottom-up proteomics experiments. Hydrolysis of proteins under certain conditions was shown to result in protein sequence coverages greater than or equal to those obtained following digestion with trypsin; however, the percentage of ions selected for fragmentation that were assigned as peptides, or peptide spectral matches (PSMs) for the samples treated with trypsin were consistently greater than for those treated with subcritical water. This observation suggests that in addition to cleavage of the peptide bond, subcritical water treatment results in other hydrolysis products, possibly due to modifications of amino acid side chains.

To investigate this further, a model peptide comprising all common amino acid residues (VQSIKADFLHYMENPTWGR) and two further model peptides (VCFQYMDRGDR and VQSIKADFLHYENPTWGR) were treated with subcritical water with the aim of probing any induced amino acid side-chain modifications. The hydrolysis products were analysed by CID and ETD MS/MS and LC CID MS/MS. Oxidation of cysteine, methionine and tryptophan residues were identified as the most common modifications.

4.2 SCW hydrolysis of model peptide VQSIKADFLHYMENPTWGR

In order to determine the effects of SCW hydrolysis on the side chains of amino acid residues, a model peptide that incorporates all 20 natural amino acids was designed and synthesized, VQSIKADFLHYMENPTWGR. An arginine residue was placed at the C-terminus of the peptide in order to allow efficient generation of a 'y' or 'z' fragment ion series following fragmentation. The acidic glutamate and aspartate residues, which were shown to direct backbone cleavage in SCW conditions in Chapter 3, were separated by five amino acid residues. The direct infusion electrospray mass spectrum of the peptide is shown in **Figure 4.1a**, with peak assignments detailed in **Appendix Table 4.1**. (Note, there are some low abundance peaks that correspond to impurities resulting from incorrect synthesis of the model peptide). In Chapter 3 hydrolysis temperatures of 160 °C were shown to be the most effective at generating peptides. In this chapter a range of temperatures around 160 °C were employed.

Samples of the peptide were subjected to SCW hydrolysis at 140 °C for 10 min, 160 °C for 10 min, 180 °C for 10 min, and 200 °C for 10 min, and the resulting hydrolysates were analysed by direct infusion electrospray mass spectrometry. A summary of the peaks observed is given in **Table 4.1**. Selected peaks were isolated and fragmented by both CID and ETD MS/MS, as described below.

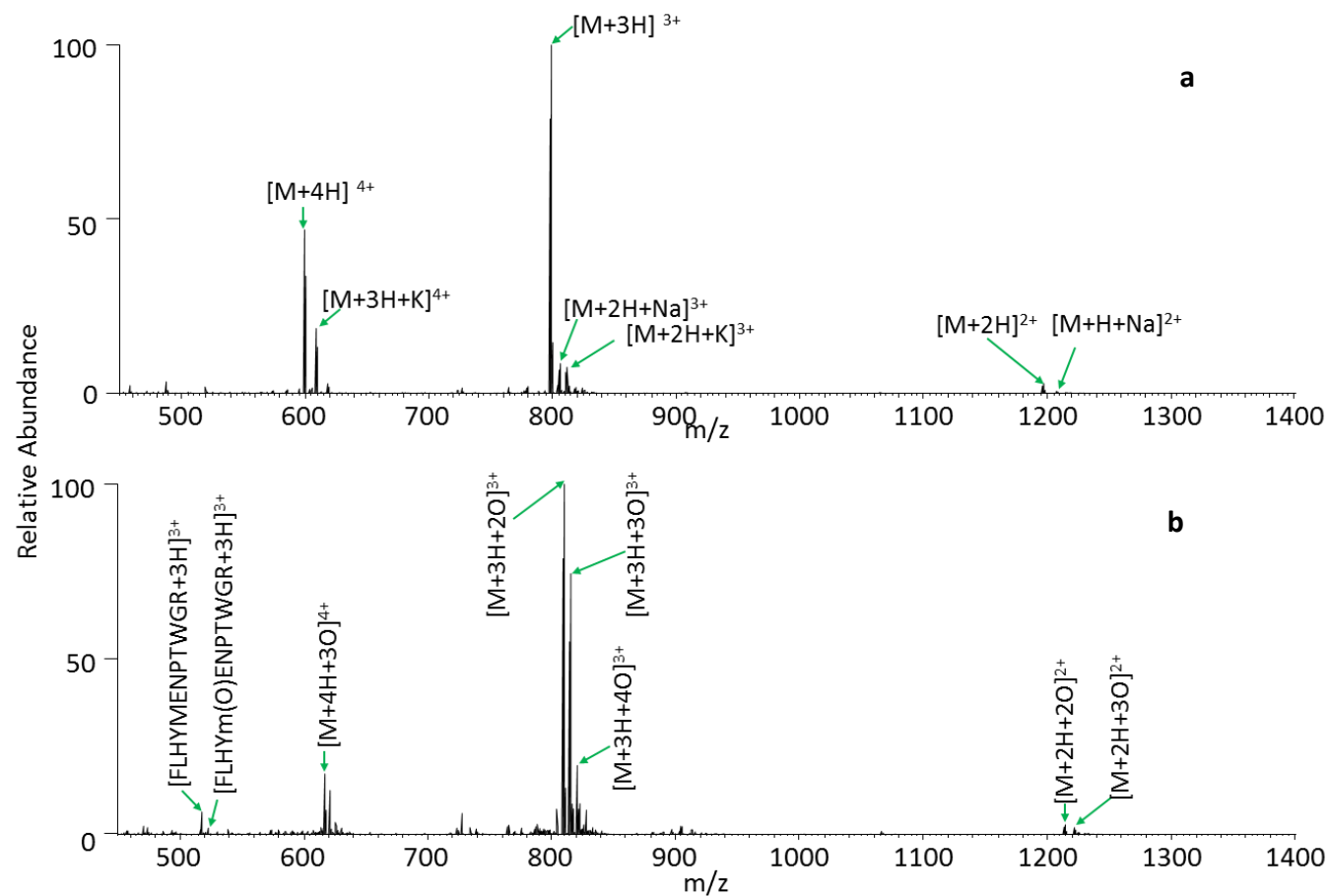


Figure 4. 1 - Direct infusion electrospray MS of **a)** untreated peptide VQSIKADFLHYMENPTWGR, **b)** peptide VQSIKADFLHYMENPTWGR treated with SCW at 140 °C for 10 min.

<u>140°C 10 minutes</u>					
<i>m/z</i>	<i>z</i>	Calculated mass (Da)	Measured mass (Da)	Peptide	ΔPPM
517.5779	3	1549.7136	1549.7119	FLHYMENPTWGR	-1.1
522.9094	3	1565.7085	1565.7064	FLHYMENPTWGR (+O)	-1.4
617.022	4	2464.0701	2464.0589	VQSIKADFLHYMENPTWGR (+K+2O)	-4.5
621.0207	4	2480.0650	2480.0537	VQSIKADFLHYMENPTWGR (+K+3O)	-4.5
809.7109	3	2426.1147	2426.1109	VQSIKADFLHYMENPTWGR (+2O)	-1.6
815.0426	3	2442.1096	2442.1060	VQSIKADFLHYMENPTWGR (+3O)	-1.5
820.3743	3	2458.1045	2458.1011	VQSIKADFLHYMENPTWGR (+4O)	-1.4
1214.0621	2	2426.1147	2426.1096	VQSIKADFLHYMENPTWGR (+2O)	-2.1
1222.0594	2	2442.1096	2442.1042	VQSIKADFLHYMENPTWGR (+3O)	-2.2
<u>160°C 10 minutes</u>					
<i>m/z</i>	<i>z</i>	Calculated mass (Da)	Measured mass (Da)	Peptide	ΔPPM
522.9093	3	1565.7085	1565.7061	FLHYMENPTWGR (+O)	-1.6
530.2266	3	1587.6689	1587.658	FLHYMENPTWGR (+ K)	-6.9
645.7868	2	1289.5611	1289.559	HYMENPTWGR	-1.6
775.8629	2	1549.7136	1549.7112	FLHYMENPTWGR	-1.5
809.7106	3	2426.1147	2426.1100	VQSIKADFLHYMENPTWGR (+2O)	-2.0
815.0424	3	2442.1096	2442.1054	VQSIKADFLHYMENPTWGR (+3O)	-1.7
<u>180°C 10 minutes</u>					
<i>m/z</i>	<i>z</i>	Calculated mass (Da)	Measured mass (Da)	Peptide	
457.2785	1			Unassigned	
517.5801	3	1549.7136	1549.7185	FLHYMENPTWGR	3.1
522.9117	3	1565.7085	1565.7133	FLHYMENPTWGR (+O)	3.0
577.2600	2	1152.5022	1152.5054	YMENPTWGR	2.8
583.7703	2	1165.5226	1165.526	FLHYMENPT (C-terminal amidation+O)	3.0
585.2570	2	1168.4971	1168.4994	YMENPTWGR (+O)	2.0
616.3218	1	615.3129	615.3145	PTWGR	2.6
645.7897	2	1289.5611	1289.5648	HYMENPTWGR	2.9
653.7871	2	1305.556	1305.5596	HYMENPTWGR (+O)	2.8
727.3919	1			Unassigned	
775.8662	2	1549.7136	1549.7178	FLHYMENPTWGR	2.7
783.8634	2	1565.7085	1565.7122	FLHYMENPTWGR (+O)	2.4
867.8906	2	1733.7621	1733.7666	ADFLHYMENPTWGR (-H ₂ O+O)	2.6

Table 4. 1 - Ions identified following SCW hydrolysis of VQSIKADFLHYMENPTWGR

200°C 10 minutes					
<i>m/z</i>	<i>z</i>	Calculated mass (Da)	Measured mass (Da)	Peptide	Δ PPM
457.2801	1			Unassigned	
517.1089	1			Unassigned	
519.2702	1	518.2601	518.2629	TWGR	5.4
573.3761	1			Unassigned	
577.2625	2	1152.5022	1152.5104	YMENPTWGR	7.1
583.7728	2	1165.5226	1165.531	FLHYMENPT (C- terminal amidation +O)	7.2
585.2600	2	1168.4971	1168.5054	YMENPTWGR (+O)	7.1
653.7898	2	1305.556	1305.565	HYMENPTWGR (+O)	6.9

Table 4.1 (continued) - Ions identified following SCW hydrolysis of

VQSIKCADFLHYMENPTWGR at 140 °C, 160 °C, 180 °C and 200 °C for 10 min.

Figure 4.1b shows the mass spectrum obtained following SCW hydrolysis of the peptide at 140 °C for 10 min. The most intense peak was observed at m/z 809.7109 and corresponds to triply protonated ions of peptide VQSIKCADFLHYMENPTWGR plus two oxygen atoms (m/z_{calc} 809.7122). Low abundance doubly protonated ions of this species were also observed at m/z 1214.0621 (m/z_{calc} 1214.0646). **Figure 4.2a** shows the ETD MS/MS spectrum of the 3+ ions and the c and z fragments are summarized in **Appendix Table 4.2**. Manual analysis of the mass spectrum revealed that both oxidations occur on the cysteine residue (i.e., sulfinic acid is formed). There are a number of peaks that correspond to amino acid side-chain losses. These fragments are commonly observed in electron-mediated dissociation [202]. Of particular note here is the peak corresponding to loss of the sulfinic acid side chain ($-\text{SO}_2\text{H}_2$) observed at m/z 1181.0746 (m/z_{calc} 1181.0756), which confirms the double oxidation on cysteine.

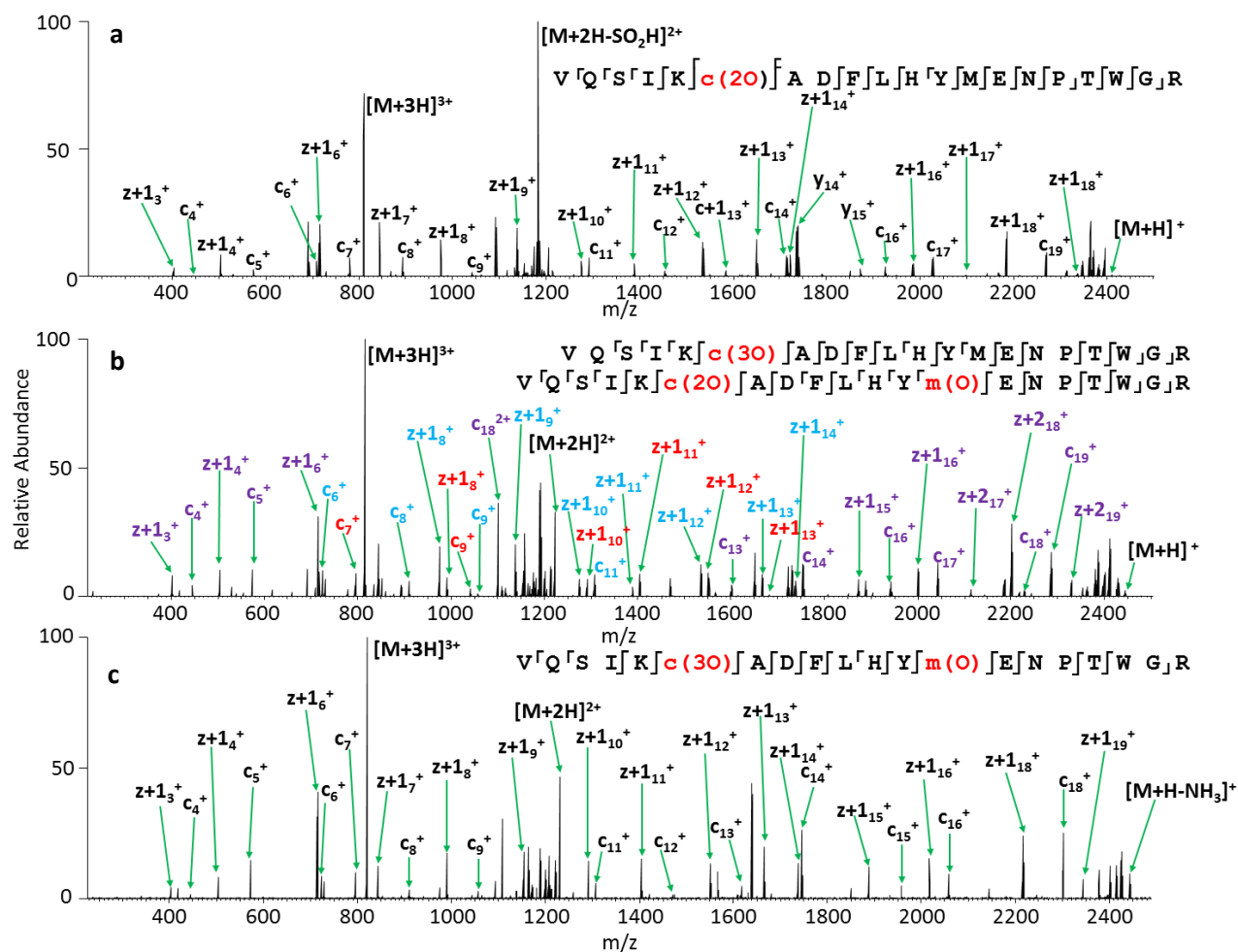


Figure 4.2 a) ETD MS/MS spectrum of 3+ ions of [VQSIKADFLHYMENPTWGR +20], **b)** ETD MS/MS fragmentation of 3+ ions of [VQSIKADFLHYMENPTWGR +30]. Fragments shown in purple can belong to either species; fragments shown in red belong to the species with two oxidations on the cysteine and one on the methionine; fragments shown in blue belong to the species with three oxidations on the cysteine, **c)** CID MS/MS fragmentation of the quadruple oxidation product of VQSIKADFLHYMENPTWGR.*Observed fragments are summarized on the peptide sequences, inset. Lower case denotes modified amino acid residues

The peak at m/z 815.0426 (**Figure 4.1b**) corresponds to triply protonated ions of the peptide plus three oxygen atoms (m/z_{calc} 815.0438). This peak was isolated and fragmented by use of ETD (**Appendix Table 4.**). Peaks corresponding to fragments from both triply oxidated cysteine (i.e., sulfonic acid) and doubly oxidated cysteine (sulfinic acid) together with methionine oxidation, were observed (**Figure 4.2b**), suggesting two species were present. Loss of both the sulfinic acid side chain (m/z 1189.0718) and (low abundance) sulfonic acid side chains were observed (m/z 1181.0777) in the +2 charge state (m/z_{calc} 1189.0731 and 1181.0756). LC CID MS/MS was performed and two species were seen to elute at retention times of ~16 min 45 s and ~19 min (**Figure 4.3**). CID MS/MS of the species eluting at RT ~16 min 45 s reveals the addition of two oxygen atoms on the cysteine residue (formation of sulfinic acid) and one oxygen atom to the methionine residue (**Appendix Table 4.4a**). CID MS/MS of the species eluting at RT 19 min shows that all three oxidations occur on the cysteine residue, forming sulfonic acid (**Appendix Table 4.4b**). The oxidation of methionine is expected as numerous studies have shown methionine to be readily oxidized to methionine sulfoxide [203].

A peak corresponding to 3+ ions of the peptide plus four oxygen atoms was observed at m/z 820.3743 (m/z_{calc} 820.3754) (**Figure 4.1b**). These ions were isolated and fragmented by ETD to reveal a single species comprising three oxidations of the cysteine residue and a single oxidation of the methionine residue (**Appendix Table 4.5** and **Figure 4.2c**).

The only peak corresponding to a SCW cleavage product was observed at m/z 517.5779 (m/z_{calc} 517.5785) and corresponds to FLHYMENPTWGR (**Figure 4.1b**). This assignment was confirmed by CID (**Appendix Figure 4.1**). The list of ions used to confirm this assignment is shown in **Appendix Table 4.6**. The peptide product is the result of cleavage C-terminal to the aspartic acid residue in the original peptide, consistent with the results presented in **Chapter 3**, which found aspartic acid to be the most common site of SCW-induced cleavage. A peak corresponding to this cleavage product plus an oxygen atom was also observed at m/z 522.9094 (m/z_{calc} 522.9105).

This ion was isolated and fragmented to reveal methionine oxidation (**Appendix Table 4.7** and **Appendix Figure 4.2**).

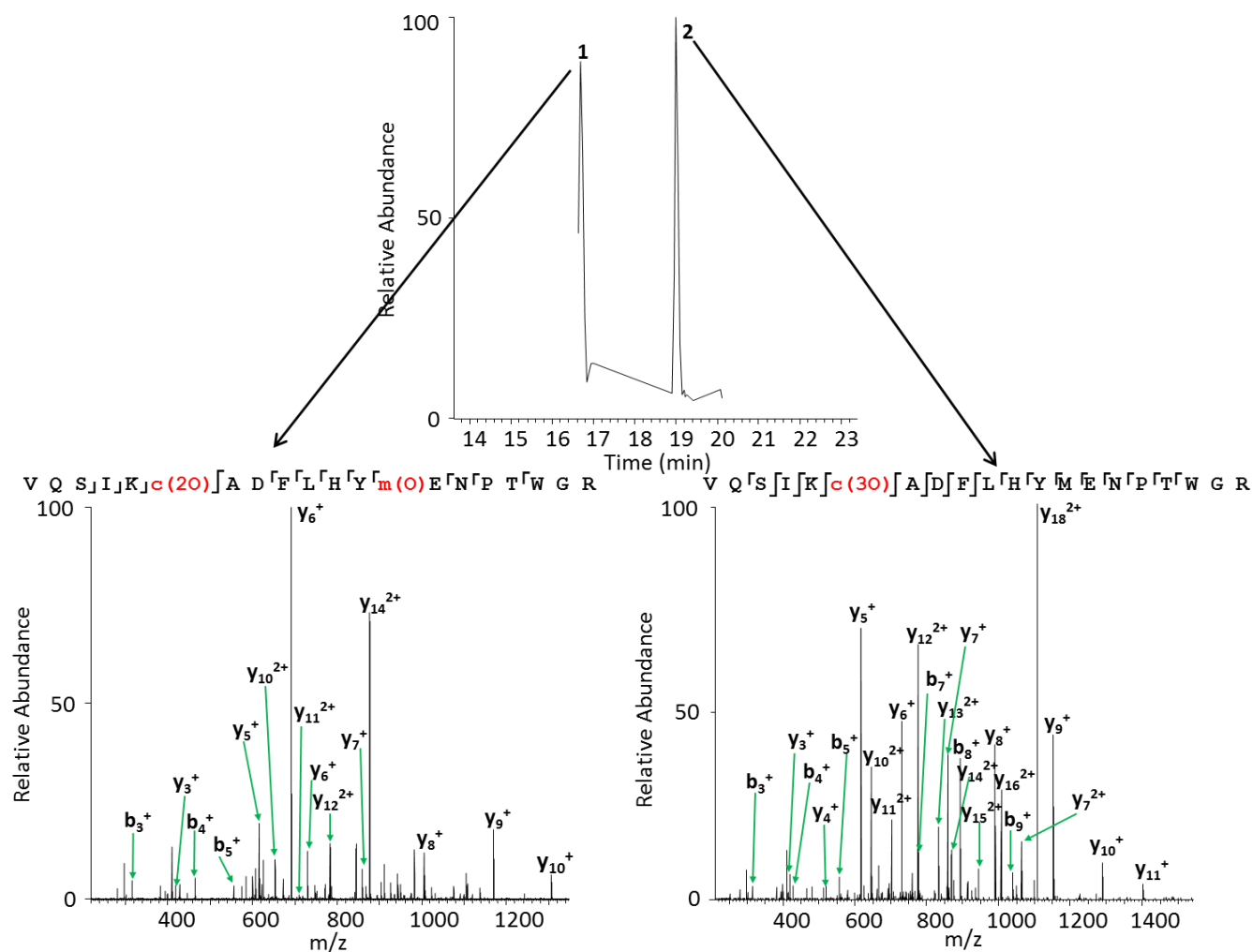


Figure 4. 3 - Extracted ion chromatogram (m/z 815.0426, [VQSIKADFLHYMENPTWGR+30]) obtained following LC CID MS/MS and the two corresponding CID MS/MS spectra at retention times 16 minutes 45 seconds and 19 minutes. Observed fragments are summarised on the peptide sequences, inset. Lower case denotes modified amino acid residues.

SCW treatment was also performed at 160 °C, 180 °C, and 200 °C (**Table 4.1** and **Figures 4.4**). In each case, the residency time was 10 min. A greater amount of peptide bond hydrolysis was observed as the temperature increased, as expected from the results in the prior chapter. Following treatment at 160 °C, the cleavage product FLHYMENPTWGR represents the base peak in the mass spectrum. At SCW conditions of 180 °C, water loss could also be detected as a modification. In the previous chapter, it was shown that inclusion of water loss as a dynamic modification in the automated protein database search of LC MS/MS data obtained from SCW hydrolysates resulted in a 9% increase in peptide identifications for α -globin, β -globin, BSA, and β -casein at SCW conditions of 160 °C (0 min), 160 °C (20 min), and 207 °C (20 min). In addition Basil *et al.* showed that in the thermal decomposition of peptides at comparable temperatures to those used here, dehydration products could be detected [204]. The identity of the specific sites of water loss could not be ascertained reliably: CID is not a reliable indicator as the CID process itself can result in water loss and no fragment ions were observed following ETD MS/MS. Interestingly, Basil *et al.* further identify C-terminal amidation as a modification through thermal denaturation. A small amount of this modification under the two harshest SCW conditions (180 °C and 200 °C) was observed: CID MS/MS was used to confirm that the amidation occurred on the C-terminus (**Figure 4.5** and **Appendix Table 4.8**).

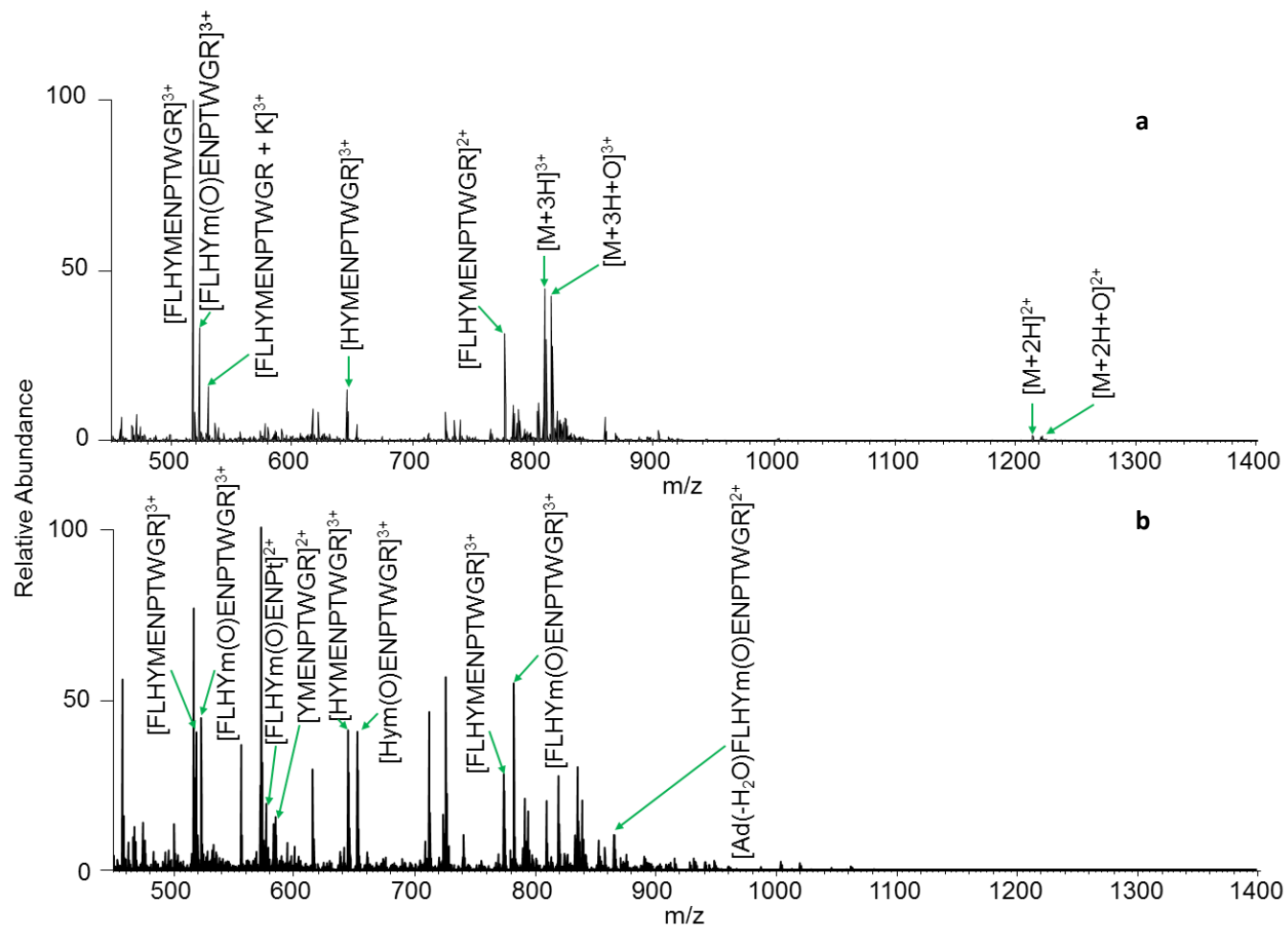


Figure 4. 4 - Direct infusion electrospray MS of peptide VQSIKADFLHYMENPTWGR treated with SCW at a) 160°C for 10 minutes; b) 180°C for 10 minutes and c) 200°C for 10 minutes.

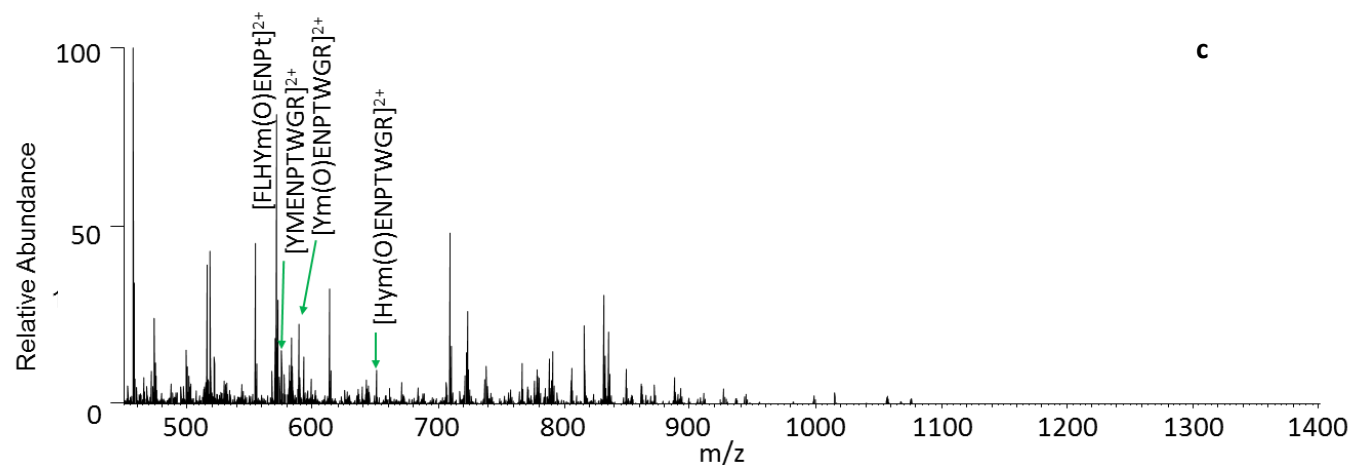


Figure 4.4 (continued) - Direct infusion electrospray MS of peptide VQSIKADFLHYMENPTWGR treated with SCW at a) 160°C for 10 minutes; b) 180°C for 10 minutes and c) 200°C for 10 minutes.

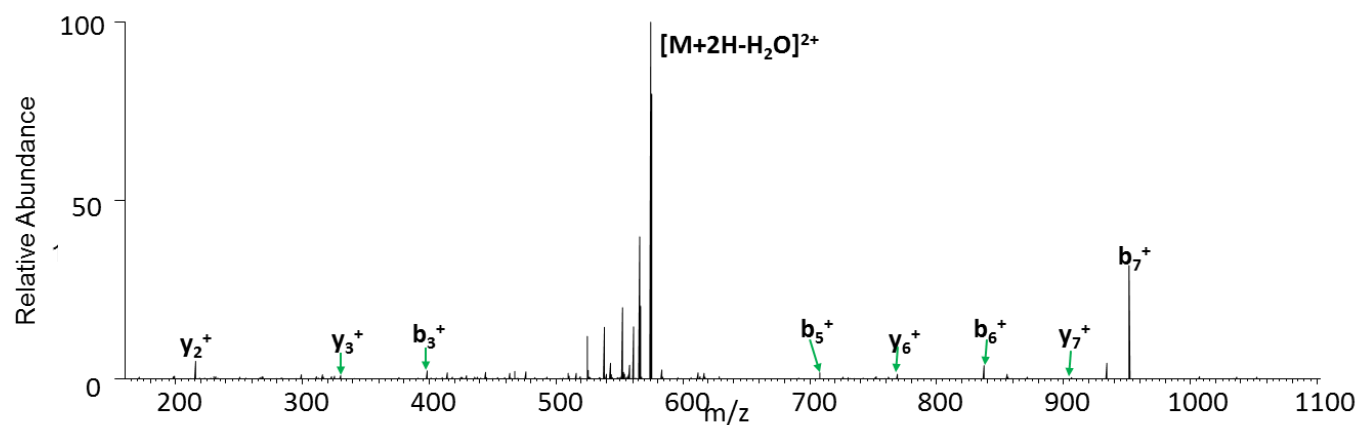


Figure 4.5 - Direct infusion electrospray MS of 3+ ions of CID MS/MS spectrum of 2+ ions of [FLHYMENPT + O + C-term amidation]

4.3 SCW hydrolysis of model peptide VCFQYMDRGDR

SCW hydrolysis was next performed under 140 °C for 10 minutes on a second peptide, which also contained cysteine and methionine, VCFQYMDRGDR. The data here was used to confirm the results from the first peptide.

The direct infusion electrospray mass spectrum of the peptide prior to subcritical treatment is shown in **Figure 4.6a**, with peak assignments detailed in **Appendix Table 4.9**. Peaks at m/z 469.2041 and 703.3028 correspond to singly oxidized species (m/z_{calc} 469.2044 and 703.3030), which CID MS/MS confirmed as methionine oxidation (**Appendix Figure 4.3** and **Appendix Table 4.10**). **Figure 4.6b** shows the direct infusion electrospray mass spectrum of the SCW hydrolysate (**see also Table 4.2**). As observed for VQSIKCADFLHYMENPTWGR, the most intense peaks correspond to oxidized forms of the peptide. Peaks observed at m/z 474.5359 (+3) and m/z 711.3004 (+2) correspond to the peptide plus the addition of two oxygen atoms (m/z_{calc} 474.5360 and 711.3000). CID MS/MS analysis of the 3+ ions confirmed that the oxidation occurs solely on the cysteine residue (**Figure 4.13** and **Appendix Table 4.11**).

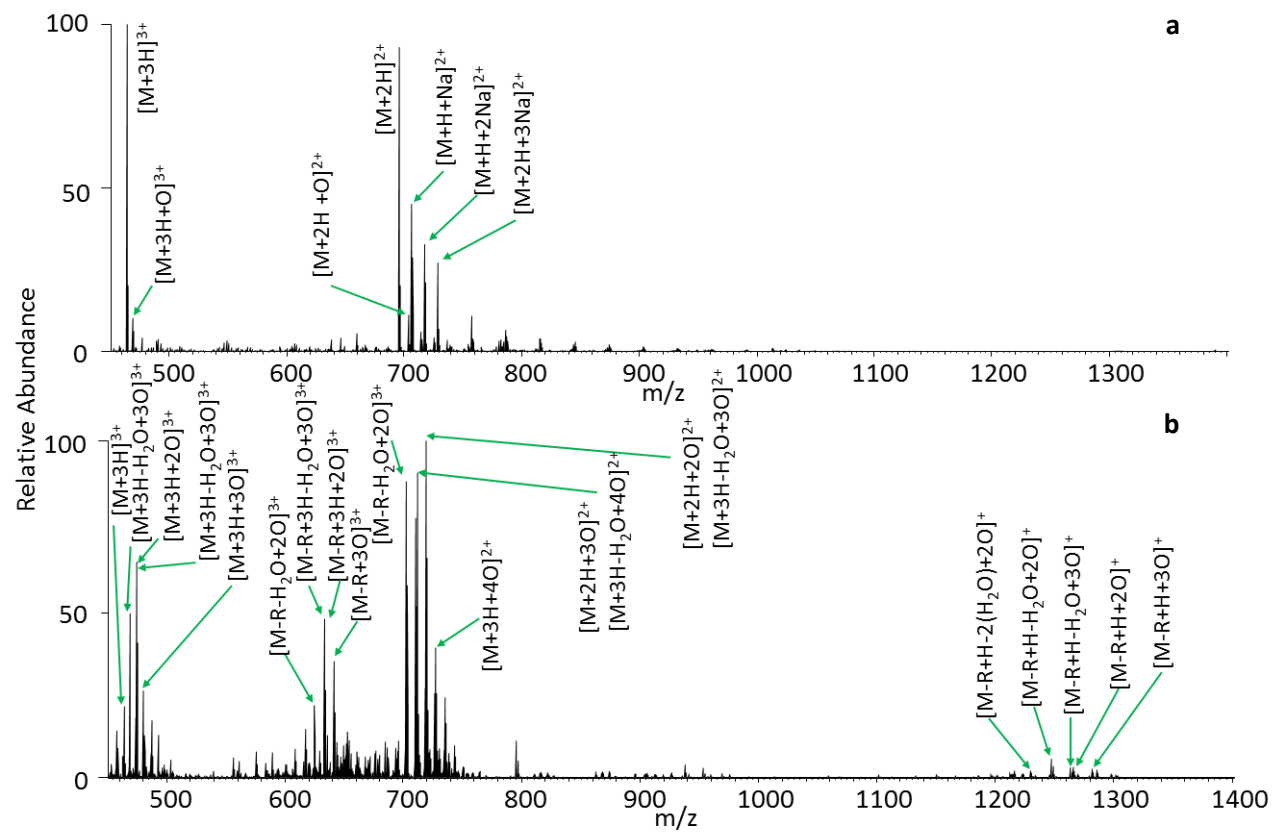


Figure 4. 6 - a) Direct infusion electrospray MS of a) untreated peptide VCFQYMDRGDR and **b)** peptide VCFQYMDRGDR treated with SCW at 140 °C for 10 min.

140°C 10 minutes					
<i>m/z</i>	<i>z</i>	Calculated mass (Da)	Measured mass (Da)	Peptide	Δ PPM
463.873	3	1388.5965	1388.5972	VCFQYMDRGDR	0.5
468.5323	3	1402.5758	1402.5751	VCFQYMDRGDR (-H ₂ O+2O)	-0.5
473.8640	3	1418.5707	1418.5702	VCFQYMDRGDR (-H ₂ O+3O)	-0.4
474.5359	3	1420.5863	1420.5859	VCFQYMDRGDR (+2O)	-0.3
479.8675	3	1436.5812	1436.5807	VCFQYMDRGDR (+3O)	-0.4
624.2444	2	1246.4747	1246.4742	VCFQYMDRGD (-H ₂ O+2O)	-0.3
632.2418	2	1262.4696	1262.4690	VCFQYMDRGD (-H ₂ O+3O)	-0.4
633.2498	2	1264.4852	1264.4850	VCFQYMDRGD (+2O)	-0.1
635.2353	2	1268.4561	1268.4560	VCFQYMDRGD (-H ₂ O+2O+Na)	0.0
641.2472	2	1280.4811	1280.4798	VCFQYMDRGD (+3O)	-1.0
643.2327	2	1284.4510	1284.4508	VCFQYMDRGD (-H ₂ O+3O+Na)	-0.1
652.2381	2	1302.4625	1302.4616	VCFQYMDRGD (+3O+Na)	-0.7
702.2950	2	1402.5758	1402.5754	VCFQYMDRGDR (-H ₂ O+2O)	-0.2
710.2924	2	1418.5707	1418.5702	VCFQYMDRGDR (-H ₂ O+3O)	-0.3
711.3004	2	1420.5863	1420.5862	VCFQYMDRGDR (+ 2O)	-0.1
718.2898	2	1434.5656	1434.5650	VCFQYMDRGDR (-H ₂ O+4O)	-0.4
719.2999	2	1436.5812	1436.5852	VCFQYMDRGDR (+3O)	2.8
727.2950	2	1452.5761	1452.5754	VCFQYMDRGDR (+4O)	-0.5
1229.4707	1	1228.4641	1228.4634	VCFQYMDRGD (-2H ₂ O+2O)	-0.6
1247.4811	1	1246.4747	1246.4738	VCFQYMDRGD (-H ₂ O+2O)	-0.7
1263.4760	1	1262.4696	1262.4687	VCFQYMDRGD (-H ₂ O+3O)	-0.7
1265.4926	1	1264.4852	1264.4853	VCFQYMDRGD (+2O)	0.1
1281.4868	1	1280.4811	1280.4795	VCFQYMDRGD (+3O)	-1.2
1285.4578	1	1284.4510	1284.4505	VCFQYMDRGD (-H ₂ O+3O+Na)	-0.3

Table 4. 2 - Ions identified following SCW hydrolysis of VCFQYMDRGDR at 140 °C for 10 min.

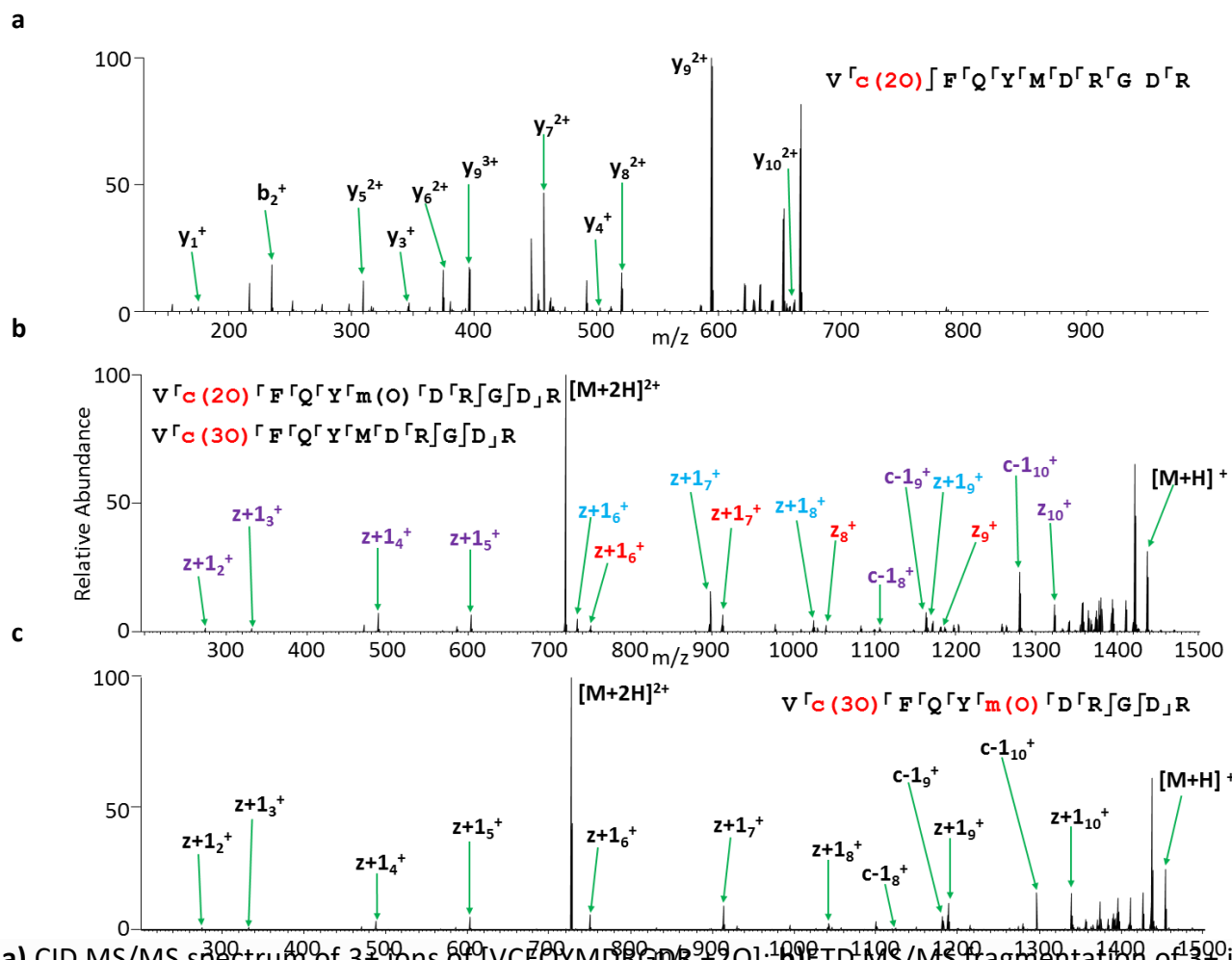


Figure 4. 7 - a) CID MS/MS spectrum of 3⁺ ions of [VCFQYMDRGDR +20]; **b)** ETD MS/MS fragmentation of 3⁺ ions of [VCFQYMDRGDR +30]. Fragments shown in purple belong to either species; fragments shown in red belong to the species with two oxidations on the cysteine and one on the methionine; fragments shown in blue belong to the species with three oxidations on the cysteine and **c)** ETD MS/MS spectrum of 2⁺ ions of [VCFQYMDRGDR +30]. Observed fragments are summarized on the peptide sequences, inset. Lower case denotes modified amino acid residues.

Peaks observed at m/z 479.8675 (+3) and m/z 719.2999 (+2) (m/z_{calc} 479.8677 and 719.2979) (**Figure 4.6b**) correspond to the peptide plus the addition of three oxygen atoms. Subsequent MS/MS analysis proved ambiguous, i.e., fragments from both Vc(3O)FQYMDRGDR and Vc(2O)FQYm(O)DRGDR were identified (**Figure 4.7b**). Furthermore, peaks corresponding to the loss of sulfinic acid (m/z 1371.6102), sulfonic acid (m/z 1355.6148), and methionine sulfoxide (m/z 1374.5942) side chains were observed (m/z_{calc} 1371.6099, 1355.6150, and 1374.5969). LC ETD MS/MS was performed and two species were seen to elute at retention times of ~11.5 min and ~13.5 min. ETD MS/MS of the species eluting at ~11.5 min revealed the presence of Vc(2O)FQYm(O)DRGDR and ETD MS/MS of the species eluting at ~13.5 min revealed the presence of Vc(3O)FQYMDRGDR (**Figure 4.8** and **Appendix Table 4.12**). Furthermore, the loss of the sulfinic acid side chain (m/z_{meas} 1371.6091, m/z_{calc} 1371.6099) was only observed in the ETD mass spectrum obtained at RT 11.5 min, and the loss of the sulfonic acid side chain (m/z_{meas} 1355.6128, m/z_{calc} 1355.6150) was only observed in the ETD mass spectrum obtained at RT 13.5 min.

The peak at m/z 727.2950 (**Figure 4.6b**), corresponding to the addition of four oxygen atoms (m/z_{calc} 727.2953), was isolated and fragmented by ETD MS/MS to reveal the addition of three oxygen atoms on the cysteine residue and the addition of one oxygen atom on the methionine residue (**Figure 4.7c** and **Appendix Table 4.13**).

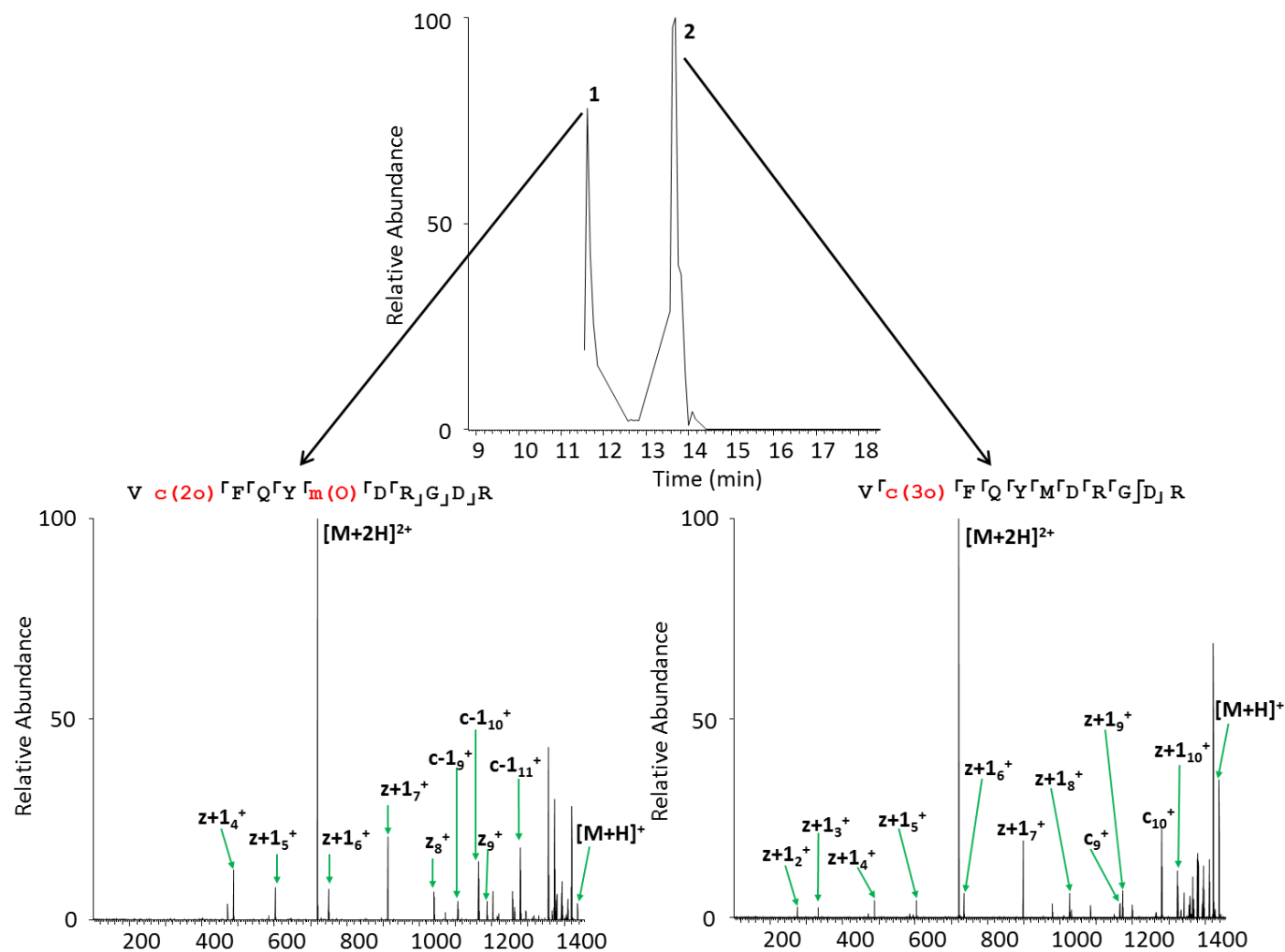


Figure 4.8 - a) - Extracted ion chromatogram (m/z 719.2973, [VCFQYMDRGDR +30]) obtained following LC ETD MS/MS and the two corresponding ETD MS/MS spectra at retention times 11 min 30 s and 13 min 30 s. Observed fragments are summarized on the peptide sequences, inset. Lower case denotes modified amino acid residues.

In addition to oxidation, extensive dehydration was observed for this peptide. This was attributed to the presence of two aspartic acid residues in the peptide sequence. Dehydration of the doubly oxidized species was observed (m/z_{meas} 468.5323 (+3) and 702.2950 (+2), m/z_{calc} 468.5322 and 702.2496), as was dehydration of the triply oxidized species (m/z_{meas} 473.8640 (+3) and 710.2924 (+2), m/z_{calc} 473.8638 and 710.2921). ETD MS/MS was performed; however, the site of water loss was ambiguous in all cases. The fragment ions observed for the species at m/z 468.5323 and 710.2924 is listed in **Appendix Tables 4.14 - 4.15**.

As with the previous peptide, cleavage at the C-terminal of the aspartic acid was also observed. Following cleavage at the Asp C-terminus peaks were observed corresponding to the addition of two oxygen atoms with (m/z 624.2444) and without water loss (m/z 633.2498) (m/z_{calc} 624.2446 and 633.2499), and addition of three oxygen atoms with (m/z 632.2418) and without water loss (m/z 641.2472) (m/z_{calc} 632.2421 and 641.2471).

The results above show that the most commonly occurring amino acid side-chain modifications following treatment with SCW are oxidation of cysteine and methionine residues. In order to determine whether other modifications might occur in the absence of those residues, SCW treatment was performed on (1) a model peptide VQSIKADFLHYENPTWGR that did not contain either cysteine or methionine and (2) the peptide VQSIKADFLHYMENPTWGR following capping of the cysteine residue.

4.4 SCW hydrolysis of model peptide VQSIKADFLHYENPTWGR

To further probe the effects of SCW hydrolysis on residues that were not cysteine or methionine, a synthetic peptide was designed, VQSIKADFLHYENPTWGR. The direct infusion ESI mass spectrum is shown in **Figure 4.9a (Appendix Table 4.16)**. The peptide was treated with SCW at 140 °C for 10 min. Direct infusion MS of the SCW-treated peptide revealed that the most abundant species was the unmodified peptide in the +3 charge state (**Figure 4.9b** and **Table 4.3**), in contrast to SCW-treated VQSIKADFLHYMENPTWGR, in which the major product was an oxidized form of the peptide.

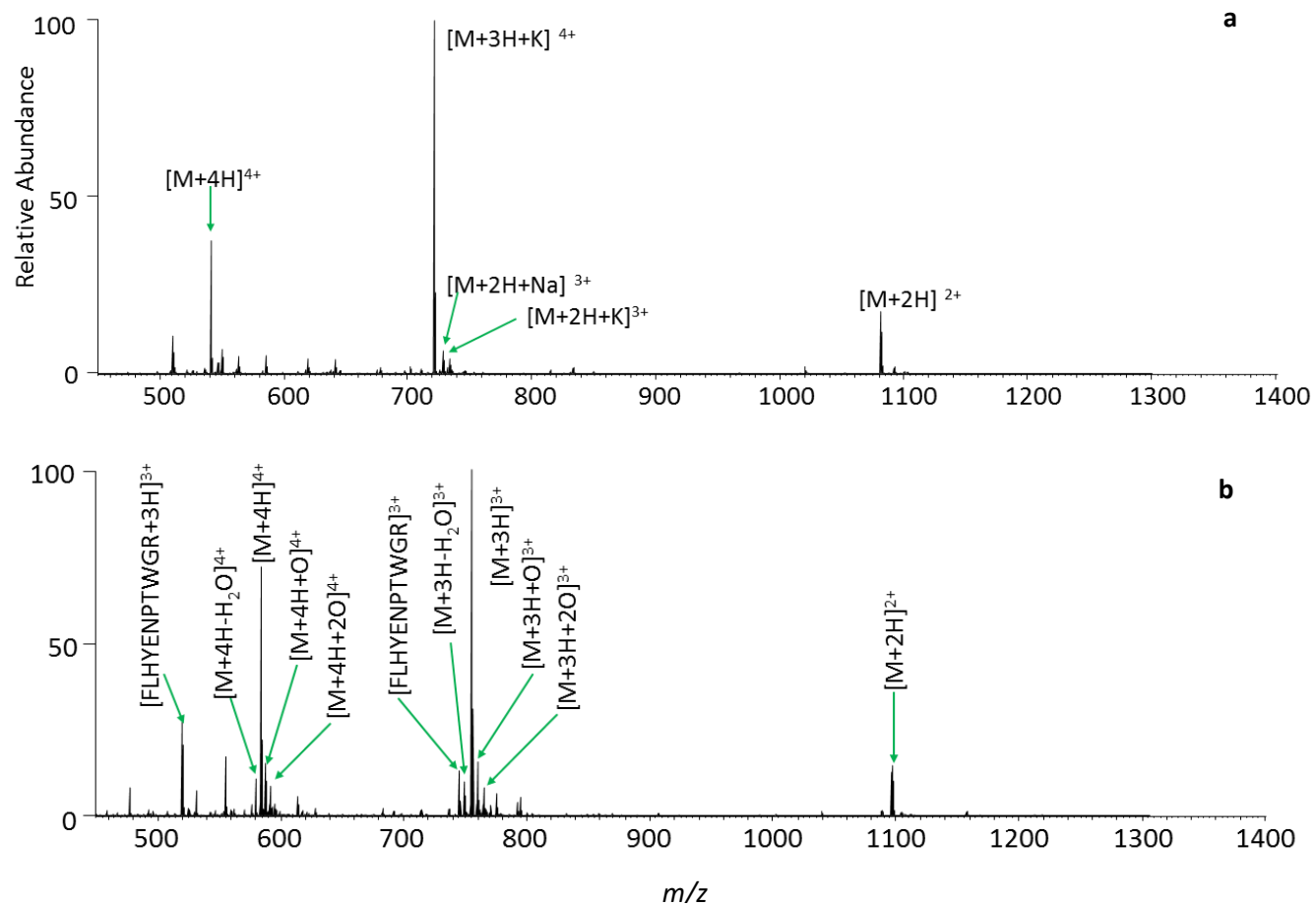


Figure 4. 9 a - Direct infusion electrospray MS of **a)** untreated peptide VQSIKADFLHYENPTWGR; **b)** of peptide VQSIKADFLHYENPTWGR treated with SCW at 140 °C for 10 min.

m/z	z	Calculated mass (Da)	Measured mass (Da)	Peptide	Δ PPM
473.9003	3	1418.6731	1418.6791	FLHYENPTWGR	4.2
536.5265	4	2142.0647	2142.0769	VQSIKADFLHYENPTWGR (-H ₂ O)	5.7
541.0280	4	2160.0752	2160.0829	VQSIKADFLHYENPTWGR	3.6
545.0272	4	2176.0701	2176.0797	VQSIKADFLHYENPTWGR (+O)	4.4
549.0260	4	2192.0650	2192.0749	VQSIKADFLHYENPTWGR (+2O)	4.5
710.3466	2	1418.6731	1418.6786	FLHYENPTWGR	3.9
715.0316	3	2142.0647	2142.0730	VQSIKADFLHYENPTWGR (-H ₂ O)	3.9
721.0348	3	2160.0752	2160.0826	VQSIKADFLHYENPTWGR	3.4
726.3670	3	2176.0701	2176.0792	VQSIKADFLHYENPTWGR (+O)	4.2
731.6989	3	2192.0650	2192.0749	VQSIKADFLHYENPTWGR (+2O)	4.5
1081.0483	2	2160.0752	2160.0820	VQSIKADFLHYENPTWGR	3.2

Table 4. 3 - Ions identified following SCW hydrolysis of VQSIKADFLHYENPTWGR at 140 °C for 10 min.

Peaks observed at m/z 545.0272 (+4) and m/z 726.3670 (+3) correspond to the peptide plus addition of a single oxygen atom (m/z_{calc} 545.0248 and 726.3640). ETD MS/MS of the ions with m/z 545.0272 confirmed that oxidation of the tryptophan residue had occurred (**Figure 4.10** and **Appendix Table 4.17**). The oxidation of tryptophan has previously been reported in proteomic studies [205, 206]. Peaks corresponding to the addition of two oxygen atoms to the peptide were also observed in the +4 and +3 charge states at m/z 549.0260 and m/z 731.6989 (m/z_{calc} 549.0235 and 731.6956). Analysis of the double oxidation product using CID MS/MS revealed that both oxidations occur on the tryptophan (**Figure 4.11** and **Appendix Table 4.18**). This is consistent with work by Taylor *et al.*, which shows tryptophan is able to adopt a second oxidation state in mitochondrial proteins [207]. A peak corresponding to the dehydrated peptide is observed under these conditions at m/z 715.0316 (m/z_{calc} 715.0288). Isolation of the ions and ETD MS/MS showed water loss to occur at the aspartic acid residue (**Figure 4.12** and **Appendix Table 4.19**). The loss of water from amino acid residues has previously been investigated by Sun *et al.*, who demonstrated that aspartic acid is a likely candidate [208]. Finally, for this peptide, an SCW hydrolysis cleavage product was observed at m/z 710.3466, corresponding to the peptide, FLHYENPTWGR (m/z_{calc} 710.3438).

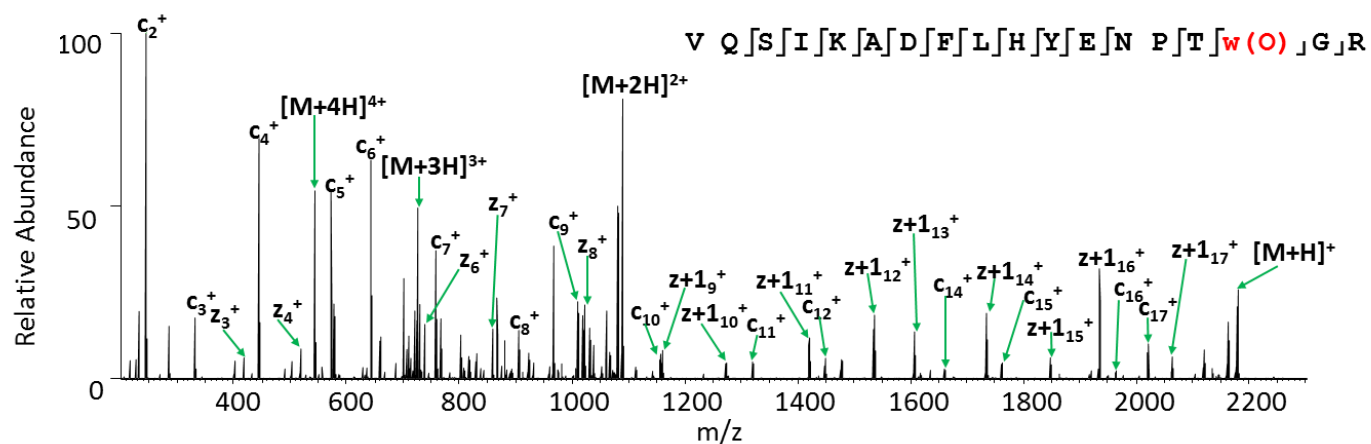


Figure 4. 10 -ETD MS/MS spectrum of 4+ ions of [VQSIKADFLHYENPTWGR+O].

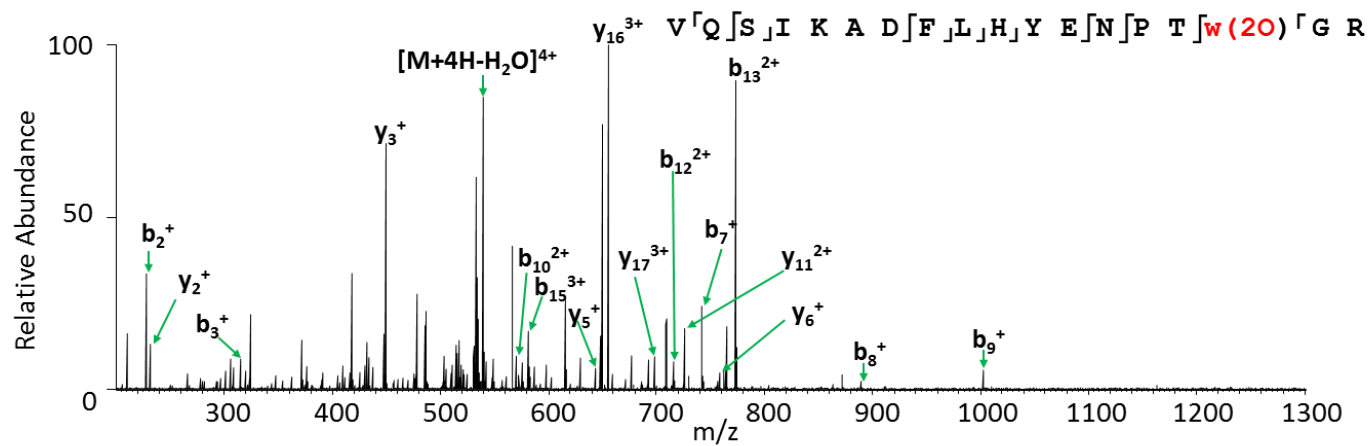


Figure 4. 11 - CID MS/MS spectrum of 4+ ions of [VQSIKADFLHYENPTWGR+2O].

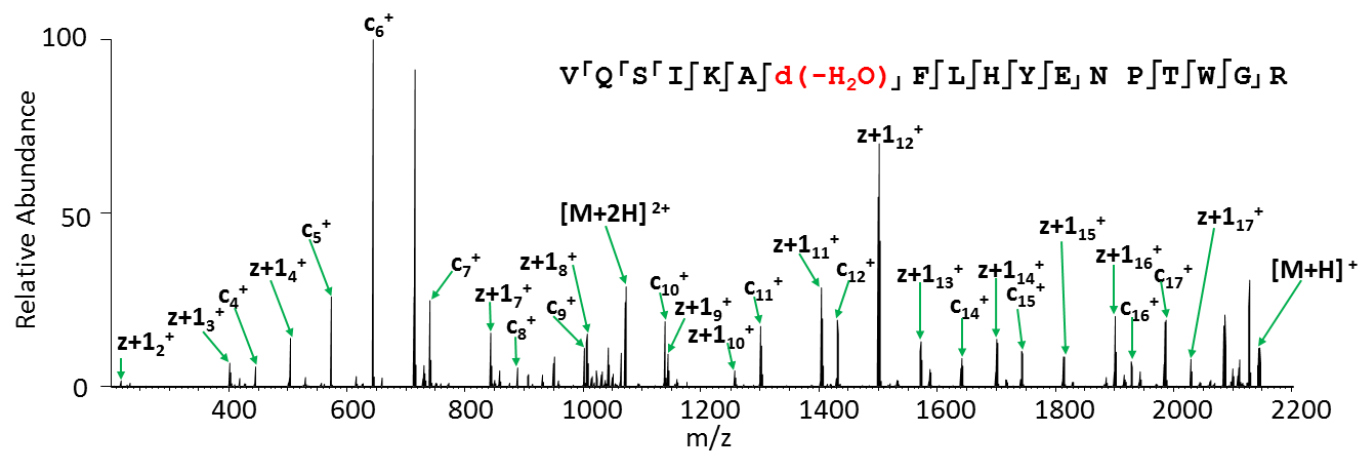


Figure 4. 12 - ETD MS/MS spectrum of 3+ ions of [VQSIKADFLHYENPTWGR- H₂O].

4.5 SCW hydrolysis of model peptide VQSIKCADFLHYMENPTWGR pre-treated with IAM

To further probe the effects of SCW hydrolysis on amino acids, the original peptide VQSIKCADFLHYMENPTWGR, was pre-treated with iodoacetamide prior to hydrolysis. This should ensure alkylation of cysteine residues and prevent its oxidation. Furthermore, it was discussed in **Chapter 3** that alkylating BSA prior to SCW hydrolysis offered increased sequence coverage under certain conditions. Understanding SCW modifications on proteins that have already been treated with IAM is therefore of interest.

Figure 4.13a shows the direct infusion electrospray mass spectrum of the iodoacetamide-treated peptide VQSIKCADFLHYMENPTWGR prior to SCW treatment (see also **Appendix Table 4.20**). CID MS/MS confirms carbamidomethylation of the cysteine residue (**Figure 4.14** and **Appendix Table 4.21**).

Figure 4.13b shows the direct infusion electrospray mass spectrum of the resulting mixture when the peptide VQSIKCADFLHYMENPTWGR pre-treated with iodoacetamide was subjected to SCW treatment at 140 °C for 10 min (see also **Table 4.4**). The most abundant multiply charged ions are the carbamidomethylated peptide ions in the 3+ charge state, observed at m/z 818.0517 (m/z_{calc} 818.0561). These species were also observed in the 4+ charge state (m/z_{meas} 613.7906; m/z_{calc} 613.7939). In addition, a single oxidation was seen to occur at m/z 617.7893 (+4) and 823.3833 (+3) (m/z_{calc} 617.7926 and 823.3877). The triply protonated species was fragmented by ETD, revealing that oxidation occurred on the methionine residue (**Figure 4.15** and **Appendix Table 4.22**).

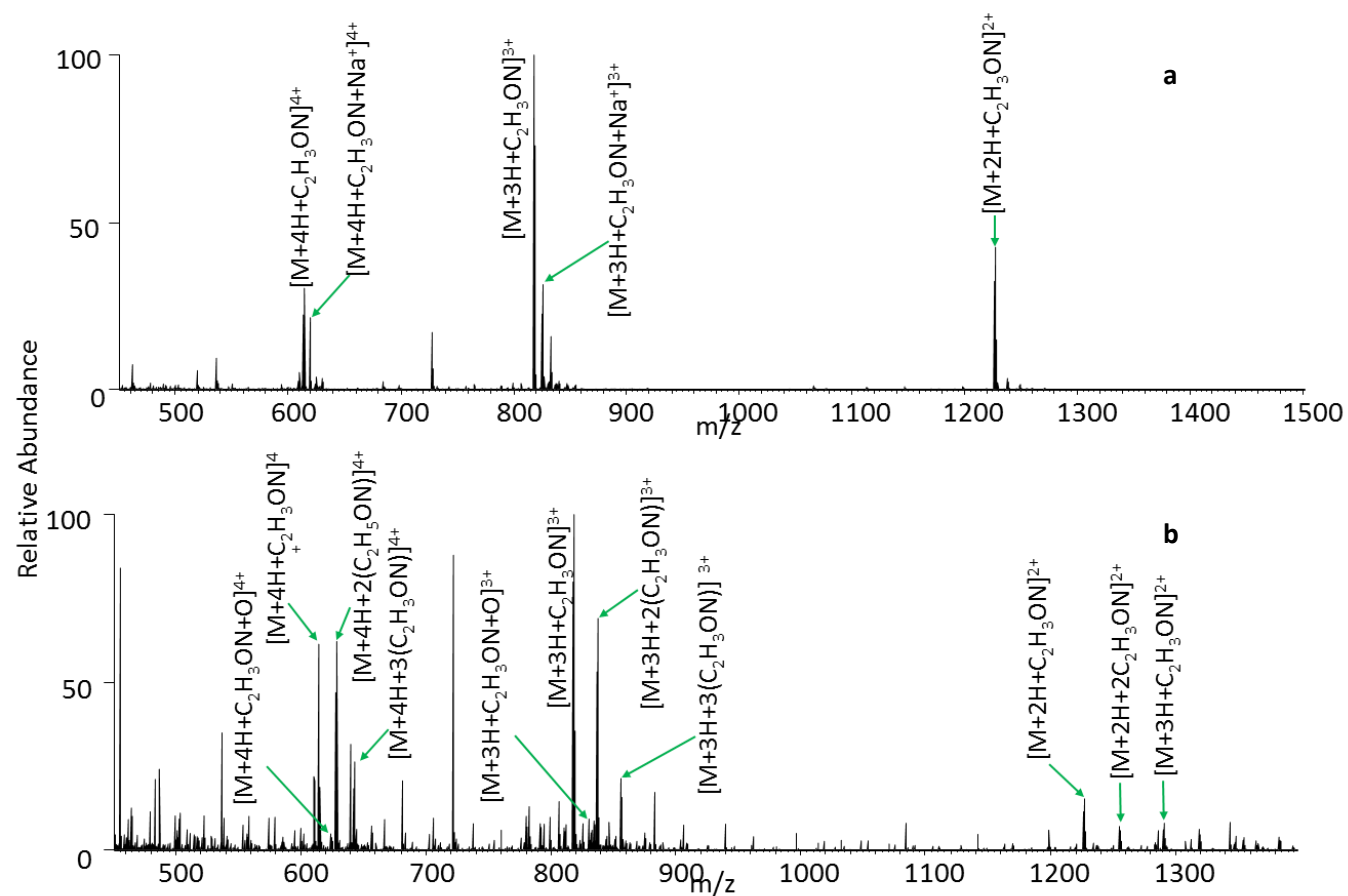
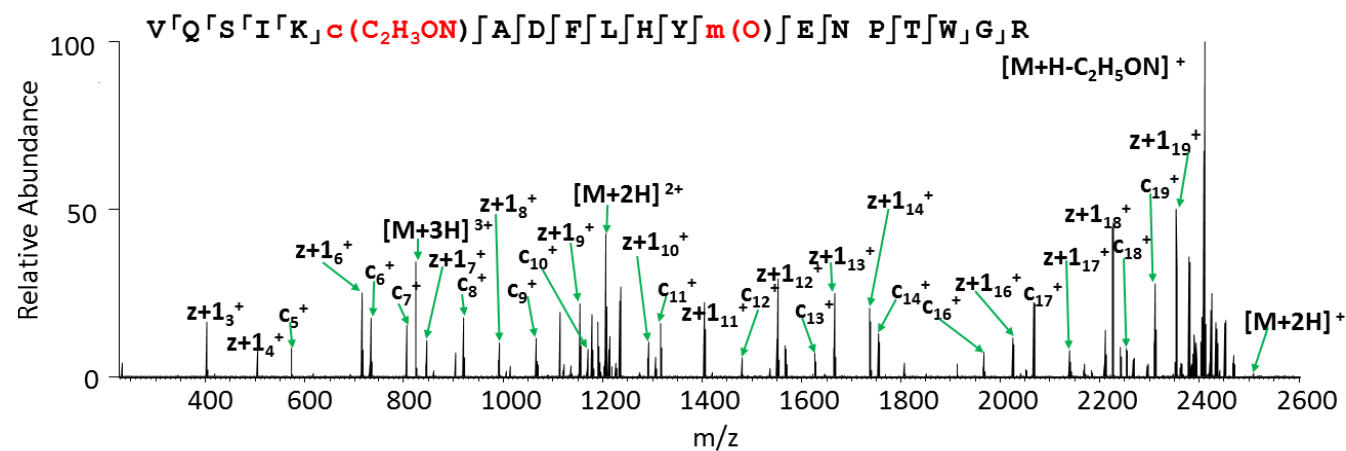
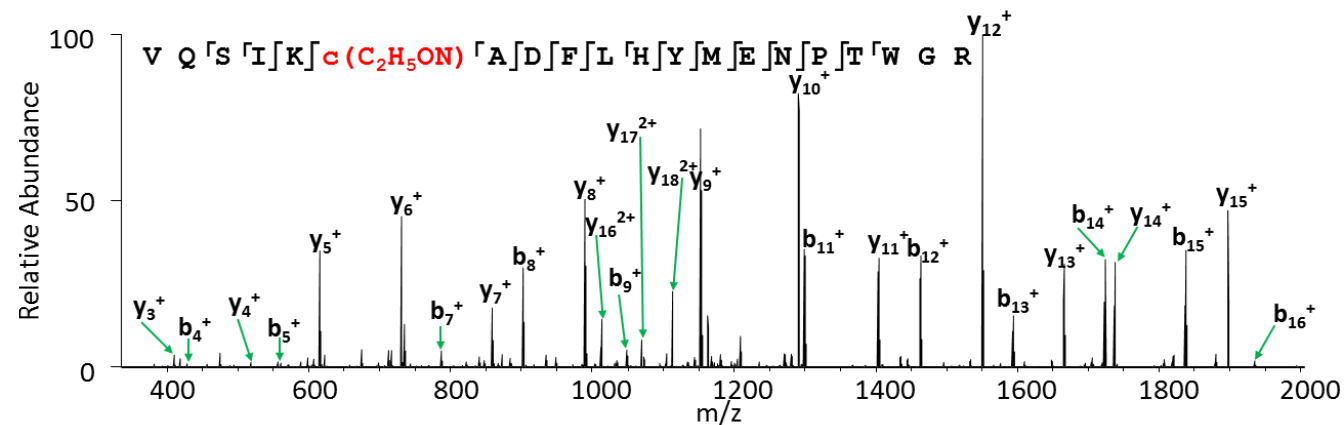


Figure 4. 13 a) Direct infusion electrospray MS of a) peptide VQSIKADFLHYMENPTWGR treated with iodoacetamide; b) VQSIKADFLHYMENPTWGR following iodoacetamide treatment treated with SCW at 140 °C for 10 min



<i>m/z</i>	<i>z</i>	Calculated mass (Da)	Measured mass (Da)	Peptide	Δ PPM
454.8248	1			Singly charged (unassigned)	
613.7906	4	2451.1464	2451.1333	VQSIKCADFLHYMENPTWGR (+ C ₂ H ₃ ON)	-5.3
617.7893	4	2467.1413	2467.1281	VQSIKCADFLHYMENPTWGR (+ C ₂ H ₃ ON + O)	-5.3
628.0459	4	2508.1678	2508.1545	VQSIKCADFLHYMENPTWGR (+2(C ₂ H ₃ ON))	-5.3
642.3011	4	2565.1893	2565.1753	VQSIKCADFLHYMENPTWGR (+3(C ₂ H ₃ ON))	-5.5
721.6640	1			Singly charged (unassigned)	
818.0517	3	2451.1464	2451.1333	VQSIKCADFLHYMENPTWGR (+ C ₂ H ₃ ON)	-5.3
823.3833	3	2467.1413	2467.1281	VQSIKCADFLHYMENPTWGR (+ C ₂ H ₃ ON + O)	-5.4
837.0587	3	2508.1678	2508.1543	VQSIKCADFLHYMENPTWGR (+2(C ₂ H ₃ ON))	-5.4
856.0685	3	2565.1893	2565.1837	VQSIKCADFLHYMENPTWGR (+3(C ₂ H ₃ ON))	-2.2
1226.5742	2	2451.1464	2451.1338	VQSIKCADFLHYMENPTWGR (+ C ₂ H ₃ ON)	-5.1
1255.0846	2	2508.1678	2508.1546	VQSIKCADFLHYMENPTWGR (+2(C ₂ H ₃ ON))	-5.3
1283.5925	2	2565.1893	2565.1704	VQSIKCADFLHYMENPTWGR (+3(C ₂ H ₃ ON))	-7.4

Table 4. 4 - Ions observed following SCW hydrolysis of iodoacetamide pre-treated VQSIKCADFLHYMENPTWGR at 140 °C for 10 min.

Interestingly, the addition of a further carbamidomethyl group to the peptide, observed at m/z 628.0459 (+4), 837.0587 (+3), 1255.0846 (+2) (m/z_{calc} 628.0492, 837.0632, and 1255.0912), as well as species with three carbamidomethyl groups at m/z 642.3011 (+4), 856.0685 (+3), and 1283.5925 (+2) (m/z_{calc} 642.3046, 837.0704, and 1283.6019) was observed. That is, the excess iodoacetamide present in the sample further alkylates the peptide under SCW conditions. Alkylation of cysteine by iodoacetamide occurs via nucleophilic substitution ($\text{S}_{\text{N}}2$) at basic pH. It is also known that under certain conditions (pH, concentration, length of incubation), alkylation of other amino acid residues (methionine, histidine, lysine, tyrosine, glutamic acid, and aspartic acid) and the N-terminus or C-terminus by iodoacetamide can occur [209-213]. The data suggests that SCW promotes substitution by other nucleophiles. It was not possible to determine the sites of modification due to the composite MS/MS spectra obtained, even when coupled with liquid chromatography. **Appendix Table 4.23** summarises the CID MS/MS for the ions observed at m/z 837.0587 demonstrating the multiple species observed.

The presence of nonspecific carbamidomethylation could be detrimental for proteomics analysis and therefore the effect of quenching excess iodoacetamide with dithiothreitol [211] prior to SCW treatment was investigated.

Figure 4.16a shows the direct infusion electrospray mass spectrum of the iodoacetamide and DTT-treated peptide VQSIKCADFLHYMENPTWGR before and after SCW treatment at 140 °C for 10 min. Both spectra are dominated by singly charged ions, likely due to the excess of both iodoacetamide and dithiothreitol. The singly carbamidomethylated peptide is observed at m/z 818.0562 (+3) and 1226.5809 (+2), and there is no evidence for multiple carbamidomethylation. Peaks corresponding to addition of hydrogen and iodine to carbamidomethylated peptides are observed in both the non-SCW treated sample at m/z 1290.5372 and m/z 1354.4932, and the SCW treated sample at m/z 1290.5365 and m/z 1354.4926 (m/z_{calc} 1290.5366 and 1354.4928). These modifications were not observed in the non-DTT treated sample. Furthermore, methionine oxidation was not observed under these conditions.

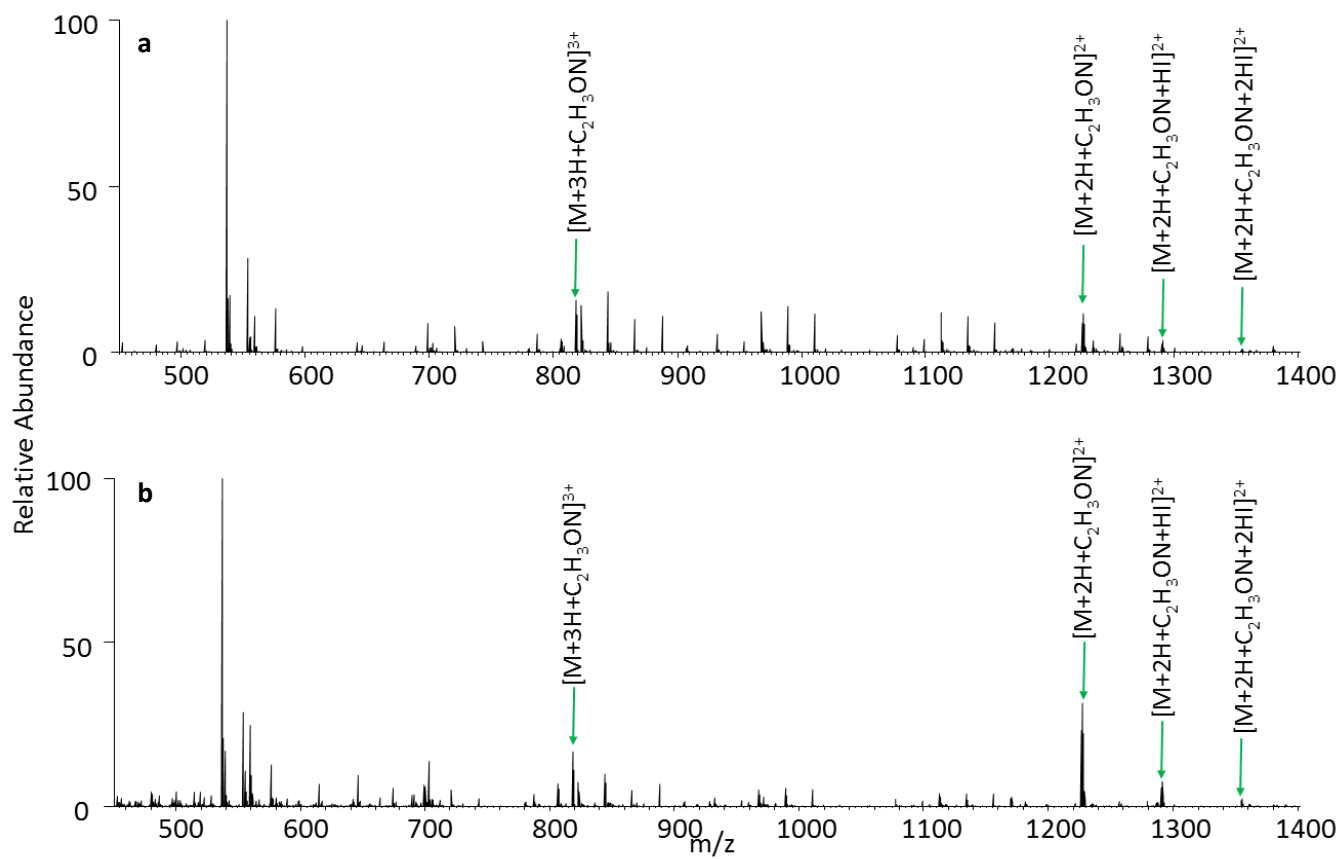


Figure 4. 16 - Direct infusion electrospray MS of peptide VQSICKADFLHYENPTWGR treated with iodoacetamide and DTT **a)** prior to SCW hydrolysis and **b)** hydrolysed at 140°C for 10 minutes.

4.6 Conjugation reactions using SCW

These results presented in section 4.4 suggest SCW could be effective in catalysing nucleophilic interactions. Whilst SCW is effective in catalysing various organic reactions [214], using this technology to promote S_N2 reactions has not been well studied.

In Section 1.5 the various benefits of dietary antioxidants are discussed. Aydemir and Yemenicioglu recently investigated the antioxidant activity of lentils, which are rich in phenolic content [215]. The authors hypothesise that phenolic compounds are initially bound to proteins, but are subsequently released in their free form during digestion. They speculate this is the major contributing factor behind the health benefits associated with phenolic rich pulses and other legume seeds. If an effective method of conjugating phenolic compounds to proteins could be realised, it may prove beneficial in the production of artificial antioxidants.

Having already demonstrated iodine as a leaving group in a SCW catalysed S_N2 reaction, investigating whether an element with similar chemical properties behaves in the same way is of interest. Secondly, it is important to investigate whether cyclic compounds would conjugate in the same way as IAM. Here the conjugation of the cyclic compound, benzyl bromide, to the peptide VQSIKCADFLHYMENPTWGR was investigated.

The peptide was incubated with an equimolar amount of benzyl bromide (15 μ M) and hydrolysed at 140 °C for 10, 30 and 60 minute time points. **Figure 4.17** shows the direct infusion electrospray mass spectrum of the peptide incubated with benzyl bromide for 10 minutes at room temperature (see also **Table 4.5**). The most intense peak in the mass spectrum at m/z 799.0440 corresponds to the triply protonated ions of the peptide with no modifications (m/z_{calc} 799.0489). This species was also observed in the +2 and +4 charge states at m/z 599.5349 and m/z 1198.0612 (m/z_{calc} 599.8385 and 1198.0697). The peak at m/z 829.0589 corresponds to the peptide with a benzyl group conjugated (m/z_{calc} 829.4003). This species was also observed in the +2 and +4 charge states, albeit at low abundance at m/z 1243.0843 and 622.0462 (m/z_{calc}

1243.0362 and 622.0502). It was not possible to determine the sites of conjugation due to the composite MS/MS spectra obtained, even when coupled with liquid chromatography. The fragment ions observed from the CID MS/MS of the ion at m/z 622.0462 are listed in **Appendix Table 4.24**.

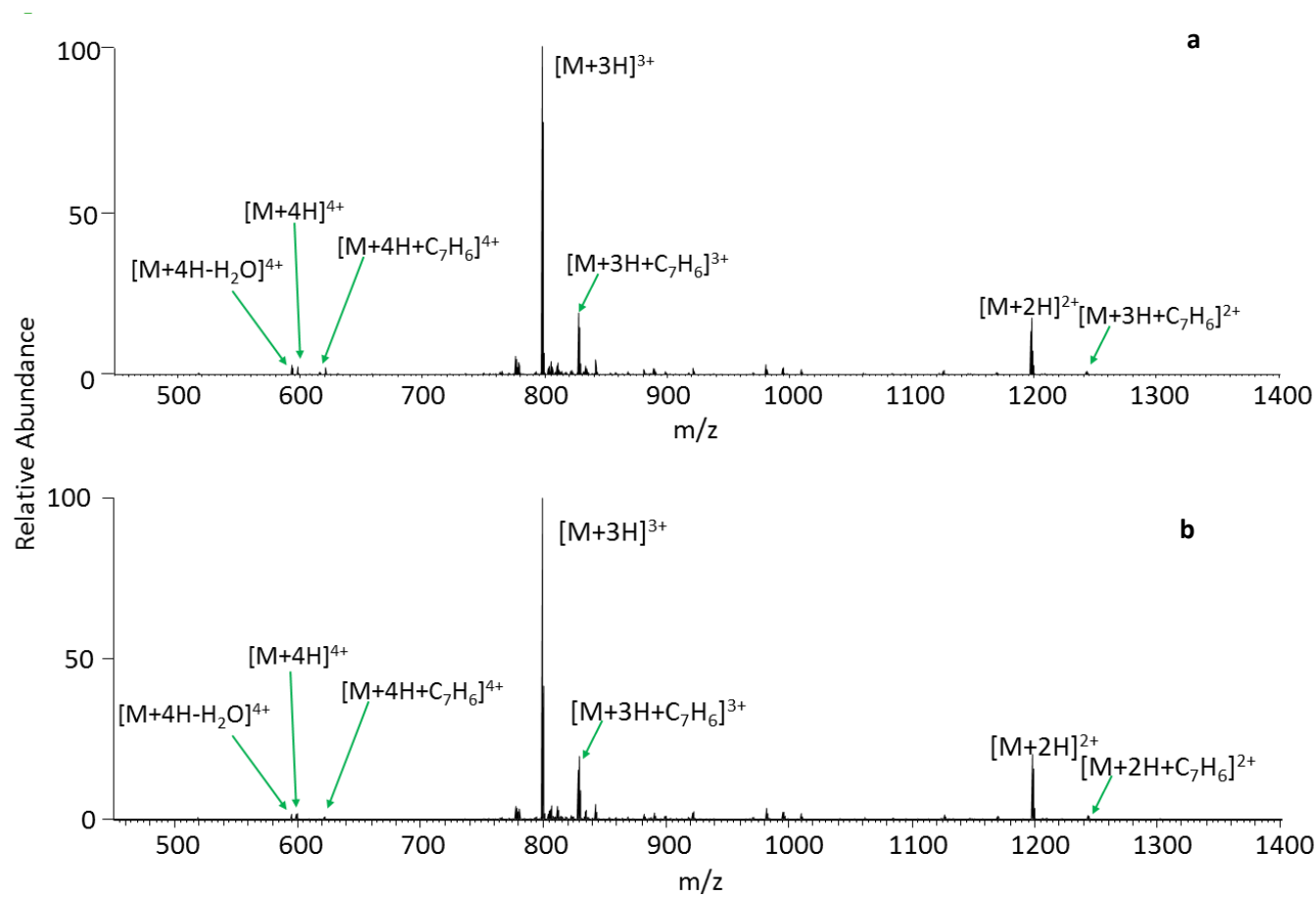


Figure 4. 17 - Direct infusion electrospray MS of peptide VQSIKCADFLHYENPTWGR incubated with benzyl bromide for **a)** 10 minutes at room temperature and **b)** 60 minutes at room temperature.

Room temperature 10 minutes					
<i>m/z</i>	<i>z</i>	Calculated mass (Da)	Measured mass (Da)	Peptide	Δ PPM
595.0323	4	2376.1144	2376.1001	VQSIKADFLHYMENPTWGR (-H ₂ O)	-6.0
599.5349	4	2394.1249	2394.1105	VQSIKADFLHYMENPTWGR	-6.0
622.0462	4	2484.1719	2484.1557	VQSIKADFLHYMENPTWGR (+C ₇ H ₆)	-6.5
799.0440	3	2394.1249	2394.1102	VQSIKADFLHYMENPTWGR	-6.2
829.0589	3	2484.1719	2484.1549	VQSIKADFLHYMENPTWGR (+C ₇ H ₆)	-6.9
1198.0612	2	2394.1249	2394.1078	VQSIKADFLHYMENPTWGR	-7.1
1243.0843	2	2484.1719	2484.1540	VQSIKADFLHYMENPTWGR (+C ₇ H ₆)	-7.2
Room temperature 60 minutes					
<i>m/z</i>	<i>z</i>	Calculated mass (Da)	Measured mass (Da)	Peptide	Δ PPM
595.0320	4	2376.1144	2376.0989	VQSIKADFLHYMENPTWGR (-H ₂ O)	-6.5
599.5349	4	2394.1249	2394.1105	VQSIKADFLHYMENPTWGR	-6.0
622.0463	4	2484.1719	2484.1561	VQSIKADFLHYMENPTWGR (+C ₇ H ₆)	-6.4
799.0440	3	2394.1249	2394.1102	VQSIKADFLHYMENPTWGR	-6.2
829.0589	3	2484.1719	2484.1549	VQSIKADFLHYMENPTWGR (+C ₇ H ₆)	-6.9
1198.0613	2	2394.1249	2394.1080	VQSIKADFLHYMENPTWGR	-7.0
1243.0844	2	2484.1719	2484.1542	VQSIKADFLHYMENPTWGR (+C ₇ H ₆)	-7.1
140°C 10 minutes					
<i>m/z</i>	<i>z</i>	Calculated mass (Da)	Measured mass (Da)	Peptide	Δ PPM
595.0324	4	2376.1144	2376.1005	VQSIKADFLHYMENPTWGR (-H ₂ O)	-5.8
599.5348	4	2394.1249	2394.1101	VQSIKADFLHYMENPTWGR	-6.2
622.0462	4	2484.1719	2484.1557	VQSIKADFLHYMENPTWGR (+C ₇ H ₆)	-6.5
799.0441	3	2394.1249	2394.1105	VQSIKADFLHYMENPTWGR	-6.0
829.0587	3	2484.1719	2484.1543	VQSIKADFLHYMENPTWGR (+C ₇ H ₆)	-7.1
1198.0613	2	2394.1249	2394.1080	VQSIKADFLHYMENPTWGR	-7.1
140°C 30 minutes					
<i>m/z</i>	<i>z</i>	Calculated mass (Da)	Measured mass (Da)	Peptide	Δ PPM
517.5785	3	1549.7136	1549.7137	FLHYMENPTWGR	0.0
547.5942	3	1639.7606	1639.7608	FLHYMENPTWGR (+C ₇ H ₆)	0.1
595.0352	4	2376.1144	2376.1117	VQSIKADFLHYMENPTWGR (-H ₂ O)	-1.1
599.5385	4	2394.1249	2394.1249	VQSIKADFLHYMENPTWGR	0.0
622.0502	4	2484.1719	2484.1717	VQSIKADFLHYMENPTWGR (+C ₇ H ₆)	-0.1
775.8644	2	1549.7136	1549.7142	FLHYMENPTWGR	0.4
799.0489	3	2394.1249	2394.1249	VQSIKADFLHYMENPTWGR	0.0
829.0647	3	2484.1719	2484.1723	VQSIKADFLHYMENPTWGR (+C ₇ H ₆)	0.1

859.0805	3	2574.2188	2574.2197	VQSIKADFLHYMENPTWGR (+2C ₇ H ₆)	0.3
1001.4988	2		2000.9830	Unassigned	
1066.0212	2		2130.0278	Unassigned	
1198.0693	2	2394.1249	2394.1240	VQSIKADFLHYMENPTWGR	-0.4
1238.0331	2	2474.0516	2474.0516	VQSIKADFLHYMENPTWGR (+HBr)	0.0
1243.0918	2	2484.1719	2484.1690	VQSIKADFLHYMENPTWGR (+C ₇ H ₆)	-1.1
1277.9962	2	2553.9783	2553.9778	VQSIKADFLHYMENPTWGR (+2HBr)	-0.2
1283.0563	2	2564.0986	2564.0980	VQSIKADFLHYMENPTWGR (+C ₇ H ₆ + HBr)	-0.2
140°C 60 minutes					
<i>m/z</i>	<i>z</i>	Calculated mass (Da)	Measured mass (Da)	Peptide	ΔPPM
502.9179	3		1505.7319	unassigned	
517.5778	3	1549.7136	1549.7116	FLHYMENPTWGR	-1.3
547.5934	3	1639.7606	1639.7584	FLHYMENPTWGR (+C ₇ H ₆)	-1.4
577.6093	3	1729.8076	1729.8061	FLHYMENPTWGR (+2C ₇ H ₆)	-0.9
595.0341	4	2376.1144	2376.1073	VQSIKADFLHYMENPTWGR (-H ₂ O)	-3.0
599.5377	4	2394.1249	2394.1217	VQSIKADFLHYMENPTWGR	-1.3
616.3193	1	615.3124	615.3120	PTWGR	-0.6
622.0494	4	2484.1719	2484.1685	VQSIKADFLHYMENPTWGR (+C ₇ H ₆)	-1.4
644.5610	4	2574.2189	2574.2149	VQSIKADFLHYMENPTWGR (+2 C ₇ H ₆)	-1.5
667.0732	4	2664.2658	2664.2637	VQSIKADFLHYMENPTWGR (+3 C ₇ H ₆)	-0.8
753.8731	2		1505.7316	unassigned	
775.8630	2	1549.7136	1549.7114	FLHYMENPTWGR	-1.4
799.0481	3	2394.1249	2394.1225	VQSIKADFLHYMENPTWGR	-1.0
820.8863	2	1639.7606	1639.7580	FLHYMENPTWGR (+C ₇ H ₆)	-1.6
829.0634	3	2484.1719	2484.1684	VQSIKADFLHYMENPTWGR (+C ₇ H ₆)	-1.4
859.0791	3	2574.2189	2574.2155	VQSIKADFLHYMENPTWGR (+2 C ₇ H ₆)	-1.3
865.9097	2	1729.8076	1729.8048	FLHYMENPTWGR (+2 C ₇ H ₆)	-1.6
889.0944	3	2664.2658	2664.2614	VQSIKADFLHYMENPTWGR (+3 C ₇ H ₆)	-1.7
1198.0662	2	2394.1249	2394.1178	VQSIKADFLHYMENPTWGR	-2.9
1238.0319	2	2474.0516	2474.0492	VQSIKADFLHYMENPTWGR (+HBr)	-1.0
1243.0912	2	2484.1719	2484.1678	VQSIKADFLHYMENPTWGR (+C ₇ H ₆)	-1.6
1277.9942	2	2553.9783	2553.9738	VQSIKADFLHYMENPTWGR (+2HBr)	-1.7
1283.0563	2	2564.0986	2564.0908	VQSIKADFLHYMENPTWGR (+C ₇ H ₆ + HBr)	-0.2
1323.0165	2	2644.0253	2644.0184	VQSIKADFLHYMENPTWGR (+C ₇ H ₆ + 2 HBr)	-2.6

Table 4. 5 - Ions Observed Following SCW hydrolysis of benzyl bromide pre-treated VQSIKADFLHYMENPTWGR at room temperature for 0 and 60 minutes and 140°C for 10, 30 and 60 minutes.

Figure 4.17b shows the direct infusion electrospray mass spectrum of the peptide incubated with benzyl bromide for 60 minutes at room temperature. There is no significant difference in the mass spectra obtained when compared to that obtained when the incubation period was 10 minutes.

The peptide-benzyl bromide mixture was hydrolysed at 140 °C for 10 minutes (**Figure 4.18a**). No additional peaks were observed under these conditions. This is in contrast to the results observed when the peptide was incubated with IAA at 140 °C for 10 minutes, where a limited amount of cleavage product was observed as well as increased conjugation. Furthermore, no additional oxidation was observed. It is unclear why these results were observed.

Figure 4.18b shows the direct infusion electrospray mass spectrum of the resulting mixture when the peptide pre-treated with benzyl bromide was hydrolysed at 140 °C for 30 min. The most abundant species observed was the peptide with no modifications at m/z 599.5385 (+4), 799.0489 (+3) and 1198.0693 (+2). I also observe a dehydration product at m/z 595.0352 as well as addition of a benzyl group at m/z 622.0502.

Increased conjugation was observed following the longer residency time. The addition of two benzyl groups to the peptide was observed at m/z 859.0805 (m/z_{calc} 859.0802). Interestingly, the addition of one (m/z 1238.0331) and two (m/z 1277.9962) hydrogen bromide (HBr) molecules to the peptide were also identified (m/z_{calc} 1238.0331 and 1277.9964). In Section 4.5 additions of hydrogen iodide were observed when the peptide was hydrolysed with IAA in the presence of DTT. This observation confirms SCW may help catalyse reactions other than nucleophilic substitution. The addition of HBr and a benzyl group to the same peptide at m/z 1283.0563 was also noted (m/z_{calc} 1283.0566).

Moreover, a cleavage product was detected at m/z 517.5785 (m/z_{calc} 517.5785). This is a result of cleavage next to the C-terminal of aspartic acid, which is consistent with the results obtained thus far. The conjugation of a benzyl group to this product was observed at m/z 547.5942 (m/z_{calc} 547.5941).

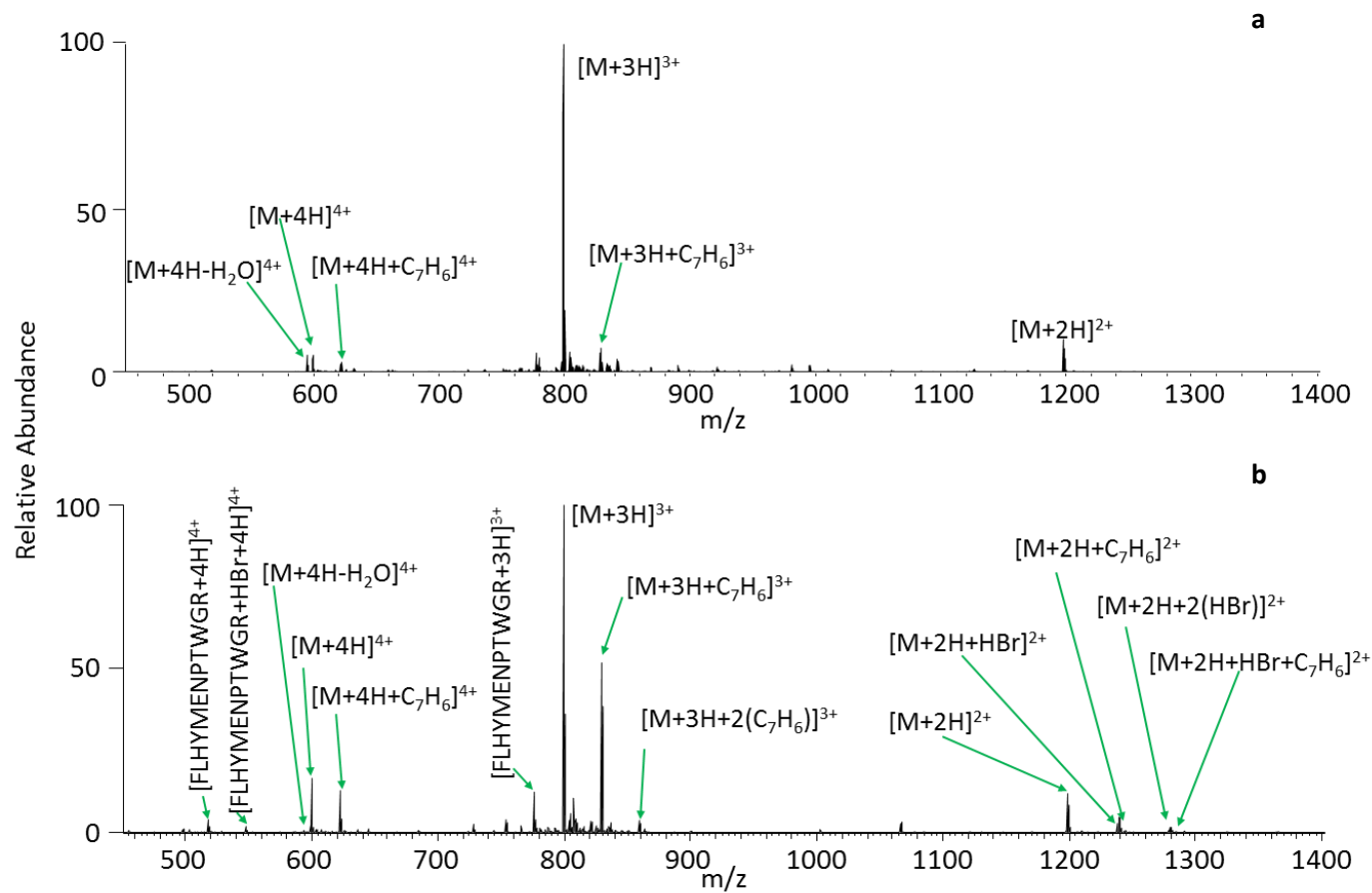


Figure 4. 18 - Direct infusion electrospray MS of peptide VQSIKADFLHYENPTWGR incubated with benzyl bromide hydrolysed at **a)** 140°C for 10 minutes; **b)** 140°C for 30 minutes and **c)** 140°C for 60 minutes.

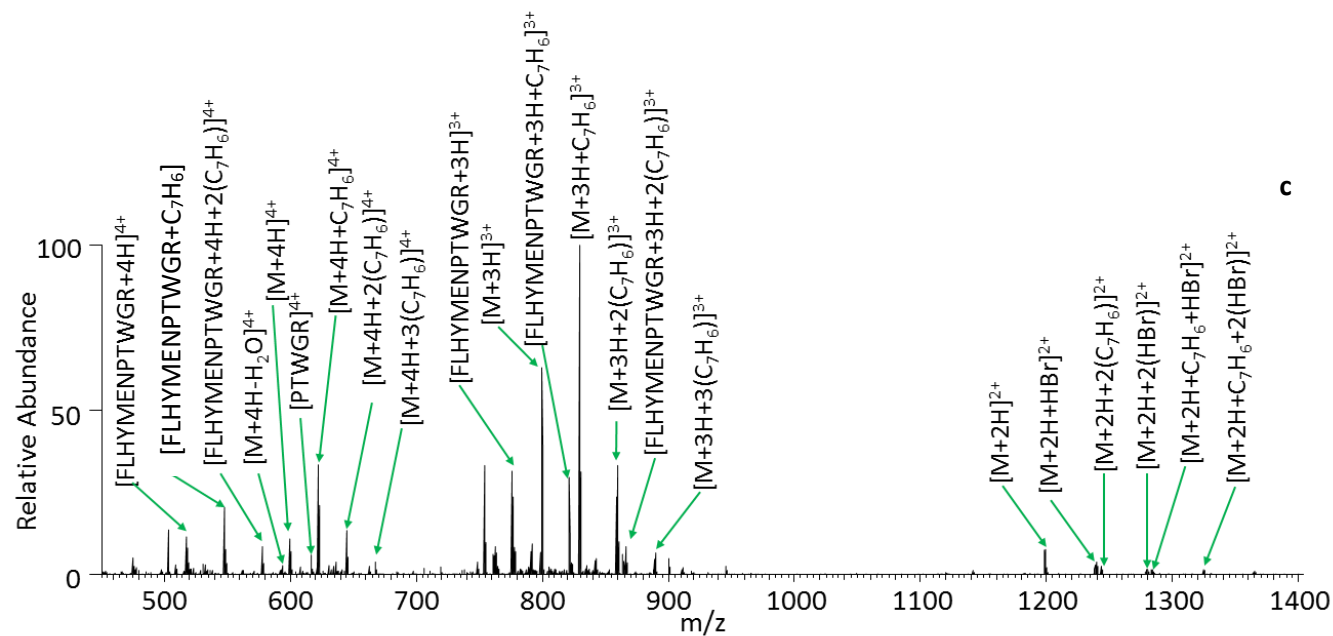


Figure 4. 18 (continued) - Direct infusion electrospray MS of peptide VQSIKADFLHYENPTWGR incubated with benzyl bromide hydrolysed at **a)** 140°C for 10 minutes; **b)** 140°C for 30 minutes and **c)** 140°C for 60 minutes.

The peptide-benzyl bromide mixture was also hydrolysed at 140 °C for 60 min. The direct infusion electrospray mass spectrum is shown in **Figure 4.18c**. Conjugation of benzyl bromide to the peptide noticeably increased under these conditions. The base peak in this mass spectrum corresponds to the addition of a benzyl group to the peptide in the +3 charge state (m/z 829.0634). This species was also observed in the +4 (m/z 622.0494) and +2 charge states (m/z 1243.0492). This observation is in contrast to the previous time points where the unmodified peptide was the base peak, observed here at m/z 599.5377 (+4), 799.0481 (+3) and 1198.0662 (+2). Furthermore, an increased abundance of the peptide which has two benzyl groups conjugated at m/z 644.5610, 859.0791 and 1277.9942 (m/z_{calc} 644.5620, 859.0802, 1277.9964) was noted. Moreover, the peptide with three benzyl groups attached was observed at m/z 667.0732 and 889.0944 (m/z_{calc} 667.0737 and 889.0959). The observation of peptide with the addition of: HBr (m/z 1238.0319), 2HBr (m/z 1277.9943), HBr and C_7H_6 (m/z 1283.0563), and 2HBr and C_7H_6 (m/z 1323.0165) were also noted (m/z_{calc} 1238.0331, 1277.9964, 1283.0566 and 1323.0199). Note the additions of multiple benzyl groups or HBr was not observed when incubated at room temperature for 60 minutes (**Figure 1.7b**).

A species resulting from cleavage at the C-terminal of aspartic acid was also observed (m/z 517.5778). Conjugation of a benzyl group to this species was observed at m/z 547.5934 (+3) and 820.8863 (+2) (m/z_{calc} 547.5941 and 820.8876). The addition of a second benzyl group to this peptide was also noted at m/z 577.6093 (m/z_{calc} 577.6098). Furthermore, under this time point the cleavage product PTWGR at m/z 616.3193 (m/z_{calc} 616.3197) resulting from non-specific cleavage was observed.

4.6 Re-analysis of Chapter 3 data

In light of the above results, the data obtained from the SCW treatment of proteins in Chapter 3 were re-analyzed. The data were searched against the relevant protein sequence as obtained from UniProt using the SEQUEST algorithm in Proteome Discoverer ver. 1.4.1.14 (Thermo Fisher Scientific). Data were searched using “nonspecific enzyme.” Precursor tolerance was 10 ppm and MS/MS tolerance was 0.5 Da. The following were allowed as dynamic modifications: addition of two and three oxygen atoms on cysteine, addition of one and two oxygen atoms on tryptophan, water loss from aspartic acid residues, C-terminal amidation and methionine oxidation. (Note that methionine oxidation was also allowed as dynamic modification in the previous analysis) The database search resulted in an increase in the number of identified peptides. An additional 108 (that is, an increase of 63.1%), 121 (38.7%), and 64 (34.2%) peptides were identified for α -globin hydrolysed at 160 °C for 0 min, 160 °C for 20 min, and 207 °C for 20 min. A further 69 (increase of 24.3%), 96 (31.1%), and 74 (48.7%) peptides were identified in β -globin hydrolysed at 160 °C for 0 min, 160 °C for 20 min, and 207 °C for 20 min. Twenty-eight (28.3%), 91 (37.0%), and 58 (25.3%) further peptides were identified for BSA hydrolysed at 160 °C for 0 min, 160 °C for 20 min, and 207 °C for 20 min. Thirteen (9%), 163 (25.2%), and 168 (23.5%) additional peptides were identified for β -casein hydrolysed at 160 °C for 0 min, 160 °C for 20 min, and 207 °C for 20 min. No significant increase in overall sequence coverage was observed, however these were already very high under these conditions. Understanding additional reactions that occur under sub critical conditions may be of further use when analysing more complex mixtures of proteins.

4.7 Conclusion

The work presented in this chapter shows that SCW hydrolysis of peptides results in efficient oxidation of the hydrolysates. SCW treatment under mild conditions (140 °C for 10 min) resulted in oxidation of cysteine and methionine residues. Oxidation of cysteine to sulfinic and sulfonic acid was observed. SCW treatment of a peptide that did not contain cysteine or methionine resulted in oxidation of tryptophan. Under harsher SCW conditions (160 °C- 200 °C), dehydration and amidation of the peptides were detected. Water loss occurs at aspartic acid. In addition, the C-terminal of aspartic acid is consistently shown to be a site of preferential cleavage for SCW.

Furthermore, these results suggest that SCW hydrolysis can catalyse nucleophilic substitution reactions. Amino acid side chains are more likely to participate in SN2 reactions with both benzyl bromide and iodoacetamide under sub-critical conditions, when compared to incubation at room temperature. The ability of SCW to catalyse conjugation reactions could be explored in future work, potentially in the binding of antioxidant compounds to proteins.

Chapter 5: Sub-critical antioxidant extraction from protein

5.1 Overview

The brewing industry generates large amounts of by-products and wastes, the most common being brewer's spent grain (BSG). A sample of BSG was supplied by Phytatec UK. A sample of barley grain that is typically used as a brewing starting reactant was also supplied as a comparison. Extraction details are described in Section 2.1.

Prior to this work, sub-critical water has been used in the extraction of antioxidant compounds from a variety of sources. This capability has been discussed in detail in Chapter 1.5. Antioxidants are substances which inhibit oxidation and can remove damaging reactive oxygen species (ROS) during oxidative stress. Oxidative stress has been linked to many diseases including cancer; Parkinson's disease and atherosclerosis [216-218].

The aim of the work presented in this chapter was to determine whether SCW treatment of BSG would result in production of peptides with antioxidant properties. The antioxidant capacity of each substance was assessed using the ORAC assay [139], a valuable tool in assessing ex-vivo antioxidant potential. To provide confirmation of the results obtained from the ORAC assay, the antioxidant potential of the generated compounds was further assessed using reducing power [134] and comet assays [136].

The results suggest that it is not in fact the peptides, but small molecule products that show antioxidant properties. The structure of these antioxidant components was identified using HCD MS/MS and potential mechanisms of formation are discussed.

5.2 Characterisation of hordein extract

Two protein extracts were supplied by Phytatec UK. The first was extract from the barley blend 'Golden Promise'. In this thesis, the protein extract is termed non-treated grain (NTG). The second extract was from the same blend which had undergone malting and mashing, i.e. 'brewer's spent grain' (BSG). Protein extraction was performed using methods described in Section 2.1. These conditions are specific for the extraction of the hordein family of proteins.

The protein extracts were analysed by SDS-PAGE, see **Figure 5.1**. Protein bands were assigned based on classifications of hordein from published work [219, 220].

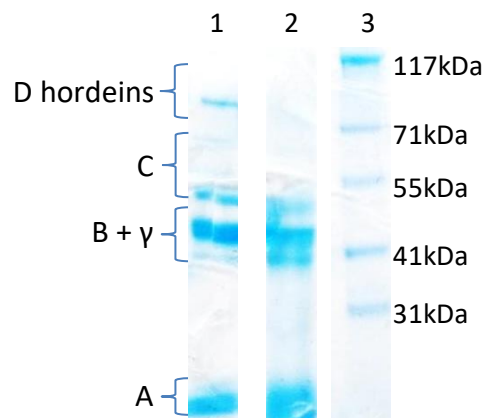


Figure 5. 1- SDS-PAGE analysis of the hordein fraction from the NTG and BSG extracts. The subgroups of hordeins (D-, C-, B-,γ- and A-hordein) are indicated. Lane 1 = NTG, lanes 2 = BSG. Markers with their molecular masses are shown in lane 3.

The band at ~100 kDa was assigned as D-hordiens, the bands between ~50 – 70 kDa were assigned as C-hordeins, the bands ~35-50kDa were assigned as a mixture of B and γ-hordeins and the low molecular weight bands were assigned as A-hordeins. In order to confirm the protein assignments, individual bands were excised and the proteins were digested with Proteinase K and subsequently analysed by LC MS/MS (described in Section 2.4). Unfortunately, this analysis failed to provide confirmation as multiple hordein classes were identified following the protein database search for each band. This results is perhaps unsurprising given the sequence homology between the

hordeins (i.e. proteolysis will result in peptides from multiple proteins with identical sequences).

The results following SDS PAGE suggest that malting and mashing have a marked effect on the hordein protein content. Previous work by Baxter *et al.* has shown that during malting, barley proteins begin to decompose into peptides and amino acid by enzymatic digestion [221]. Here, the larger D hordeins are not detected in the BSG sample, suggesting they have been degraded. The patterns are similar for the other hordein classes between the two samples. Previous work has shown that B and D hordeins are more liable for degradation [222, 223]. During malting, disulfide bonds are reduced and B and D hordeins are in part subjected to proteolysis.

5.3 Preparation of hydrolysates

NTG and BSG were hydrolysed at 160 °C for 0 minutes, 160 °C for 20 minutes, 207 °C for 20 minutes, 253 °C for 20 minutes and 300 °C for 20 minutes. **Figure 5.2** shows the number of peptides that could be identified using LC MS/MS from each of the hydrolysates. A full list of the peptides identified is listed in **Appendix Tables 5.1- 5.14**. Few peptides could be identified from these hydrolysates. This is consistent with the results to be discussed in Chapter 6 where few peptides were identified from SCW hydrolysates of a complex mixture using LC MS/MS via the Orbitrap Elite.

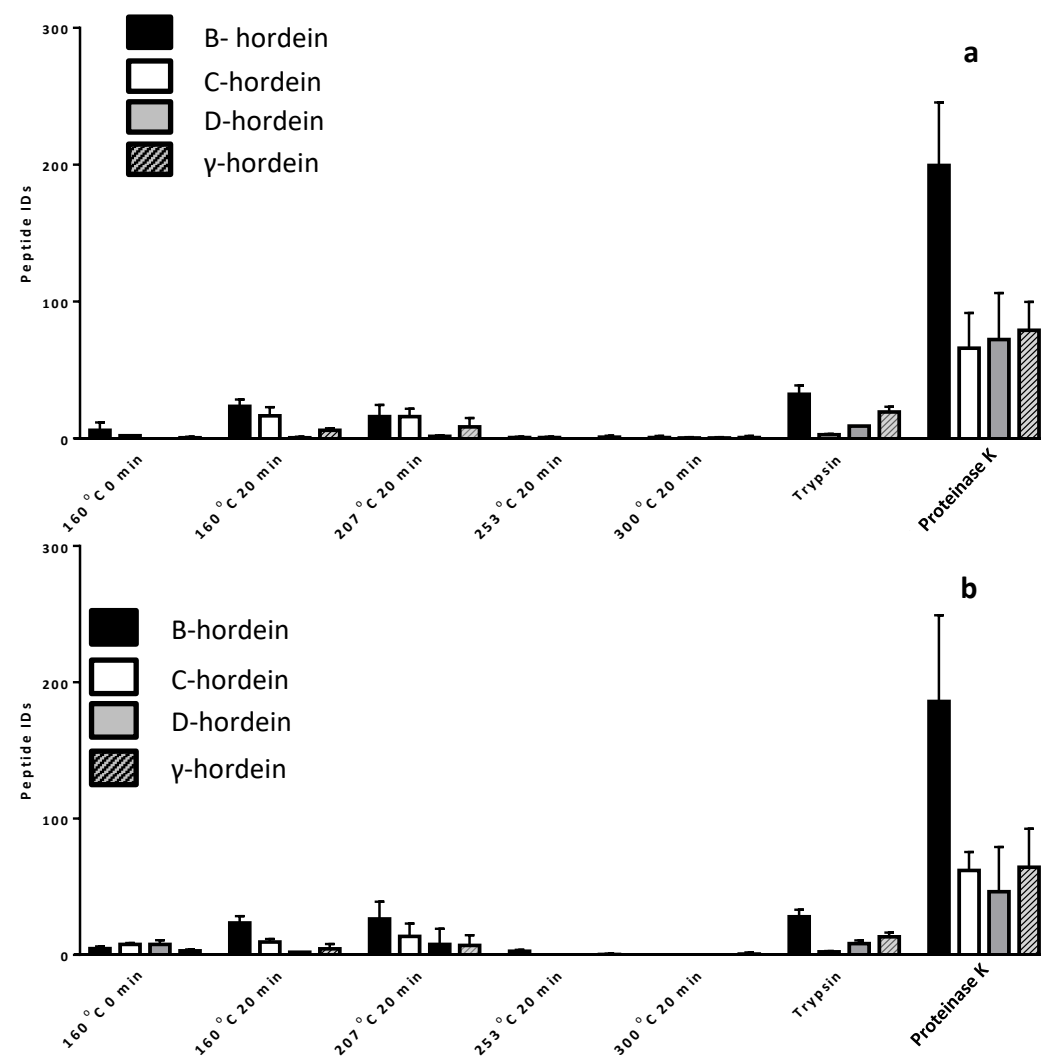
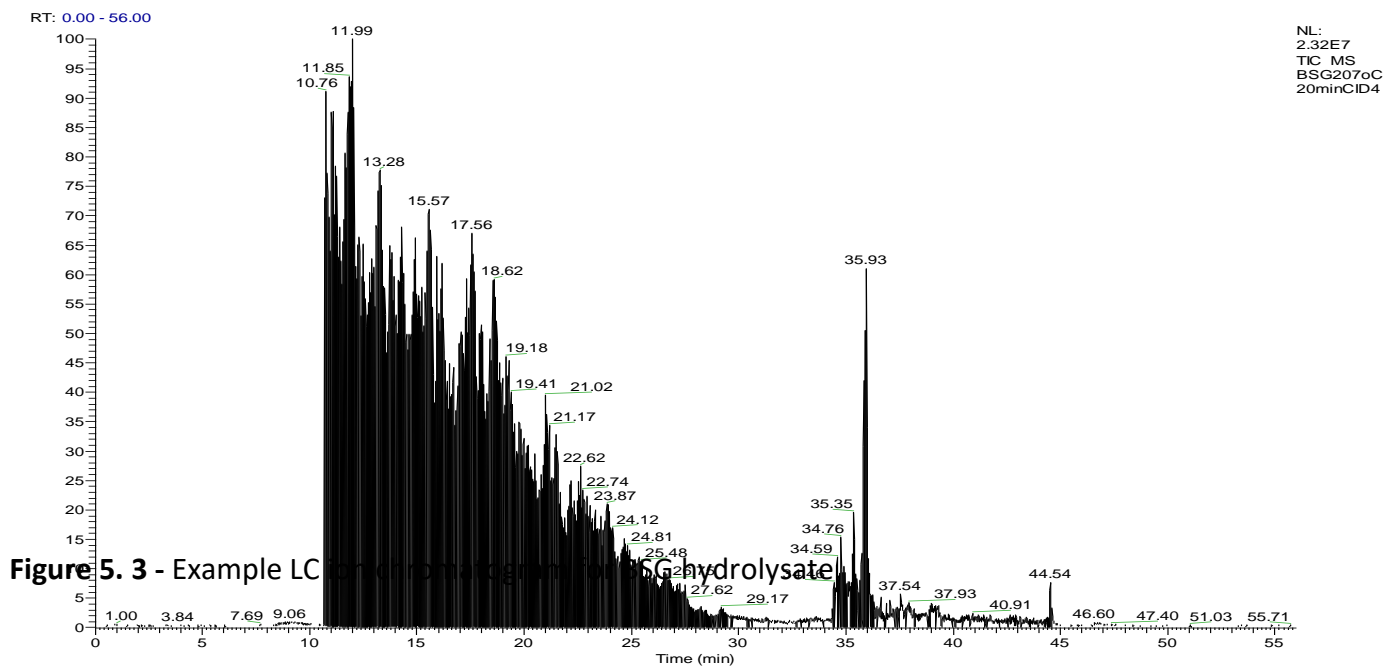


Figure 5. 2 - Number of Peptide identifications for LC MS/MS analyses from SCW hydrolysates and enzymatic digests for **a)** NTG and **b)** BSG. n=3. Error bars represent 1 S.D.

The results observed here are in agreement with this observed in Chapter 6. Here it is hypothesised the low peptide identifications was due to mixture complexity, this is investigated further in Chapter 6. **Figure 5.3** shows an example screenshot of the HPLC chromatogram, illustrating the large amounts of peptides that are eluted.

To confirm the presence of hordeins in the NTG and BSG provided, proteins were tryptically digested in solution and analysed using LC MS/MS, again using the Orbitrap Elite (**Figure 5.2**). As with the SCW hydrolysates, this mixture resulted in few peptide identifications. This is likely due to the lack of arginine and lysine residues in the amino acid sequences of the hordeins. Proteins were next digested using proteinase K, a non-specific enzyme. A large increase in protein IDs was observed, where ~50% peptides assigned were a result of digestion from B-hordeins.



5.4 Antioxidant Potential of SCW hydrolysates

ORAC, comet and reducing power assays have been used extensively to assess both the direct and indirect antioxidant activity of a range of mixtures [146, 224-229]. These are described in more detail in Chapter 1.5.4.

5.4.1 ORAC assay

The total antioxidant capacity (TAC) of a substance can be crudely described using the ORAC assay, through estimation of the antioxidant components of a sample in a global manner. The ORAC assay measures the ability of a substance to quench free radicals by hydrogen donation. A detailed overview of the method is discussed in Chapter 1.5.4.1. The ORAC assay was used to assess the TAC of the NTG and BSG hydrolysates as well as those from the standard protein BSA under the same hydrolysis conditions. Here, Trolox (6-hydroxy-2,5,7,8-tetrametmethylchroman-2-carboxylic acid), a water soluble vitamin E analog, is used as the calibration standard and ORAC results are expressed as μM Trolox equivalents.

Figure 5.4 shows the effect of SCW reaction time and temperature on total antioxidant capacity of NTG and BSG. Values are reported as the concentration of Trolox standard that was required to achieve the same antioxidant capacity (Trolox Equivalence (TE) Value). SCW conditions were 160 °C for 0 min, 160 °C for 20 min, 207 °C for 20 min, 253 °C for 20 min and 300 °C for 20 min.

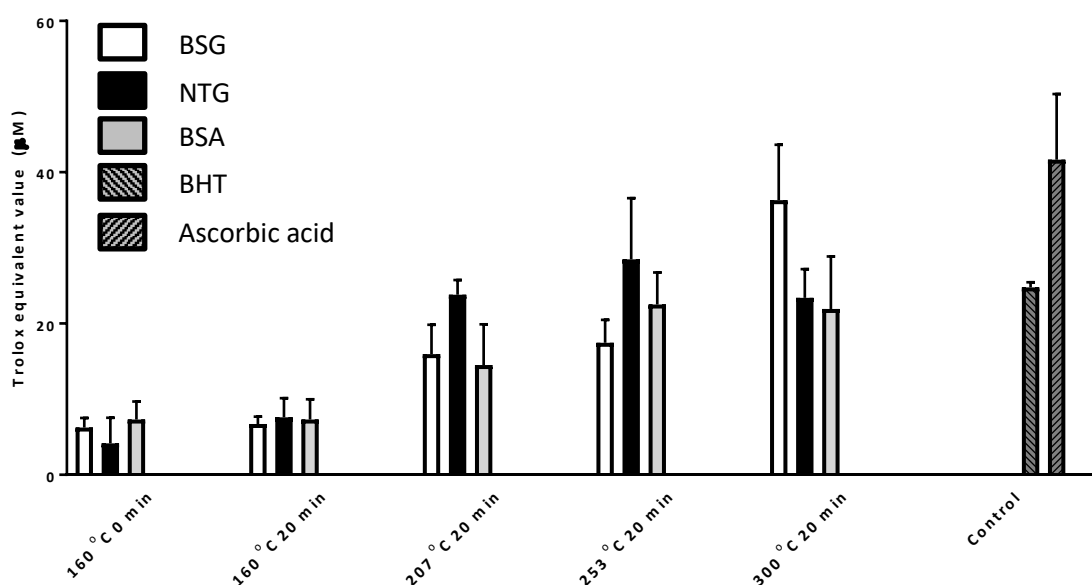


Figure 5. 4 - ORAC assay of NTG, BSG and BSA hydrolysates compared to commercial antioxidants at 0.05mg/ml. Absorbance was recorded at 700 nm. Data represent mean \pm SD of three replicates.

TE values of 6.3 ± 1.0 and 6.7 ± 0.8 μ M were reported for SCW hydrolysis of BSG at 160 °C for 0 and 20 minutes. When the hydrolysis temperature was increased from 160 °C to 207 °C, a significant increase in TE was observed (16.0 ± 3.2 μ M) ($p < 0.05$). A similar level of antioxidant capacity was obtained at 253 °C (17.5 ± 2.5 μ M). A sharp increase in TE value was observed following SCW hydrolysis at 300 °C (36.3 ± 5.2 μ M) ($p < 0.05$).

A positive correlation between hydrolysis temperature and antioxidant capacity was observed for NTG. SCW hydrolysis at 160 °C for 0 min gave a TE value of 4.2 ± 2.8 μ M. Extension of the reaction time to 20 min resulted in a similar level of antioxidant

capacity ($7.6 \pm 2.1 \mu\text{M}$). A significant increase in antioxidant capacity was observed at 207°C ($23.8 \pm 1.6 \mu\text{M}$) ($p < 0.05$). Comparable levels of antioxidant activity were observed at 253°C and 300°C ($28.5 \pm 6.6 \mu\text{M}$ and $23.4 \pm 3.1 \mu\text{M}$).

To compare the TAC of hordein hydrolysates against those of a standard protein, BSA was hydrolysed under the same conditions. The TE values for BSA hydrolysates from 160°C for 0 and 20 min treatments were $7.3 \pm 1.9 \mu\text{M}$ and $7.3 \pm 2.7 \mu\text{M}$. An increase in TAC was again observed at 207°C ($14.5 \pm 4.4 \mu\text{M}$). High TE values were also obtained at 253°C and 300°C ($22.5 \mu\text{M} \pm 3.5$ and $21.9 \pm 5.7 \mu\text{M}$).

Two antioxidants that are routinely used as supplements within the food and pharmaceutical industries are Butylated hydroxytoluene (BHT) and ascorbic acid. The TACs observed following hydrolysis at the higher temperature points of all three reactants compared favourably against the same w/v of BHT ($24.8 \pm 0.6 \mu\text{M}$) and ascorbic acid ($41.7 \pm 6.1 \mu\text{M}$).

These results suggest that SCW hydrolysis of protein results in the efficient formation of a powerful antioxidant mixture under increasing temperatures points, regardless of the starting protein. A general correlation between temperature and TAC was observed. Significant increases in TAC were observed between hydrolysates obtained at 160°C and 207°C for BSG and NTG. Whilst the realisation of a process to produce a valuable product from BSG has economic potential for the brewing industry, providing a standard methodology for the transformation of any protein-based waste into a powerful antioxidant has increased commercial applications.

5.4.2 Reducing Power assay

Reducing power serves as a reflection of antioxidant activity. This assay is based on the reduction of Fe^{3+} to Fe^{2+} and subsequently monitoring the increase in absorbance at 700nm. As with the ORAC assay, the biological relevance of this assay is uncertain, particularly given the electron transfer mechanism of action. This is described in more detail in Chapter 1.5.4.2.

Figure 5.5 shows the $\text{Abs}_{700\text{nm}}$ against each hydrolysis condition. A substance exhibiting reducing power will cause the complex to be reduced to the ferrous (Fe^{2+}) form, resulting in an increased absorbance recorded at 700nm.

The reducing power consistently increased with the harshness of the hydrolysis conditions. Under hydrolysis conditions of 160 °C for 0 minutes, no $\text{Abs}_{700\text{nm}}$ was recorded for BSG or NTG (both 0.00 ± 0.00) whilst a limited amount was recorded for BSA (0.06 ± 0.03). Under hydrolysis conditions of 160 °C for 20 minutes little $\text{Abs}_{700\text{nm}}$ was again recorded for NTG or BSG (again both 0.00 ± 0.00), whilst a moderate increase in BSA was observed (0.11 ± 0.02). Hydrolysates from 207 °C for 20 minutes showed significant increases in $\text{Abs}_{700\text{nm}}$ for all three mixtures: 0.04 ± 0.01 for BSG, 0.08 ± 0.02 for NTG and 0.20 ± 0.01 for BSA ($p < 0.005$ in all cases). Significant increases in $\text{Abs}_{700\text{nm}}$ were also increased between 207 and 253 °C for 20 minutes: 0.16 ± 0.02 ($p < 0.001$) for BSG, 0.18 ± 0.02 for NTG and 0.26 ± 0.03 for BSA (both $p < 0.05$). The highest levels of $\text{Abs}_{700\text{nm}}$ were recorded for hydrolysates from 300 °C for 20 minutes for NTG (0.29 ± 0.04), BSG (0.26 ± 0.04) and BSA (0.31 ± 0.03). These represented significant increases in $\text{Abs}_{700\text{nm}}$ for BSG and NTG compared to the values obtained at 253 °C for 20 minutes ($p < 0.05$). Here, the reducing power of the hydrolysates was not as high as that observed in the commercial antioxidants BHT (0.65 ± 0.02) and ascorbic acid (0.64 ± 0.02).

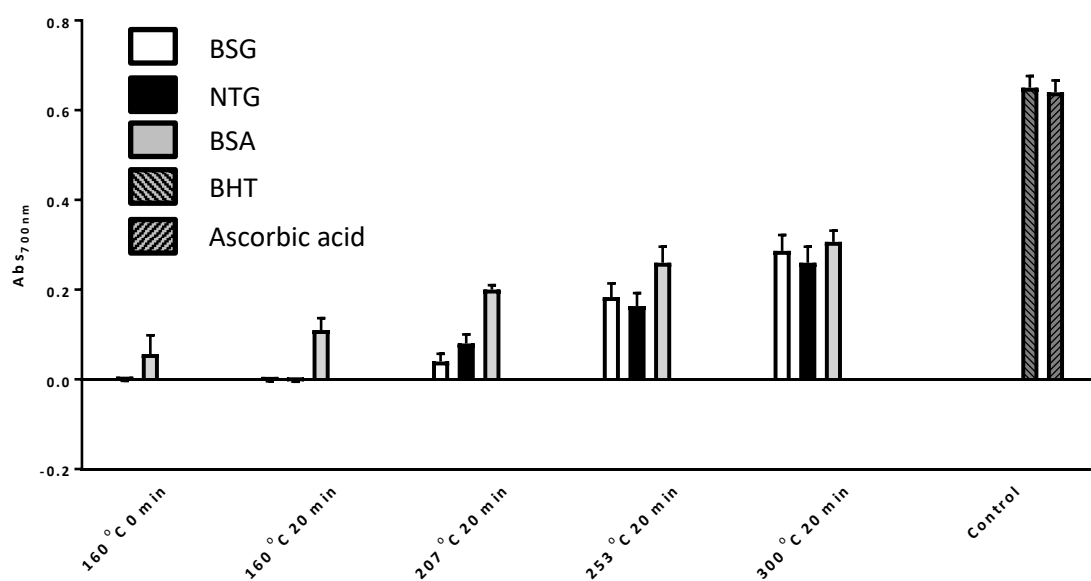


Figure 5. 5 - Reducing power assay of NTG, BSG and BSA hydrolysates and commercial antioxidants at 0.05mg/ml. Absorbance was recorded at 700 nm. n=3. Data represent mean \pm SD of three replicates.

5.4.3 Comet assay

To confirm the results described above, the more rigorous comet assay was applied, in which the antioxidant potential is assessed on live cells. The comet assay offers a sensitive method for measuring DNA strand breaks in individual cells. A comprehensive explanation of the assay is detailed in Chapter 1.5.4.3.

Prior to performing the comet assay, HaCaT cells were incubated in NTG, BSG and BSA hydrolysates from 160 °C for 0 min, 160 °C for 20 min, 207 °C for 20 min, 253 °C for 20 min and 300 °C for 20 min. The incubation period was 24 hours and the cell viability was assessed using trypan blue exclusion. This assay is discussed in Chapter 1.5.4.3. The % cell viability was recorded to ensure each hydrolysate mixture did not produce any unwanted cytotoxic effects.

Figure 5.6 shows the results of trypan blue staining of HaCaT cells after 24 h of incubation with different concentration of the test compounds. Cell viability following the various treatments was >90 % and no floating cells were noticed in the medium. This is comparable to untreated cells. The presence of 50 μ M H₂O₂ for the final 30 minutes of incubation caused a slight decrease in viability to ~90%.

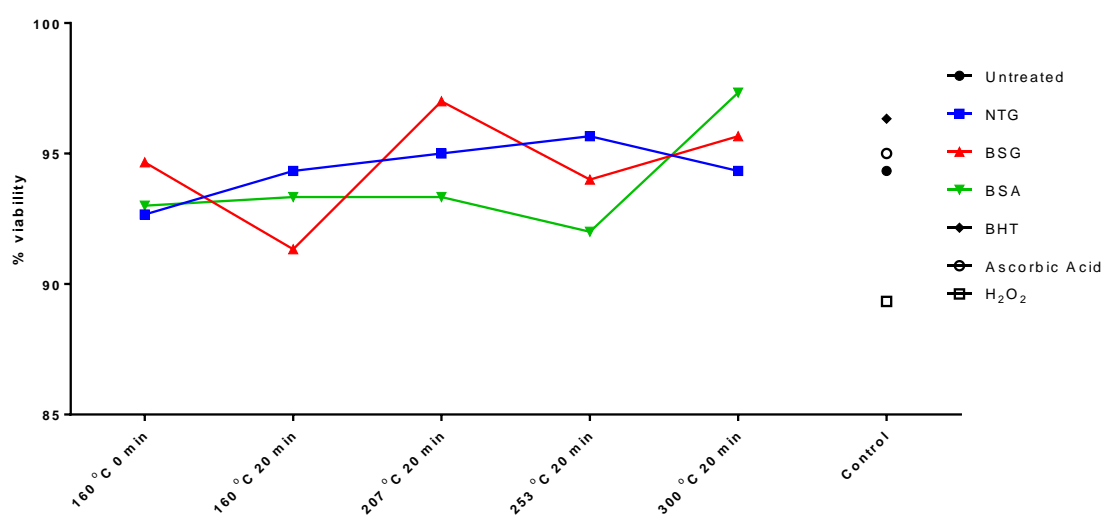


Figure 5. 6- Viability of HaCaT cells incubated in SCW hydrolysates and commercial antioxidants for 24h. n=3. Data represent mean values.

DNA damage was analysed by the comet assay. Following single-cell electrophoresis, the relative tail length was measured, with longer tails representing increased DNA damage. Cells were pre-incubated with protein hydrolysates (specific experimental details described in Chapter 2.9) and exposed to 50 μM H_2O_2 for the last 30 minutes of treatment.

Figure 5.7 shows the mean amount of DNA in comet tails for each experimental condition. **Figure 5.8** shows an example screenshot of comets visualised from the comet assay. The bright circles represent a comets 'head'. In this example the DNA has migrated a large distance away from the head to generate a characteristic 'tail'. The % of DNA that is in the comet's tail is proportional to the amount of DNA damage induced by H_2O_2 treatment.

Following incubation of HaCaT cells with 50 μM H_2O_2 for 30 minutes a large amount of DNA in comet tails (55.2 ± 3.0 %) was observed (the positive control). When pre-incubated in protein hydrolysates from 160 $^\circ\text{C}$ for 0 min treatment a reduction in tail length was observed for BSG (45.5 ± 2.0 %), NTG (47.5 ± 0.7 %) and BSA (43.5 ± 1.0 %, statistically significant $p < 0.05$). Pre-incubation in hydrolysates from 160 $^\circ\text{C}$ for 20 min treatment yielded a similar level of % tail DNA for all three proteins (50.7 ± 2.8 % for NTG, 50.6 ± 0.11 % for BSG and 39.0 ± 6.3 % for BSA). A steady reduction in % tail DNA with respect to hydrolysis temperature was observed over the remaining pre-incubation conditions. After treatment with hydrolysates from 207 $^\circ\text{C}$ for 20 min a decrease in DNA migration in the comet tails was noted and for BSG, NTG and BSA (43.5 ± 2.1 %, 42.0 ± 2.1 % and 37.7 ± 1.9 %). A further decrease in % tail DNA was observed in incubation solutions from 253 $^\circ\text{C}$ for 20 min for BSG (36.8 ± 2.1 %) and BSA (30.3 ± 1.9 %) whilst similar results were obtained for NTG (42.9 ± 1.6 %). The % tail DNA further decreased when pre-incubated in solutions from 300 $^\circ\text{C}$ for 20 min treatment for BSG (39.5 ± 0.3 %), NTG (26.1 ± 3.3 %) and BSA (29.8 ± 2.5 %).

In contrast to the results obtained from the ORAC assay, SCW hydrolysates were not shown to convey a comparable level of antioxidant activity compared to either of the commercial antioxidants. % tail DNA was reported as 17.3 ± 3.5 % for BHT and $14.9 \pm$

1.1 % for ascorbic acid. These results suggest a disparity between the ex vivo and in vivo antioxidant activity of the hydrolysates, thereby underlying the limitations of the ORAC assay. However, a large decrease in DNA damage observed when incubating in hydrolysates under certain conditions remains encouraging. Furthermore, the general positive correlation between antioxidant power and hydrolysis temperature is consistent with the ORAC assay results.

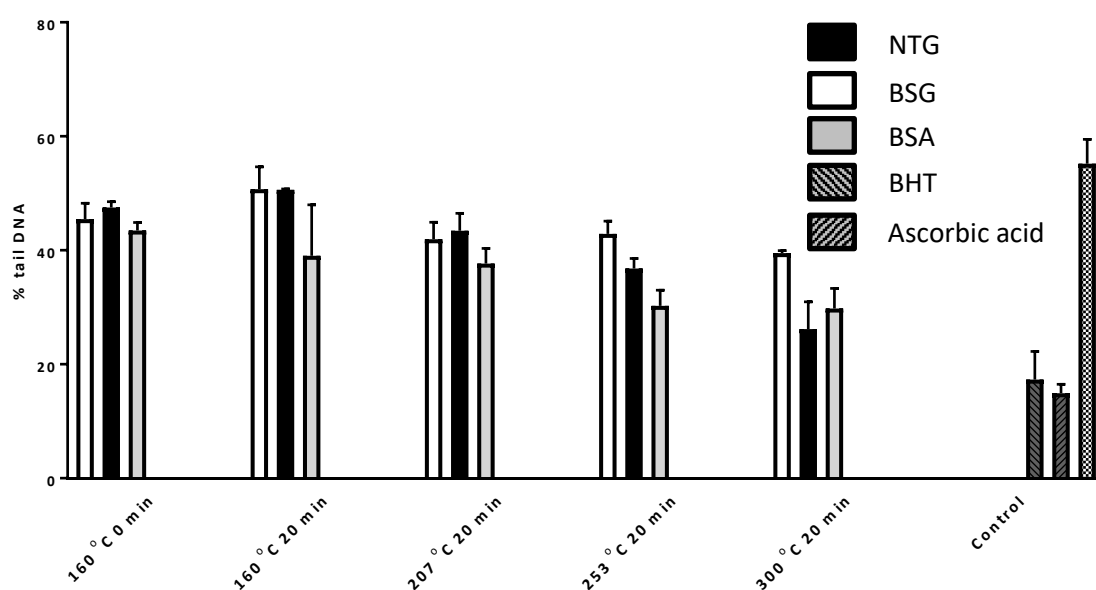


Figure 5. 7 - DNA strand breakage detected by the comet assay using a HaCaTs. Values represent the mean tail movement, where n = 2. Data represent mean \pm SD of two replicates.

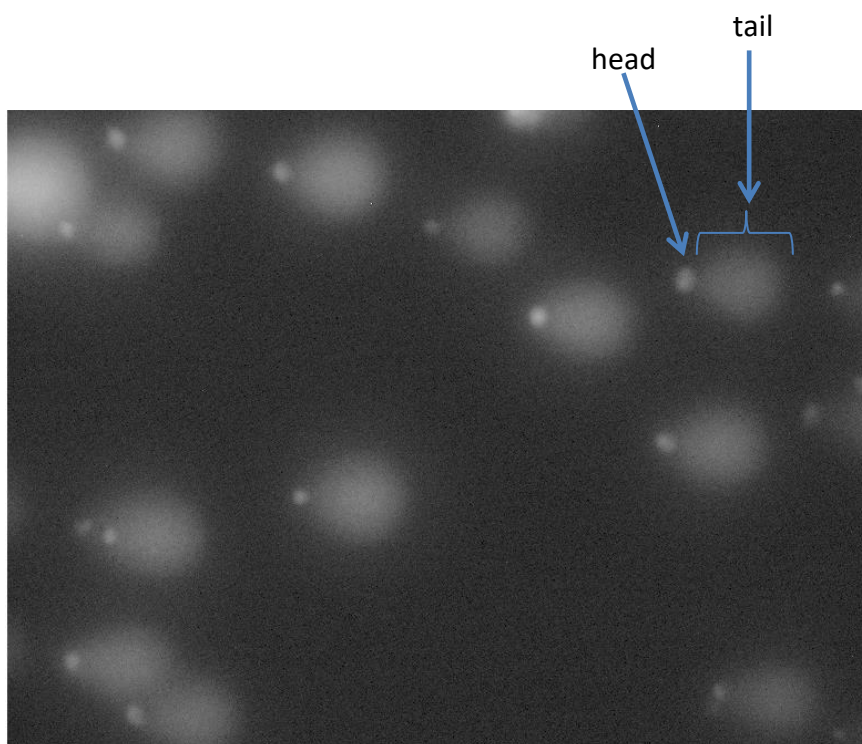


Figure 5. 8 - Example screenshot of comets visualised in the comet assay.

5.3.4 Identification of the molecular origin of the antioxidant activity

The results presented in Chapter 3 indicate that hydrolysis conditions of 160 °C for 20 mins results in production of peptides, and that the peptides are gradually decomposed into smaller molecules at temperatures above this. Given the results of the antioxidant assays above, it is hypothesised that the small molecules produced under hydrolysis conditions of 207 °C and greater are responsible for the antioxidant capacity, rather than the peptides.

Enzymatic digests of hordeins have previously shown evidence of antioxidant activity[230]. Bamdad *et al.* showed the digestion of hordein extract using alcalase, flavorzyme and pepsin can produce extracts with strong radical scavenging, metal chelating and oxidative reducing power. Whilst some antioxidant power from the protein had been converted to peptides (hydrolysis conditions of 160 °C for 0 and 20 minutes) was observed, it is at temperatures ≥ 207 °C that we observe the strongest antioxidant capacity.

Figure 5.9 shows the TE values obtained from an ORAC assay of a tryptic and proteinase K digests BSG, NTG and BSA. Whilst modest antioxidant activity could be obtained from both the tryptic (8.8 ± 1.5 μ M for BSG; 4.9 ± 0.9 μ M for NTG and 3.7 ± 1.1 μ M for BSA) and proteinase K digests (6.6 ± 1.7 μ M for BSG; 10.9 ± 3.0 μ M for NTG and 5.2 ± 1.8 μ M for BSA), they do not substantially differ to those obtained for corresponding samples which had not been digested (6.3 ± 0.9 μ M for NTG; 5.2 ± 2.4 for BSG and 4.9 ± 2.4 μ M for BSA).

Previous work has shown that amino acid side chains either in their free form or within protein and peptide structures can provide strong antioxidant activity [231, 232]. To assess whether free amino acids directly contribute to increased antioxidant activity, the TAC of an equimolar solution of all 20 natural amino acids was also assessed via the ORAC assay. The TE value obtained was comparable to those obtained under the enzymatic digests (9.4 ± 2.5 μ M). It is hypothesised that under hydrolysis conditions of 207 °C and above, rather than release the component amino acids, their lysis from the peptide chain would involve modification of the molecules and that these would be

directly responsible for the very high levels of antioxidant activity observed under the most harsh hydrolysis conditions.

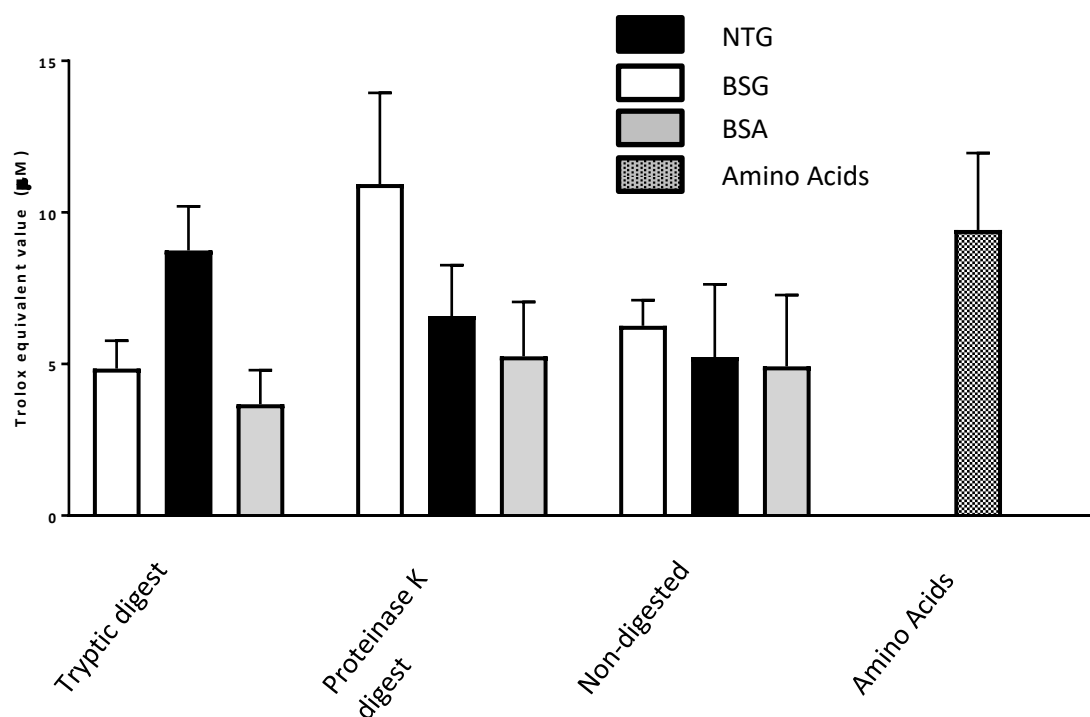


Figure 5. 9 - TE values obtained for enzymatic digests of NTG, BSG and BSA and equimolar amino acid mixture using the ORAC assay. n=3. Data represent mean \pm SD of three replicates.

5.5 Small molecule analysis

To better understand the bioactive behaviour of the decomposition products of proteins in sub critical conditions, it is necessary to characterise the compounds formed. Although decomposition pathways of proteins and amino acids in SCW have been previously studied, these studies focus on the identification of pre-selected compounds using a HPLC system, with post column electro conductivity detection [185, 233]. The aim here was to identify unknown components in a SCW mixture and to propose mechanisms for their formation.

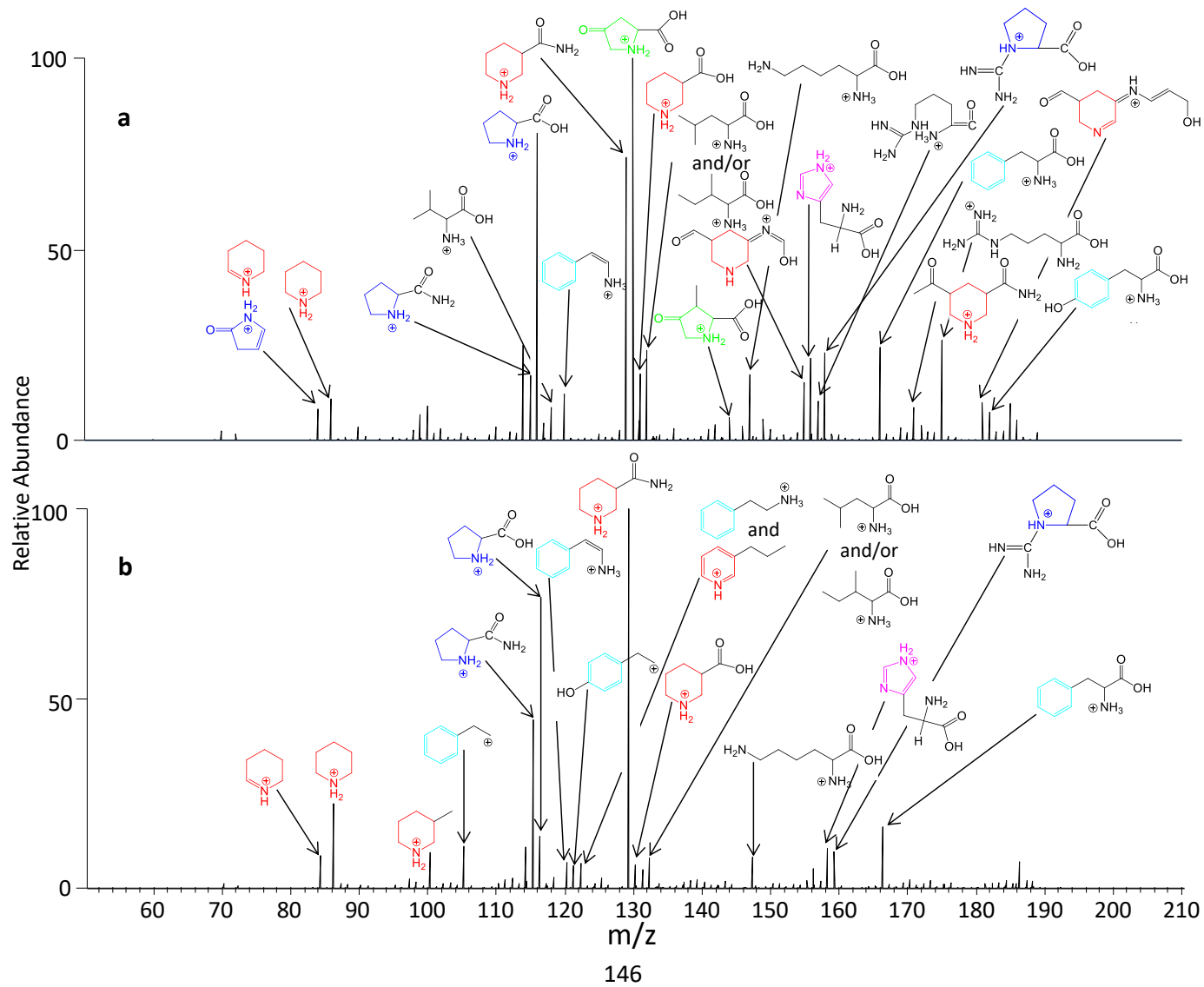
To identify the decomposition products from the SCW hydrolysis of proteins, hydrolysates were analysed by direct infusion electrospray mass spectrometry. Ions of relative abundance >5% were isolated and fragmented using higher energy collisional dissociation (HCD) MS/MS. A list of all ions isolated and fragmented using HCD are listed in **Appendix Figures 5.1-5.60** in order of mass-to-charge ratio. Figures are annotated with predicted structures of precursor and fragment ions.

The mass spectra obtained for the hydrolysates in the mass range of 50 - 210 m/z for the 160 °C for 0 min and 20 min hydrolysates can be viewed in **Appendix Figures 5.61-5.69 (See also Appendix Tables 5.15-5.22)**. The most abundant peaks in each spectrum correspond to solvent and very few molecules were identified in this range.

5.5.1 BSA hydrolysate analysis

Figure 5.10a shows the mass spectrum obtained following SCW hydrolysis of BSA at 207 °C for 20 minutes. A summary of the peaks observed is listed in **Table 5.1**.

The most intense peak was observed at m/z 130.0503. This corresponds to a molecular formula of $C_5H_8NO_3$. HCD MS/MS suggests that this peak corresponded to singly-charged pyroglutamic acid (**Appendix Figure 5.27**). It has previously been shown in the SCW hydrolysis of BSA that pyroglutamic acid is a major reactant product under comparable conditions [233]. This study differed from this experiment, not only in the hydrolysis conditions, but also that pre-selected products were quantitated, rather than providing a qualitative analysis. In a separate study Abdelmoez. *et al.* studied the decomposition of 17 of the 20 natural amino acids [185]. Pyroglutamate was identified as the sole decomposition product from the SCW hydrolysis of glutamate, resulting from its dehydration. The mechanism of pyroglutamate formation is shown in Scheme **5.1 a**. However, the decomposition of glutamine was not discussed in their study. In Chapter 4 deamination was identified as a SCW induced modification. Deamination of glutamine can also result in the formation of pyroglutamate (**Scheme 5.1a**) [234].



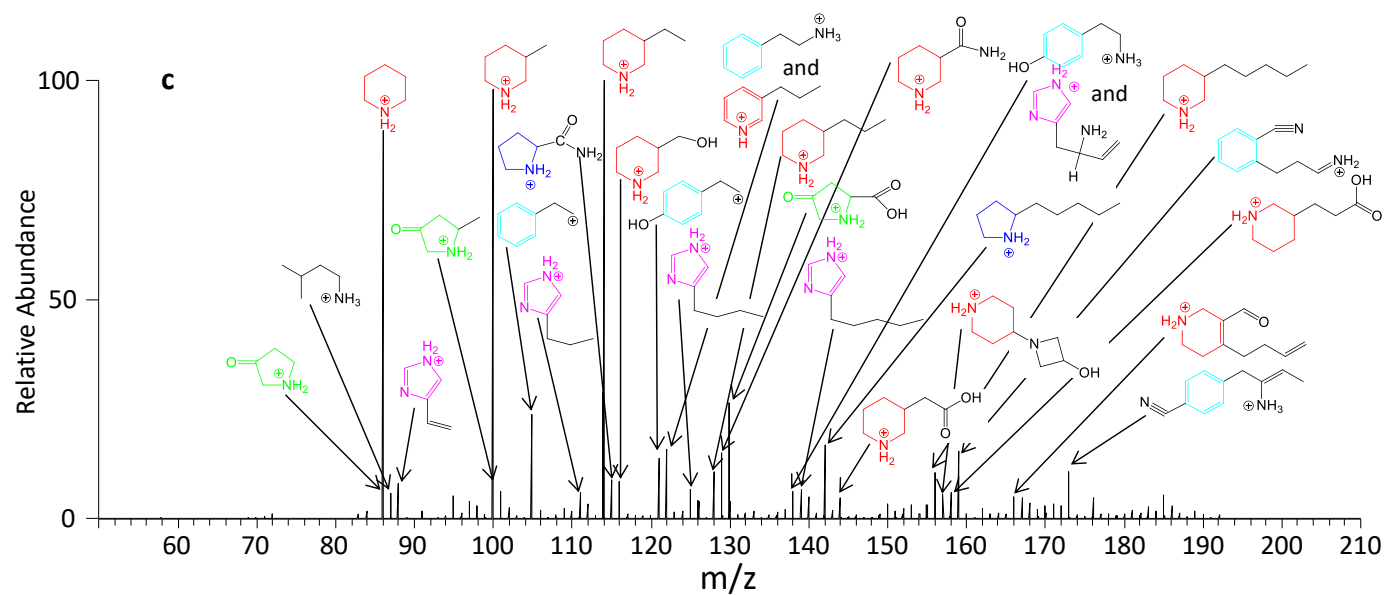
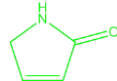
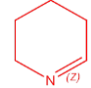
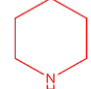
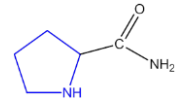
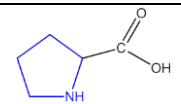
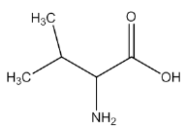
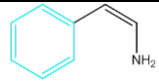
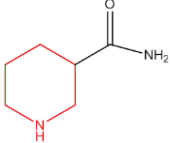
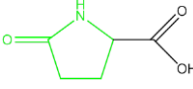
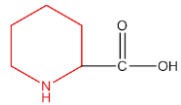
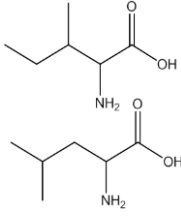
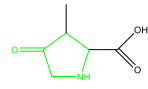
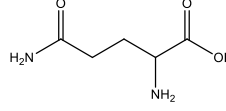
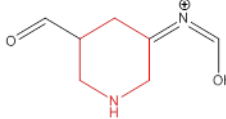
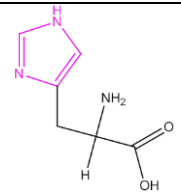
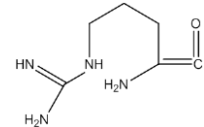
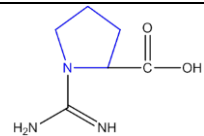
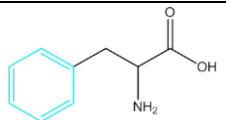
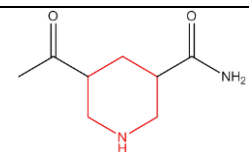


Figure 5. 10 - Direct infusion ESI MS of BSA hydrolysed at **a)** 207°C for 20 min, **b)** 253 °C for 20 min and **c)** 300 °C for 20 min.

<u>m/z</u>	<u>Calculated mass (Da)</u>	<u>Measured mass (Da)</u>	<u>Formula</u>	<u>Proposed Structure</u>	<u>HCD MS/MS</u>	<u>ΔPPM</u>	<u>Relative abundance</u>
84.0446	83.0371	83.0373	C ₄ H ₅ ON		No	2.7	7.65
84.0809	83.0735	83.0736	C ₅ H ₉ N		No	1.5	8.24
86.0966	85.0892	85.0893	C ₅ H ₁₁ N		No	1.5	10.89
98.9756	n/a	n/a	solvent	n/a	n/a	n/a	6.86
100.0759	n/a	n/a	solvent	n/a	n/a	n/a	9.12
115.0870	114.0793	114.0797	C ₅ H ₁₀ ON ₂		Appendix Figure 5.13	3.7	17.22
116.0709	115.0633	115.0636	C ₅ H ₉ O ₂ N		Appendix Figure 5.14	2.8	83.26
118.0866	117.0790	117.0793	C ₅ H ₁₁ O ₂ N		Appendix Figure 5.16	2.8	8.72
120.0812	119.0735	119.0739	C ₈ H ₉ N		Appendix Figure 5.18	3.6	12.35

129.1027	128.0950	128.0954	C ₆ H ₁₂ N ₂ O		Appendix Figure 5.26	3.3	75.26
130.0503	129.0426	129.0430	C ₅ H ₇ O ₃ N		Appendix Figure 5.27	3.3	100.00
130.0867	129.0790	129.0794	C ₆ H ₁₁ O ₂ N		Appendix Figure 5.28	3.3	9.07
131.1183	130.1106	130.1110	C ₆ H ₁₄ ON ₂	Unassigned	No	3.3	17.70
132.1023	131.0946	131.0950	C ₆ H ₁₃ ON ₂		Appendix Figure 5.29	3.2	23.61
144.0660	143.0582	143.0587	C ₆ H ₉ O ₃ N		No	3.7	6.10
147.1133	146.1055	146.1060	C ₆ H ₁₄ O ₂ N ₂		Appendix Figure 5.38	3.6	17.74

155.0821	154.0742	154.0748	C ₇ H ₁₀ O ₂ N ₂		Appendix Figure 5.43	4.0	15.81
156.0773	155.0695	155.0700	C ₆ H ₉ O ₂ N ₃		Appendix Figure 5.44	3.4	23.43
157.1089	156.1011	156.1016	C ₆ H ₁₂ ON ₄		Appendix Figure 5.46	3.4	10.89
158.0929	157.0851	157.0856	C ₆ H ₁₁ O ₂ N ₃		Appendix Figure 5.48	3.3	22.77
166.0868	165.0790	165.0795	C ₉ H ₁₁ O ₂ N		Appendix Figure 5.51	3.2	24.52
171.1134	170.1055	170.1061	C ₈ H ₁₄ O ₂ N ₂		Appendix Figure 5.53	3.7	8.66

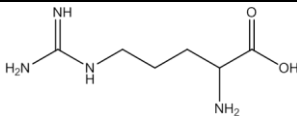
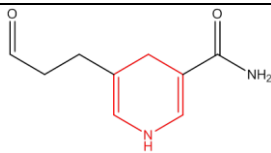
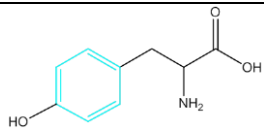
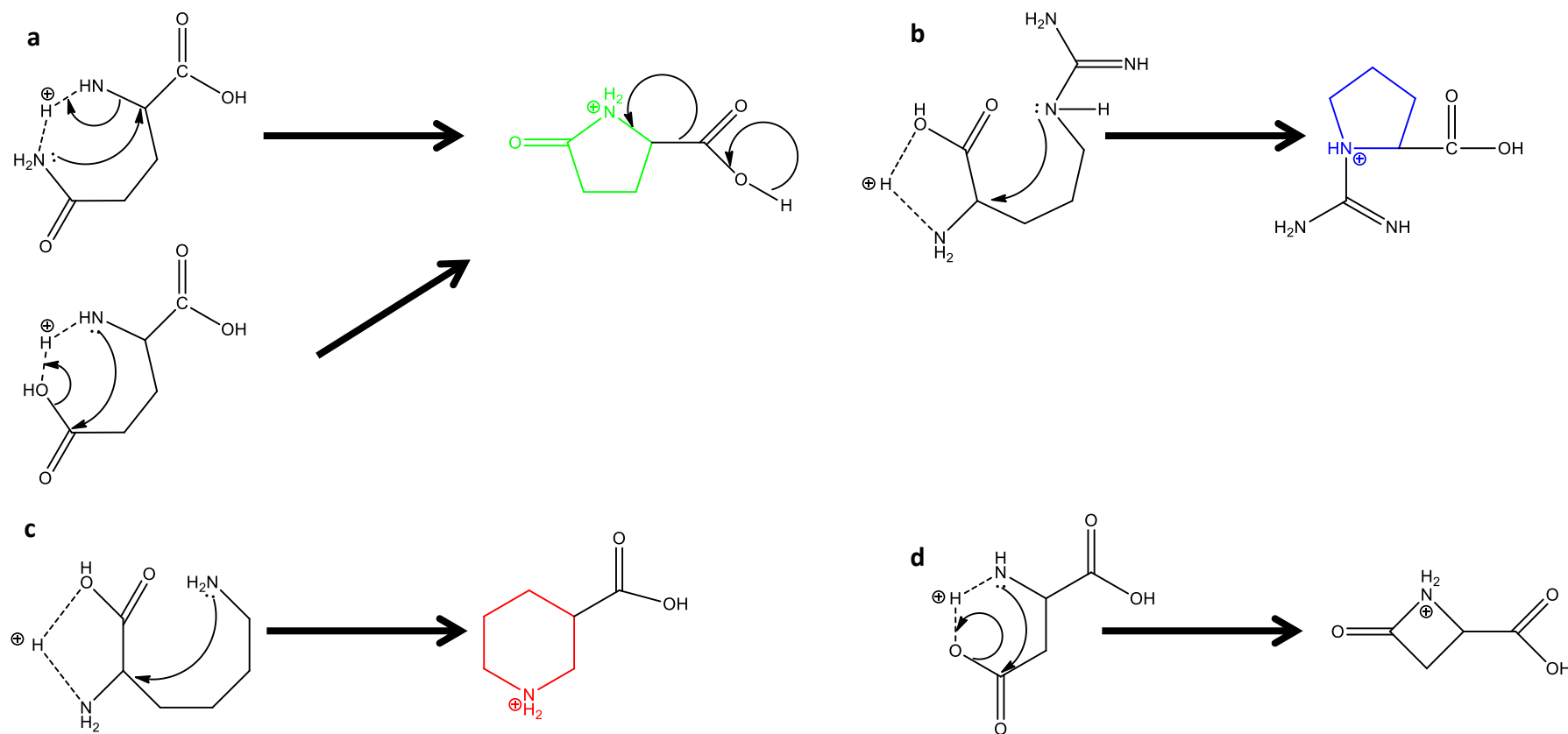
175.1195	174.1117	174.1122	C ₆ H ₁₄ O ₄ N ₂		Appendix Figure 5.55	3.0	28.64
181.0978	180.0899	180.0905	C ₉ H ₁₂ O ₂ N ₂		Appendix Figure 5.57	3.5	10.24
182.0818	181.0739	181.0745	C ₉ H ₁₁ O ₃ N		Appendix Figure 5.58	3.4	7.34
185.0927	184.0847	184.0854	C ₈ H ₁₂ O ₃ N ₂	Unassigned	No	3.9	5.88
185.1291	184.1212	184.1218	C ₉ H ₁₆ O ₂ N ₂	Unassigned	No	3.4	9.63
186.1243	185.1164	185.1170	C ₈ H ₁₅ O ₂ N ₃	Unassigned	No	3.4	5.51

Table 5. 1 - Ions Observed Following SCW Hydrolysis of BSA at 207 °C for 20 min.



Scheme 5. 1 - Proposed mechanism for **a)** Deamination of glutamine and dehydration of glutamic acid, **b)** deamination of arginine, **c)** deamination of lysine and **d)** dehydration of aspartic acid.

A peak was observed at m/z 144.0660 corresponding to singly protonated ions of $C_6H_9O_3N$. This ion may correspond to methylation of pyroglutamic acid, although no HCD MS/MS data was collected to support this, due to difficulties in peak isolation. In addition a peak was observed at m/z 84.0446. The mass difference suggests this could be the result of decarboxylation of pyro glutamic acid ($-CO_2$). No fragments could be observed from the HCD of this ion due to the limited sensitivity of the instrument at the lower mass range and the relatively high energies that are needed to fragment cyclic structures. Decarboxylation has been identified as a major reaction pathway in SCW hydrolysis [185]. Abdelmoez. *et al.* were able to show in the SCW hydrolysis of 17 of the natural amino acids that 13 of them produced formic acid, the leaving group from decarboxylation.

Ions were also detected at m/z 120.0812 and 157.1089. The mass differences observed between these ions and the masses of the natural amino acids suggest that these could be products of phenylalanine decarboxylation and arginine dehydration. The structure of these compounds was confirmed using HCD MS/MS (**Appendix Figures 5.18 and 5.46**).

As well as the data collected from the SCW hydrolysis of peptides in Chapter 4, dehydration and deamination reactions have been identified as reaction pathways in other SCW treated molecules. Decarboxylation of indole-2-carboxylic acid to unsubstituted indole has been shown under conditions of 255 °C for 20 minutes [235], as has the decarboxylation of an ester to produce a styrene[236]. Additionally, in previous work by Kuhlmann *et al.* cyclohexanol was shown to be dehydrated under sub-critical conditions of 250-300 °C, although this was in deuterium oxide rather than water [237].

The peak at m/z 116.0709 corresponds to singly protonated $C_5H_9O_2N$, the elemental composition of proline (+1). This assignment was confirmed using HCD MS/MS (**Appendix Figure 5.13**). The transformation of arginine to proline is a common biological reaction. This reaction has previously been demonstrated in sub-critical conditions [185].

Other peaks corresponding to the m/z of amino acids were observed. HCD MS/MS was used to confirm their assignment. Amino acids liberated from BSA under these conditions including valine (m/z 118.0866) (HCD MS/MS analysis in **Appendix Figure 5.16**), leucine and isoleucine (m/z 132.1023) (HCD MS/MS analysis in **Appendix Figure 5.29**), lysine (m/z 147.1123) (HCD MS/MS analysis in **Appendix Figure 5.39**), histidine (m/z 156.0773) (HCD MS/MS analysis in **Appendix Figure 5.44**), phenylalanine (m/z 166.0868) (HCD MS/MS analysis in **Appendix Figure 5.51**), arginine (m/z 175.1195) (HCD MS/MS analysis in **Appendix Figure 5.55**) and tyrosine (m/z 182.0818) (HCD MS/MS analysis in **Appendix Figure 5.58**).

The peak at m/z 115.0870 corresponds to singly protonated $C_5H_{10}ON_2$. HCD MS/MS analysis suggests that this peak corresponds to proline that has undergone amidation – a SCW induced modification established in Chapter 4 (HCD MS/MS analysis in **Appendix Figure 5.13**). The results suggest a further pyrrolidine-based structure observed at m/z 158.0929. The mass difference suggests that this ion could be a result of arginine deamination. Deamination was established as a modification induced under certain SCW conditions in Chapter 4. A mechanism for arginine deamination has been previously been proposed (**Scheme 5.1b**) [238]. HCD MS/MS produced fragment ions that are consistent with this structure (**Appendix Figure 5.48**).

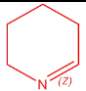
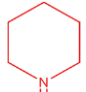
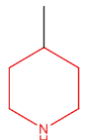
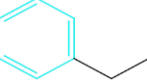
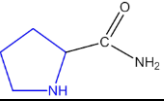
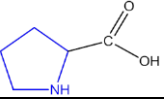
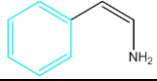
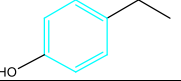
The ion observed at m/z 130.0837 may be the result of lysine deamination. This reaction has previously been predicted to form pipecolic acid (**Scheme 5.1c**) [238]. The fragment ions observed in the HCD MS/MS spectra of this species were consistent with this structure (**Appendix Figure 5.28**). A peak corresponding to the subsequent amidation of this species was observed at m/z 129.1027, and confirmed by HCD MS/MS (**Appendix Figure 5.26**). These structures share a common piperidine ring, which may correspond to the peak observed at m/z 86.0966, although this was not confirmed by HCD MS/MS due to the limited mass range of the instrument. Similarly, decarboxylation of pipecolic acid may be responsible for the ion observed at m/z 84.0809, although the structure was not confirmed. It is hypothesised that the piperidine-based structure forms the basis for ions observed at m/z 155.0821 (HCD

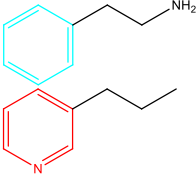
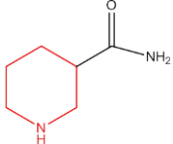
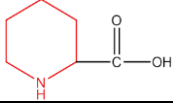
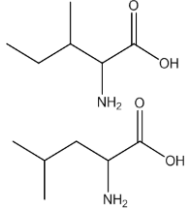
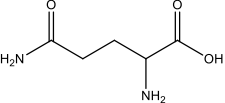
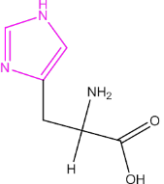
MS/MS analysis in **Appendix Figure 5.43**), 171.1134 (HCD MS/MS analysis in **Appendix Figure 5.53**), 181.0978 (HCD MS/MS analysis in **Appendix Figure 5.57**).

MS analysis was next performed on hydrolysates from the SCW treatment of BSA at 253°C for 20 minutes (**Figure 5.10b** and **Table 5.2**). Peaks observed in the mass spectra that had not been detected following SCW treatment at 207 °C were selected for fragmentation and are highlighted in **Table 5.2**.

The most abundant peak in the mass spectrum was observed at m/z 129.1024. In the analysis of the data observed when BSA was hydrolysed at 207 °C for 20 minutes it was suggested that this ion corresponds to amidation of the species observed at m/z 130.0865. Under hydrolysis conditions of 253 °C for 20 minutes, a greater abundance of amidated species are observed relative to their non-amidated counterparts. The species at m/z 129.1024 has a relative abundance of 100% compared to the non-amidated species at m/z 130.0865 which has a relative abundance of 6.14%. In contrast, under conditions of 207 °C for 20 minutes the ion at m/z 130.0865 was observed in greater abundance. Additionally, an ion of m/z 115.0867 is observed. It is hypothesised that this ion is prolinimide (a proline residue that has undergone amidation). The ion observed at m/z 116.0708 was assigned as proline. Prolinamide has a relative abundance $\sim 4\times$ greater than that of proline. This observation is in contrast to the results obtained following hydrolysis at 207 °C for 20 min where the opposite was true.

An ion was observed at m/z 122.0966. The mass suggests the ion could be a result of Phe-CO₂. Two possible structures were assigned using HCD MS/MS (**Appendix Figure 5.21**). Coupling liquid chromatography to HCD MS/MS could be an effective method of separating the possible isomers and confirming their assignment. Furthermore an ion was observed at m/z 105.0700, which could be a result of NH₃ loss from the ion at m/z 122.0966. Its structure was hypothesised (HCD MS/MS analysis in **Appendix Figure 5.5**). In addition, an ion was observed at m/z 158.0927 which was previously attributed to Arg-NH₃ (HCD MS/MS analysis in **Appendix Figure 5.48**).

<u>m/z</u>	<u>Calculated mass (Da)</u>	<u>Measured mass (Da)</u>	<u>Formula</u>	<u>Proposed Structure</u>	<u>HCD MS/MS</u>	<u>PPM</u>	<u>Relative abundance</u>
84.0808	83.0735	83.0735	C ₅ H ₉ N		No	0.3	8.84
86.0965	85.0892	85.0892	C ₅ H ₁₁ N		No	0.3	22.36
100.0758	n/a	n/a	solvent	n/a	No	n/a	8.86
100.1122	99.1048	99.1049	C ₆ H ₁₃ N		Appendix Figure 5.4	1.3	9.37
105.0700	104.0626	104.0627	C ₈ H ₈		Appendix Figure 5.5	1.2	11.01
114.0915	n/a	n/a	solvent	n/a	n/a	n/a	11.00
115.0867	114.0793	114.0794	C ₅ H ₁₀ ON ₂		Appendix Figure 5.13	1.1	44.49
116.0708	115.0633	115.0635	C ₅ H ₉ O ₂ N		Appendix 5.14	1.9	14.47
120.0810	119.0735	119.0737	C ₈ H ₉ N		Appendix 5.18	1.9	7.31
121.0650	120.0575	120.0577	C ₈ H ₁₀ O		Appendix 5.20	1.9	6.09

122.0966	121.0891	121.0893	C ₈ H ₁₁ N		Appendix 5.21	1.8	6.66
129.1024	128.0950	128.0951	C ₆ H ₁₂ ON ₂		Appendix 5.26	1.0	100
130.0865	129.0790	129.0792	C ₆ H ₁₁ O ₂ N		Appendix 5.27	1.7	6.14
130.1058	Unassigned	129.0985	Unassigned	Unassigned	n/a	n/a	6.43
132.1021	131.0946	131.0948	C ₆ H ₁₃ O ₂ N		Appendix 5.29	1.7	8.18
147.1131	146.1055	146.1058	C ₆ H ₁₄ O ₂ N ₂		Appendix 5.39	2.2	8.45
156.0770	155.0695	155.0697	C ₆ H ₉ O ₂ N ₂		Appendix 5.44	1.4	5.38

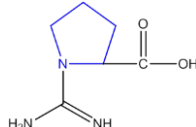
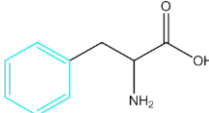
158.0927	157.0851	157.0854	C ₆ H ₁₁ O ₂ N ₃		Appendix 5.48	2.1	10.77
159.0919	158.0844	158.0846	C ₁₀ H ₁₁ N ₂	Unassigned	n/a	8.4	9.69
166.0865	165.0790	165.0792	C ₉ H ₁₁ O ₂ N		Appendix 5.51	1.4	16.98
186.1240	185.1164	185.1167	C ₈ H ₁₅ O ₂ N ₃	Unassigned	n/a	1.8	7.04

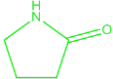
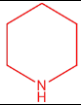
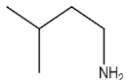
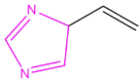
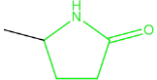
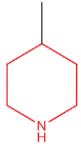
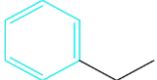
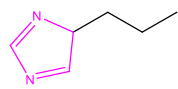
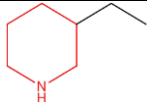
Table 5. 2 - Ions Observed Following SCW Hydrolysis of BSA at 253 °C for 20 min.

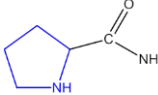
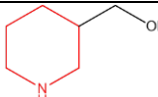
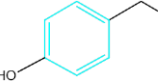
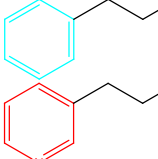
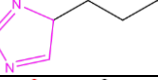
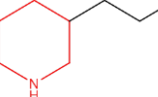
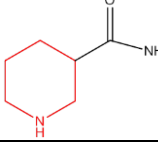
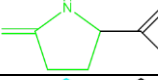
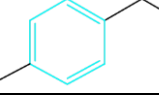
Furthermore, the ion observed at m/z 121.0650 has a mass difference corresponding to CO_2 and NH_2 loss from tyrosine. The assignment and structure were confirmed using HCD MS/MS (**Appendix Figure 5.20**). The further loss of the hydroxyl group from this structure was observed at m/z 105.0700 (HCD MS/MS analysis in **Appendix Figure 5.21**). Moreover, decarboxylation of phenylalanine was observed at m/z 120.0810 (HCD MS/MS analysis in **Appendix Figure 5.18**).

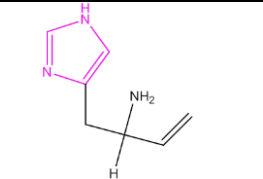
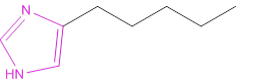
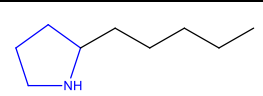
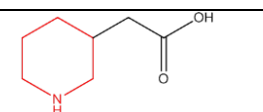
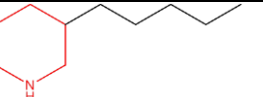
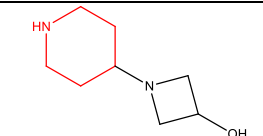
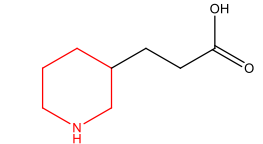
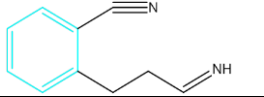
Free amino acids were also observed under these conditions, although fewer and at lower relative abundances compared to those at 207 °C. This observation suggests that amino acids are initially liberated under lower temperature points and then further modified as temperatures increase. Peaks corresponding to proline (m/z 116.0708), leucine and isoleucine (m/z 132.1021), lysine (m/z 147.1131), histidine (m/z 156.0770) and phenylalanine (m/z 166.0865) were observed.

Peaks that were speculated to correspond to tetrahydropyridine and piperidine were again observed at m/z 84.0808 and m/z 86.0965. As with the previous temperature point, further modifications on tetrahydropyridine and piperidine molecules are apparent (m/z 100.1131 and m/z 122.0966). Structures for these ions are proposed in **Appendix Figures 5.4** and **5.21**. Work in Chapter 4 suggested the propensity of sub-critical water to catalyse organic reactions. Moreover, sub-critical water has also been shown to catalyse alkylation reactions specifically. Aria *et al.* demonstrated the alkylation of phenol with propionaldehyde in the absence of a catalyst under sub-critical water conditions[239]. Additionally, Eckart *et al.* showed increased alkylation of phenol and p-cresol with tert-butanol shown at a temperature of 250 - 300 °C. [240]

MS analysis was also performed on hydrolysates obtained from BSA hydrolysed at 300 °C for 20 minutes (**Figure 5.10c** and **Table 5.3**). Peaks not observed under 207°C or 253°C for 20 minutes are highlighted in **Table 5.3**. The main reaction products that were detected under these conditions were additions of hydrocarbon chains to cyclic structures formed in the more moderate conditions.

<u>m/z</u>	<u>Calculated mass (Da)</u>	<u>Measured mass (Da)</u>	<u>Formula</u>	<u>Proposed Structure</u>	<u>HCD MS/MS</u>	<u>PPM</u>	<u>Relative abundance</u>
86.0600	85.0528	85.0527	C ₄ H ₇ NO		No	-0.4	5.77
86.0963	85.0892	85.0890	C ₅ H ₁₁ N		No	-2.1	96.88
88.1120	87.1048	87.1047	C ₅ H ₁₃ N		No	-0.9	10.77
95.0603	94.0531	94.0530	C ₅ H ₆ N ₂		No	-0.8	6.70
100.0757	99.0684	99.0684	C ₅ H ₉ ON		No	0.2	22.27
100.1120	99.1048	99.1047	C ₆ H ₁₃ N		Appendix Figure 5.4	-0.8	98.56
105.0698	106.0783	106.0782	C ₈ H ₁₀		Appendix Figure 5.5	-1.2	6.42
111.0917	110.0844	110.0844	C ₆ H ₁₀ N ₂		Appendix Figure 5.9	0.2	5.58
114.0914	n/a	n/a	solvent	n/a	n/a	n/a	41.40
114.1277	113.1204	113.1204	C ₇ H ₁₅ N		Appendix Figure 5.12	0.2	100.00

115.0866	114.0793	114.0793	C ₅ H ₁₀ ON ₂		Appendix Figure 5.13	0.2	15.84
116.1070	115.0997	115.0997	C ₆ H ₁₃ ON		Appendix Figure 5.15	0.2	14.47
121.0648	120.0575	120.0575	C ₈ H ₉ O		Appendix Figure 5.20	0.2	22.89
122.0965	121.0891	121.0892	C ₈ H ₁₂ N		Appendix Figure 5.21	1.0	22.11
125.1074	124.1000	124.1001	C ₇ H ₁₂ N ₂		Appendix Figure 5.24	1.0	5.41
128.1434	127.1361	127.1361	C ₈ H ₁₇ N		Appendix Figure 5.25	0.2	10.23
129.1023	128.0950	128.0950	C ₆ H ₁₂ ON ₂		Appendix Figure 5.26	0.2	23.79
130.0503	129.0426	129.0430	C ₅ H ₇ O ₃ N		Appendix Figure 5.27	3.3	31.56
138.0913	137.0841	137.0840	C ₈ H ₁₁ ON		Appendix Figure 5.33	-0.6	9.27

138.1027	137.0953	137.0954	C ₇ H ₁₁ N ₃		Appendix Figure 5.34	0.9	7.16
139.1231	138.1157	138.1158	C ₈ H ₁₄ N ₂		Appendix Figure 5.35	0.9	6.06
142.1591	141.1518	141.1518	C ₉ H ₁₉ N		Appendix Figure 5.36	0.2	16.10
144.1020	143.0946	143.0947	C ₇ H ₁₃ NO ₂		No	0.9	6.29
156.1748	155.1674	155.1675	C ₁₀ H ₂₁ N		Appendix Figure 5.45	0.8	10.33
157.1336	156.1263	156.1263	C ₈ H ₁₆ N ₂ O		Appendix Figure 5.47	0.2	7.24
158.1176	157.1103	157.1103	C ₈ H ₁₅ NO ₂		Appendix Figure 5.49	0.2	7.65
159.0917	158.0844	158.0844	C ₁₀ H ₁₀ N ₂		Appendix Figure 5.50	0.2	16.7

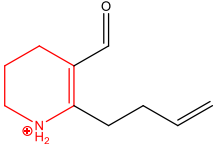
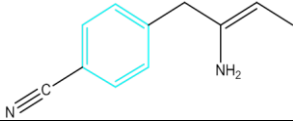
166.1228	165.1154	165.1155	C ₁₀ H ₁₆ ON		Appendix Figure 5.52	0.8	6.1
173.1074	172.1001	172.1001	C ₁₁ H ₁₃ N ₂		Appendix Figure 5.54	0.1	9.4
185.1286	184.1212	184.1213	C ₉ H ₁₇ O ₂ N ₂	Unassigned	No	0.7	8.4

Table 5. 3 - Ions Observed Following SCW Hydrolysis of BSA at 300 °C for 20 min.

The base peak in the spectrum was observed at m/z 114.1277, corresponding to singly protonated $C_7H_{15}N$. This ion could represent piperidine with the addition of a C_2H_4 group. Fragment ions consistent with this structure were identified following HCD MS/MS (**Appendix Figure 5.12**). Moreover, the peak hypothesised to correspond to piperidine was observed at m/z 86.0963. Additional peaks with mass differences corresponding to piperidine plus : CH_2 at m/z 100.1120 (HCD MS/MS analysis in **Appendix Figure 5.3**), C_3H at m/z 122.0965 (HCD MS/MS analysis in **Appendix Figure 5.21b**), C_3H_6 at m/z 128.1434 (HCD MS/MS analysis in **Appendix Figure 5.25**), C_5H_{10} at m/z 156.1748 (HCD MS/MS analysis in **Appendix Figure 5.45**), CH_2O at m/z 116.1070 (HCD MS/MS analysis in **Appendix Figure 5.15**), $C_3H_4O_2$ (HCD MS/MS analysis in **Appendix Figure 5.49**), C_5H_5O at m/z 166.1228 (HCD MS/MS analysis in **Appendix Figure 5.52**) were also noted.

The results also suggest that an imidazole ring can be observed with various additions. These included C_2H_2 at m/z 95.0603 (proposed structure is listed in **Table 5.3** despite no HCD MS/MS data being collected for this ion), C_3H_6 at m/z 111.0917 (HCD MS/MS analysis in **Appendix Figure 5.9**), C_4H_8 at m/z 125.1074 (HCD MS/MS analysis in **Appendix Figure 5.24**), C_4N_2 at m/z 138.1027 (HCD MS/MS analysis in **Appendix Figure 5.34**) and C_5H_{10} at m/z 139.1231 (HCD MS/MS analysis in **Appendix Figure 5.35**). Additions to benzene were also identified: additions of C_2H_4 at m/z 105.0698 (HCD MS/MS analysis in **Appendix Figure 5.5**), $C_4H_4N_2$ at m/z 159.0917 (HCD MS/MS analysis in **Appendix Figure 5.50**).

Interestingly, an ion is observed at m/z 157.1336. HCD MS/MS analysis confirmed the structure to involve the conjugation of piperidine to azetidine (**Appendix Figure 5.47**). Azetidine has previously been shown to be a deamination product of asparagine (**Scheme 5.1d**) [238]. Parsons *et al.* have performed similar coupling reactions on arenes with various alkenes at temperatures of 260 °C - 400°C. However, these reactions were performed with a Pd catalyst and its removal was shown to be detrimental to the yield [241].

Unlike the analyses of BSA hydrolysates obtained from hydrolysis at 207 and 253 °C for 20 minutes, a peak corresponding to pipecolic acid was not observed. Possible methylation and ethylation products of this species were observed at m/z 144.1020 and 158.1176). HCD MS/MS analysis was only performed on the ion at m/z 158.1176 due to difficulties in isolation, however fragment ions consistent with this assignment were observed (**Appendix Figure 5.49**). Furthermore, the ion at m/z 129.1023 corresponds to amidation of pipecolic acid (**Appendix Figure 5.26**).

A peak corresponding to pyroglutamate was observed during these conditions at m/z 130.0503. The neutral loss of carbon dioxide was observed at m/z 86.0600 to form pyrrolidone. The additions of CH₂ at m/z 100.0757 (no HCD MS/MS data collected due to difficulties in isolation) and C₅H₁₀ at m/z 142.1591 (HCD MS/MS analysis in **Appendix Figure 5.45**) were observed.

Additional ions identified under these conditions included peaks at m/z 138.091, which was attributed to Tyr-CO₂, m/z 121.0698 which was attributed to Tyr-CO₂-NH₃, m/z 88.1120, which was attributed to Ile/Leu-CO₂. The structure of the ions at m/z 138.09 and 121.0698 was solved using HCD MS/MS analysis (**Appendix Figure 5.33** and **5.20**). No fragment ions were observed when this peak was isolated and subjected to HCD due to the limited sensitivity of the instrument at this mass range.

Furthermore, when BSA was hydrolysed at 253 °C for 20 mins an increase in amidated species (compared to hydrolysis conditions 207 °C for 20 minutes) was noted. The amidated form of proline (prolinamide) being observed at higher abundance than proline itself. Under hydrolysis conditions of 300 °C for 20 minutes, prolinamide was observed at m/z 115.0866, whilst no ion corresponding to proline was detected. This suggests amidation continues to become a more favourable reaction as temperature increases.

A further ion was observed at m/z 173.1074 which was unique to these conditions. The structure was determined using HCD MS/MS analysis (**Appendix Figure 5.54**).

The results above are consistent with the prior findings from the SCW hydrolysis of peptides in Chapter 4. Commonly occurring amino acid modifications following treatment with SCW are dehydration, deamination and amidation. Furthermore decarboxylation was identified as a major modification which is consistent with previous studies on the SCW of amino acids.

5.5.2 NTG hydrolysate analysis

Figure 5.11a shows the direct infusion electrospray mass spectrum of the NTG hydrolysed at 207 °C for 20 minutes (see also **Table 5.4**). As with the hydrolysis of BSA, amino acids were liberated from the protein under these conditions. Peaks hypothesised to corresponding to the alanine at m/z 90.0550, proline at m/z 116.0708 (**Appendix Figure 5.14**) , valine at m/z 118.0865 (**Appendix Figure 5.16**), lysine and isoleucine at m/z 132.1022 (**Appendix Figure 5.29**), aspartic acid at m/z 134.0451 (**Appendix Figure 5.32**), histidine at m/z 156.0771 (**Appendix Figure 5.44**), phenylalanine at m/z 166.867 (**Appendix Figure 5.51**) and arginine at m/z 175.1194 (**Appendix Figure 5.55**) were observed. HCD analysis of the ion observed at m/z 90.05 failed to provide confirmation of alanine, due to the limited sensitivity of the Orbitrap mass analyser under these conditions. A solution of pure alanine was analysed using the same electrospray and HCD conditions and no fragment ions could be detected.

The base peak in the spectrum was observed at m/z 130.0501. This peak was observed in the SCW hydrolysis of BSA and attributed to pyroglutamate. Ions observed at m/z 84.0445 and 86.0601 correspond to decomposition products of pyroglutamate, as well as a peak corresponding to piperidine at m/z 86.0965.

Two hydrolysis products that are observed specifically in NTG are ions at m/z 96.0445 and m/z 102.1279. These species are hypothesised aspyridinol and hexylamine, although these structures are inconsistent with the reactions already identified and the HCD data acquired were not of good quality.

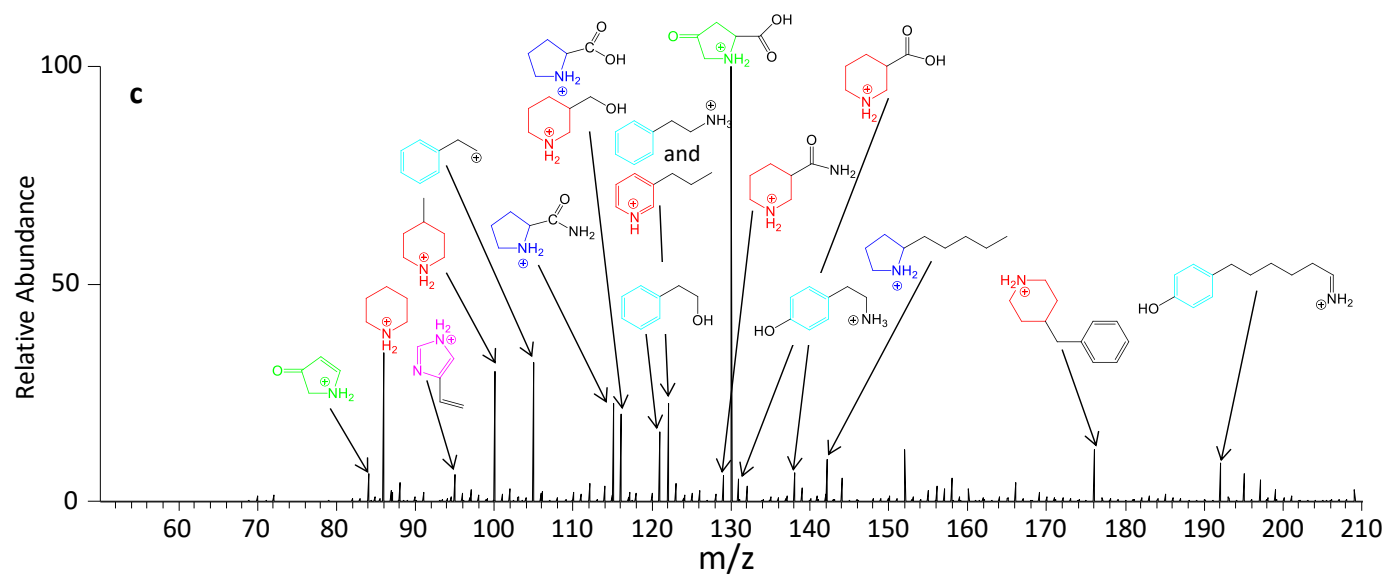
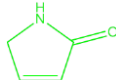
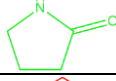
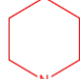
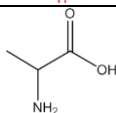
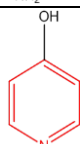
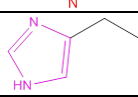
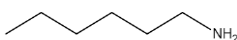
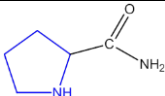
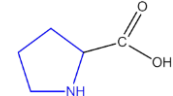
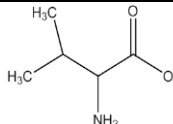
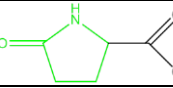
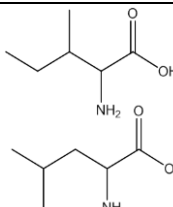
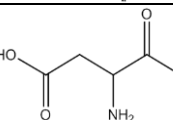
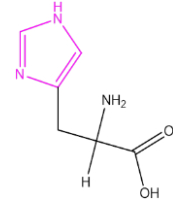
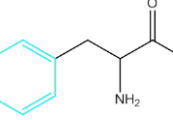


Figure 5. 11 - Direct infusion ESI MS of BSA hydrolysed at **a)** 207°C for 20 min, **b)** 253 °C for 20 min and **c)** 300 °C for 20 min.

<u>m/z</u>	<u>Calculated mass (Da)</u>	<u>Measured mass (Da)</u>	<u>Formula</u>	<u>Proposed Structure</u>	<u>HCD MS/MS</u>	<u>PPM</u>	<u>Relative abundance</u>
84.0445	83.0371	83.0372	C ₄ H ₅ ON		No	1.5	6.11
86.0601	85.0528	85.0528	C ₄ H ₇ ON		No	0.3	8.58
86.0965	85.0892	85.0892	C ₅ H ₁₂ N		No	0.3	11.71
90.0550	89.0477	89.0477	C ₃ H ₈ O ₂ N		No	0.3	6.46
96.0445	95.0371	95.0372	C ₅ H ₅ ON		No	1.3	8.81
97.0761	96.0688	96.0689	C ₅ H ₈ N ₂		Appendix Figure 5.2	0.8	5.49
102.1279	101.1205	101.1206	C ₆ H ₁₅ N		No	1.2	41.02
106.0500	n/a	n/a	Solvent	n/a	n/a	n/a	5.55
114.0916	n/a	n/a	Solvent	n/a	n/a	n/a	17.4
115.0868	114.0793	114.0795	C ₅ H ₁₀ ON ₂		Appendix Figure 5.12	2.0	15.04

116.0708	115.0633	115.0635	C ₅ H ₉ O ₂ N		Appendix Figure 5.13	1.9	100
118.0865	117.0790	117.0792	C ₅ H ₁₁ O ₂ N		Appendix Figure 5.15	1.9	24.28
130.0501	129.0426	129.0428	C ₅ H ₇ O ₃ N		Appendix Figure 5.26	1.7	89.63
130.0978	129.0902	129.0905	C ₅ H ₁₂ ON ₃	Unassinged	n/a	2.5	10.49
132.1022	131.0946	131.0949	C ₆ H ₁₃ O ₂ N		Appendix Figure 5.28	2.5	49.88
134.0451	133.0375	133.0378	C ₄ H ₇ O ₄ N		Appendix Figure 5.31	2.4	8.57
156.0771	155.0695	155.0698	C ₆ H ₉ O ₂ N ₃		Appendix Figure 5.43	2.1	6.88
166.0867	165.0790	165.0794	C ₉ H ₁₁ O ₂ N		Appendix Figure 5.50	2.6	8.36

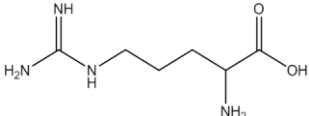
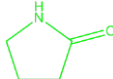
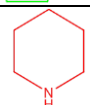
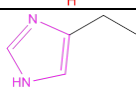
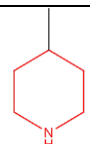
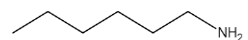
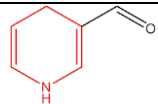
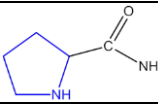
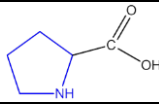
175.1194	174.1117	174.1121	C ₆ H ₁₄ O ₂ N ₄		Appendix Figure 5.54	2.4	7.54
----------	----------	----------	--	--	-------------------------	-----	------

Table 5. 4 - Ions Observed Following SCW Hydrolysis of NTG at 207 °C for 20 min.

In addition ions were observed at m/z 84.0445, 86.0601, 86.0965 and 97.0761. These were attributed to neutral losses from the structures previously established under these conditions.

Hydrolysates obtained from SCW treatment of NTG at 253 °C for 20 minutes were next analysed (**Figure 5.11b** and **Table 5.5**). Peaks not observed at 207 °C for 20 minutes are highlighted in **Table 5.5**. Fewer peaks corresponding to amino acids could be detected at this increased temperature. Ions were observed m/z 116.0708, 118.0865, 132.1022, 166.0867, corresponding to proline, valine, leucine and/or isoleucine and phenylalanine.

Ions were also observed that were previously identified in hydrolysates as pyrrol-2-one (m/z 86.0601), ethylimidazole (m/z 97.0762), piperidine (m/z 86.0965), pipecoline (m/z 100.1122), prolinamide (m/z 115.0868), pyroglutamate (m/z 130.0502) and pipecolic acid (m/z 130.0865). Additional ions, not previously detected, were observed at m/z 110.0602 and 116.1072. The structures of the two ions were determined using HCD MS/MS (**Appendix Figure 5.7** and **5.15**).

<u>m/z</u>	<u>Calculated mass (Da)</u>	<u>Measured mass (Da)</u>	<u>Formula</u>	<u>Proposed Structure</u>	<u>HCD MS/MS</u>	<u>PPM</u>	<u>Relative abundance</u>
86.0601	85.0528	85.0528	C ₄ H ₇ ON		No	0.3	5.21
86.0965	85.0892	85.0892	C ₅ H ₁₁ N		No	0.3	30.17
97.0762	96.0688	96.0689	C ₅ H ₈ N ₂		Appendix Figure 5.2	1.8	5.49
100.1122	99.1048	99.1049	C ₆ H ₁₃ N		Appendix Figure 5.3	1.3	12.28
102.1279	101.1205	101.1206	C ₆ H ₁₅ N		No	1.2	9.87
104.1071	103.0997	103.0998	C ₅ H ₁₃ ON	Unassigned	No	1.2	13.44
110.0602	109.0528	109.0529	C ₆ H ₇ ON		Appendix Figure 5.7	1.1	9.57
114.0916	n/a	n/a	Solvent	n/a	n/a	n/a	6.54
115.0868	114.0793	114.0795	C ₅ H ₁₀ ON ₂		Appendix Figure 5.13	2.0	10.45
116.0708	115.0633	115.0635	C ₅ H ₉ O ₂ N		Appendix Figure 5.14	1.9	100.00

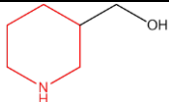
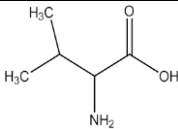
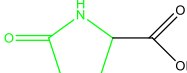
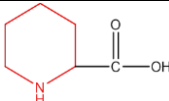
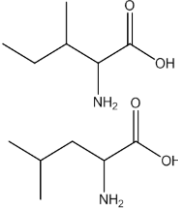
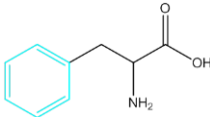
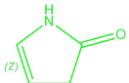
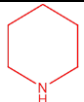
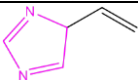
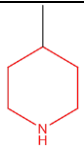
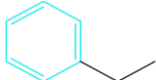
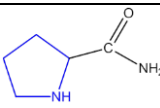
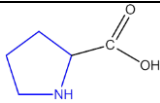
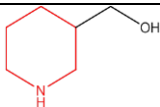
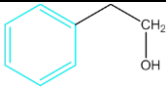
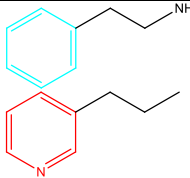
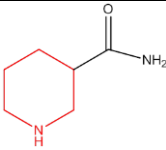
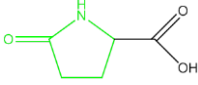
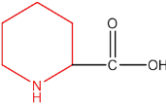
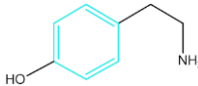
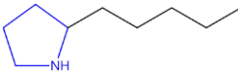
116.1072	115.0997	115.0999	C ₆ H ₁₃ ON		Appendix Figure 5.15	1.9	10.17
117.0742	n/a	n/a	Solvent	n/a	n/a	n/a	6.76
118.0865	117.0790	117.0792	C ₅ H ₁₁ O ₂ N		Appendix Figure 5.16	1.9	11.05
130.0502	129.0426	129.0429	C ₅ H ₇ O ₃ N		Appendix Figure 5.27	2.5	56.13
130.0865	129.0790	129.0792	C ₆ H ₁₁ O ₂ N		Appendix Figure 5.28	1.7	6.25
132.1022	131.0946	131.0949	C ₆ H ₁₃ O ₂ N		Appendix Figure 5.29	2.5	22.22
166.0867	165.0790	165.0794	C ₉ H ₁₁ O ₂ N		Appendix Figure 5.51	2.6	7.85

Table 5. 5 - Ions Observed Following SCW Hydrolysis of NTG at 253 °C for 20 min.

Figure 5.11c shows the direct infusion electrospray mass spectrum of NTG hydrolysed at 300 °C for 20 minutes (see also **Table 5.6**). Peaks not observed under 207°C or 253 °C for 20 minutes are highlighted in **Table 5.6**. Only one unmodified amino acid was observed under these conditions, and that was proline (m/z 116.0706). The base peak in the mass spectrum was at m/z 130.0498, which was again attributed to pyroglutamate.

Furthermore, the deamination of lysine to pipecolic acid (m/z 130.0862) and its subsequent amidation to piperidine-4-carboxamide (m/z 129.1023) were again noted. Species corresponding to the amidation of proline (m/z 115.0865) as well as a decarboxylation of phenylalanine (m/z 120.0805) were also noted. As with the BSA hydrolysates, an increased amount of addition reactions occurred under these conditions. The conjugation of piperidine to CH_2 (m/z 100.1120) (HCD MS/MS analysis in **Appendix Figure 5.3**), CH_3O (m/z 116.1069) (HCD MS/MS analysis in **Appendix Figure 5.15**) and C_3 (m/z 122.0964) (HCD MS/MS analysis in **Appendix Figure 5.21**) were apparent. The conjugation of piperidine to a benzene ring (m/z 176.1433) was also identified (HCD MS/MS analysis in **Appendix Figure 5.56**). The benzene ring, which is formed from the decomposition of phenylalanine or tyrosine, was itself speculated to have additions of C_2H_4 , $\text{C}_2\text{H}_4\text{O}$, $\text{C}_2\text{H}_5\text{N}$, and $\text{C}_6\text{H}_{12}\text{ON}$ (m/z 105.0698, 121.0648, 122.0964 and 192.1383) (HCD MS/MS analysis in **Appendix Figure 5.5, 5.20, 5.21, 5.59**). Additions of C_2H_2 to an imidazole ring and C_5H_{10} to pyrrolidine were also speculated (m/z 95.0603 and m/z 142.1590). No HCD MS/MS data were collected for the ion at 95.0603, although the structure of the ion at m/z 142.1590 was speculated in **Appendix Figure 5.36**.

<u>m/z</u>	<u>Calculated mass (Da)</u>	<u>Measured mass (Da)</u>	<u>Formula</u>	<u>Proposed Structure</u>	<u>HCD MS/MS</u>	<u>PPM</u>	<u>Relative abundance</u>
84.0443	83.0371	83.0370	C ₄ H ₅ ON		No	-0.9	6.10
86.0963	85.0892	85.0890	C ₅ H ₁₁ N		No	-2.1	30.70
95.0603	94.0531	94.0530	C ₅ H ₆ N ₂		No	-0.8	5.76
100.1120	99.1048	99.1047	C ₆ H ₁₃ N		Appendix Figure 5.3	-0.8	26.85
105.0698	106.0783	106.0782	C ₈ H ₁₀		Appendix Figure 5.5	-1.2	27.37
115.0865	114.0793	114.0792	C ₅ H ₁₀ ON ₂		Appendix Figure 5.13	-0.7	19.97
116.0706	115.0633	115.0633	C ₅ H ₉ O ₂ N		Appendix Figure 5.14	0.2	18.17
116.1069	115.0997	115.0996	C ₆ H ₁₄ ON		Appendix Figure 5.15	-0.7	12.14

121.0648	122.0732	122.0732	C ₈ H ₁₀ O		Appendix Figure 5.20	14.70	121.0648
122.0964	121.0892	121.0891	C ₈ H ₁₁ N		Appendix Figure 5.21	-0.6	19.96
129.1023	128.0950	128.0950	C ₆ H ₁₂ ON ₂		Appendix Figure 5.26	0.2	5.29
130.0498	129.0426	129.0425	C ₅ H ₇ O ₃ N		Appendix Figure 5.27	-0.6	100.00
130.0862	129.0790	129.0789	C ₆ H ₁₁ O ₂ N		Appendix Figure 5.28	-0.6	8.81
138.0914	137.0841	137.0841	C ₈ H ₁₁ ON		Appendix Figure 5.33	0.5	5.97
142.1590	141.1518	141.1517	C ₉ H ₁₉ N		Appendix Figure 5.36	-0.5	8.20

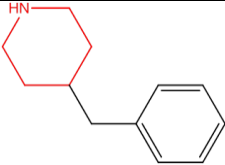
152.0318	n/a	151.0245	n/a	Unassigned	n/a	n/a	11.81
176.1433	175.1361	175.1360	C ₁₂ H ₁₇ N		Appendix Figure 5.56	-0.4	9.99

Table 5. 6- Ions Observed Following SCW Hydrolysis of NTG at 300 °C for 20 min.

5.5.3 BSG hydrolysate analysis

Figure 5.12a shows the direct infusion electrospray mass spectrum of the BSG hydrolysed at 207°C for 20 minutes. A list of predicted structures for all ions is shown in **Table 5.7**. Under hydrolysis conditions of 207°C for 20 minutes, amino acids were efficiently generated under these conditions and ions corresponding to proline (m/z 116.0700), valine (m/z 118.0856), leucine and/or isoleucine (m/z 132.1013), glutamine (m/z 147.0757), lysine (m/z 147.1121), glutamate (m/z 148.0597), histidine (m/z 156.0760), phenylalanine (m/z 166.0854), arginine (m/z 175.1181) and tyrosine (m/z 182.0803) were observed. Additional ions at m/z 86.0959, 97.0755, 120.0802 and 130.0492 were observed. These were detected in previous hydrolysates and structures were determined using HCD MS/MS.

Figure 5.12b shows the direct infusion electrospray mass spectrum of the BSG hydrolysed at 253°C for 20 minutes (see also **Table 5.8**). Peaks not observed under 207°C are highlighted in **Table 5.8**. Under these conditions the base peak in the mass spectrum remains m/z 116.0700, which was attributed to proline. Under these conditions, an increased amount of proline amidation is observed (m/z 115.0860). The amino acids valine (m/z 118.0856), leucine and/or isoleucine (m/z 132.1012) and phenylalanine (m/z 166.0854) were also detected. Pyroglutamate was also observed at an increased abundance (m/z 130.0492). Piperidine (m/z 86.0659) and its methylated product (m/z 100.1115) were also observed.

Figure 5.12b shows the direct infusion electrospray mass spectrum of the BSG hydrolysed at 300°C for 20 minutes (see also **Table 5.9**). Peaks not observed under 207 °C or 253 °C are highlighted in **Table 5.9**. Very few ions representing unmodified amino acids were observed under these conditions. This was consistent with BSA and NTG hydrolysates from the same hydrolysis conditions. Only ions corresponding to proline (m/z 116.0700) and leucine and/or isoleucine (m/z 132.1013) were observed. Piperidine was observed in high abundance (m/z 86.0959), with speculated additions of CH_2 (m/z 100.1115), C_2H_2 (m/z 112.1115), C_2H_4 (m/z 114.1271), CH_2O (m/z 86.0959) and $\text{C}_2\text{H}_2\text{O}_2$ (m/z 144.1012) as well as a species at m/z 110.0595.

Similar additions were speculated on the imidazole ring of histidine of CH_2 (m/z 97.0755), C_3H_6 (m/z 111.0911), C_4H_6 (m/z 123.0911), C_4H_8 (m/z 125.1067), C_5H_{10} (m/z 139.1223) and C_6H_{12} (m/z 153.1378). The addition of C_3H to piperidine and the decarboxylation of phenylalanine were again observed as hydrolysis of BSA under these conditions (both m/z 122.0962). Prolinamide and pyroglutamate were again detected at m/z 115.0860 and m/z 130.0492.

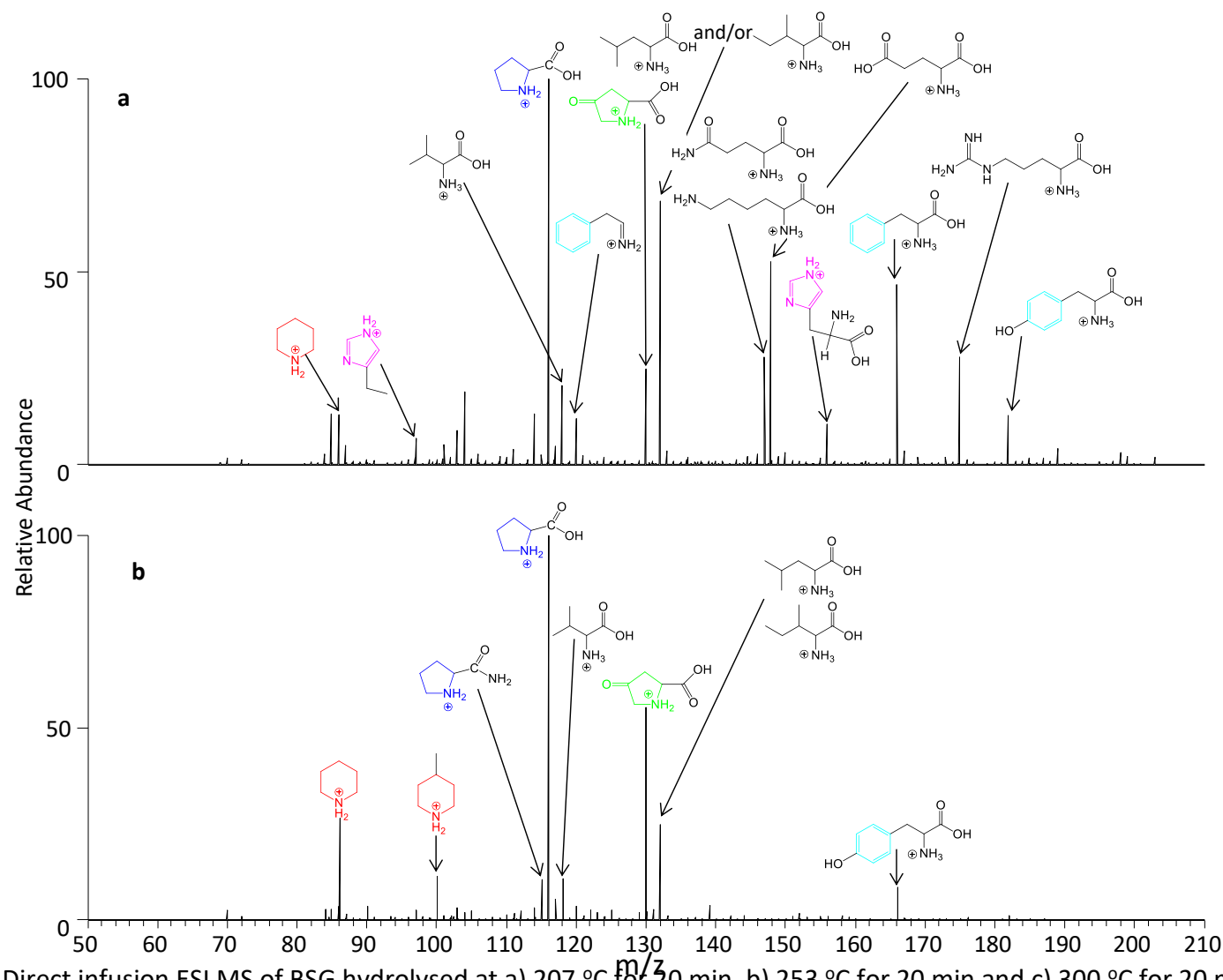


Figure 5. 12- Direct infusion ESI MS of BSG hydrolysed at a) 207 °C for 20 min, b) 253 °C for 20 min and c) 300 °C for 20 min.

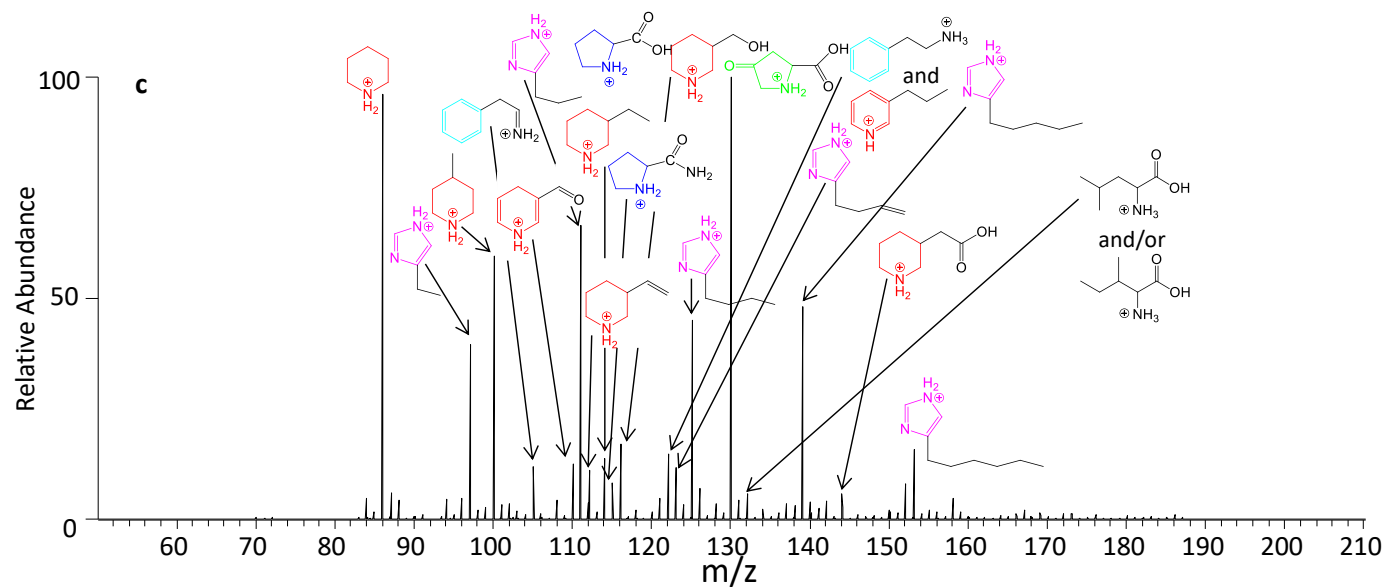
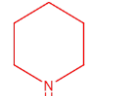
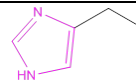
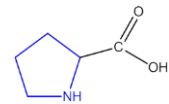
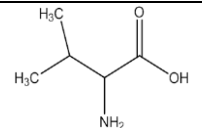
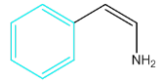
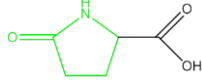
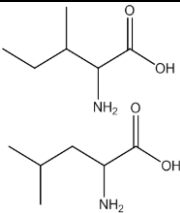
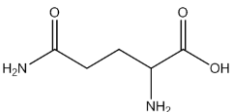
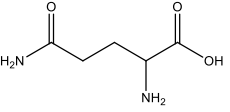
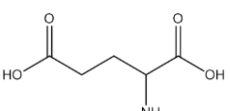
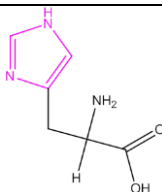


Figure 5. 12 (continued) - Direct infusion ESI MS of BSG hydrolysed at a) 207 °C for 20 min, b) 253 °C for 20 min and c) 300 °C for 20 min.

<u>m/z</u>	<u>Calculated mass (Da)</u>	<u>Measured mass (Da)</u>	<u>Formula</u>	<u>Proposed Structure</u>	<u>HCD MS/MS</u>	<u>PPM</u>	<u>Relative abundance</u>
84.9592	n/a	n/a	Solvent	n/a	No	n/a	12.79
86.0959	85.0892	85.0886	C ₅ H ₁₁ N		No	-6.8	12.69
97.0755	96.0688	96.0682	C ₅ H ₈ N ₂		Appendix Figure 5.2	-5.5	6.84
102.9697	n/a	n/a	Solvent	n/a	No	n/a	8.79
104.1064	103.0997	103.0991	CH ₁₃ ON	Unassigned	No	-5.7	18.62
114.0907	n/a	n/a	Solvent	n/a	No	n/a	12.87
116.0700	115.0633	115.0627	C ₅ H ₉ O ₂ N		Appendix Figure 5.14	-5.0	100
118.0856	117.0790	117.0783	C ₅ H ₁₁ O ₂ N		Appendix Figure 5.16	-5.8	20.18
120.0802	119.0735	119.0729	C ₈ H ₉ N		Appendix Figure 5.18	-4.8	11.75
130.0492	129.0426	129.0419	C ₅ H ₇ O ₃ N		Appendix Figure 5.27	-5.2	24.76

132.1013	131.0946	131.0940	C ₆ H ₁₃ O ₂ N		Appendix Figure 5.29	-4.4	68.32
147.0757	146.0691	146.0684	C ₅ H ₁₀ O ₃ N ₂		Appendix Figure 5.38	-4.8	28.24
147.1121	146.1055	146.1048	C ₆ H ₁₄ O ₂ N ₂		Appendix Figure 5.39	-4.6	6.78
148.0597	147.0532	147.0524	C ₅ H ₉ O ₄ N		Appendix Figure 5.40	-5.3	52.91
156.0760	155.0695	155.0687	C ₆ H ₉ O ₂ N ₃		Appendix Figure 5.44	-5.0	10.27

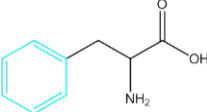
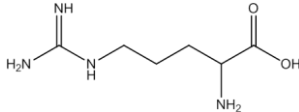
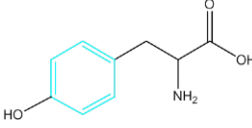
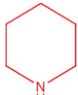
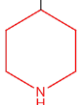
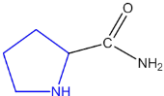
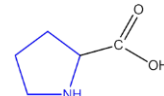
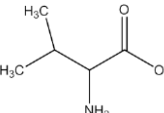
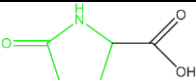
166.0854	165.0790	165.0781	C ₉ H ₁₁ O ₂ N		Appendix Figure 5.51	-5.3	47.07
175.1181	174.1118	174.1108	C ₆ H ₁₄ O ₄ N ₂		Appendix Figure 5.55	-5.6	28.23
182.0803	181.0739	181.0730	C ₉ H ₁₁ O ₃ N		Appendix Figure 5.58	-4.8	12.96

Table 5. 7 - Ions Observed Following SCW Hydrolysis of BSG at 207 °C for 20 min.

<u>m/z</u>	<u>Calculated mass (Da)</u>	<u>Measured mass (Da)</u>	<u>Formula</u>	<u>Structure</u>	<u>HCD MS/MS</u>	<u>PPM</u>	<u>Relative abundance</u>
86.0959	85.0892	85.0886	C ₅ H ₁₁ N		No	-6.8	28.34
100.1115	99.1048	99.1042	C ₆ H ₁₃ N		Appendix Figure 5.3	-5.8	13.45
115.0860	114.0793	114.0787	C ₅ H ₁₀ ON ₂		Appendix Figure 5.13	-5.0	10.65
116.0700	115.0633	115.0627	C ₅ H ₉ O ₂ N		Appendix Figure 5.14	-5.0	100
118.0856	117.0790	117.0783	C ₅ H ₁₁ O ₂ N		Appendix Figure 5.16	-5.8	10.11
130.0492	129.0426	129.0419	C ₅ H ₇ O ₃ N		Appendix Figure 5.27	-5.2	49.95

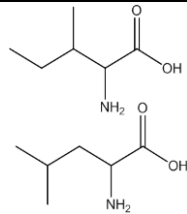
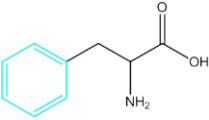
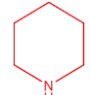
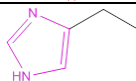
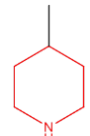
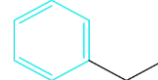
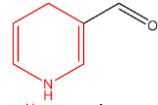
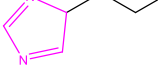
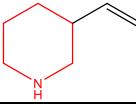
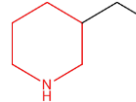
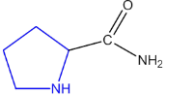
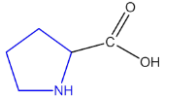
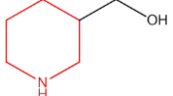
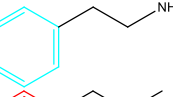
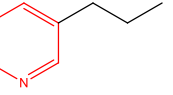
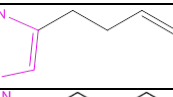
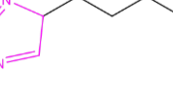
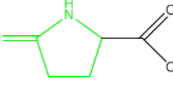
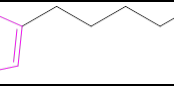
132.1012	131.0946	131.0939	C ₆ H ₁₃ O ₂ N		Appendix Figure 5.29	-5.2	24.41
166.0854	165.0790	165.0781	C ₉ H ₁₁ O ₂ N		Appendix Figure 5.50	-5.3	6.51

Table 5. 8 - Ions Observed Following SCW Hydrolysis of BSG at 253 °C for 20 min.

6.10	<u>Calculated mass (Da)</u>	<u>Measured mass (Da)</u>	<u>Formula</u>	<u>Proposed Structure</u>	<u>HCD MS/MS</u>	<u>PPM</u>	<u>Relative abundance</u>
86.0959	85.0892	85.0886	C ₅ H ₁₁ N		No	-6.8	91.94
97.0755	96.0688	96.0682	C ₅ H ₈ N ₂		Appendix Figure 5.2	-5.5	38.51
100.0751	n/a	n/a	solvent	n/a	n/a	n/a	17.35
100.1115	99.1048	99.1042	C ₆ H ₁₃ N		Appendix Figure 5.3	-5.8	58.1
105.0693	104.0626	104.0620	C ₈ H ₈		Appendix Figure 5.5	-5.5	11.49
110.0595	109.0528	109.0522	C ₆ H ₇ ON		Appendix Figure 5.7	-5.3	12.04
111.0911	110.0844	110.0838	C ₆ H ₁₀ N ₂		Appendix Figure 5.9	-5.2	63.15
112.1115	111.1048	111.1042	C ₇ H ₁₃ N		Appendix Figure 5.11	-5.2	10.8
114.0908	n/a	n/a	Solvent	n/a	n/a	n/a	6.47
114.1271	113.1204	113.1198	C ₇ H ₁₅ N		Appendix Figure 5.12	-5.1	13.61

115.086	114.0793	114.0787	C ₅ H ₁₀ ON ₂		Appendix Figure 5.13	-5.0	7.98
116.0700	115.0633	115.0627	C ₅ H ₉ O ₂ N		Appendix Figure 5.14	-5.0	15.38
116.1064	115.0997	115.0991	C ₆ H ₁₃ ON		Appendix Figure 5.15	-5.0	16.21
122.0958	121.0891	121.0885	C ₈ H ₁₂ N	 	Appendix Figure 5.21	-4.8	14.18
123.0911	122.0844	122.0838	C ₇ H ₁₀ N ₂		Appendix Figure 5.22	-4.7	11.28
125.1067	124.1000	124.0994	C ₇ H ₁₂ N ₂		Appendix Figure 5.24	-4.6	43.89
130.0492	129.0426	129.0419	C ₅ H ₇ O ₃ N		Appendix Figure 5.27	-5.2	100
139.1223	138.1157	138.1150	C ₈ H ₁₄ N ₂		Appendix Figure 5.35	-4.9	45.91

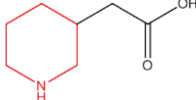
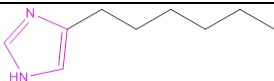
144.1012	143.0946	143.0939	C ₇ H ₁₃ NO ₂		No	-4.7	5.56
152.0311	n/a	151.0245	n/a	Unassigned	n/a	n/a	7.43
153.1378	152.1314	152.1305	C ₉ H ₁₆ N ₂		Appendix Figure 5.42	-5.8	15.52

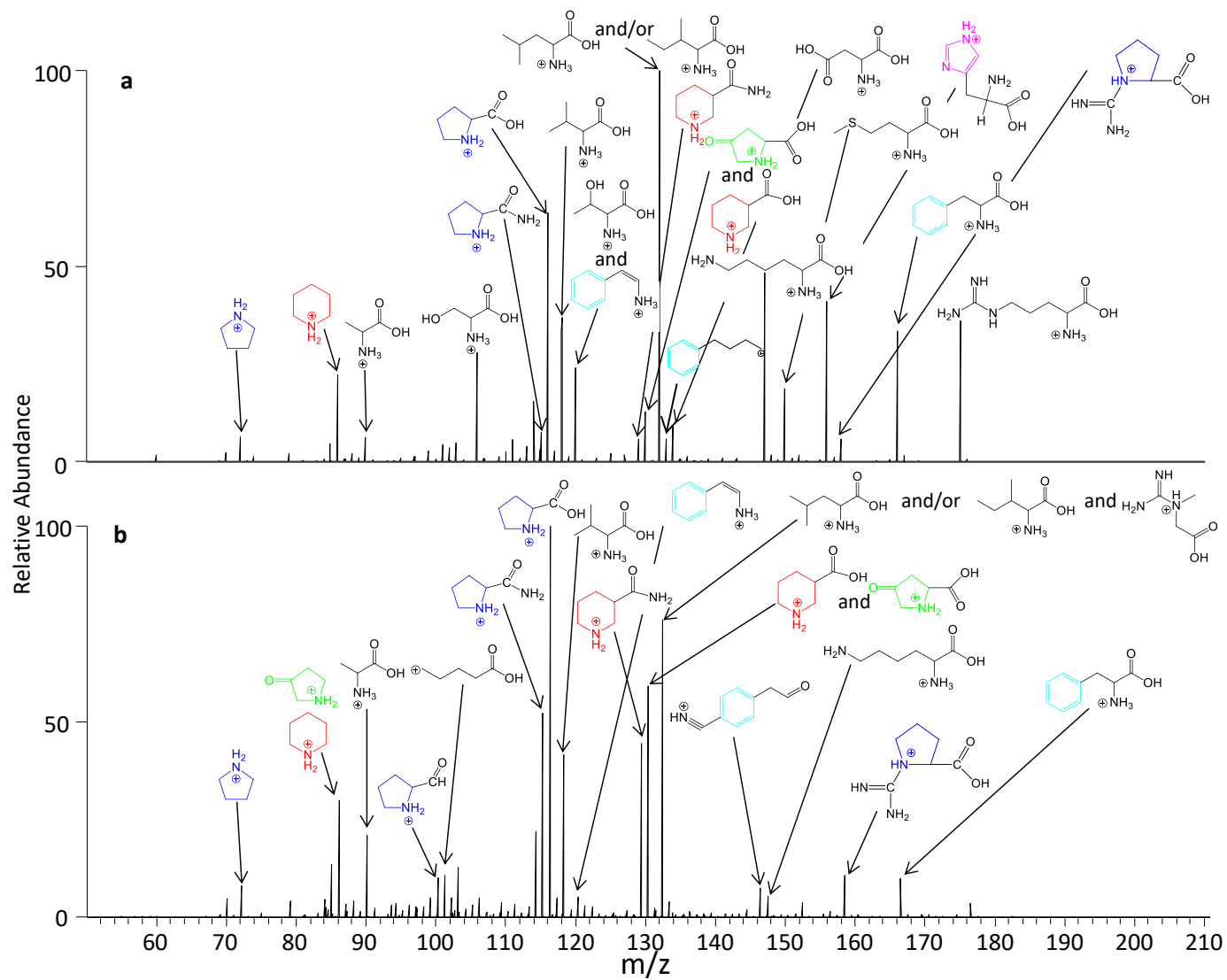
Table 5. 9 - Ions Observed Following SCW Hydrolysis of BSG at 300 °C for 20 min.

5.5.4 Amino acid hydrolysate analysis

To further probe the pathway of protein degradation in SCW, an equimolar mixture of all 20 natural amino acids was hydrolysed. The direct infusion electrospray mass spectrum of this mixture prior to SCW treatment is shown in **Appendix Figure 5.67** (see also **Appendix Table 5.8**). Peaks were observed corresponding to 19 of the 20 amino acids and the structures were confirmed using HCD MS/MS. Ions corresponding to the amino acids were observed: alanine at m/z 90.0550 (HCD MS/MS analysis did not result in the observation of fragment ions) serine at m/z 106.0500 (HCD MS/MS analysis in **Appendix Figure 5.5**), proline at m/z 116.0708 (HCD MS/MS analysis in **Appendix Figure 5.14**), valine at m/z 118.0864 (HCD MS/MS analysis in **Appendix Figure 5.16**), threonine at m/z 120.0657 (HCD MS/MS analysis in **Appendix Figure 5.17**), leucine and isoleucine at m/z 132.1021 (HCD MS/MS analysis in **Appendix Figure 5.29**), asparagine at m/z 133.0605 (HCD MS/MS analysis in **Appendix Figure 5.30**), aspartic acid at m/z 134.0445 (HCD MS/MS analysis in **Appendix Figure 5.32**), glutamine at m/z 147.0767 (HCD MS/MS analysis in **Appendix Figure 5.38**), lysine at m/z 147.1131 (HCD MS/MS analysis in **Appendix Figure 5.39**) glutamate at m/z 148.0607 (HCD MS/MS analysis in **Appendix Figure 5.40**), methionine at m/z 150.0586 (HCD MS/MS analysis in **Appendix Figure 5.41**), histidine at m/z 156.0770 (HCD MS/MS analysis in **Appendix Figure 5.43**), phenylalanine at m/z 166.0866 (HCD MS/MS analysis in **Appendix Figure 5.51**) and arginine at m/z 175.1193 HCD MS/MS analysis in (**Appendix Figure 5.55**), tyrosine at m/z 182.0816 (HCD MS/MS analysis in **Appendix Figure 5.58**) and tryptophan tyrosine at m/z 205.0967 (HCD MS/MS analysis in **Appendix Figure 5.60**). Glycine could not be detected in the mass spectrum due to the limited sensitivity of the orbitrap in this mass range. A solution of pure glycine was analysed by direct infusion ESI and could not be detected in the orbitrap.

A peak hypothesised to correspond to piperidine, at m/z 86.0962, was observed. It is unclear whether these ions are a result of incorrect amino acid synthesis or the ionisation procedure.

Figure 5.13 shows the direct infusion electrospray mass spectrum of the 20 amino acid mixture hydrolysed at 207 °C for 20 minutes (see **Table 5.10**). Under these conditions the majority of observed ions were assigned as unmodified amino acids. Here, the mass spectra obtained are not dissimilar to that observed when not treated with SCW. Ions were observed at m/z 90.0547 (alanine) m/z 106.0496 (serine), m/z 116.0704 (proline), m/z 118.0860 (valine), m/z 120.0653 (threonine), m/z 132.1017 (leucine and/or isoleucine), m/z 134.0446 (aspartic acid), m/z 147.1127 (lysine), m/z 150.0581 (methionine), m/z 156.0765 (histidine), m/z 166.0859 (phenylalanine) and m/z 175.1186 (arginine).



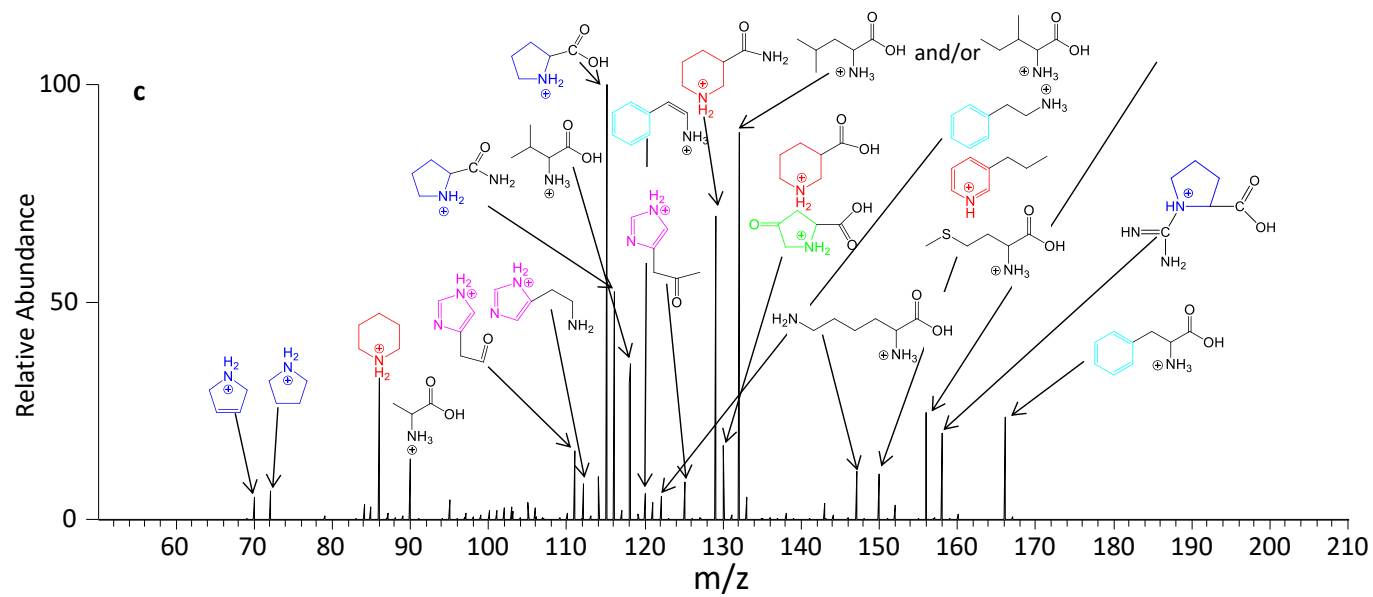
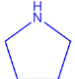
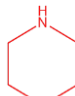
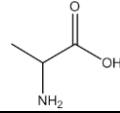
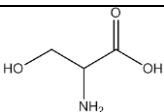
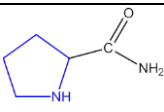
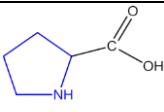
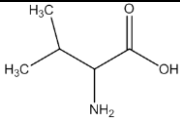
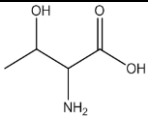
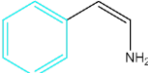
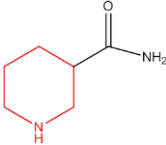
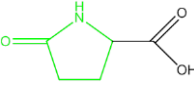
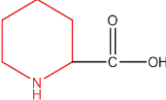
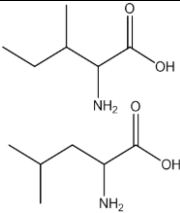
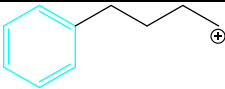
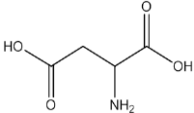
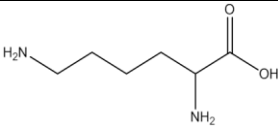
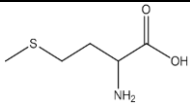
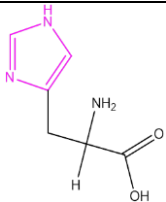
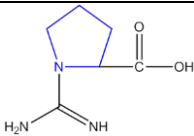


Figure 5. 13 - Direct infusion ESI MS of 20 aa mixture at **a)** 207 °C for 20 min, **b)** 253 °C for 20 min and **c)** 300 °C for 20 min.

<u>m/z</u>	<u>Calculated mass (Da)</u>	<u>Measured mass (Da)</u>	<u>Formula</u>	<u>Proposed Structure</u>	<u>HCD MS/MS</u>	<u>PPM</u>	<u>Relative abundance</u>
72.0806	71.0735	71.0733	C ₄ H ₉ N		No	-2.5	6.70
84.9595	n/a	n/a	Solvent	n/a	No	n/a	5.20
86.0962	85.0892	85.0889	C ₅ H ₁₁ N		No	-2.7	22.66
90.0547	89.0477	89.0474	C ₃ H ₇ NO ₂		No	-3.1	6.63
102.9700	n/a	n/a	Solvent	n/a	No	n/a	5.41
106.0496	105.0426	105.0423	C ₃ H ₇ NO ₃		Appendix Figure 5.6	-2.6	29.40
114.0912	n/a	n/a	Solvent	n/a	n/a	n/a	17.00
115.0864	114.0793	114.0791	C ₅ H ₁₀ ON ₂		Appendix Figure 5.13	-1.5	7.51
116.0704	115.0633	115.0631	C ₅ H ₉ O ₂ N		Appendix Figure 5.14	-1.5	67.38

118.0860	117.0790	117.0787	C ₅ H ₁₁ O ₂ N		Appendix Figure 5.16	-2.4	37.86
120.0653	119.0582	119.0580	C ₄ H ₉ O ₃ N		Appendix Figure 5.17	-1.5	24.63
120.0805	119.0735	119.0732	C ₈ H ₉ N		Appendix Figure 5.18	-2.3	7.31
129.1021	128.0950	128.0948	C ₆ H ₁₂ ON ₂		Appendix Figure 5.26	-1.4	5.64
130.0497	129.0426	129.0424	C ₅ H ₇ O ₃ N		Appendix Figure 5.27	-1.4	12.95
130.0861	129.0790	129.0788	C ₆ H ₁₁ O ₂ N		Appendix Figure 5.28	-1.4	10.12
132.1017	131.0946	131.0944	C ₆ H ₁₄ ON ₂		Appendix Figure 5.29	-1.3	100.00

133.1050	n/a	n/a	Solvent		Appendix Figure 5.31	n/a	6.00
134.0446	133.0375	133.0373	C ₇ H ₇ O ₄ N		Appendix Figure 5.32	-1.3	9.54
147.1126	146.1055	146.1053	C ₆ H ₁₄ O ₂ N ₂		Appendix Figure 5.39	-1.2	47.52
150.0581	149.0511	149.0508	C ₅ H ₁₁ O ₂ NS		Appendix Figure 5.41	-1.9	18.09
156.0765	155.0695	155.0692	C ₆ H ₉ O ₂ N ₃		Appendix Figure 5.44	-1.9	38.79
158.0921	157.0851	157.0848	C ₆ H ₁₁ O ₂ N ₃		Appendix Figure 5.48	-1.8	5.27

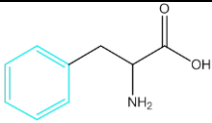
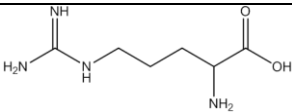
166.0859	165.0790	165.0786	C ₉ H ₁₁ O ₂ N		Appendix Figure 5.51	-2.3	33.31
175.1186	174.1118	174.1113	C ₆ H ₁₄ O ₄ N ₂		Appendix Figure 5.55	-2.7	37.99

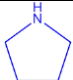
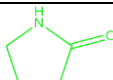
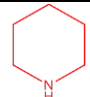
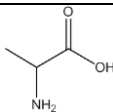
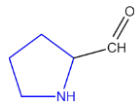
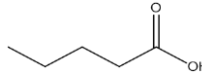
Table 5. 10 - Ions Observed Following SCW Hydrolysis of AA at 207 °C for 20 min.

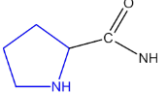
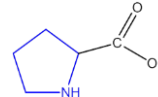
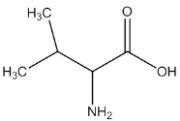
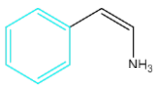
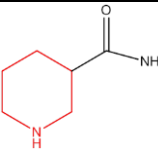
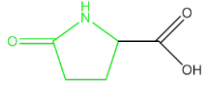
Ions were also observed at m/z 115.0864, 129.1021 and 158.0921. The ion at m/z 115.0864 has previously been assigned as prolinamide (HCD MS/MS analysis in **Appendix Figure 5.13**) and the ion at m/z 129.1021 to be piperidine-4-carboxamide (HCD MS/MS analysis in **Appendix Figure 5.26**). These were attributed to be a result of proline and pipecolic acid amidation. Furthermore, the species observed at m/z 158.0921, was previously speculated to be the result of arginine deamination. The HCD MS/MS spectrum of this ion is shown in **Appendix Figure 5.48**.

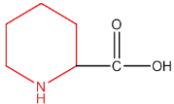
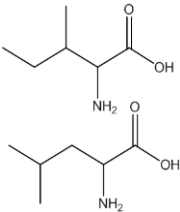
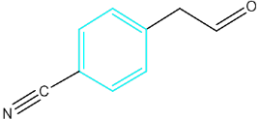
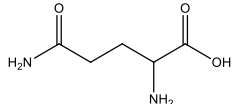
MS analysis was next performed on the hydrolysates of the equimolar amino acid mixture from 253 °C for 20 minutes SCW treatment (**Figure 5.13b** and **Table 5.11**). Peaks not observed under 207 °C for 20 minutes are highlighted in **Table 5.11**. As with hydrolysis on protein mixtures, fewer unmodified amino acids could be observed under these harsher conditions. Only ions corresponding to alanine (m/z 90.0548), proline (m/z 116.0705), valine (m/z 118.0861), leucine and isoleucine (m/z 132.1018), lysine (m/z 147.1127) and phenylalanine (m/z 166.0861) were noted. It has previously been shown that decomposition products under SCW conditions of serine and cysteine include alanine. Serine or cysteine were not observed at this temperature. Furthermore valine has previously been shown to be a decomposition product of lysine [185].

At this temperature point, arginine is no longer detected however its deamination product, 1-carbamimidoylproline (m/z 158.0923) is observed. Furthermore a marked increase in the relative abundance of ions speculated to correspond to pyroglutamate were noted (at m/z 130.0498) as well as the subsequent decarboxylation to pyrrolidone (m/z 86.0599). Under these conditions an increased amount of amidation on pipecolic acid to piperidine-4-carboxamide (m/z 129.1022) as well as its deamination product piperidine (m/z 86.0963) was noted.

Species corresponding to valeric acid (m/z 101.0596) (HCD MS/MS analysis in **Appendix Figure 5.4**), as well a benzene based structure at m/z 146.0600 (HCD MS/MS analysis in **Appendix Figure 5.37**), were observed although the mechanism of formation process remains elusive.

<u>m/z</u>	<u>Calculated mass (Da)</u>	<u>Measured mass (Da)</u>	<u>Formula</u>	<u>Proposed Structure</u>	<u>HCD MS/MS</u>	<u>PPM</u>	<u>Relative abundance</u>
72.0806	71.0735	71.0733	C ₄ H ₉ N		No	-2.5	7.88
84.9596	n/a	n/a	Solvent	n/a	n/a	n/a	13.13
86.0599	85.0528	85.0526	C ₄ H ₇ ON		No	-2.1	8.32
86.0963	85.0892	85.0890	C ₅ H ₁₁ N		No	-1.5	29.27
90.0548	89.0477	89.0475	C ₄ H ₇ NO ₂		No	-1.8	20.49
100.0756	99.0684	99.0683	C ₅ H ₉ NO		No	-0.9	10.09
101.0596	102.0681	102.0680	C ₅ H ₁₀ O ₂		Appendix Figure 5.4	-1.0	11.00
102.9701	n/a	n/a	Solvent	n/a	n/a	n/a	12.99
114.0913	n/a	n/a	solvent	n/a	n/a	n/a	21.57

115.0865	114.0793	114.0792	C ₅ H ₁₀ ON ₂		Appendix Figure 5.13	-0.7	51.04
116.0705	115.0633	115.0632	C ₅ H ₉ O ₂ N		Appendix Figure 5.13	-0.7	100.00
118.0861	115.0633	115.0632	C ₅ H ₉ O ₂ N		Appendix Figure 5.16	-1.5	42.71
120.0807	119.0735	119.0734	C ₈ H ₉ N		Appendix Figure 5.18	-0.6	5.31
129.1022	128.0950	128.0949	C ₆ H ₁₂ N ₂ O		Appendix Figure 5.26	-0.6	43.44
130.0498	129.0426	129.0425	C ₅ H ₇ O ₃ N		Appendix Figure 5.27	-0.6	58.12

130.0862	129.0790	129.0789	C ₆ H ₁₁ O ₂ N		Appendix Figure 5.28	-0.6	11.04
132.0767	131.0695	131.0694	C ₄ H ₉ O ₂ N ₃	Unassigned	No	-0.6	8.80
132.1018	131.0946	131.0945	C ₆ H ₁₄ ON ₂		Appendix Figure 5.29	-0.6	74.65
146.0600	145.0528	145.0527	C ₉ H ₇ ON		Appendix Figure 5.37	-0.5	7.39
147.1127	146.1055	146.1054	C ₆ H ₁₄ O ₂ N ₂		Appendix Figure 5.39	-0.5	5.30

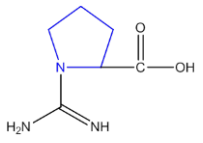
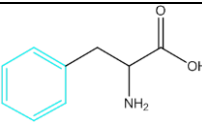
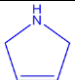
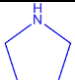

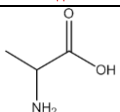
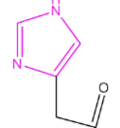
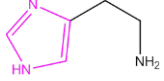
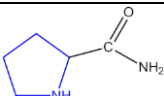
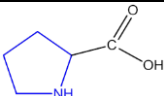
158.0923	157.0851	157.0850	C ₆ H ₁₁ O ₂ N ₃		Appendix Figure 5.48	-0.5	10.88
166.0861	165.0790	165.0788	C ₉ H ₁₁ O ₂ N		Appendix Figure 5.51	-1.1	9.98

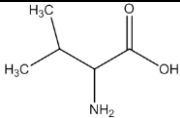
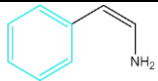
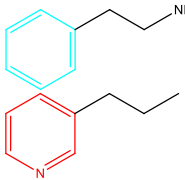
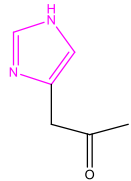
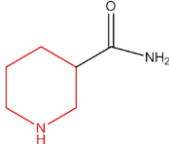
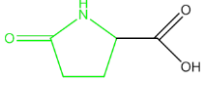
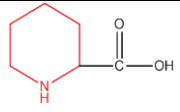
Table 5. 11 - Ions Observed Following SCW Hydrolysis of AA at 253 °C for 20 min.

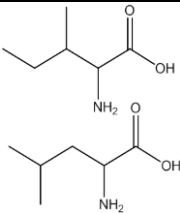
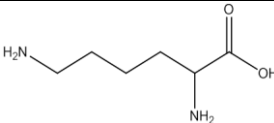
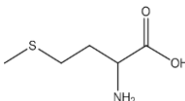
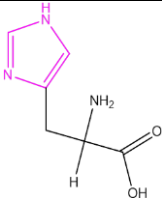
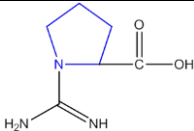
Figure 5.13c shows the direct infusion electrospray mass spectrum of the 20 amino acid mixture hydrolysed at 300 °C for 20 minutes (see also **Table 5.12**). Peaks not observe under 207 °C or 253 °C are highlighted in **Table 5.12**. In contrast to the degradation of BSA, unmodified amino acids were still observed at this temperature point. Unmodified alanine (m/z 90.0547), proline (m/z 116.0703), valine (m/z 118.0860), leucine and isoleucine (m/z 132.1016), lysine (m/z 147.1125), proline (m/z 116.0703), methionine (m/z 150.0581), histidine (m/z 156.0765) and phenylalanine (m/z 166.0859) were observed. The two most abundant peaks in the mass spectrum correspond to prolinamide (m/z 115.0765) and piperidine-4-carboxamide (m/z 129.1020) form through amidation. The ratio of prolinamide:proline increases with temperature. This pattern is consistent in all of the results, reflecting a correlation between temperature and amidation levels.

Various modifications on histidine including decarboxylation (m/z 112.0867) (HCD MS/MS analysis in **Appendix Figure 5.10**) as well as the addition of C_2H_2O and C_3H_4O the imidoazole ring (m/z 111.0551 and 125.0707) (HCD MS/MS analysis in **Appendix Figure 5.8** and **5.23**) were observed. The addition of C_3H to piperidine and the decarboxylation of phenylalanine were again observed as hydrolysis of BSA under these conditions (both m/z 122.0962). Deamination of arginine was also observed (m/z 158.0921).

The results above confirm that in the SCW temperature range of 207 °C - 253 °C, the most commonly occurring reactions are amidation, deamination, dehydration, and decarboxylation of amino acid side chains. Interestingly as the temperature is raised to 300 °C further addition reactions on amino acid side chains were identified.

<u>m/z</u>	<u>Calculated mass (Da)</u>	<u>Measured mass (Da)</u>	<u>Formula</u>	<u>Proposed Structure</u>	<u>HCD MS/MS</u>	<u>PPM</u>	<u>Relative abundance</u>
70.0649	69.0579	69.0576	C ₄ H ₇ N		No	-4.0	5.1200
72.0805	71.0735	71.0732	C ₄ H ₉ N		No	-3.9	6.4100
86.0962	85.0892	85.0889	C ₅ H ₁₁ N		No	-3.24	31.7300
90.0547	89.0477	89.0474	C ₅ H ₁₁ N		No	-3.1	13.8300
111.0551	110.0480	110.0478	C ₅ H ₆ ON ₂		Appendix Figure 5.8	-1.6	16.0100
112.0867	111.0797	111.0794	C ₅ H ₆ ON ₃		Appendix Figure 5.10	-2.5	8.5600
114.0912	n/a	n/a	Solvent	n/a	n/a	n/a	9.7900
115.0863	114.0793	114.0790	C ₅ H ₁₀ ON ₂		Appendix Figure 5.13	-2.4	100.0000
116.0703	115.0633	115.0630	C ₅ H ₉ O ₂ N		Appendix Figure 5.14	-2.4	53.1000

118.0860	117.0790	117.0787	C ₅ H ₁₁ O ₂ N		Appendix Figure 5.16	-2.4	35.0100
120.0805	119.0735	119.0732	C ₈ H ₉ N		Appendix Figure 5.18	-2.3	5.9500
122.0962	121.0892	121.0889	C ₈ H ₁₁ N		Appendix Figure 5.21	-2.3	5.3500
125.0707	124.0637	124.0634	C ₆ H ₈ N ₂ O		Appendix Figure 5.23	-2.2	8.9900
129.1020	128.0950	128.0947	C ₆ H ₁₂ N ₂ O		Appendix Figure 5.26	-2.2	68.2600
130.0497	129.0426	129.0424	C ₅ H ₇ O ₃ N		Appendix Figure 5.27	-1.4	12.3800
130.0860	129.0790	129.0787	C ₆ H ₁₁ O ₂ N		Appendix Figure 5.28	-2.1	16.9600

132.1016	131.0946	131.0943	C ₆ H ₁₄ ON ₂		Appendix Figure 5.29	-2.1	87.1700
147.1125	146.1055	146.1052	C ₆ H ₁₄ O ₂ N ₂		Appendix Figure 5.39	-1.9	11.1700
150.0581	149.0511	149.0508	C ₅ H ₁₁ O ₂ NS		Appendix Figure 5.41	-1.9	10.5900
156.0765	155.0695	155.0692	C ₆ H ₉ O ₂ N ₃		Appendix Figure 5.44	-1.8	25.0700
158.0921	157.0851	157.0848	C ₆ H ₁₁ O ₂ N ₃		Appendix Figure 5.48	-1.8	19.6000

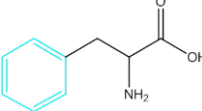
166.0859	165.0790	165.0786	C ₉ H ₁₁ O ₂ N	 <chem>N[C@@H](Cc1ccccc1)C(=O)O</chem>	Appendix Figure 5.52	-2.3	23.2600
----------	----------	----------	---	---	-------------------------	------	---------

Table 5. 12 - Ions Observed Following SCW Hydrolysis of AA at 300 °C for 20 min.

5.6 Conclusion

The work described in this chapter shows the transformation of protein into mixtures with antioxidant properties using SCW as a reagent. A strong correlation between reaction temperature and the antioxidant capacity of the resulting hydrolysates was observed in ORAC, comet and reducing power assays.

To better understand the bioactive behaviour of the decomposition products of proteins in sub critical conditions, the compounds formed were analysed. Although decomposition pathways of proteins have been previously studied, there is a lack of structural data on the compounds that are formed from the SCW hydrolysis of proteins. Here, compounds obtained following the SCW hydrolysis of NTG, BSG and BSA was identified. The products of SCW hydrolysis were analysed by mass spectrometry. Structural characterisation of the resulting compounds was obtained by higher energy collision dissociation (HCD). The influence of SCW on proteins was shown to be release of amino acids followed by amidation, decarboxylation and deamination. The results also support previous work which states the transformation of more complex amino acids into simpler ones (Ala, Val and Pro). To further probe the pathway of thermal decomposition SCW treatment was applied to an equimolar mixture of all 20 natural amino acids and the chemical reactions were consistent with those obtained for the protein.

Chapter 6: Sub-critical water applications in proteomics

6.1 Overview

The work presented in Chapters 3 and 4 suggested that SCW may find a role as a proteolytic reagent within in the context of a standard bottom-up proteomics workflow. For individual proteins, the sequence coverages obtained following SCW hydrolysis were comparable to those obtained when using trypsin. In this Chapter, the results observed following SCW hydrolysis of a more complex protein mixture are presented. Whilst the eventual aim of this technology would be to provide efficient proteolysis of an extremely complex sample, e.g., a cell lysate, here the focus is on a mixture of six proteins.

The Pierce 6 protein digest is a protein digest mixture used as a quality control standard for LC MS/MS of proteomic samples. It contains the tryptic digest of the following proteins: BSA, bovine cytochrome C, chicken lysozyme, *E-coli* β -galactosidase, bovine apo-transferrin and *S.cerevisiae* alcohol dehydrogenase. The sequence coverage for each of the proteins offered by Pierce 6 protein mixture is typically high (reported as >70% on average) [242].

In the work presented in this Chapter the same six proteins were tryptically digested in house and the sequence coverages observed were compared to those of a corresponding SCW hydrolysate of the same mixture. During the work completed in this Chapter it became apparent that optimisation of MS, HPLC and database search parameters would be required for SCW hydrolysates to offer sequence coverages comparable to those of the tryptic digests. These included comparing the data collected from different mass spectrometers (the Orbitrap Elite and the Q Exactive HF), gradient and column lengths as well as dynamic modifications included in search parameters.

6.2 Preparation of six protein mixture

Lyophilized samples of Bovine Serum Albumin (BSA) (Uniprot accession P02769), Bovine Cytochrome C (Uniprot accession P62894), Chicken Lysozyme (Uniprot accession P00698), E-coli β -galactosidase (Uniprot accession P00722), Bovine Apo-transferrin (Uniprot accession Q29443) and *S.cerevisiae* Alcohol Dehydrogenase (Uniprot accession P00330) were acquired individually. Three 15 ml solution containing 0.01mg/ml of each protein was hydrolysed at 160 °C for 20 minutes - conditions shown to obtain high sequence coverage in Chapter 3. Hydrolysates were desalted and analysed via LC - CID MS/MS using parameters described in Section 2.7. Peptides were identified using Proteome discoverer using methods described in Section 2.8. Parameters included dynamic modifications of N/Q and single oxidation of C/M. Data were searched using “nonspecific enzyme”.

6.3 LC MS/MS analysis using Orbitrap Elite

Figure 6.1 shows the sequence coverage that was acquired for each protein in the six protein mixture following SCW hydrolysis. The values are calculated from the Proteome Discoverer searches, with errors representing the standard deviation across three replicates. The data obtained shows that SCW hydrolysis of a mixture of proteins provides less sequence coverage per protein compared to when proteins were hydrolysed individually under the same conditions ($97.4 \pm 3.9\%$ for α -globin and $96.2 \pm 0.8\%$ for β -globin, $69.0 \pm 12.5\%$ for BSA and $100.0 \pm 0.0\%$ for β -casein from the data analysed in Chapter 3). The raw peptides identified are listed in **Appendix Table 6.1**.

The sequence coverage obtained for each proteins were as follows: $9.3 \pm 2.7\%$ for BSA, $11.1 \pm 0.5\%$ for cytochrome C, $32.7 \pm 1.2\%$ for lysozyme, $3.7 \pm 1.0\%$ for β -galactosidase, $21.1 \pm 1.6\%$ for apo-transferrin and $45.4 \pm 3.8\%$ for alcohol dehydrogenase. For comparison, the six protein mixture was tryptically digested and analysed using LC MS/MS (see **Figure 6.1**). The data obtained demonstrates that tryptic digestion of this mixture results in greater sequence coverage than SCW hydrolysis. This was proven for each protein. BSA presented sequence coverage of 51.6

± 4.9 , cytochrome C, coverage of 72.4 ± 9.1 %, lysozyme, coverage of 68.7 ± 3.0 %, β -galactosidase, coverage of 52.0 ± 5.9 %, apo-transferrin, coverage of 62.3 ± 3.8 % and alcohol dehydrogenase, coverage of 59.9 ± 4.3 %. The raw peptides identified are listed in **Appendix Table 6.2**.

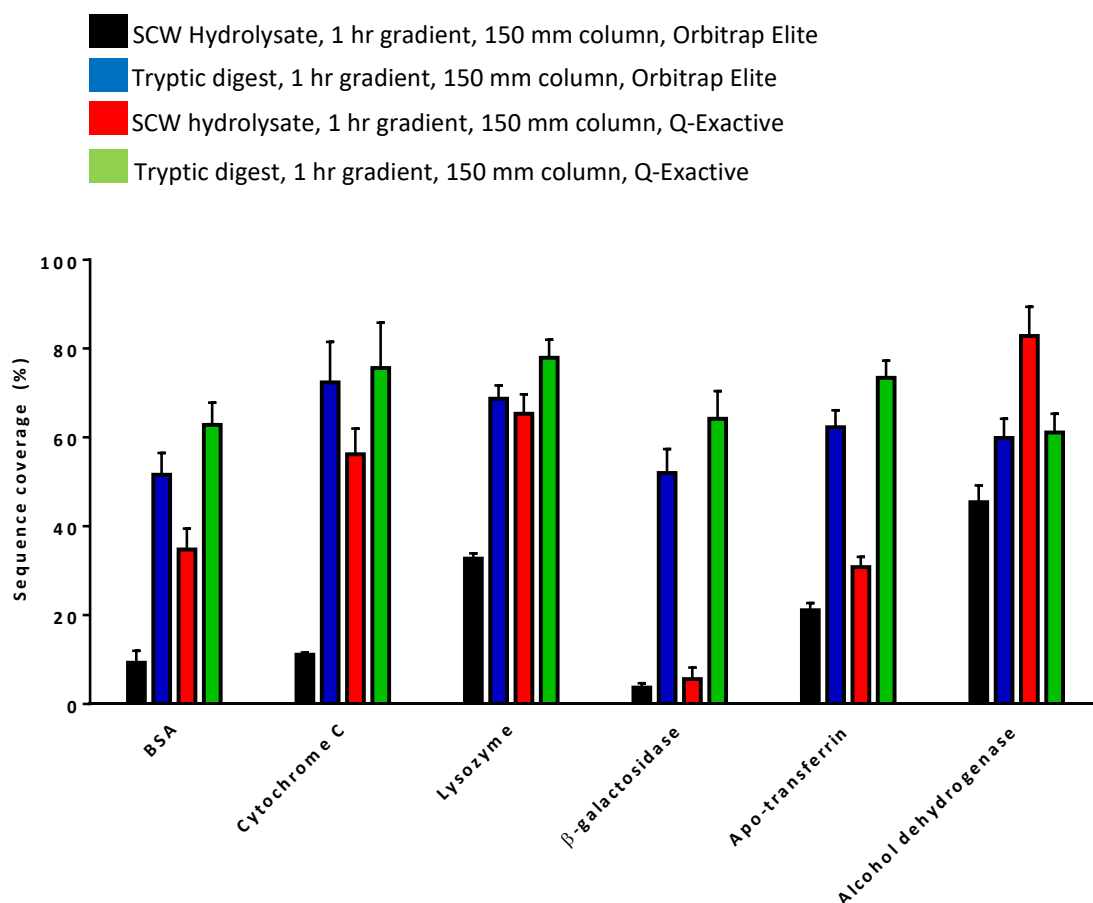


Figure 6. 1 - Mean sequence coverage obtained for trypsin digests and SCW hydrolysis at 160 °C for 20 min for six protein mixture. n = 3. Error bars represent one standard deviation.

6.4 Optimisation of HPLC parameters

Figure 6.2 shows example screenshots of fragmentation spectra that were observed for tryptic digests and **Figure 6.3** shows example screenshots of fragmentation spectra that were observed for SCW hydrolysates in the Orbitrap Elite. The quality of the MS/MS data collected for the tryptic digests was far superior to that observed for the corresponding SCW hydrolysates.

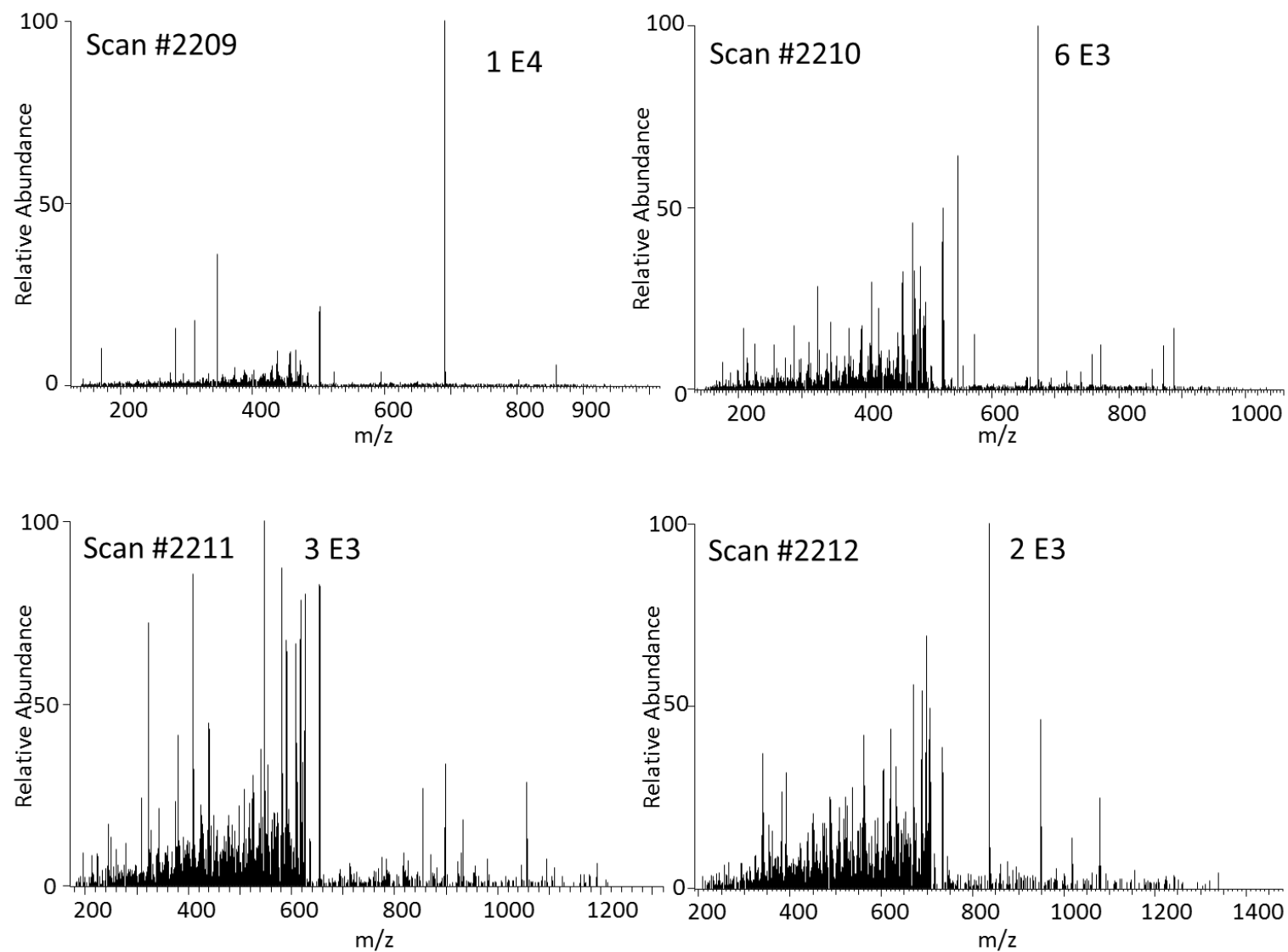


Figure 6. 2 - Representative CID MS/MS spectrum from six protein mixture tryptic digest.

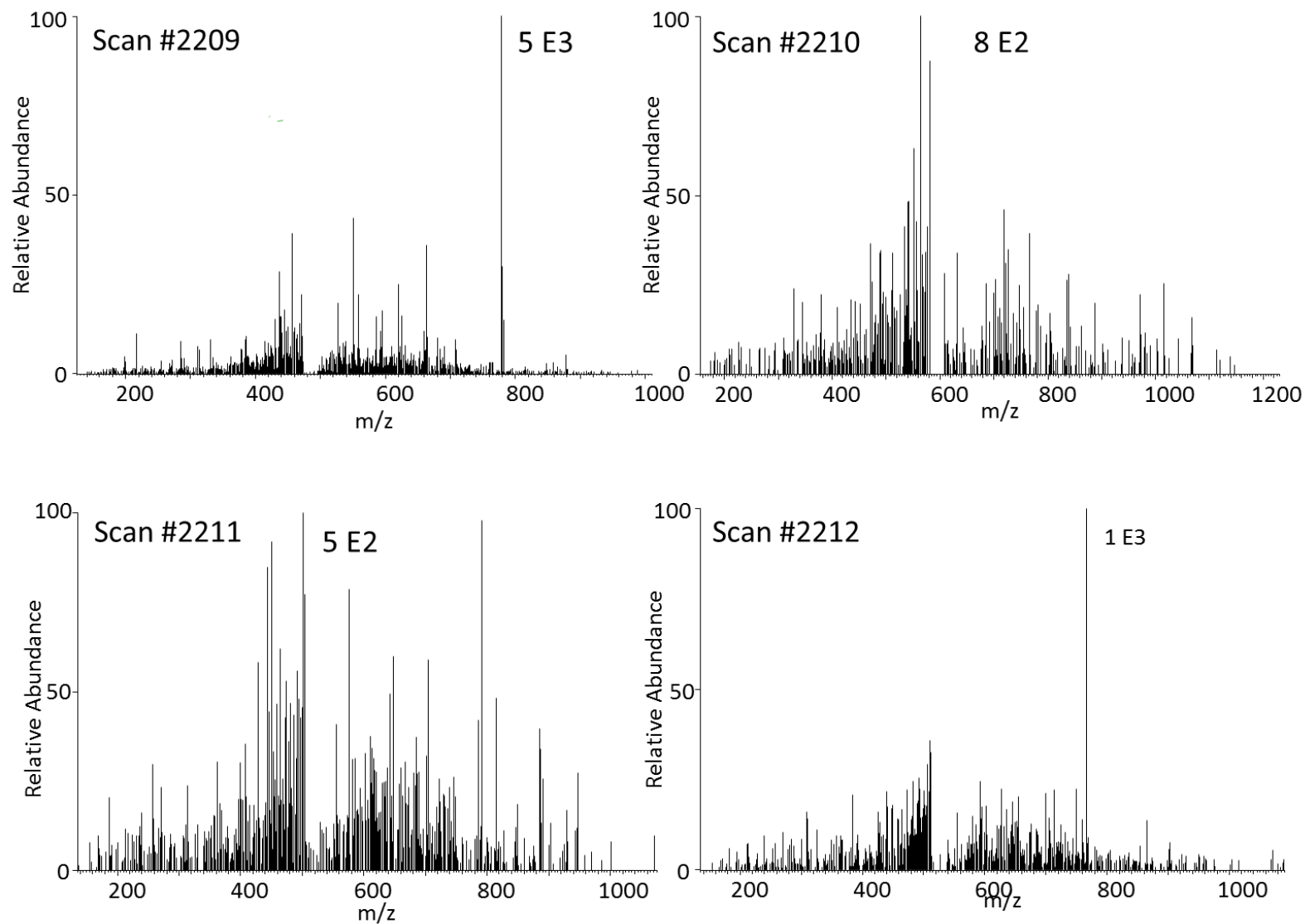


Figure 6. 3 - Representative CID MS/MS spectrum from six protein mixture hydrolysate.

I hypothesise that the reduced sequence coverage observed for the proteins was due to the vast numbers of peptides that are generated during SCW hydrolysis. Whilst trypsin is a fully specific enzyme and is only liable to cleave at R and K residues, SCW (as shown in Chapter 3) displays only partial specificity towards D and E residues. This results in the production of an increased number of peptides, and therefore an amplified number being eluted during the same time period during HPLC separation. The co-elution of peptides results in poor MS/MS data observed, for the SCW hydrolysates, and therefore fewer peptide matches.

6.4.1 LC MS/MS analysis using Q-Exactive

To increase peptide identifications the analysis was repeated using the Q-Exactive mass spectrometer, using HCD as a fragmentation method. The Q-Exactive makes use of a quadrupole mass filter coupled to an orbitrap, rather than an ion trap coupled to an orbitrap used the LTQ Orbitrap Elite. The Q-Exactive has been compared favourably to the LTQ Orbitrap Elite in both peptide and protein identifications from complex mixtures [243]. The quadrupole mass filter achieves peptide separation nearly instantaneously. In contrast, the linear ion trap applies external RF-DC fields that allow only a certain ion population to stably remain in the trap. The scan rate for the Q-exactive is therefore much higher. Moreover, the fragmentation data collected using HCD in the Q-Exactive is of higher resolution than the CID data collected in the LTQ Orbitrap Elite. In the Q-Exactive the fragment ions are analysed using the Orbitrap, rather than the lower resolution ion-trap which was used to monitor the CID fragment ions in the LTQ Orbitrap Elite. Higher resolution results in a lower mass error of product ions, leading to smaller number of peptides matched to the reversed database and therefore a lower score threshold.

A large increase in sequence coverage for BSA (34.8 ± 4.7 %), cytochrome C (56.2 ± 5.8 %), lysozyme (65.3 ± 4.4 %) and alcohol dehydrogenase (82.8 ± 6.6 %) was observed when re-analysing the SCW hydrolysates analysing using HCD MS/MS via the Q-Exactive (**Figure 6.1**). No improvement in sequence coverage was observed for β -

galactosidase (5.6 ± 2.6 %). **Figure 6.4** shows an example of the MS/MS data obtained from the Q-E analysis of the six protein mixture hydrolysate. This is of much better quality than that observed in the Orbitrap Elite (**Figure 6.3**). Note the increased mass range to facilitate lower mass fragment ions also. The raw peptides identified are listed in **Appendix Table 6.3**.

Q-Exactive analysis of the tryptic digests also increased in comparison to data collected in the Orbitrap Elite (see **Figure 6.1**). However, the increased coverage for the SCW hydrolysates was much more marked. Sequence coverages observed were $62.8 \pm 5.0\%$ for BSA, $75.6 \pm 10.2\%$ for cytochrome C, $77.9 \pm 4.1\%$ for lysozyme, $64.2 \pm 6.2\%$ for β -galactosidase, $73.4 \pm 3\%$ for apo-transferrin and $61.1 \pm 4.2\%$ for alcohol dehydrogenase. The raw peptides identified are listed in **Appendix Table 6.4**.

To investigate the low sequence coverage observed for β -galactosidase, the protein was hydrolysed individually under the same hydrolysis conditions and analysed using the Q-Exactive. The coverage garnered was 42.8 ± 3.7 , ~tenfold higher than that observed when hydrolysing within the mixture. Furthermore the coverage observed for BSA was $69.0 \pm 12.5\%$ when hydrolysed individually in (see Chapter 3), significantly higher than that observed from the six protein mixture analysis (although it should be noted that starting material concentrations were higher in the earlier experiments).

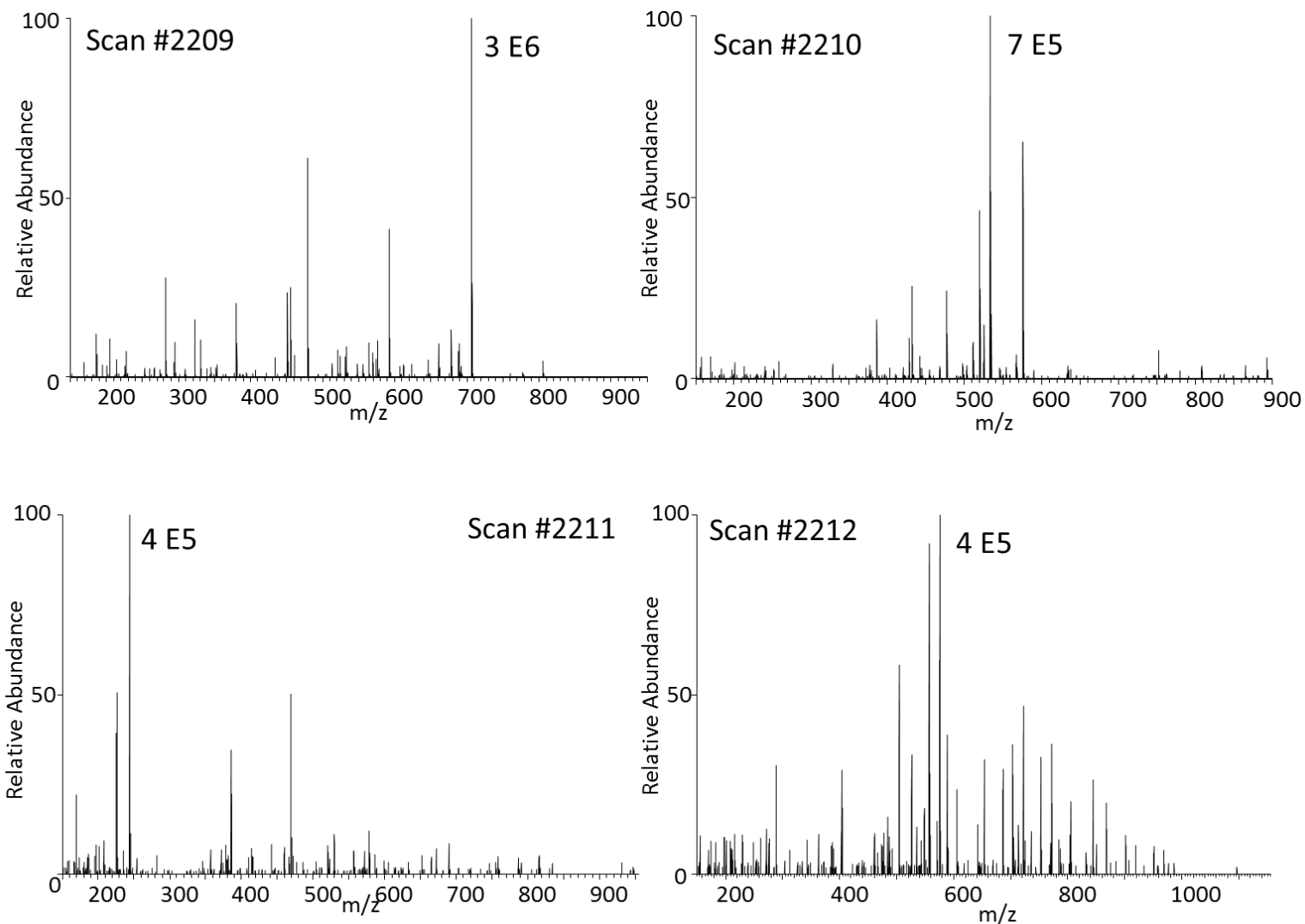


Figure 6. 4 - Representative CID MS/MS spectrum from Six Protein Mixture SCW hydrolysate using the Q Exactive.

6.4.2 Optimisation of search parameters

The data observed thus far in Chapter 6 was searched using the same dynamic modifications that were used in Chapter 3, i.e. deamidation of asparagine/ glutamine residues and oxidation on cysteine/methionine residues. However, from data observed in Chapters 4 and 5 the results suggests that modifications induced by SCW are primarily single oxidation of methionine or tryptophan, double or triple oxidation of cysteine, C-terminal amidation, water loss and deamination. **Table 6.1** shows the sequence coverages that were obtained by sequentially searching the data acquired using Q-Exactive HF these modifications. A column listing the coverages observed when no dynamic modifications were included is shown as a comparison.

	Dynamic modification									
	No Mods	Deam Oxidation (1,2)	Oxidation (1)	Oxidation (2,3)	Oxidation (1,2,3)	Amidation	- H ₂ O	- NH ₃	All	Oxidation
	Residues affected									
		N/Q/C/M	M/W	C	C/M/W	C-terminal	D	N	C/M/D/E/C -term	M/W + AspC
Aldehyde Dehydrogenase	78.4 ± 2.6	82.8 ± 2.6	85.9 ± 2.7	83.4 ± 1.8	80.8 ± 3.9	78.7 ± 4.4	80.5 ± 4.2	78.9 ± 3.0	55.8 ± 4.1	36.1 ± 2.1
Lysozyme	57.1 ± 4.4	65.3 ± 4.4	68.0 ± 3.3	67.8 ± 4.0	66.7 ± 4.8	63.4 ± 4.0	71.4 ± 4.7	62.8 ± 3.3	69.8 ± 4.2	71.4 ± 7.3
Apo Transferrin	28.8 ± 2.5	30.8 ± 2.3	33.7 ± 4.7	33.5 ± 2.9	32.5 ± 4.9	34.5 ± 5.4	25.0 ± 2.6	24.3 ± 4.5	20.5 ± 5.1	25.0 ± 4.8
BSA	29.8 ± 2.3	34.8 ± 4.7	35.3 ± 3.6	33.3 ± 3.1	33.1 ± 5.9	41.0 ± 5.9	19.7 ± 5.1	26.4 ± 6.2	17.5 ± 4.3	19.7 ± 6.5
Cytochrome C	43.9 ± 6.7	56.2 ± 5.8	57.3 ± 5.0	55.1 ± 4.9	52.2 ± 4.6	60.0 ± 5.3	55.2 ± 6.6	52.9 ± 3.5	39.1 ± 4.0	55.2 ± 5.2
β-galactosidase	4.9 ± 2.4	5.6 ± 2.6	4.6 ± 1.9	4.1 ± 1.4	4.7 ± 1.7	2.8 ± 1.5	2.8 ± 1.5	1.9 ± 1.0	2.8 ± 1.3	2.8 ± 1.3

Table 6. 1 - Percentage sequence coverage obtained for six protein mixture using different search parameters.

Interestingly, the overall highest sequence coverages were observed when dynamic modifications listed included single oxidation of methionine and tryptophan only. The raw peptides identified are listed in **Appendix Table 6.5**. These parameters were subsequently used for all further analyses described in this chapter. This data is not consistent with the data obtained in Chapter 4 which suggest that double and triple oxidation of cysteine are the most common modifications. A reduction in sequence coverage was noted when the search parameters included double and triple oxidation of cysteine.

In Chapter 3 and 4, I also observe semi-specific cleavage towards aspartic acid residues. When the enzyme specificity was changed from 'non-specific' to 'semi-specificity at Asp C-terminal' a reduction in sequence coverage was observed for 5/6 proteins. Whilst identifying the cleavage mechanism of SCW was not helpful in peptide identifications, it will be of further use in the field for understanding the sub-critical reactions on proteins and peptides.

Introducing a variable modification allows the chosen PTM to occur in any instance on the selected amino acid residue, in all theoretical peptides within the chosen data. This approach offers an effective method at identifying peptides with known PTM sites. However, the introduction of PTMs also substantially increases the database size required for the search [244]. The increased database size leads to an increase in spectra being assigned to peptides incorrectly (false positive) [245, 246]. Maintaining the FDR at 1% means that peptides now typically require a higher score to be listed as 'high confidence' peptides [247]. There is now an increased chance of spectra not being assigned (false negatives).

The introduction of each modification lists peptides that are unique to that search. Furthermore, each search gives consistently higher sequence coverage for all proteins compared to when no dynamic modifications were listed in the search parameters. This data suggests all of these modifications are induced during SCW hydrolysis. When all dynamic modifications were included in the same search a large reduction in sequence coverage was observed for all proteins, with the exception of lysozyme. This

reduction is likely due to rise of false positives and subsequently false negatives as a result of many dynamic modifications in the same search.

6.4.2 LC MS/MS analysis using longer column

Next, the effect of column length on protein identification was examined (**Figure 6.4**). Here, the column length was increased from 150 mm to 500 mm. Increasing the column length will allow greater separation of peptides and improve the resolution of the chromatograph. Increasing the column length is an important parameter to optimise for SCW hydrolysates where co-elution of peptides using the shorter column was predicted. Modest increases in sequence coverages were observed for BSA (44.7 ± 9.4), cytochrome C (69.8 ± 4.0 %), β -galactosidase (8.9 ± 6.9 %) and apo-transferrin (40.2 ± 6.1 %). Comparable data was observed for alcohol dehydrogenase (83.0 ± 6.7 %) and lysozyme (72.0 ± 5.9 %). The raw peptides identified are listed in **Appendix Table 6.6**.

6.4.3 LC MS/MS analysis using longer gradient

The effect of gradient length on the sequence coverage observed for the SCW hydrolysates was also examined. Here, the gradient was increased from 1 hour to 4.5 hours. Further increases in sequence coverages for BSA (49.1 ± 5.5 %), lysozyme (82.1 ± 5.4 %), β -galactosidase (9.4 ± 3.5 %) and apotransferrin (43.5 ± 7.9 %) were noted. Comparable data was observed for aldehyde dehydrogenase (81.1 ± 8.0 %) and a decrease was observed for cytochrome C (60.0 ± 16.2 %). The raw peptides identified are listed in **Appendix Table 6.7**.

MacCoss *et al.* investigated the effects of using both a longer column and longer gradient lengths on Peptide IDs in proteomic samples [177]. Longer gradients were effective at increasing peptide IDs. The use of longer columns also showed increased peptide IDs, but only when longer gradients were also used. This is in contrast to our

data which suggest using a longer column is effective in improving peptide IDs in its own right.

Whilst these latter two parameters show limited improvement in the sequence coverage observed for all 6 proteins, they are likely to be of more use when more complex samples are used.

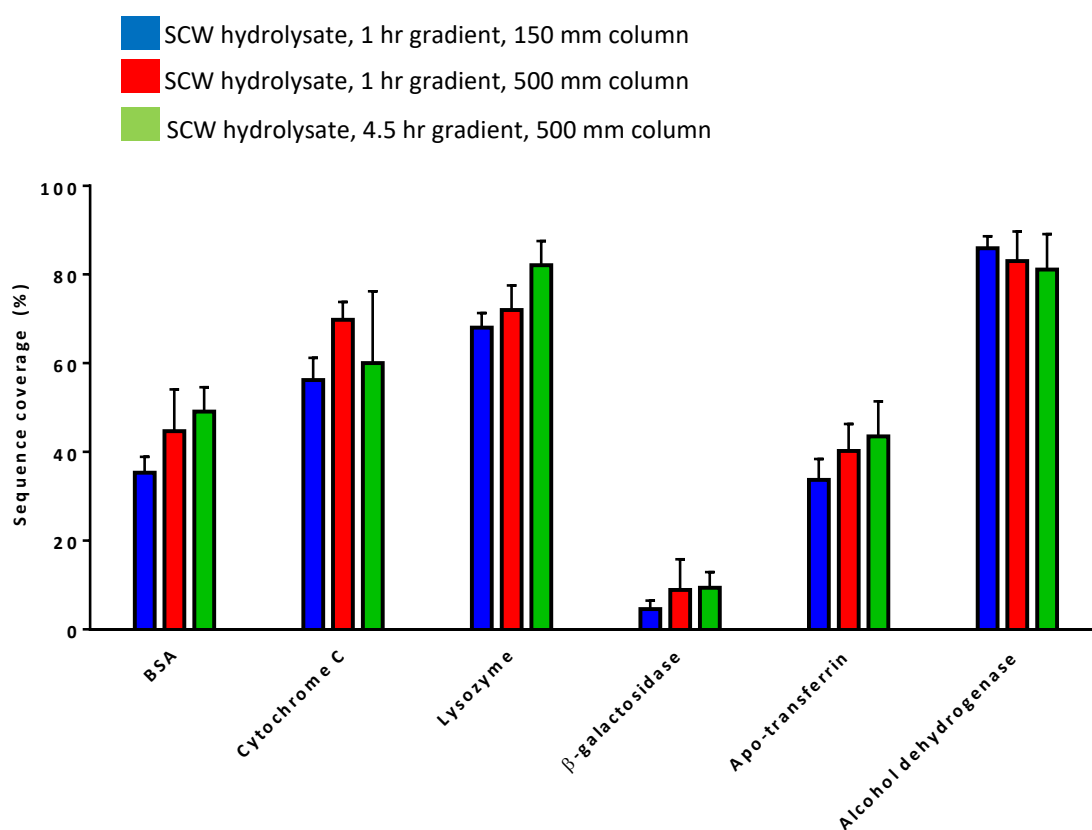


Figure 6. 5 - Mean sequence coverage obtained for SCW hydrolysis at 160 °C for 20 min for six protein mixture using Q-exactive. n = 3. Error bars represent one standard deviation.

6.5 Conclusion

The work presented in this chapter builds on data obtained in Chapters 3 and 4. Here, I continue the development of SCW as an alternative proteolysis reagent. I have optimised the parameters required to reliably identify the components of a mixture of BSA, cytochrome C, lysozyme, β -galactosidase, apo-transferrin and alcohol dehydrogenase.

Using SCW as a reagent on this mixture did not garner the same sequence coverages that were observed when performing SCW hydrolysis on mixtures of single proteins, therefore a thorough optimisation of several areas of the proteomics protocol needed to be assessed. Firstly, the use of the Q-Exactive mass spectrometer offered increased peptide IDs compared to the Orbitrap Elite, which was used for prior analysis. The use of the Q-Exactive was more advantageous for SCW generated peptides than tryptic peptides. Furthermore the search parameters were optimised, and the dynamic modifications included in the Proteome Discoverer search were altered. The use of a longer LC column and gradient showed modest increases in protein identification. Changing these parameters allowed the identification of 5 of the 6 proteins to excellent certainty (sequence coverage 40-80%). The data observed for β -galactosidase was consistently of poor quality (sequence coverage <10 %), although unique peptides to this protein were observed in each of the replicates.

Chapter 7: Conclusion and Future Work

SCW hydrolysis is an emerging technology in antioxidant extraction from industrial waste, in particular waste which is rich in protein. The brewing industry generates huge volumes of residues and by products. The most common is brewers spent grain (BSG) which is extremely rich in protein. In the work presented in this thesis I aim to demonstrate antioxidant extraction from BSG using SCW.

To address the aim, the behaviour of protein during SCW hydrolysis was investigated (Chapter 3). The results obtained within this chapter led to the possibility of using SCW as an alternative proteolytic reagent for proteomics experiments. Investigating the modifications that SCW induces on amino acid side chains to assist in peptide identification was completed in Chapter 4. The work presented in Chapter 5 focused on assessing the antioxidant activity of the small molecule products of SCW hydrolysis.

Chapter 6 further explored the potential of utilising SCW within a proteomic workflow. HPLC MS/MS conditions, including column and gradient length, as well as search parameters were optimised.

7.1 Sub-critical water hydrolysis of proteins: specificity and post translational modifications

In order to better understand the mechanisms of SCW hydrolysis, three model proteins (haemoglobin, BSA, β -casein) were hydrolysed using SCW at a wide range of temperatures (160 °C - 300 °C) at different time points (0 min and 20 min). The resulting hydrolysates were analysed using LC MS/MS as a method of peptide identification. The peptide products generated resulted in high protein sequence coverages, indeed the sequence coverages obtained were comparable to those obtained with trypsin, the choice method for proteomic studies. In addition SCW was effective at maintaining PTMs under certain conditions and displayed partial specificity towards negatively charged residues.

The percentage of PSMs for the samples treated with trypsin was consistently greater than for those treated with SCW. This observation suggests that in addition to

hydrolysis of the peptide bond, SCW treatment results in other chemical reactions, potentially including modification of amino acid side chains. This was explored further in Chapter 4.

7.2 Sub-critical water hydrolysis of peptides: amino acid modifications and conjugation

In Chapter 4 the effect of SCW on amino acid side chains was determined using a model peptide approach. The synthetic peptide VQSIKCADFLHYMENPTWGR, which contains all 20 commonly-occurring amino acid residues, was synthesized and treated with SCW at one of four temperature points (140, 160, 180, 200 °C) for 10 min. SCW hydrolysis of peptides resulted in efficient oxidation of the hydrolysates. SCW treatment under mild conditions (140 °C for 10 min) resulted in oxidation of cysteine and methionine residues. Oxidation of cysteine to sulfinic and sulfonic acid was also observed. SCW treatment of a peptide that did not contain cysteine or methionine resulted in oxidation of tryptophan. Under harsher SCW conditions (160 °C - 180 °C), dehydration, amidation and deamination of the peptides was detected. Water loss occurs at aspartic acid. In addition, the C-terminal of aspartic acid is consistently shown to be a site of preferential cleavage for SCW.

Additionally, when the peptide was incubated with a nucleophile, SCW was shown to promote S_N2 reactions. Using SCW to promote nucleophilic interactions could present an interesting alternative to traditional catalysts. To investigate this more rigorous testing is required. I propose a study involving incubating a variety of nucleophiles with the 20 aa synthetic peptide under a wide range of temperature and time points.

7.3 Sub-critical antioxidant extraction from protein

Chapter 5 was aimed at exploring the antioxidant capacity of SCW hydrolysates using ORAC, reducing power and comet assays. SCW hydrolysis was performed on a blend of barley that had not undergone brewing (Non-treated grain (NTG)), brewers spent grain (BSG) and BSA. Antioxidant capacity was identified in all hydrolysates and comparable antioxidant activity to commercial antioxidants was obtained under certain hydrolysis conditions. The results inferred that it is not in fact the peptides, but small molecule products that show antioxidant properties. The structure of these antioxidant components was speculated using HCD MS/MS. In the work presented in this thesis ions of the same m/z were assumed to have the same chemical structure despite originating from different starting reactants and/or hydrolysis conditions. A more complete analysis would have involved collecting HCD MS/MS of each selected ion for each hydrolysate.

In future work, the propensity of SCW to produce mixtures with antioxidant properties from any protein will be explored. A general procedure for antioxidant extraction from any protein mixture has huge economic potential. I would aim to hydrolyse standard proteins at time and temperature points shown to be most efficient at generating strong antioxidant power (300 °C and 20 minutes). As well as assessing antioxidant activity via the assays already discussed, I would also complete other assays such as the FRAP assay which assess other aspects of antioxidant mechanisms.

Furthermore, a more thorough analysis of the small compounds produced during SCW hydrolysis is needed. I propose a study where hydrolysates are fractionated using HPLC and the antioxidant activity of each fraction is assessed. The compounds present in each fraction would be assessed using a mass spectrometer with a lower mass range than that used in this study to facilitate the assignment of compounds which showed no fragmentation data in the results presented in this thesis. This would provide data on which of the specific compounds provides the most antioxidant power.

7.4 Sub-critical water applications in proteomics

The idea of pursuing SCW hydrolysis as an alternative proteolytic reagent was further explored in Chapter 6 by completing SCW hydrolysis on a mixture of 6 proteins. SCW hydrolysis initially failed to provide comparable sequence coverage to tryptic digests using the same mass spectrometry and chromatography conditions. An enhancement in protein IDs was offered using a Q-Exactive HF mass spectrometer compared to the Orbitrap Elite that was used in previous experiments. Further improvements in protein sequence coverage were offered by increasing column and gradient length.

If further time was provided future experiments would be completed to validate some of the data I presented in this Chapter. In the work presented in this thesis I do not complete HCD analysis using the Orbitrap Elite, and therefore have no direct comparison between fragmentation methods on the same instrument. Moreover, I do not complete an experiment to directly measure effect of gradient length against peptide IDs whilst using the 150 mm column.

The ultimate aim of the SCW technology would be to supply a faster, cheaper alternative to trypsin in a proteomic experiment. These typically involve the analysis of a complex mixture of many proteins e.g. from a cell lysate. A future study may involve cell lysates being digested using trypsin and equivalent volumes of extracted protein also hydrolysed using SCW hydrolysis. The number and type of proteins identified at each hydrolysis condition will be compared against the corresponding tryptic digest. Peptides would be fractionated by both gel-free and/or gel-based approaches prior to analysis.

Furthermore, I hypothesise using SCW may be able remove the need for the lysis cocktail in lysate extraction. I propose an experiment where cells will be directly introduced into the SCW reaction vessels. I hypothesise the harsh conditions involved in SCW hydrolysis will prove sufficient to lyse the cell walls and subsequently hydrolyse the proteins into peptides. This will remove the need for many of the expensive and time consuming chemical processes necessary during the preparation of samples prior to LC MS/MS and will represent a significant contribution to the proteomics field.

1. Carr, A.G., R. Mammucari, and N.R. Foster, *A review of subcritical water as a solvent and its utilisation for the processing of hydrophobic organic compounds*. Chemical Engineering Journal, 2011. **172**(1): p. 1-17.
2. Griffiths, J., *A brief history of mass spectrometry*. Analytical Chemistry, 2008. **80**(15): p. 5678-5683.
3. Morris, H.R., et al., *Fast atom bombardment: A new mass spectrometric method for peptide sequence analysis*. Biochemical and Biophysical Research Communications, 1981. **101**(2): p. 623-631.
4. Depauw, E., A. Agnello, and F. Derwa, *Liquid matrices for liquid secondary ion mass-spectrometry fast-atom-bombardment - an update*. Mass Spectrometry Reviews, 1991. **10**(4): p. 283-301.
5. Karas, M. and F. Hillenkamp, *Laser desorption ionization of proteins with molecular masses exceeding 10000 Daltons*. Analytical Chemistry, 1988. **60**(20): p. 2299-2301.
6. Fenn, J.B., et al., *Electrospray ionization for mass-spectrometry of large biomolecules*. Science, 1989. **246**(4926): p. 64-71.
7. Konijnenberg, A., A. Butterer, and F. Sobott, *Native ion mobility-mass spectrometry and related methods in structural biology*. Biochimica Et Biophysica Acta-Proteins and Proteomics, 2013. **1834**(6): p. 1239-1256.
8. Taylor, F.R.S., *Disintegration of water drops in an electric field*. Proceedings of the Royal Society of London. Series A. Mathematical and Physical Sciences, 1964. **280**(1382): p. 383-397.
9. Rohner, T.C., N. Lion, and H.H. Girault, *Electrochemical and theoretical aspects of electrospray ionisation*. Physical Chemistry Chemical Physics, 2004. **6**(12): p. 3056-3068.
10. Kebarle, P. and U.H. Verkerk, *Electrospray: from ions in solution to ions in the gas phase, what we know*. Mass Spectrometry Reviews, 2009. **28**(6): p. 898-917.
11. Ahadi, E. and L. Konermann, *Ejection of Solvated Ions from Electrosprayed Methanol/Water Nanodroplets Studied by Molecular Dynamics Simulations*. Journal of the American Chemical Society, 2011. **133**(24): p. 9354-9363.
12. Wang, R. and R. Zenobi, *Evolution of the Solvent Polarity in an Electrospray Plume*. Journal of the American Society for Mass Spectrometry, 2010. **21**(3): p. 378-385.
13. Thomson, B.A. and J.V. Iribarne, *Field-induced ion evaporation from liquid surfaces at atmospheric-pressure*. Journal of Chemical Physics, 1979. **71**(11): p. 4451-4463.
14. Iribarne, J.V. and B.A. Thomson, *On the evaporation of small ions from charged droplets*. Journal of Chemical Physics, 1976. **64**(6): p. 2287-2294.
15. Dole, M., L.L. Mack, and R.L. Hines, *Molecular beams of macroions*. Journal of Chemical Physics, 1968. **49**(5): p. 2240-&.
16. Konermann, L., A.D. Rodriguez, and J.J. Liu, *On the Formation of Highly Charged Gaseous Ions from Unfolded Proteins by Electrospray Ionization*. Analytical Chemistry, 2012. **84**(15): p. 6798-6804.

17. Ahadi, E. and L. Konermann, *Modeling the Behavior of Coarse-Grained Polymer Chains in Charged Water Droplets: Implications for the Mechanism of Electrospray Ionization*. Journal of Physical Chemistry B, 2012. **116**(1): p. 104-112.
18. Nguyen, S. and J.B. Fenn, *Gas-phase ions of solute species from charged droplets of solutions*. Proceedings of the National Academy of Sciences of the United States of America, 2007. **104**(4): p. 1111-1117.
19. Wilm, M. and M. Mann, *Analytical properties of the nanoelectrospray ion source*. Analytical chemistry, 1996. **68**(1): p. 1-8.
20. Juraschek, R., T. Dulcks, and M. Karas, *Nanoelectrospray - More than just a minimized-flow electrospray ionization source*. Journal of the American Society for Mass Spectrometry, 1999. **10**(4): p. 300-308.
21. Schultz, G.A., et al., *A fully integrated monolithic microchip electrospray device for mass spectrometry*. Analytical Chemistry, 2000. **72**(17): p. 4058-4063.
22. Van Pelt, C.K., S. Zhang, and J.D. Henion, *Characterization of a fully automated nanoelectrospray system with mass spectrometric detection for proteomic analyses*. J Biomol Tech, 2002. **13**(2): p. 72-84.
23. Makarov, A., et al., *Performance evaluation of a hybrid linear ion trap/orbitrap mass spectrometer*. Analytical chemistry, 2006. **78**(7): p. 2113-2120.
24. DiMaggio, J., Peter A, et al., *A hybrid method for peptide identification using integer linear optimization, local database search, and quadrupole time-of-flight or Orbitrap tandem mass spectrometry*. Journal of proteome research, 2008. **7**(4): p. 1584-1593.
25. Frank, A.M., et al., *De novo peptide sequencing and identification with precision mass spectrometry*. Journal of proteome research, 2007. **6**(1): p. 114-123.
26. Thermo Fisher Scientific Orbitrap Elite Hardware Manual. 2011.
27. Stafford, G.C., et al., *Recent improvements in and analytical applications of advanced ion trap technology*. International Journal of Mass Spectrometry, 1984. **60**(SEP): p. 85-98.
28. Martin, N.J., *Surface analysis for proteomics via liquid extraction surface analysis mass spectrometry and liquid chromatography mass spectrometry*. 2016, University of Birmingham.
29. Olsen, J.V., et al., *A dual pressure linear ion trap Orbitrap instrument with very high sequencing speed*. Mol Cell Proteomics, 2009. **8**(12): p. 2759-69.
30. Perry, R.H., R.G. Cooks, and R.J. Noll, *Orbitrap mass spectrometry: instrumentation, ion motion and applications*. Mass Spectrom Rev, 2008. **27**(6): p. 661-99.
31. Hu, Q., et al., *The Orbitrap: a new mass spectrometer*. J Mass Spectrom, 2005. **40**(4): p. 430-43.
32. De Hoffmann, E. and V. Stroobant, *Mass spectrometry: principles and applications*. 2007: John Wiley & Sons.
33. Makarov, A., *Electrostatic axially harmonic orbital trapping: a high-performance technique of mass analysis*. Analytical chemistry, 2000. **72**(6): p. 1156-1162.
34. Thermo Fisher Scientific Exactive Operating Manual. 2010.

35. El-Aneed, A., A. Cohen, and J. Banoub, *Mass Spectrometry, Review of the Basics: Electrospray, MALDI, and Commonly Used Mass Analyzers*. Applied Spectroscopy Reviews, 2009. **44**(3): p. 210-230.
36. Michalski, A., et al., *Mass spectrometry-based proteomics using Q Exactive, a high-performance benchtop quadrupole Orbitrap mass spectrometer*. Mol Cell Proteomics, 2011. **10**(9): p. M111.011015.
37. Quan, L. and M. Liu, *CID, ETD and HCD fragmentation to study protein post-translational modifications*. Mod Chem Appl, 2013. **1**(1): p. 1-5.
38. Wysocki, V.H., et al., *Mass spectrometry of peptides and proteins*. Methods, 2005. **35**(3): p. 211-222.
39. Roepstorff, P., *PROPOSAL FOR A COMMON NOMENCLATURE FOR SEQUENCE IONS IN MASS-SPECTRA OF PEPTIDES-REPLY*. Biomedical Mass Spectrometry, 1985. **12**(10): p. 631-631.
40. Steen, H. and M. Mann, *The ABC's (and XYZ's) of peptide sequencing*. Nature Reviews Molecular Cell Biology, 2004. **5**(9): p. 699-711.
41. Wysocki, V.H., et al., *Mobile and localized protons: a framework for understanding peptide dissociation*. J Mass Spectrom, 2000. **35**(12): p. 1399-406.
42. Salek, M. and W.D. Lehmann, *Neutral loss of amino acid residues from protonated peptides in collision-induced dissociation generates N- or C-terminal sequence ladders*. J Mass Spectrom, 2003. **38**(11): p. 1143-9.
43. Annan, R.S., et al., *A multidimensional electrospray MS-based approach to phosphopeptide mapping*. Anal Chem, 2001. **73**(3): p. 393-404.
44. Mirgorodskaya, E., P. Roepstorff, and R.A. Zubarev, *Localization of O-glycosylation sites in peptides by electron capture dissociation in a fourier transform mass spectrometer*. Analytical Chemistry, 1999. **71**(20): p. 4431-4436.
45. Kelleher, R.L., et al., *Localization of labile posttranslational modifications by electron capture dissociation: The case of gamma-carboxyglutamic acid*. Analytical Chemistry, 1999. **71**(19): p. 4250-4253.
46. Stensballe, A., S. Andersen, and O.N. Jensen, *Characterization of phosphoproteins from electrophoretic gels by nanoscale Fe(III) affinity chromatography with off-line mass spectrometry analysis*. Proteomics, 2001. **1**(2): p. 207-222.
47. Hakansson, K., et al., *High resolution tandem mass spectrometry for structural biochemistry*. Current Organic Chemistry, 2003. **7**(15): p. 1503-1525.
48. Zabrouskov, V., et al., *New approach for plant proteomics - Characterization of chloroplast proteins of Arabidopsis thaliana by top-down mass spectrometry*. Molecular & Cellular Proteomics, 2003. **2**(12): p. 1253-1260.
49. Syka, J.E., et al., *Peptide and protein sequence analysis by electron transfer dissociation mass spectrometry*. Proceedings of the National Academy of Sciences of the United States of America, 2004. **101**(26): p. 9528-9533.
50. Zubarev, R.A., N.L. Kelleher, and F.W. McLafferty, *Electron Capture Dissociation of Multiply Charged Protein Cations. A Nonergodic Process*. Journal of the American Chemical Society, 1998. **120**(13): p. 3265-3266.

51. Sawicka, A., *et al.*, *Model calculations relevant to disulfide bond cleavage via electron capture influenced by positively charged groups*. Journal of Physical Chemistry B, 2003. **107**(48): p. 13505-13511.
52. Iavarone, A.T., K. Paech, and E.R. Williams, *Effects of charge state and cationizing agent on the electron capture dissociation of a peptide*. Analytical Chemistry, 2004. **76**(8): p. 2231-2238.
53. Chamot-Rooke, J., *et al.*, *Electron capture in charge-tagged peptides. Evidence for the role of excited electronic states*. Journal of the American Society for Mass Spectrometry, 2007. **18**(12): p. 2146-2161.
54. Syrtstad, E.A. and F. Turecek, *Toward a general mechanism of electron capture dissociation*. Journal of the American Society for Mass Spectrometry, 2005. **16**(2): p. 208-224.
55. Turecek, F., X.H. Chen, and C.T. Hao, *Where does the electron go? Electron distribution and reactivity of peptide cation radicals formed by electron transfer in the gas phase*. Journal of the American Chemical Society, 2008. **130**(27): p. 8818-8833.
56. Sobczyk, M., *et al.*, *Coulomb-assisted dissociative electron attachment: Application to a model peptide*. Journal of Physical Chemistry A, 2005. **109**(1): p. 250-258.
57. Zhurov, K.O., *et al.*, *Principles of electron capture and transfer dissociation mass spectrometry applied to peptide and protein structure analysis*. Chemical Society Reviews, 2013. **42**(12): p. 5014-5030.
58. McAlister, G.C., *et al.*, *Higher-energy collision-activated dissociation without a dedicated collision cell*. Molecular & Cellular Proteomics, 2011. **10**(5): p. O111. 009456.
59. Jedrychowski, M.P., *et al.*, *Evaluation of HCD-and CID-type fragmentation within their respective detection platforms for murine phosphoproteomics*. Molecular & Cellular Proteomics, 2011. **10**(12): p. M111. 009910.
60. Lee, M.S. and E.H. Kerns, *LC/MS applications in drug development*. Mass Spectrometry Reviews, 1999. **18**(3-4): p. 187-279.
61. Eaglesham, G.K., *et al.*, *Use of HPLC-MS/MS to monitor cylindrospermopsin, a blue-green algal toxin, for public health purposes*. Environmental Toxicology, 1999. **14**(1): p. 151-154.
62. Shou, W.Z., *et al.*, *A novel approach to perform metabolite screening during the quantitative LC-MS/MS analyses of in vitro metabolic stability samples using a hybrid triple-quadrupole linear ion trap mass spectrometer*. Journal of mass spectrometry, 2005. **40**(10): p. 1347-1356.
63. Bolmatov, D., V.V. Brazhkin, and K. Trachenko, *Thermodynamic behaviour of supercritical matter*. Nature Communications, 2013. **4**.
64. Uematsu, M. and E.U. Franck, *Static dielectric-constant of water and steam*. Journal of Physical and Chemical Reference Data, 1980. **9**(4): p. 1291-1306.
65. Mohsen-Nia, M., H. Amiri, and B. Jazi, *Dielectric Constants of Water, Methanol, Ethanol, Butanol and Acetone: Measurement and Computational Study*. Journal of Solution Chemistry, 2010. **39**(5): p. 701-708.

66. Simsek Kus, N., *Organic reactions in subcritical and supercritical water*. Tetrahedron, 2012. **68**(4): p. 949-958.
67. Yoshida, H., M. Terashima, and Y. Takahashi, *Production of organic acids and amino acids from fish meat by sub-critical water hydrolysis*. Biotechnology Progress, 1999. **15**(6): p. 1090-1094.
68. Sereewatthanawut, I., et al., *Extraction of protein and amino acids from deoiled rice bran by subcritical water hydrolysis*. Bioresour Technol, 2008. **99**(3): p. 555-61.
69. Watchararujji, K., et al., *Value-added subcritical water hydrolysate from rice bran and soybean meal*. Bioresource Technology, 2008. **99**(14): p. 6207-6213.
70. Kaspar, A.A. and J.M. Reichert, *Future directions for peptide therapeutics development*. Drug Discovery Today, 2013. **18**(17-18): p. 807-817.
71. Tavakoli, O. and H. Yoshida, *Conversion of scallop viscera wastes to valuable compounds using sub-critical water*. Green Chemistry, 2006. **8**(1): p. 100-106.
72. Sereewatthanawut, I., et al., *Extraction of protein and amino acids from deoiled rice bran by subcritical water hydrolysis*. Bioresource Technology, 2008. **99**(3): p. 555-561.
73. Wataniyakul, P., et al., *Microwave pretreatment of defatted rice bran for enhanced recovery of total phenolic compounds extracted by subcritical water*. Bioresource Technology, 2012. **124**: p. 18-22.
74. Teresa Fernandez-Ponce, M., et al., *Extraction of antioxidant compounds from different varieties of Mangifera indica leaves using green technologies*. Journal of Supercritical Fluids, 2012. **72**: p. 168-175.
75. Ibanez, E., et al., *Subcritical water extraction of antioxidant compounds from rosemary plants*. Journal of Agricultural and Food Chemistry, 2003. **51**(2): p. 375-382.
76. Xu, H.G., et al., *Subcritical water extraction and antioxidant activity evaluation with on-line HPLC-ABTS(center dot+) assay of phenolic compounds from marigold (Tagetes erecta L.) flower residues*. Journal of Food Science and Technology-Mysore, 2015. **52**(6): p. 3803-3811.
77. Murugan, R. and T. Parimelazhagan, *Comparative evaluation of different extraction methods for antioxidant and anti-inflammatory properties from Osbeckia parvifolia Arn. – An in vitro approach*. Journal of King Saud University - Science, 2014. **26**(4): p. 267-275.
78. Wang, L. and C.L. Weller, *Recent advances in extraction of nutraceuticals from plants*. Trends in Food Science & Technology, 2006. **17**(6): p. 300-312.
79. Khajenoori, M., et al., *Subcritical Water Extraction of Essential Oils from Zataria Multiflora Boiss*. Journal of Food Process Engineering, 2009. **32**(6): p. 804-816.
80. Giray, E.S., et al., *Comparing the effect of sub-critical water extraction with conventional extraction methods on the chemical composition of Lavandula stoechas*. Talanta, 2008. **74**(4): p. 930-5.
81. Gamiz-Gracia, L. and M.D.L. de Castro, *Continuous subcritical water extraction of medicinal plant essential oil: comparison with conventional techniques*. Talanta, 2000. **51**(6): p. 1179-1185.

82. Yu, X.M., et al., *Subcritical water extraction of antioxidant phenolic compounds from XiLan olive fruit dreg*. Journal of Food Science and Technology-Mysore, 2015. **52**(8): p. 5012-5020.
83. Vergara-Salinas, J.R., et al., *Effect of Pressurized Hot Water Extraction on Antioxidants from Grape Pomace before and after Enological Fermentation*. Journal of Agricultural and Food Chemistry, 2013. **61**(28): p. 6929-6936.
84. Xiao, S.Z., et al., *Subcritical Water Extraction of Ursolic Acid from Hedyotis diffusa*. Applied Sciences-Basel, 2017. **7**(2).
85. Casas, L., et al., *Extraction of resveratrol from the pomace of Palomino fino grapes by supercritical carbon dioxide*. Journal of Food Engineering, 2010. **96**(2): p. 304-308.
86. Awaluddin, S.A., et al., *Subcritical Water Technology for Enhanced Extraction of Biochemical Compounds from Chlorella vulgaris*. Biomed Research International, 2016.
87. Hawthorne, S.B., Y. Yang, and D.J. Miller, *Extraction of organic pollutants from environmental solids with sub- and supercritical water*. Anal. Chem., 1995. **66**(18): p. 2912-2920.
88. Deng, C.H., N. Li, and X.M. Zhang, *Rapid determination of essential oil in Acorus tatarinowii Schott. by pressurized hot water extraction followed by solid-phase microextraction and gas chromatography-mass spectrometry*. Journal of Chromatography A, 2004. **1059**(1-2): p. 149-155.
89. Kronholm, J., et al., *Comparison of gas chromatography-mass spectrometry and capillary electrophoresis in analysis of phenolic compounds extracted from solid matrices with pressurized hot water*. Journal of Chromatography A, 2004. **1022**(1-2): p. 9-16.
90. Ramos, L., E.M. Kristenson, and U.A.T. Brinkman, *Current use of pressurised liquid extraction and subcritical water extraction in environmental analysis*. Journal of Chromatography A, 2002. **975**(1): p. 3-29.
91. Brovchenko, I. and A. Oleinikova, *Multiple Phases of Liquid Water*. Chemphyschem, 2008. **9**(18): p. 2660-2675.
92. Hanim, S.S., et al., *Effects of temperature, time and pressure on the hemicelluloses yield extracted using subcritical water extraction*, in Chisa 2012, P. Kluson, Editor. 2012. p. 562-565.
93. Czuchajowska, Z., et al., *Structure and functionality of barley starches*. Cereal Chemistry, 1998. **75**(5): p. 747-754.
94. Izydorczyk, M., et al., *Variation in total and soluble β -glucan content in hullless barley: effects of thermal, physical, and enzymic treatments*. Journal of Agricultural and Food Chemistry, 2000. **48**(4): p. 982-989.
95. Quinde, Z., S. Ullrich, and B.-K. Baik, *Genotypic variation in color and discoloration potential of barley-based food products*. Cereal Chemistry, 2004. **81**(6): p. 752-758.
96. Brookes, P., D. Lovett, and I. MacWilliam, *The steeping of barley. A review of the metabolic consequences of water uptake, and their practical implications*. Journal of the Institute of Brewing, 1976. **82**(1): p. 14-26.

97. Mussatto, S.I., G. Dragone, and I.C. Roberto, *Brewers' spent grain: generation, characteristics and potential applications*. Journal of Cereal Science, 2006. **43**(1): p. 1-14.
98. Petters, H., B. Flannigan, and B. Austin, *Quantitative and qualitative studies of the microflora of barley malt production*. Journal of Applied Microbiology, 1988. **65**(4): p. 279-297.
99. O'Sullivan, T., et al., *A comparative study of malthouse and brewhouse microflora*. Journal of the Institute of Brewing, 1999. **105**(1): p. 55-61.
100. Tang, D.-S., et al., *Recovery of protein from brewer's spent grain by ultrafiltration*. Biochemical Engineering Journal, 2009. **48**(1): p. 1-5.
101. Szponar, B., et al., *Protein fraction of barley spent grain as a new simple medium for growth and sporulation of soil actinobacteria*. Biotechnology Letters, 2003. **25**(20): p. 1717-1721.
102. Bisaria, R., M. Madan, and P. Vasudevan, *Utilisation of agro-residues as animal feed through bioconversion*. Bioresource Technology, 1997. **59**(1): p. 5-8.
103. Macgregor, A.W. and G.B. Fincher, *Carbohydrates of the barley grain*. Barley: Chemistry and technology, ed. A.W. MacGregor and R.S. Bhatti. 1993. 73-130.
104. Shewry, P.R. and N.G. Halford, *Cereal seed storage proteins: structures, properties and role in grain utilization*. Journal of Experimental Botany, 2002. **53**(370): p. 947-958.
105. Morgan, A.G. and T.J. Riggs, *Effects of drought on yield and on grain and malt characteristics in spring barley*. Journal of the Science of Food and Agriculture, 1981. **32**(4): p. 339-346.
106. Qi, J.C., et al., *Protein and hordein fraction content in barley seeds as affected by sowing date and their relations to malting quality*. J Zhejiang Univ Sci B, 2005. **6**(11): p. 1069-75.
107. Rival, S.G., C.G. Boeriu, and H.J. Wichers, *Caseins and casein hydrolysates. 2. Antioxidative properties and relevance to lipooxygenase inhibition*. Journal of Agricultural and Food Chemistry, 2001. **49**(1): p. 295-302.
108. Bamdad, F., J. Wu, and L. Chen, *Effects of enzymatic hydrolysis on molecular structure and antioxidant activity of barley hordein*. Journal of Cereal Science, 2011. **54**(1): p. 20-28.
109. Bamdad, F. and L. Chen, *Antioxidant capacities of fractionated barley hordein hydrolysates in relation to peptide structures*. Molecular Nutrition & Food Research, 2013. **57**(3): p. 493-503.
110. Reed, D.J., *Toxicity of oxygen*. Molecular and cellular mechanisms of toxicity, 1995: p. 35-68.
111. Sies, H., *BIOCHEMISTRY OF OXIDATIVE STRESS*. Angewandte Chemie-International Edition in English, 1986. **25**(12): p. 1058-1071.
112. Samali, A., et al., *A comparative study of apoptosis and necrosis in HepG2 cells: oxidant-induced caspase inactivation leads to necrosis*. Biochem Biophys Res Commun, 1999. **255**(1): p. 6-11.
113. del Rio, L.A., *ROS and RNS in plant physiology: an overview*. Journal of Experimental Botany, 2015. **66**(10): p. 2827-2837.

114. Giles, G.I., K.M. Tasker, and C. Jacob, *Hypothesis: The role of reactive sulfur species in oxidative stress*. Free Radical Biology and Medicine, 2001. **31**(10): p. 1279-1283.
115. Moldovan, L. and N.I. Moldovan, *Oxygen free radicals and redox biology of organelles*. Histochem Cell Biol, 2004. **122**(4): p. 395-412.
116. Giles, G.I., et al., *Reactive sulphur species: an in vitro investigation of the oxidation properties of disulphide S-oxides*. Biochemical Journal, 2002. **364**: p. 579-585.
117. Flora, S.J.S., *Structural, chemical and biological aspects of antioxidants for strategies against metal and metalloid exposure*. Oxidative Medicine and Cellular Longevity, 2009. **2**(4): p. 191-206.
118. Venero, J.L., et al., *Evidence for dopamine-derived hydroxyl radical formation in the nigrostriatal system in response to axotomy*. Free Radic Biol Med, 2003. **34**(1): p. 111-23.
119. Castellani, R.J., et al., *Contribution of redox-active iron and copper to oxidative damage in Alzheimer disease*. Ageing Res Rev, 2004. **3**(3): p. 319-26.
120. Dizdaroglu, M. and P. Jaruga, *Mechanisms of free radical-induced damage to DNA*. Free Radic Res, 2012. **46**(4): p. 382-419.
121. Kanno, T., et al., *Literature review of the role of hydroxyl radicals in chemically-induced mutagenicity and carcinogenicity for the risk assessment of a disinfection system utilizing photolysis of hydrogen peroxide*. Journal of clinical biochemistry and nutrition, 2012. **51**(1): p. 9-14.
122. Weydert, C.J. and J.J. Cullen, *Measurement of superoxide dismutase, catalase, and glutathione peroxidase in cultured cells and tissue*. Nature protocols, 2010. **5**(1): p. 51-66.
123. Kulbacka, J., et al., *Apoptosis, free radicals and antioxidant defense in antitumor therapy*, in *Antioxidant enzyme*. 2012, InTech.
124. Lu, J.M., et al., *Chemical and molecular mechanisms of antioxidants: experimental approaches and model systems*. Journal of Cellular and Molecular Medicine, 2010. **14**(4): p. 840-860.
125. Kumar, S., A. Mishra, and A.K. Pandey, *Antioxidant mediated protective effect of Parthenium hysterophorus against oxidative damage using in vitro models*. BMC complementary and alternative medicine, 2013. **13**(1): p. 120.
126. Pandey, A.K. and S. Kumar, *Antioxidant, lipo-protective and antibacterial activities of phytoconstituents present in Solanum xanthocarpum root*. International Review of Biophysical Chemistry (IREBIC), 2012. **3**(3): p. 42-47.
127. Huang, D.J., B.X. Ou, and R.L. Prior, *The chemistry behind antioxidant capacity assays*. Journal of Agricultural and Food Chemistry, 2005. **53**(6): p. 1841-1856.
128. Glazer, A.N., *Phycoerythrin fluorescence-based assay for reactive oxygen species*. Methods Enzymol, 1990. **186**: p. 161-8.
129. Ghiselli, A., et al., *A fluorescence-based method for measuring total plasma antioxidant capability*. Free Radical Biology and Medicine, 1995. **18**(1): p. 29-36.
130. Bors, W., C. Michel, and M. Saran, *Inhibition of the bleaching of the carotenoid crocin a rapid test for quantifying antioxidant activity*. Biochimica et Biophysica Acta (BBA)-Lipids and Lipid Metabolism, 1984. **796**(3): p. 312-319.

131. Singleton, V.L., R. Orthofer, and R.M. Lamuela-Raventós, [14] *Analysis of total phenols and other oxidation substrates and antioxidants by means of folin-ciocalteu reagent*, in *Methods in enzymology*. 1999, Elsevier. p. 152-178.
132. Re, R., et al., *Antioxidant activity applying an improved ABTS radical cation decolorization assay*. *Free radical biology and medicine*, 1999. **26**(9-10): p. 1231-1237.
133. Pulido, R., L. Bravo, and F. Saura-Calixto, *Antioxidant activity of dietary polyphenols as determined by a modified ferric reducing/antioxidant power assay*. *Journal of agricultural and food chemistry*, 2000. **48**(8): p. 3396-3402.
134. Oyaizu, M., *Studies on products of browning reaction*. *The Japanese Journal of Nutrition and Dietetics*, 1986. **44**(6): p. 307-315.
135. Wolfe, K.L. and R.H. Liu, *Cellular antioxidant activity (CAA) assay for assessing antioxidants, foods, and dietary supplements*. *Journal of agricultural and food chemistry*, 2007. **55**(22): p. 8896-8907.
136. Collins, A.R., *The comet assay for DNA damage and repair: principles, applications, and limitations*. *Mol Biotechnol*, 2004. **26**(3): p. 249-61.
137. Cao, G.H., H.M. Alessio, and R.G. Cutler, *Oxygen-radical absorbency capacity assay for antioxidants*. *Free Radical Biology and Medicine*, 1993. **14**(3): p. 303-311.
138. Ou, B.X., M. Hampsch-Woodill, and R.L. Prior, *Development and validation of an improved oxygen radical absorbance capacity assay using fluorescein as the fluorescent probe*. *Journal of Agricultural and Food Chemistry*, 2001. **49**(10): p. 4619-4626.
139. Huang, D.J., et al., *Development and validation of oxygen radical absorbance capacity assay for lipophilic antioxidants using randomly methylated beta-cyclodextrin as the solubility enhancer*. *Journal of Agricultural and Food Chemistry*, 2002. **50**(7): p. 1815-1821.
140. Jaime, L., et al., *Pressurized liquids as an alternative process to antioxidant carotenoids' extraction from Haematococcus pluvialis microalgae*. *Lwt-Food Science and Technology*, 2010. **43**(1): p. 105-112.
141. Prior, R.L., X.L. Wu, and K. Schaich, *Standardized methods for the determination of antioxidant capacity and phenolics in foods and dietary supplements*. *Journal of Agricultural and Food Chemistry*, 2005. **53**(10): p. 4290-4302.
142. Ninfali, P., et al., *Antioxidant capacity of vegetables, spices and dressings relevant to nutrition*. *British Journal of Nutrition*, 2005. **93**(2): p. 257-266.
143. Bondet, V., W. Brand-Williams, and C. Berset, *Kinetics and mechanisms of antioxidant activity using the DPPH. free radical method*. *LWT-Food Science and Technology*, 1997. **30**(6): p. 609-615.
144. Walker, R.B. and J.D. Everette, *Comparative reaction rates of various antioxidants with ABTS radical cation*. *Journal of Agricultural and Food Chemistry*, 2009. **57**(4): p. 1156-1161.
145. P Jayanthi, P.L., *Reducing power of the solvent extracts of Eichhornia crassipes (Mart.) Solms*. *International Journal of Pharmacy and Pharmaceutical Sciences*, 2011. **3**(3): p. 126-128.

146. Vijayalakshmi, M. and K. Ruckmani, *Ferric reducing anti-oxidant power assay in plant extract*. Bangladesh Journal of Pharmacology, 2016. **11**(3): p. 570-572.
147. Ostling, O. and K.J. Johanson, *Microelectrophoretic study of radiation-induced DNA damages in individual mammalian cells*. Biochemical and biophysical research communications, 1984. **123**(1): p. 291-298.
148. Singh, N.P., *et al.*, *A simple technique for quantitation of low-levels of DNA-damage in individual cells*. Experimental Cell Research, 1988. **175**(1): p. 184-191.
149. Bajpayee, M., A. Kumar, and A. Dhawan, *The comet assay: assessment of in vitro and in vivo DNA damage*. Methods Mol Biol, 2013. **1044**: p. 325-45.
150. Hartmann, A., *et al.*, *Use of the alkaline in vivo Comet assay for mechanistic genotoxicity investigations*. Mutagenesis, 2004. **19**(1): p. 51-59.
151. Remenyik, É., *et al.*, *Comet Assay to Study UV-Induced DNA Damage*, in *Biologic Effects of Light 1998*. 1999, Springer. p. 41-43.
152. Leandro, L.F., *et al.*, *Assessment of the genotoxicity and antigenotoxicity of (+)-usnic acid in V79 cells and Swiss mice by the micronucleus and comet assays*. Mutation Research/Genetic Toxicology and Environmental Mutagenesis, 2013. **753**(2): p. 101-106.
153. Leandro, L.F., *et al.*, *Assessment of the genotoxicity and antigenotoxicity of (+)-usnic acid in V79 cells and Swiss mice by the micronucleus and comet assays*. Mutation Research/Genetic Toxicology and Environmental Mutagenesis, 2013. **753**(2): p. 101-106.
154. Munari, C.C., *et al.*, *In vivo assessment of genotoxic, antigenotoxic and anticarcinogenic activities of Solanum lycocarpum fruits glycoalkaloidic extract*. PloS one, 2014. **9**(11): p. e111999.
155. Bakuradze, T. and E. Richling, *Comparison of different DNA staining methods in the comet assay*. Frontiers in Genetics, 2015. **6**(1): p. 1-1.
156. Albertini, R.J., *et al.*, *IPCS guidelines for the monitoring of genotoxic effects of carcinogens in humans*. Mutation Research/Reviews in Mutation Research, 2000. **463**(2): p. 111-172.
157. Hartmann, A., *et al.*, *Recommendations for conducting the in vivo alkaline Comet assay*. Mutagenesis, 2003. **18**(1): p. 45-51.
158. Collins, A.R., *et al.*, *The comet assay: topical issues*. Mutagenesis, 2008. **23**(3): p. 143-151.
159. Yarmush, M.L. and A. Jayaraman, *Advances in proteomic technologies*. Annual review of biomedical engineering, 2002. **4**(1): p. 349-373.
160. Mitulović, G. and K. Mechtler, *HPLC techniques for proteomics analysis—a short overview of latest developments*. Briefings in Functional Genomics, 2006. **5**(4): p. 249-260.
161. Bruce, C., *et al.*, *Proteomics and the analysis of proteomic data: 2013 overview of current protein-profiling technologies*. Current protocols in bioinformatics, 2013: p. 13.21. 1-13.21. 17.
162. Catherman, A.D., O.S. Skinner, and N.L. Kelleher, *Top down proteomics: facts and perspectives*. Biochemical and biophysical research communications, 2014. **445**(4): p. 683-693.

163. Zhang, Y., *et al.*, *Protein analysis by shotgun/bottom-up proteomics*. Chemical reviews, 2013. **113**(4): p. 2343-2394.
164. Kurien, B.T. and R.H. Scofield, *Extraction of proteins from gels: a brief review*. Methods Mol Biol, 2012. **869**: p. 403-5.
165. Gauci, V.J., M.P. Padula, and J.R. Coorssen, *Coomassie blue staining for high sensitivity gel-based proteomics*. Journal of proteomics, 2013. **90**: p. 96-106.
166. Wray, W., *et al.*, *Silver staining of proteins in polyacrylamide gels*. Analytical biochemistry, 1981. **118**(1): p. 197-203.
167. Dyballa, N. and S. Metzger, *Fast and sensitive colloidal coomassie G-250 staining for proteins in polyacrylamide gels*. Journal of visualized experiments: JoVE, 2009(30).
168. D'Souza, R.C., *et al.*, *Time-resolved dissection of early phosphoproteome and ensuing proteome changes in response to TGF- β* . Sci. Signal., 2014. **7**(335): p. rs5-rs5.
169. Gruhler, A., *et al.*, *Quantitative phosphoproteomics applied to the yeast pheromone signaling pathway*. Molecular & Cellular Proteomics, 2005. **4**(3): p. 310-327.
170. Huttlin, E.L., *et al.*, *A tissue-specific atlas of mouse protein phosphorylation and expression*. Cell, 2010. **143**(7): p. 1174-1189.
171. Pinkse, M.W., *et al.*, *Highly robust, automated, and sensitive online TiO₂-based phosphoproteomics applied to study endogenous phosphorylation in Drosophila melanogaster*. Journal of proteome research, 2007. **7**(2): p. 687-697.
172. McNulty, D.E. and R.S. Annan, *Hydrophilic interaction chromatography reduces the complexity of the phosphoproteome and improves global phosphopeptide isolation and detection*. Molecular & cellular proteomics, 2008. **7**(5): p. 971-980.
173. Batth, T.S., C. Francavilla, and J.V. Olsen, *Off-line high-pH reversed-phase fractionation for in-depth phosphoproteomics*. Journal of proteome research, 2014. **13**(12): p. 6176-6186.
174. Boone, C. and J. Adamec, *10 - Top-Down Proteomics A2 - Ciborowski, P*, in *Proteomic Profiling and Analytical Chemistry (Second Edition)*, J. Silberring, Editor. 2016, Elsevier: Boston. p. 175-191.
175. Köcher, T., R. Swart, and K. Mechtler, *Ultra-high-pressure RPLC hyphenated to an LTQ-Orbitrap Velos reveals a linear relation between peak capacity and number of identified peptides*. Analytical chemistry, 2011. **83**(7): p. 2699-2704.
176. Eeltink, S., *et al.*, *Optimizing the peak capacity per unit time in one-dimensional and off-line two-dimensional liquid chromatography for the separation of complex peptide samples*. Journal of Chromatography A, 2009. **1216**(44): p. 7368-7374.
177. Hsieh, E.J., *et al.*, *Effects of column and gradient lengths on peak capacity and peptide identification in nanoflow LC-MS/MS of complex proteomic samples*. Journal of the American Society for Mass Spectrometry, 2013. **24**(1): p. 148-153.

178. Köcher, T., *et al.*, *Analysis of protein mixtures from whole-cell extracts by single-run nanoLC-MS/MS using ultralong gradients*. *Nature protocols*, 2012. **7**(5): p. 882-890.
179. Bauer, M., *et al.*, *Evaluation of Data-Dependent and -Independent Mass Spectrometric Workflows for Sensitive Quantification of Proteins and Phosphorylation Sites*. *Journal of Proteome Research*, 2014. **13**(12): p. 5973-5988.
180. Eng, J.K., A.L. McCormack, and J.R. Yates, *An approach to correlate tandem mass spectral data of peptides with amino acid sequences in a protein database*. *Journal of the American Society for Mass Spectrometry*, 1994. **5**(11): p. 976-989.
181. Cottrell, J.S. and U. London, *Probability-based protein identification by searching sequence databases using mass spectrometry data*. *electrophoresis*, 1999. **20**(18): p. 3551-3567.
182. Geer, L.Y., *et al.*, *Open mass spectrometry search algorithm*. *Journal of proteome research*, 2004. **3**(5): p. 958-964.
183. Craig, R. and R.C. Beavis, *TANDEM: matching proteins with tandem mass spectra*. *Bioinformatics*, 2004. **20**(9): p. 1466-1467.
184. Aggarwal, S. and A.K. Yadav, *False Discovery Rate Estimation in Proteomics*. *Methods Mol Biol*, 2016. **1362**: p. 119-28.
185. Abdelmoez, W., H. Yoshida, and T. Nakahasi, *Pathways of Amino Acid Transformation and Decomposition in Saturated Subcritical Water Conditions*. *International Journal of Chemical Reactor Engineering*, 2010. **8**.
186. Powell, T., S. Bowra, and H.J. Cooper, *Subcritical Water Processing of Proteins: An Alternative to Enzymatic Digestion?* *Anal Chem*, 2016. **88**(12): p. 6425-32.
187. Swaney, D.L., C.D. Wenger, and J.J. Coon, *Value of using multiple proteases for large-scale mass spectrometry-based proteomics*. *Journal of proteome research*, 2010. **9**(3): p. 1323-1329.
188. Lopez-Ferrer, D., *et al.*, *Sample treatment for protein identification by mass spectrometry-based techniques*. *TrAC Trends in Analytical Chemistry*, 2006. **25**(10): p. 996-1005.
189. Kang, K.Y. and B.S. Chun, *Behavior of amino acid production from hydrothermal treatment of fish-derived wastes*. *Korean Journal of Chemical Engineering*, 2004. **21**(6): p. 1147-1152.
190. Partridge, S.M. and H.F. Davis, *PREFERENTIAL RELEASE OF ASPARTIC ACID DURING THE HYDROLYSIS OF PROTEINS*. *Nature*, 1950. **165**(4185): p. 62-63.
191. Li, A.Q., *et al.*, *Chemical cleavage at aspartyl residues for protein identification*. *Analytical Chemistry*, 2001. **73**(22): p. 5395-5402.
192. Inglis, A.S., *Cleavage at aspartic-acid*. *Methods in Enzymology*, 1983. **91**: p. 324-332.
193. Smith, B.J., *Chemical cleavage of proteins at aspartyl residues*. *The protein protocols handbook*, ed. J.M. Walker. 1996. 381-384.
194. Zhong, H.Y., *et al.*, *Protein sequencing by mass analysis of polypeptide ladders after controlled protein hydrolysis*. *Nature Biotechnology*, 2004. **22**(10): p. 1291-1296.

195. Zhong, H.Y., S.L. Marcus, and L. Li, *Microwave-assisted acid hydrolysis of proteins combined with liquid chromatography MALDI MS/MS for protein identification*. Journal of the American Society for Mass Spectrometry, 2005. **16**(4): p. 471-481.
196. Hua, L., T.Y. Low, and S.K. Sze, *Microwave-assisted specific chemical digestion for rapid protein identification*. Proteomics, 2006. **6**(2): p. 586-591.
197. Swatkoski, S., et al., *Evaluation of microwave-accelerated residue-specific acid cleavage for proteomic applications*. Journal of Proteome Research, 2008. **7**(2): p. 579-586.
198. Plaza, M. and C. Turner, *Pressurized hot water extraction of bioactives*. Trac-Trends in Analytical Chemistry, 2015. **71**: p. 39-54.
199. Espinoza, A.D., R.O. Morawicki, and T. Hager, *Hydrolysis of Whey Protein Isolate Using Subcritical Water*. Journal of Food Science, 2012. **77**(1): p. C20-C26.
200. Syka, J.E.P., et al., *Peptide and protein sequence analysis by electron transfer dissociation mass spectrometry*. Proceedings of the National Academy of Sciences of the United States of America, 2004. **101**(26): p. 9528-9533.
201. Powell, T., S. Bowra, and H.J. Cooper, *Subcritical Water Hydrolysis of Peptides: Amino Acid Side-Chain Modifications*. Journal of the American Society for Mass Spectrometry, 2017. **28**(9): p. 1775-1786.
202. Cooper, H.J., et al., *Characterization of amino acid side chain losses in electron capture dissociation*. Journal of the American Society for Mass Spectrometry, 2002. **13**(3): p. 241-249.
203. Vogt, W., *OXIDATION OF METHIONYL RESIDUES IN PROTEINS - TOOLS, TARGETS, AND REVERSAL*. Free Radical Biology and Medicine, 1995. **18**(1): p. 93-105.
204. Basile, F., et al., *Mass Spectrometry Characterization of the Thermal Decomposition/Digestion (TDD) at Cysteine in Peptides and Proteins in the Condensed Phase*. Journal of the American Society for Mass Spectrometry, 2011. **22**(11): p. 1926-1940.
205. Moller, I.M. and B.K. Kristensen, *Protein oxidation in plant mitochondria detected as oxidized tryptophan*. Free Radical Biology and Medicine, 2006. **40**(3): p. 430-435.
206. Lemma-Gray, P., et al., *Tryptophan 334 oxidation in bovine cytochrome c oxidase subunit I involves free radical migration*. Febs Letters, 2007. **581**(3): p. 437-442.
207. Taylor, S.W., et al., *Oxidative post-translational modification of tryptophan residues in cardiac mitochondrial proteins*. Journal of Biological Chemistry, 2003. **278**(22): p. 19587-19590.
208. Sun, S.W., et al., *Deriving the probabilities of water loss and ammonia loss for amino acids from tandem mass spectra*. Journal of Proteome Research, 2008. **7**(1): p. 202-208.
209. Boja, E.S. and H.M. Fales, *Overalkylation of a protein digest with iodoacetamide*. Analytical Chemistry, 2001. **73**(15): p. 3576-3582.

210. Yang, Z.H. and A.B. Attygalle, *LC/MS characterization of undesired products formed during iodoacetamide derivatization of sulfhydryl groups of peptides*. Journal of Mass Spectrometry, 2007. **42**(2): p. 233-243.
211. Rebecchi, K.R., et al., *A General Protease Digestion Procedure for Optimal Protein Sequence Coverage and Post-Translational Modifications Analysis of Recombinant Glycoproteins: Application to the Characterization of Human Lysyl Oxidase-like 2 Glycosylation*. Analytical Chemistry, 2011. **83**(22): p. 8484-8491.
212. Nielsen, M.L., et al., *Iodoacetamide-induced artifact mimics ubiquitination in mass spectrometry*. Nature Methods, 2008. **5**(6): p. 459-460.
213. Lapko, V.N., D.L. Smith, and J.B. Smith, *Identification of an artifact in the mass spectrometry of proteins derivatized with iodoacetamide*. Journal of Mass Spectrometry, 2000. **35**(4): p. 572-575.
214. Savage, P.E., *Organic Chemical Reactions in Supercritical Water*. Chemical Reviews, 1999. **99**(2): p. 603-622.
215. Yemenicioglu, L.Y.A.a.A., *Are Protein-bound Phenolic Antioxidants in Pulses Unseen Part of Iceberg?* Journal of Plant Biochemistry & Physiology, 2011. **1**(4).
216. Reuter, S., et al., *Oxidative stress, inflammation, and cancer: How are they linked?* Free radical biology & medicine, 2010. **49**(11): p. 1603-1616.
217. Hwang, O., *Role of Oxidative Stress in Parkinson's Disease*. Experimental Neurobiology, 2013. **22**(1): p. 11-17.
218. Kattoor, A.J., et al., *Oxidative Stress in Atherosclerosis*. Curr Atheroscler Rep, 2017. **19**(11): p. 42.
219. Shewry, P.R., H.M. Pratt, and B.J. Mifflin, *Varietal identification of single seeds of barley by analysis of hordein polypeptides*. Journal of the Science of Food and Agriculture, 1978. **29**(7): p. 587-596.
220. Schmidt, D., et al., *Lysine metabolism in antisense C-hordein barley grains*. Plant Physiology and Biochemistry, 2015. **87**: p. 73-83.
221. Baxter, E.D., *Hordein in barley and malt - a review*. Journal of the Institute of Brewing, 1981. **87**(3): p. 173-176.
222. Marchylo, B.A., J.E. Kruger, and D. Hatcher, *High-performance liquid-chromatographic and electrophoretic analysis of hordein during malting for 2 barley varieties of contrasting malting quality*. Cereal Chemistry, 1986. **63**(3): p. 219-231.
223. Tatham, A.S. and P.R. Shewry, *The S-poor prolamins of wheat, barley and rye*. Journal of Cereal Science, 1995. **22**(1): p. 1-16.
224. Ou, B.X., et al., *Analysis of antioxidant activities of common vegetables employing oxygen radical absorbance capacity (ORAC) and ferric reducing antioxidant power (FRAP) assays: A comparative study*. Journal of Agricultural and Food Chemistry, 2002. **50**(11): p. 3122-3128.
225. Li, C.Y., et al., *Oxygen Radical Absorbance Capacity of Different Varieties of Strawberry and the Antioxidant Stability in Storage*. Molecules, 2013. **18**(2): p. 1528-1539.
226. Ehlenfeldt, M.K. and R.L. Prior, *Oxygen Radical Absorbance Capacity (ORAC) and Phenolic and Anthocyanin Concentrations in Fruit and Leaf Tissues of*

- Highbush Blueberry*. Journal of Agricultural and Food Chemistry, 2001. **49**(5): p. 2222-2227.
227. Cemeli, E., A. Baumgartner, and D. Anderson, *Antioxidants and the Comet assay*. Mutation Research/Reviews in Mutation Research, 2009. **681**(1): p. 51-67.
 228. Festa, F., *et al.*, *Strong antioxidant activity of ellagic acid in mammalian cells in vitro revealed by the comet assay*. Anticancer Res, 2001. **21**(6a): p. 3903-8.
 229. Lin, K.-H., *et al.*, *Antioxidant activity of herbaceous plant extracts protect against hydrogenperoxide-induced DNA damage in human lymphocytes*. BMC Research Notes, 2013. **6**(1): p. 490.
 230. Bamdad, F., J.P. Wu, and L.Y. Chen, *Effects of enzymatic hydrolysis on molecular structure and antioxidant activity of barley hordein*. Journal of Cereal Science, 2011. **54**(1): p. 20-28.
 231. Wu, H.-C., H.-M. Chen, and C.-Y. Shiau, *Free amino acids and peptides as related to antioxidant properties in protein hydrolysates of mackerel (Scomber austriasicus)*. Food Research International, 2003. **36**(9): p. 949-957.
 232. Zhang, J., *et al.*, *Antioxidant activities of the rice endosperm protein hydrolysate: identification of the active peptide*. European Food Research and Technology, 2009. **229**(4): p. 709-719.
 233. Abdelmoez, W. and H. Yoshida, *Production of Amino and Organic Acids from Protein Using Sub-Critical Water Technology*. International Journal of Chemical Reactor Engineering, 2013. **11**: p. 369-384.
 234. Moorhouse, K.G., *et al.*, *Validation of an HPLC method for the analysis of the charge heterogeneity of the recombinant monoclonal antibody IDEC-C2B8 after papain digestion*. J Pharm Biomed Anal, 1997. **16**(4): p. 593-603.
 235. Wang, Z., *Fischer Indole Synthesis*, in *Comprehensive Organic Name Reactions and Reagents*. 2010, John Wiley & Sons, Inc.
 236. An, J.Y., *et al.*, *Applications of high-temperature aqueous media for synthetic organic reactions*. Journal of Organic Chemistry, 1997. **62**(8): p. 2505-2511.
 237. Kuhlmann, B., E.M. Arnett, and M. Siskin, *Classical Organic-Reactions In Pure Superheated Water*. Journal of Organic Chemistry, 1994. **59**(11): p. 3098-3101.
 238. Choi, S.S., *et al.*, *Fragmentation patterns of protonated amino acids formed by atmospheric pressure chemical ionization*. Rapid Communications in Mass Spectrometry, 2013. **27**(1): p. 143-151.
 239. Sato, T., *et al.*, *Alkylation of phenol with carbonyl compounds in supercritical water*. Journal of Chemical Engineering of Japan, 2003. **36**(3): p. 339-342.
 240. Chandler, K., *et al.*, *Tuning alkylation reactions with temperature in near-critical water*. Aiche Journal, 1998. **44**(9): p. 2080-2087.
 241. Reardon, P., *et al.*, *Palladium-Catalyzed Coupling Reactions In Superheated Water*. Organometallics, 1995. **14**(8): p. 3810-3816.
 242. <https://www.thermofisher.com/order/catalog/product/88342>.
 243. Sun, L., G. Zhu, and N.J. Dovichi, *Comparison of the LTQ-Orbitrap Velos and the Q-Exactive for proteomic analysis of 1–1000 ng RAW 264.7 cell lysate digests*. Rapid Communications in Mass Spectrometry, 2013. **27**(1): p. 157-162.

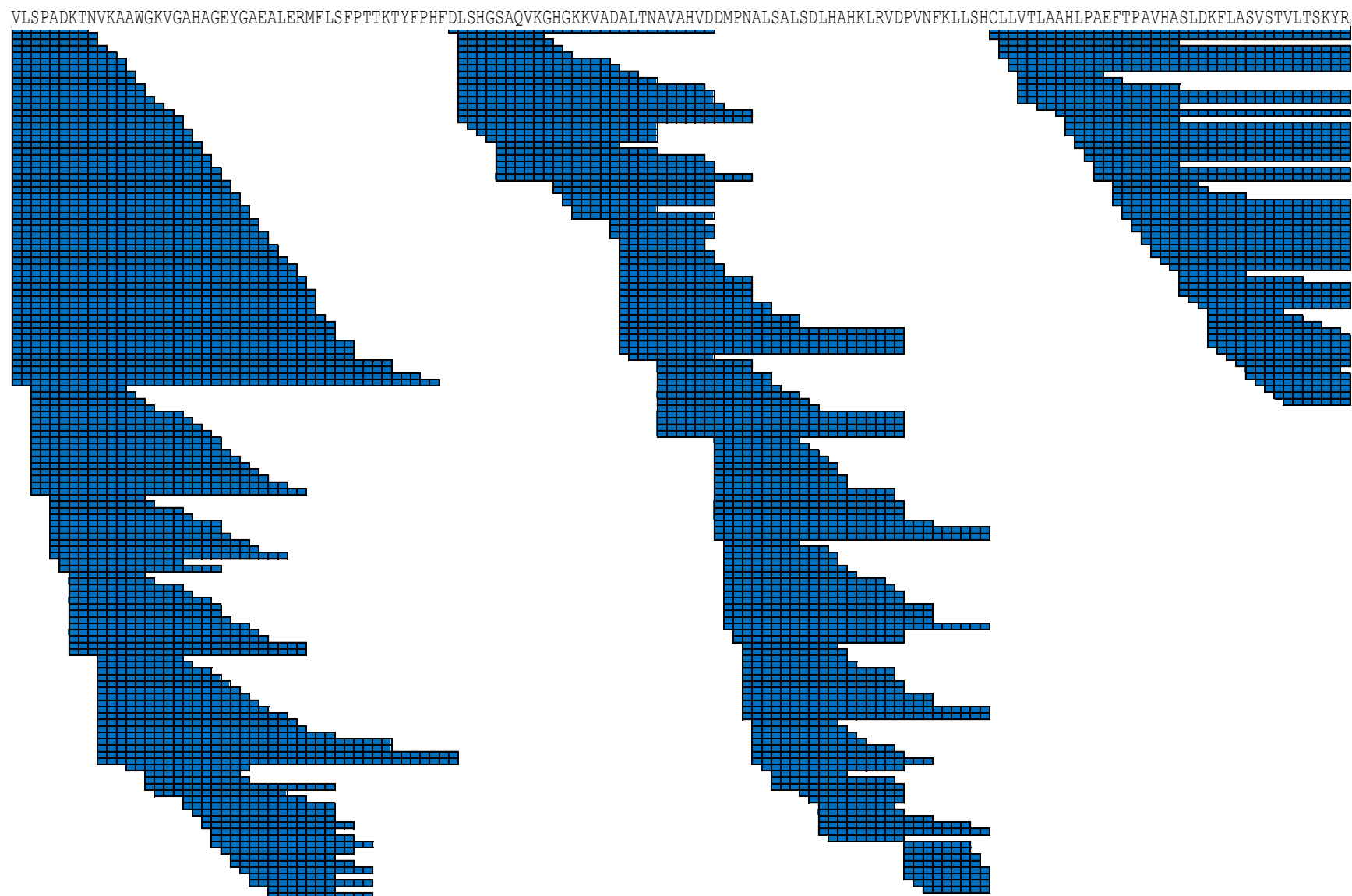
- 244. Zhao, Y. and O.N. Jensen, *Modification-specific proteomics: strategies for characterization of post-translational modifications using enrichment techniques*. Proteomics, 2009. **9**(20): p. 4632-4641.
- 245. Tanner, S., et al., *Accurate annotation of peptide modifications through unrestrictive database search*. Journal of proteome research, 2007. **7**(01): p. 170-181.
- 246. Ong, S.-E., G. Mittler, and M. Mann, *Identifying and quantifying in vivo methylation sites by heavy methyl SILAC*. Nature methods, 2004. **1**(2): p. 119-126.
- 247. Na, S., N. Bandeira, and E. Paek, *Fast Multi-blind Modification Search through Tandem Mass Spectrometry*. Molecular & Cellular Proteomics : MCP, 2012. **11**(4): p. M111.010199.

Appendix

Appendix Figure 3. 1 - Summary of peptides identified following SCW hydrolysis of **a)** α -globin, **b)** β - globin, **c)**BSA and **d)** β -casein under conditions 160 °C for 0 minutes, 160 °C for 20 minutes, 207 °C for 20 minutes, 253 °C for 20 minutes and 300 °C for 20 minutes.



Appendix Figure 3.1 a) SCW hydrolysis of α - globin at 160⁰C for 0 minutes.

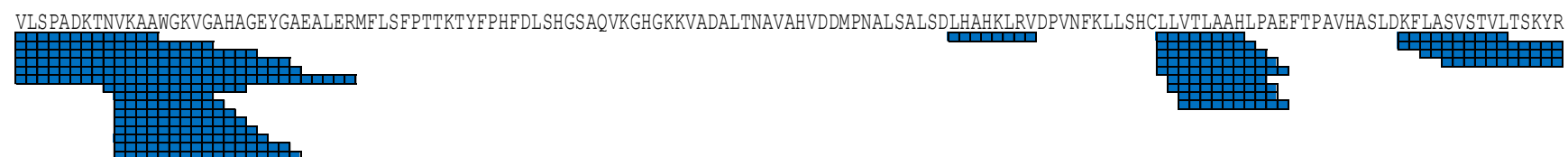


Appendix Figure 3.1 a) SCW hydrolysis of α -globin at 160°C for 20 minutes.

VLSPADKTNVKAANGKVGAGAHAGEYGAEALERMFLSFPTTKTYFPHFDLSHGSAQVKGHGKKVADALTNAVAHVDDMPNALSALSDLHAHKLRVDPVNFKLLSHCLLVTLAAHLPAEFTPAVHASLDKFLASVSTVLTISKYR



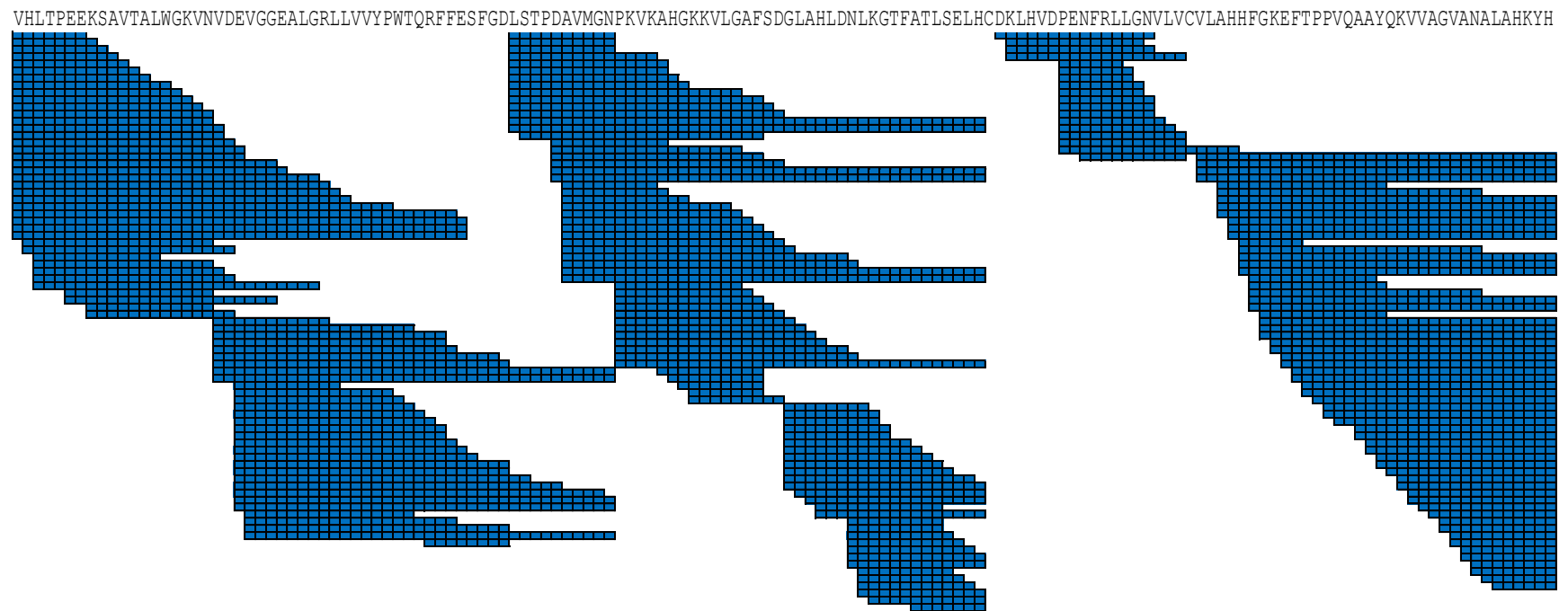
Appendix Figure 3.1 a) SCW hydrolysis of α -globin at 207⁰C for 20 minutes.



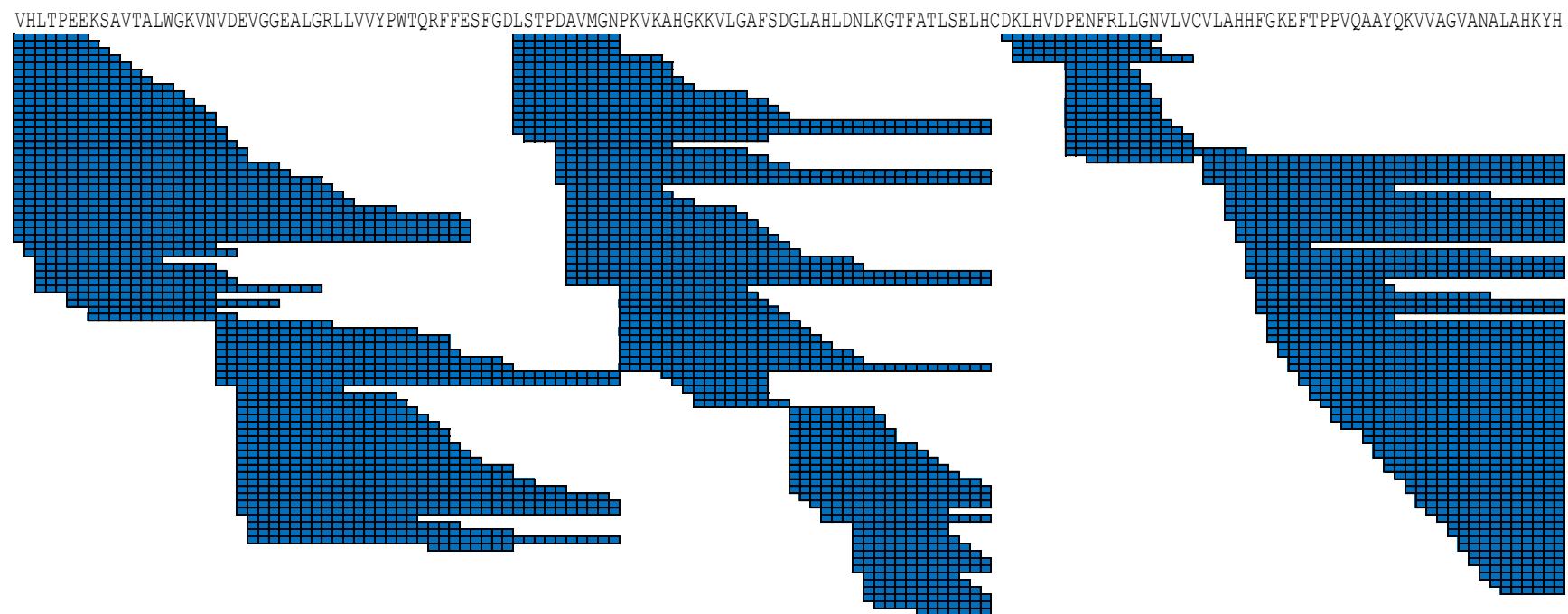
Appendix Figure 3.1 a) SCW hydrolysis of α - globin at 253⁰C for 20 minutes.

VLSPADKTNVKAANGKVGAGAGEYGAELERMFLSFPTTKTYFPHFDLSHGSAQVKGHGKKVADALTNAVAHVDDMPNALSALSDLHAHKLRVDPVNFKLLSHCLLVTLAAHLPAEFTPAVHASLDKFLASVSTVLTSKYR

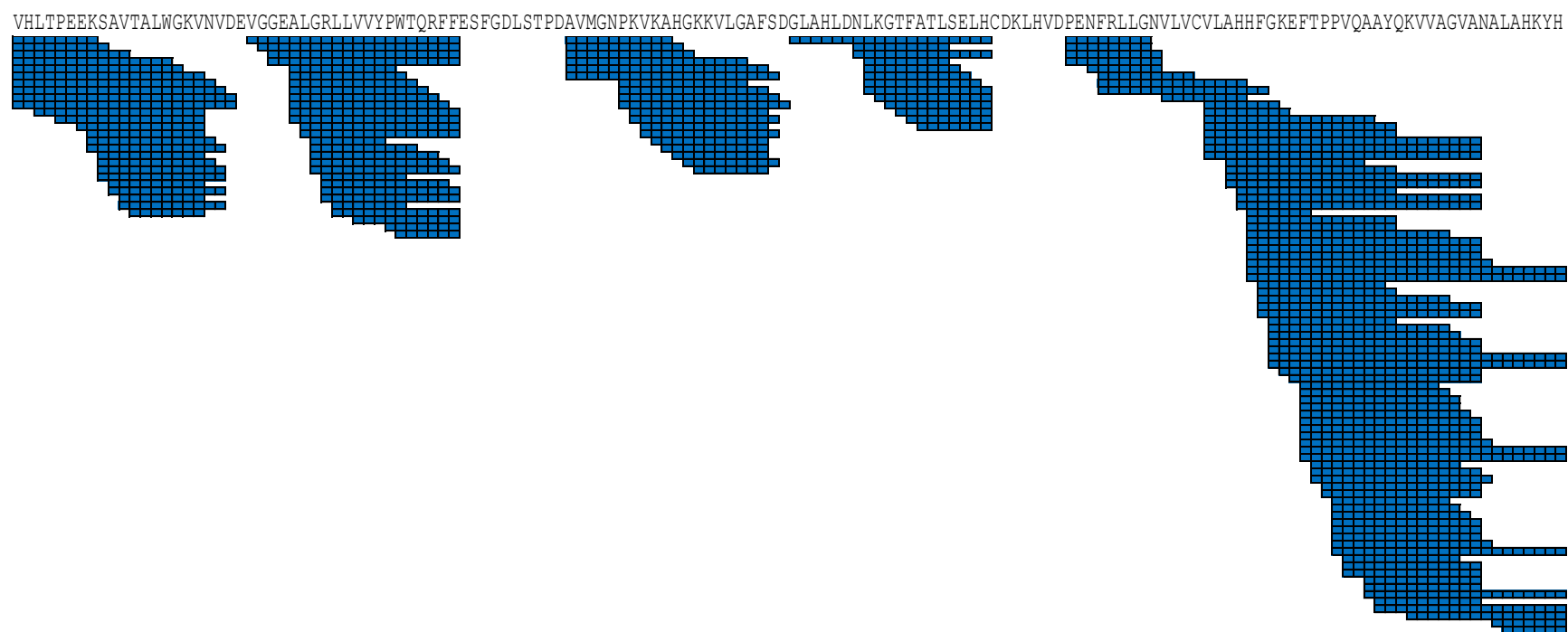
Appendix Figure 3.1 a) SCW hydrolysis of α - globin at 300⁰C for 20 minutes.



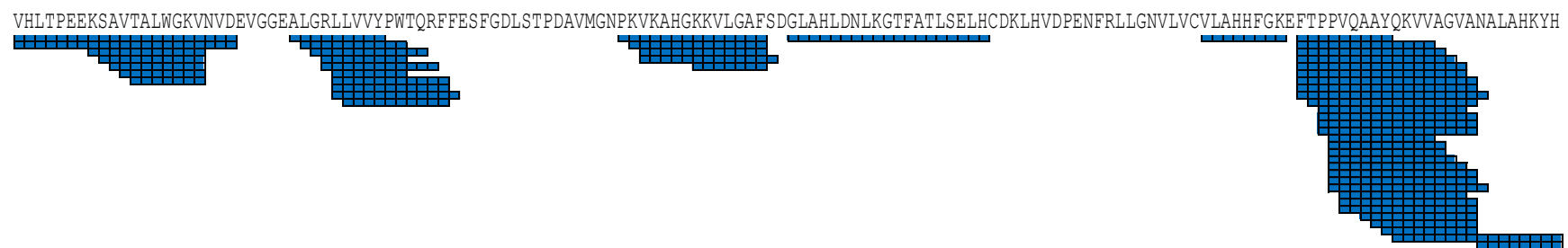
Appendix Figure 3.1 b) SCW hydrolysis of β - globin at 160⁰C for 0 minutes.



Appendix Figure 3.1 b) SCW hydrolysis of β -globin at 160 °C for 20 minutes.



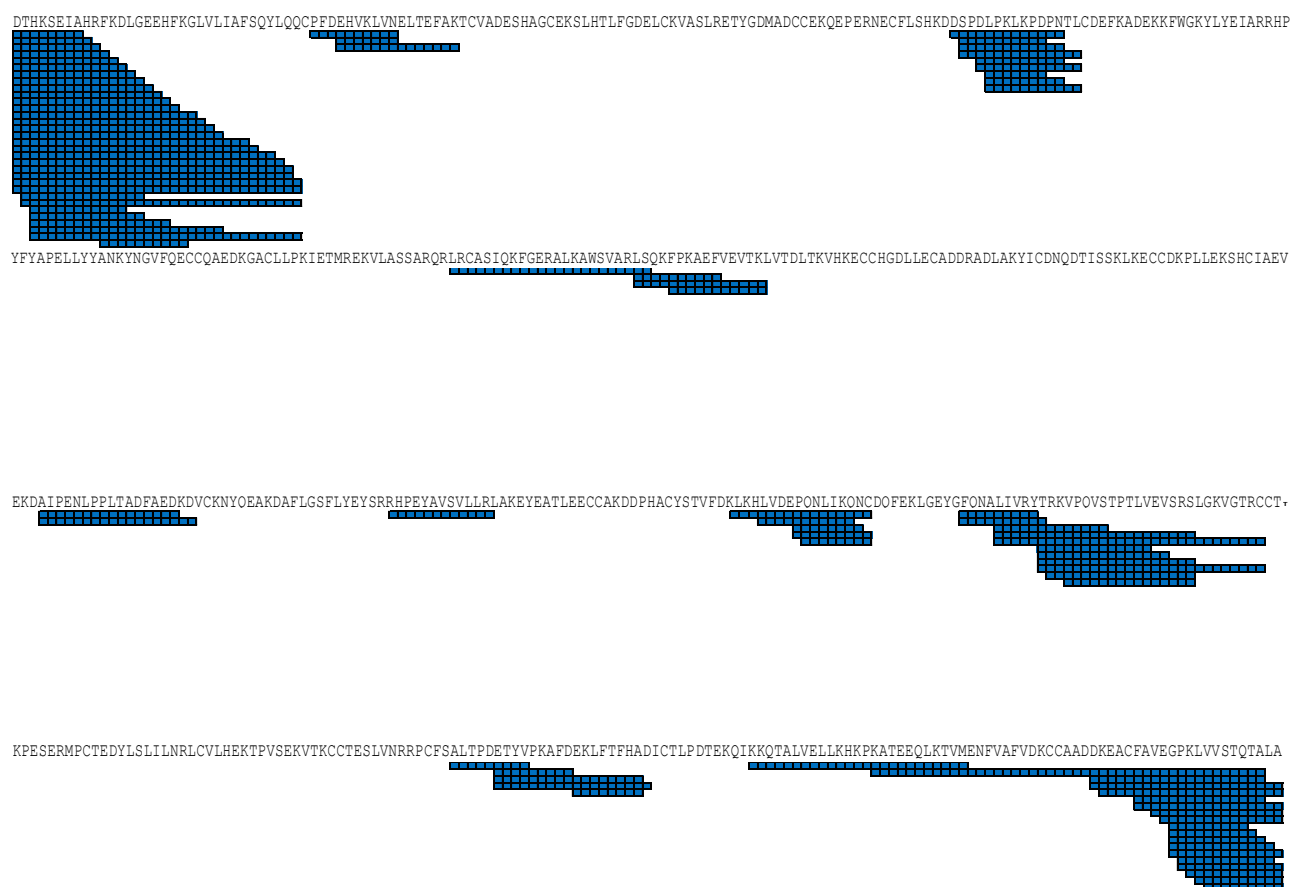
Appendix Figure 3.1 b) SCW hydrolysis of β - globin at 207⁰C for 20 minutes.



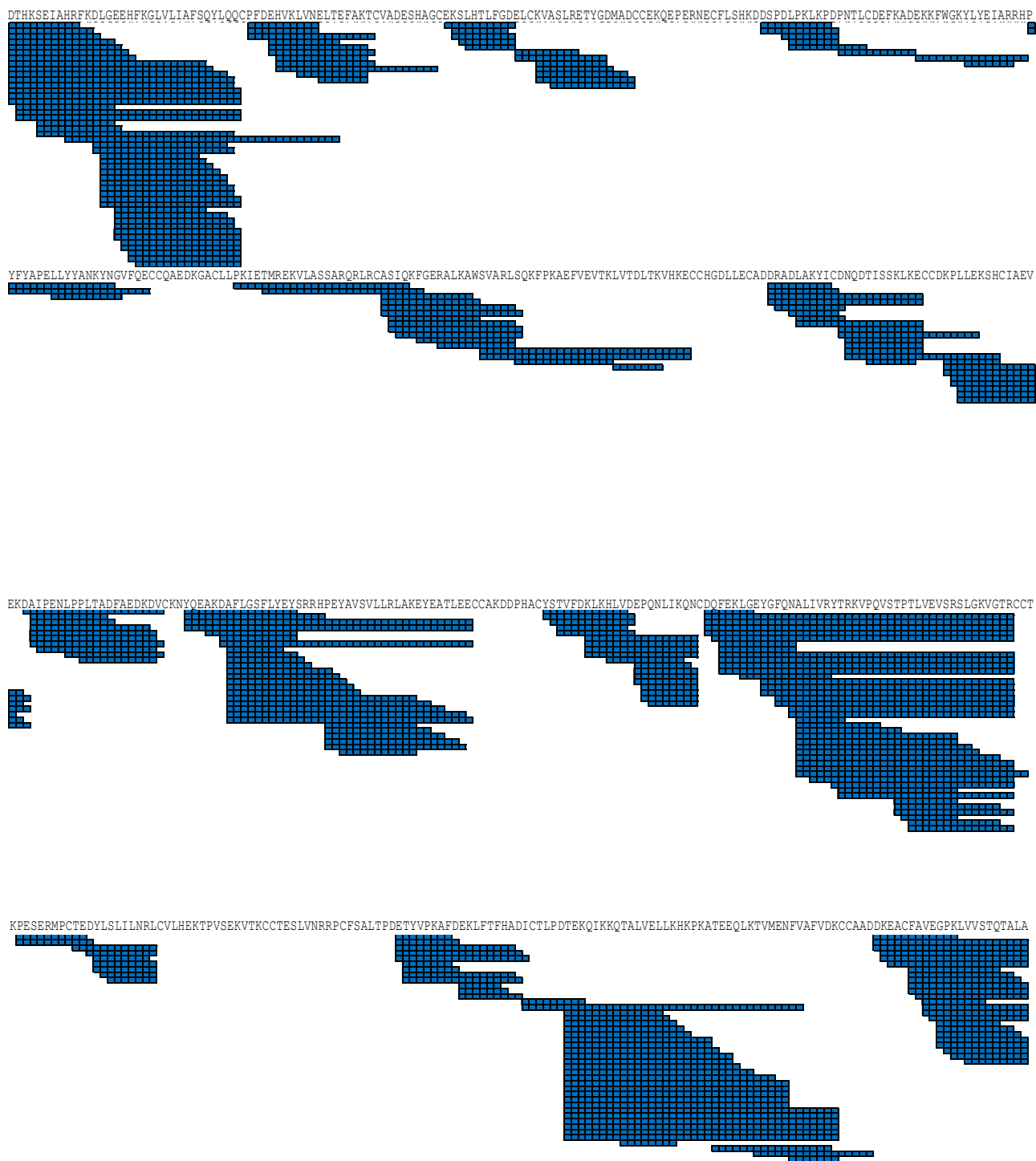
Appendix Figure 3.1 b) SCW hydrolysis of β - globin at 253⁰ C for 20 minutes.

VHLTPEEKSAVTALWGKVNVDEVGGEALGRLLVVYPWTQRFFESFGDLSTPDAMGNPKVKAHGKKVLGAFSDGLAHLNLTGTATLSELHCDKLHVDPENFRLLGNVLCVLAHHFGKEFTPPVQAAYQKVVAGVANALAHKYH

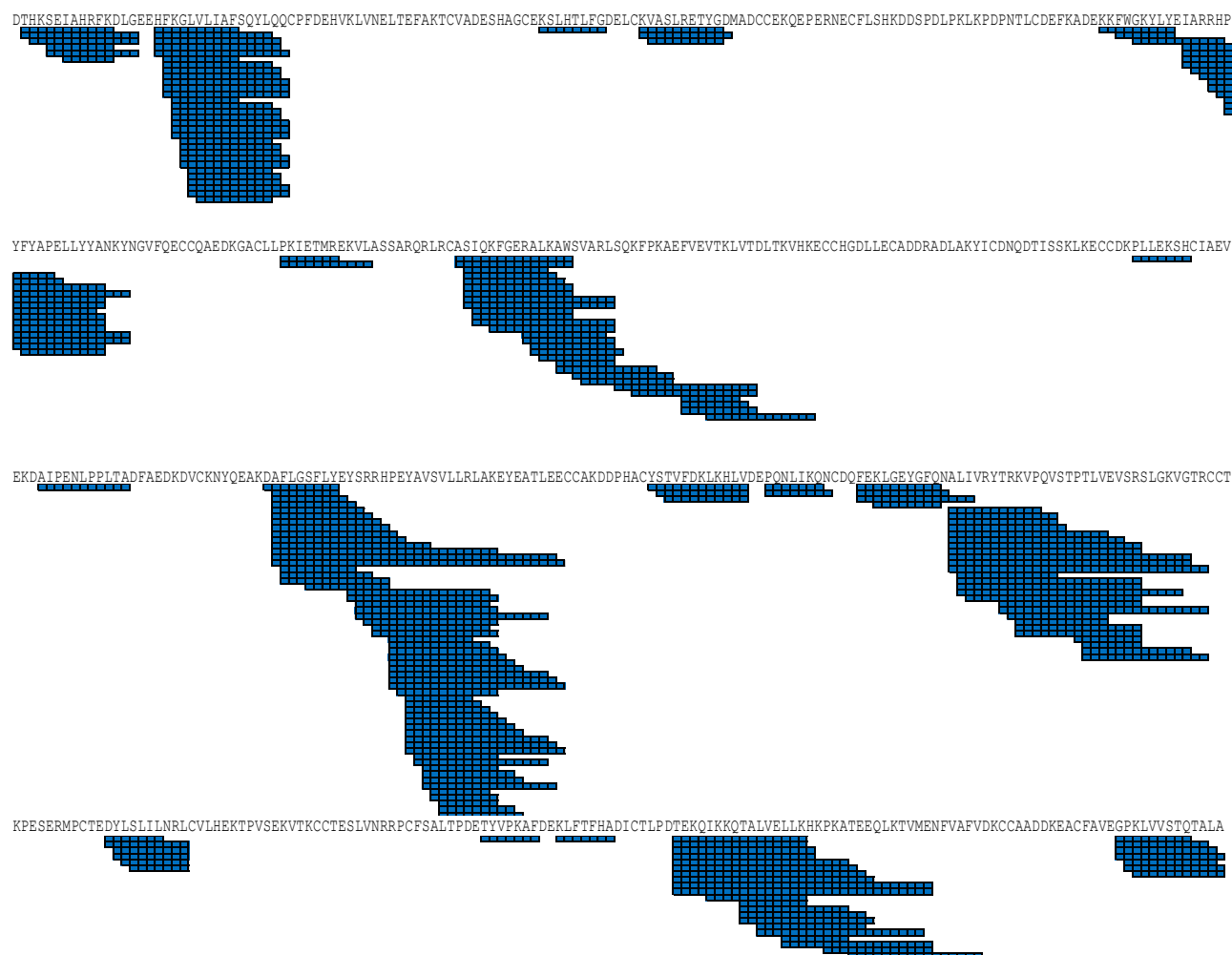
Appendix Figure 3.1 b) SCW hydrolysis of β - globin at 300⁰C for 0 minutes.



Appendix Figure 3.1 c) SCW hydrolysis of untreated BSA at 160⁰C for 0 minutes.

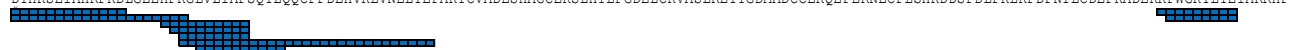


Appendix Figure 3.1 c) SCW hydrolysis of untreated BSA at 160°C for 20 minutes.

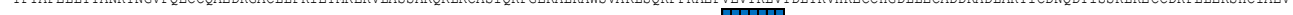


Appendix Figure 3.1 c) SCW hydrolysis of untreated BSA at 207⁰C for 20 minutes.

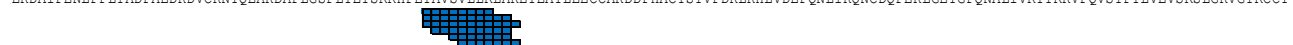
DTHKSEIAHRFKDLGEEHFKGLVLIAFSQVLQQCPFDEHVKLVNELTEFAKTCVADESHAGCEKSLHTLFGDELCKVASLRETYGDMADCEKQEPPERNECFLSHKDDSPDLPKLPDPNTLCDEFKADEKKFWGKYLVEIARRHP



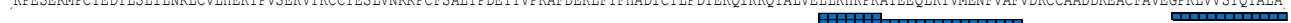
YFYAPELLYYANKYNGVFQECQAEDEKGCALLPKIETMREKVLASSARQRLRCASIQKFGERALKAWSVARLSQKFPKAEFVEVTKLVTDLTGVHKECCHGDLLECADDRADLAKYICDNQDTISSKLECCDKPLEKSHCIAEV



EKDAIPENLPPLTADFAEDKDVCKNYQEAQDAFLGSFLYEYSRRHPEYAVSVLLRLAKEYEATLEECCAKDDPHACYSTVFDKCLKHLVDEPQNLIKQNCQFEKLGEYGFQNALIVRYTRKVPQVSTPTLVEVSRLGKVGTRCCT



KPESERMPCTEDYLSLILNRLCVLHEKTPVSEKVKCTESLVNRRPCFSALTPDETYVPKAFDEKLFTHADICTLPDTEKQIKKQTALVELLKHKPKATEEQLKTVMENFVAFVDKCCAADDKEACFAVEGPKLVVSTQTALA



Appendix Figure 3.1 c) SCW hydrolysis of untreated BSA at 253⁰C for 20 minutes.

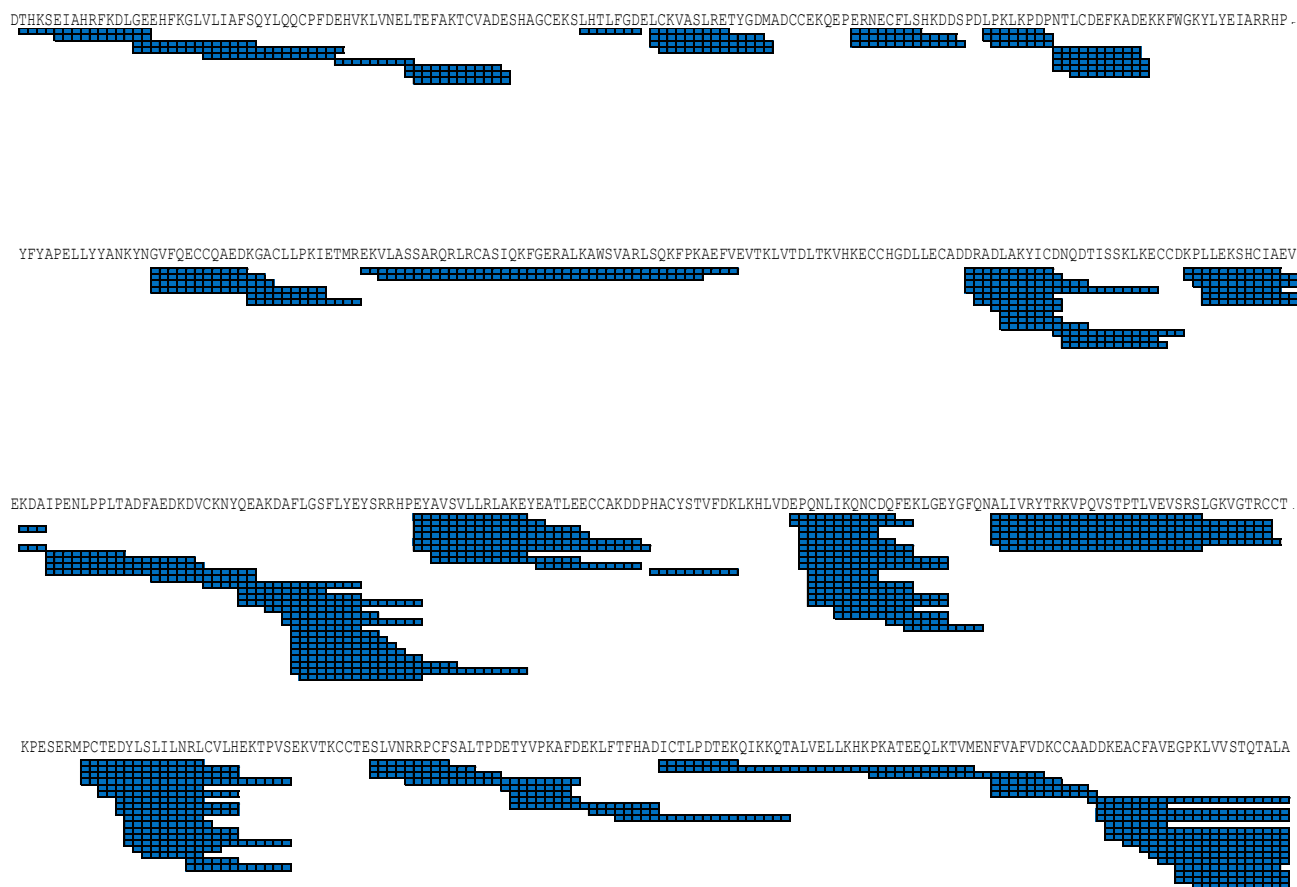
DTHKSEIAHRFKDLGEEHFKGLVLIAFSQYLQCPFDEHVKLVLNELTEFAKTCVADESHAGCEKSLHTLFGDELCKVASLRETYGDMADCEKQEPERNECFLSHKDDSPDLPKLKPDNPNTLCDEFKADEKKFWGKYLYEIARRHP

YFYAPELLYYANKYNGVFQECCQAEDKGACLLPKIETMREKVLASSARQRLRCASIQKFGERALKAWSVARLSQKFPKAEFEVETKLVTDLTKVHKECCHGDLLECADDRADLAKYICDNQDTISSKLECCDKP LLEKSHCIAEV

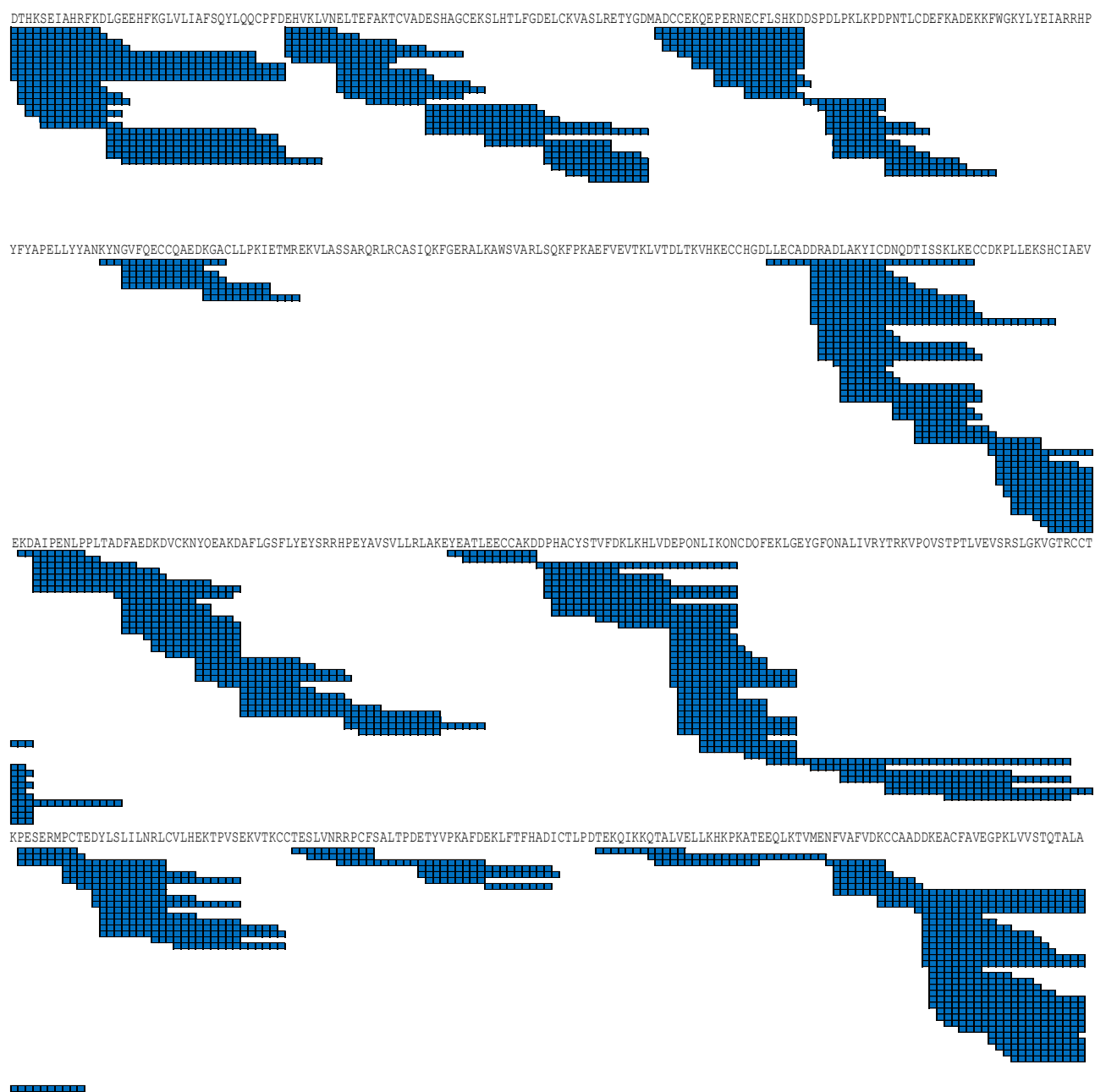
EKDAIPENLPPLTADFAEDKDVCNKYQEAQDAFLGSLYYSRRHPEYAVSVLLRLAKEYEATLECCAKDDPHACYSTVFDKLKHLVDEPQNLIKQNCQFEKLGEYGFQNALIVRYTRKVPQVSTPTLVEVSRSLGKVGTRCCT

KPESERMPC TEDYLSLILNRLCVLHEKTPVSEKVT KCCTESLVNRRPCFSALTPDETYVPKAFDEKLFTFHADICTLPDTEKQIKQTALVELLKHHPKATEEQ LKTVMENFVAFVDKCCAADDKEACFAVEGPKLVVSTQTALA

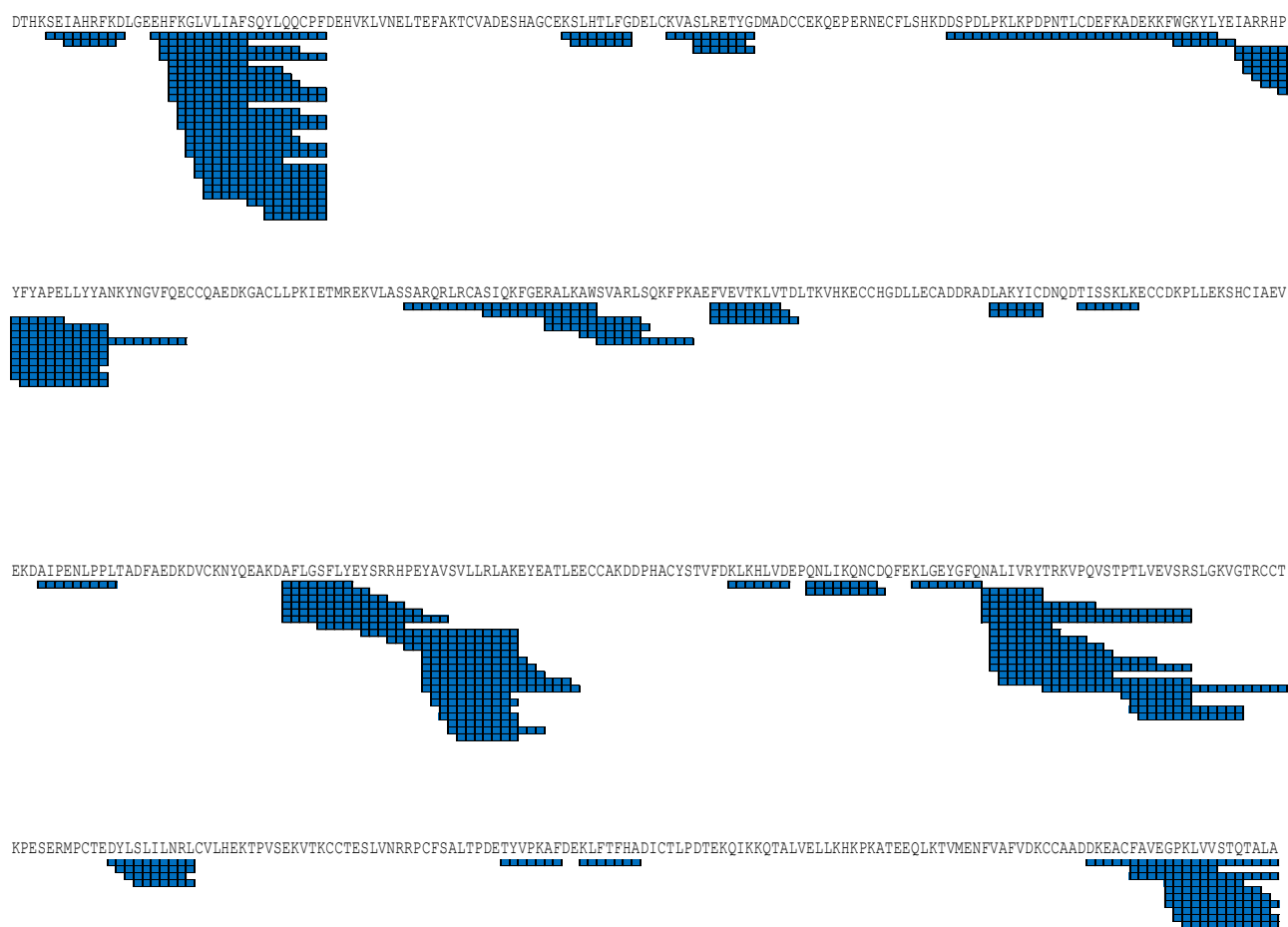
Appendix Figure 3.1 c) SCW hydrolysis of untreated BSA at 300⁰C for 20 minutes.



Appendix Figure 3.1 c) BSA reduction pre- SCW hydrolysis at 160⁰ C for 0 minutes.



Appendix Figure 3.1 c) BSA reduction pre- SCW hydrolysis at 160⁰ C for 20 minutes.



Appendix Figure 3.1 c) BSA reduction pre- SCW hydrolysis at 207⁰C for 20 minutes.

DTHKSEIAHRFKDLGEEHFKGLVLIAFSQYLQQCPFDEHVKLVNELTEFAKTCVADESHAGCEKSLHTLFGDELCKVASLRETYGDMADCEKQEPERNECFLSHKDDSPDLPLKLPDPNTLCDEFKADEKKFWGKYLYEIARRHP

YFYAPELLYYANKYNGVFQECQAEDKGACLLPKIETMREKVLASSARQRLRCASIQKFGERALKAMSVARLSQKFPKAEFVEVTKLVTDLTKEVHKECCHGDLLECADDRADLAKYICDNQDTISSKLKECCDKPLEKSHCIAEV

EKDAIPENLPPLTADFAEDKDVCKNYOEAKDAFLGSFLYEYSRRHPEYAVSVLLRLAKEYEATLEECCAKDDPHACYSTVFDKHLVDEPONLIKONCDOFEKLGEYGFONALIVRYTRKVPVSTPTLVEVSRSLGKVGTRCCT

KPESERMPCTEDYLSLIINRLCVLHEKTPVSEKVTCKCTESLVNRRPCFSALTPDETYVPKAFDEKLFTHADICTLPDTEKQIKQTALVELLKHKKPKATEEQIKTMENFVAFVDKCCAADDKEACFAVEGPKLVVSTQTALA

Appendix Figure 3.1 c) BSA reduction pre- SCW hydrolysis at 253⁰C for 20 minutes.

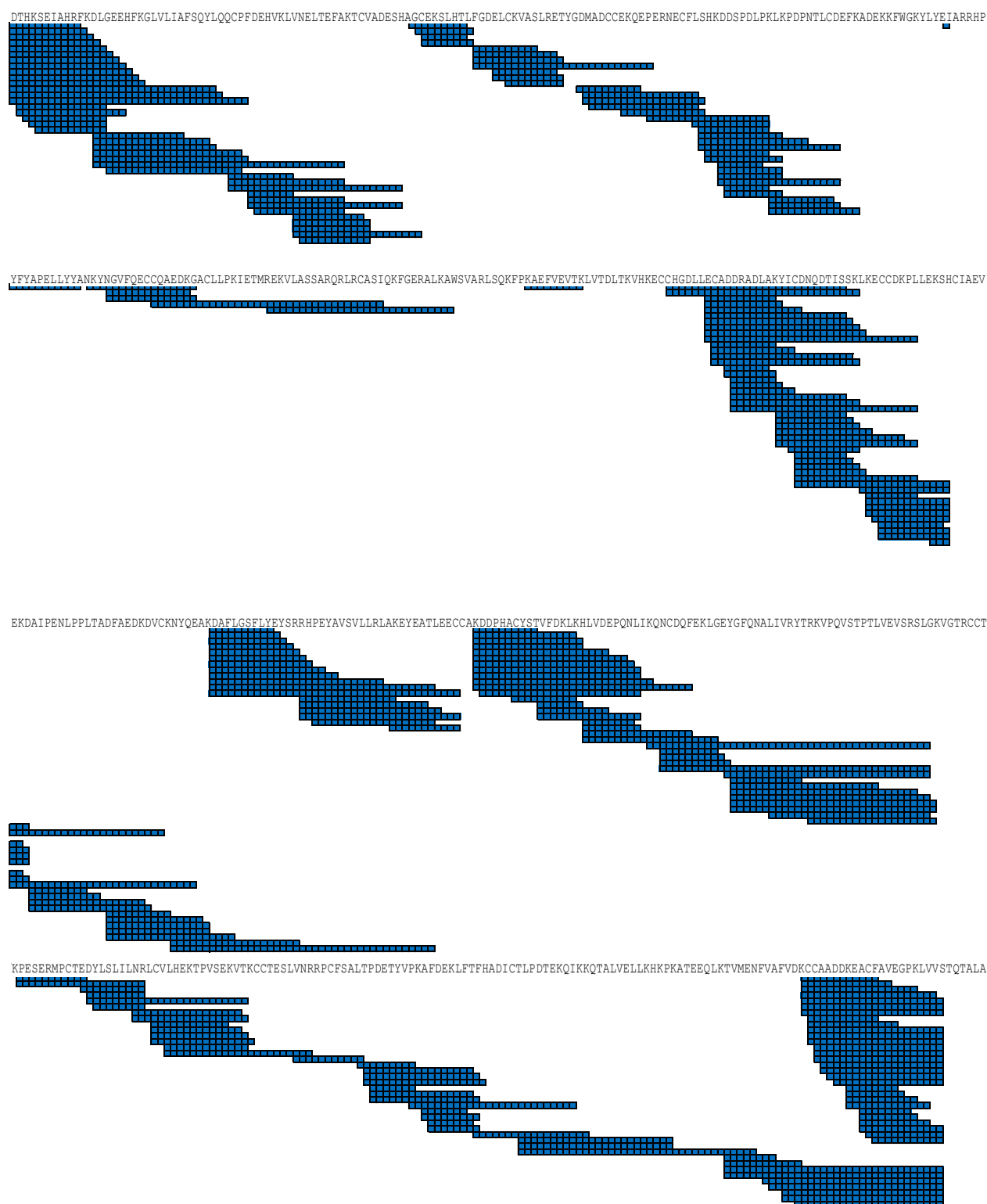
DTHKSEIAHRFKDLGEEHFKGLVLIAFSQYLQCPFDEHVKLVNELTEFAKTCVADESHAGCEKSLHTLFGDELCKVASLRETYGDMADCEKQEPERNECFLSHKDDSPDLPKLKPDNPNTLCDEFKADEKKFWGKYLVEIARRHP

YFYAPELLYYANKYNGVFQECQQAEDKGACLLPKIETMREKVLASSARQLRCASIQKFGERALKAWSVARLSQKFFKAEFVEVTKLVTDLTQVHKECCHGDLLECADDRADLAKYICDNQDTISSKLECCDKPILLEKSHCIAEV

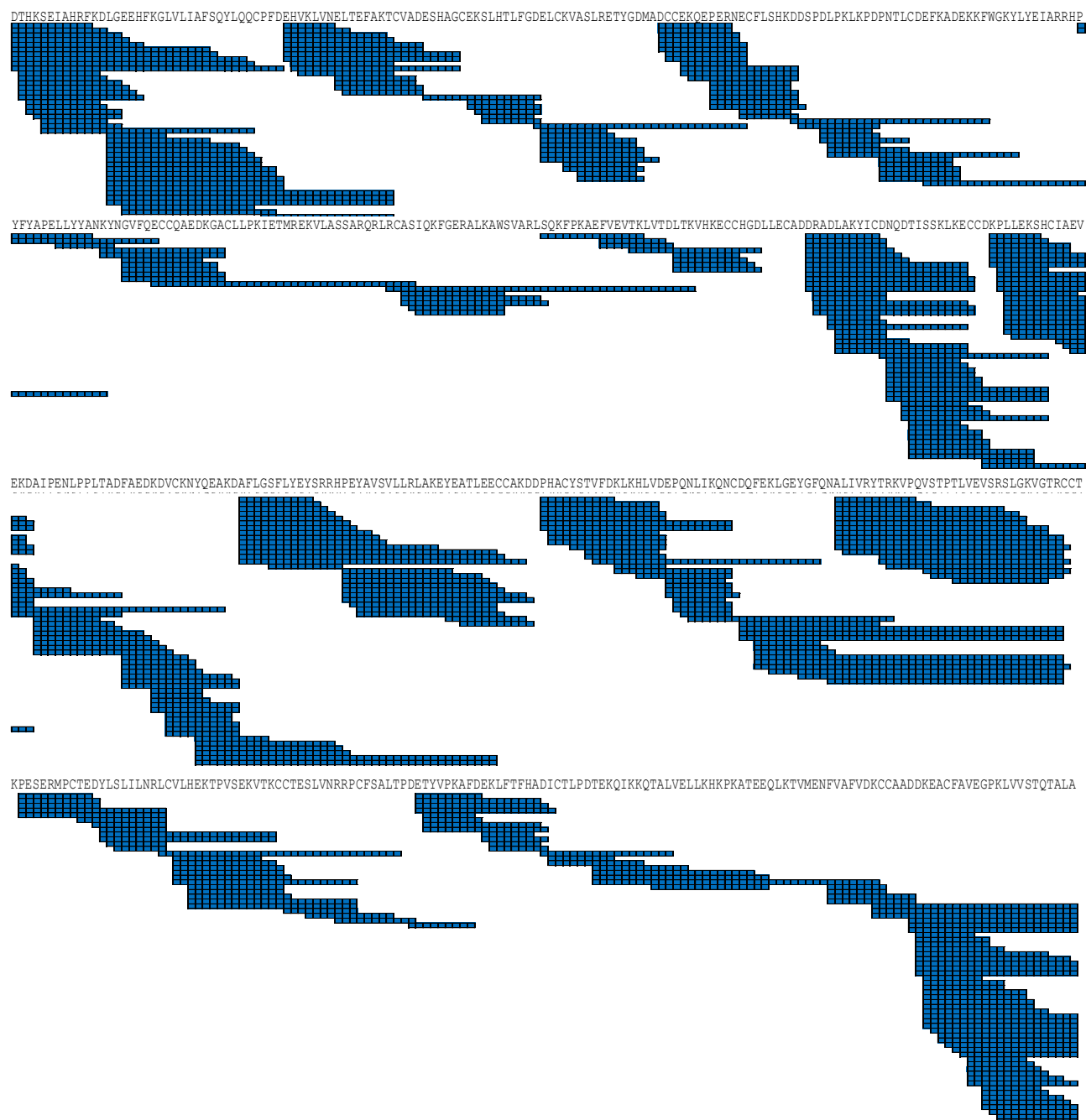
EKDAIPENLPPLTADFAEDKDVCNKYQEAQDAFLGSFLYEYSRRHPEYAVSVLLRLAKEYEATLEECCAKDDPHACYSTVFDKCLKHLVDEPQNLIKQNCQDFEKLGEYGFQNALIVRYTRKVPQVSTPTLVEVSRLGKVGTRCCT

KPESERMPCTEDYLSLIILNRLCVLHEKTPVSEKVKCCTESLVNRRPCFSALTPDETYVPKAFDEKLFTFHADICTLPDTEKQIKKQTAELVELLKHKPKATEEQKKTVMENFVAFVDKCCAADDKEACFAVEGPKLVVSTQTALA

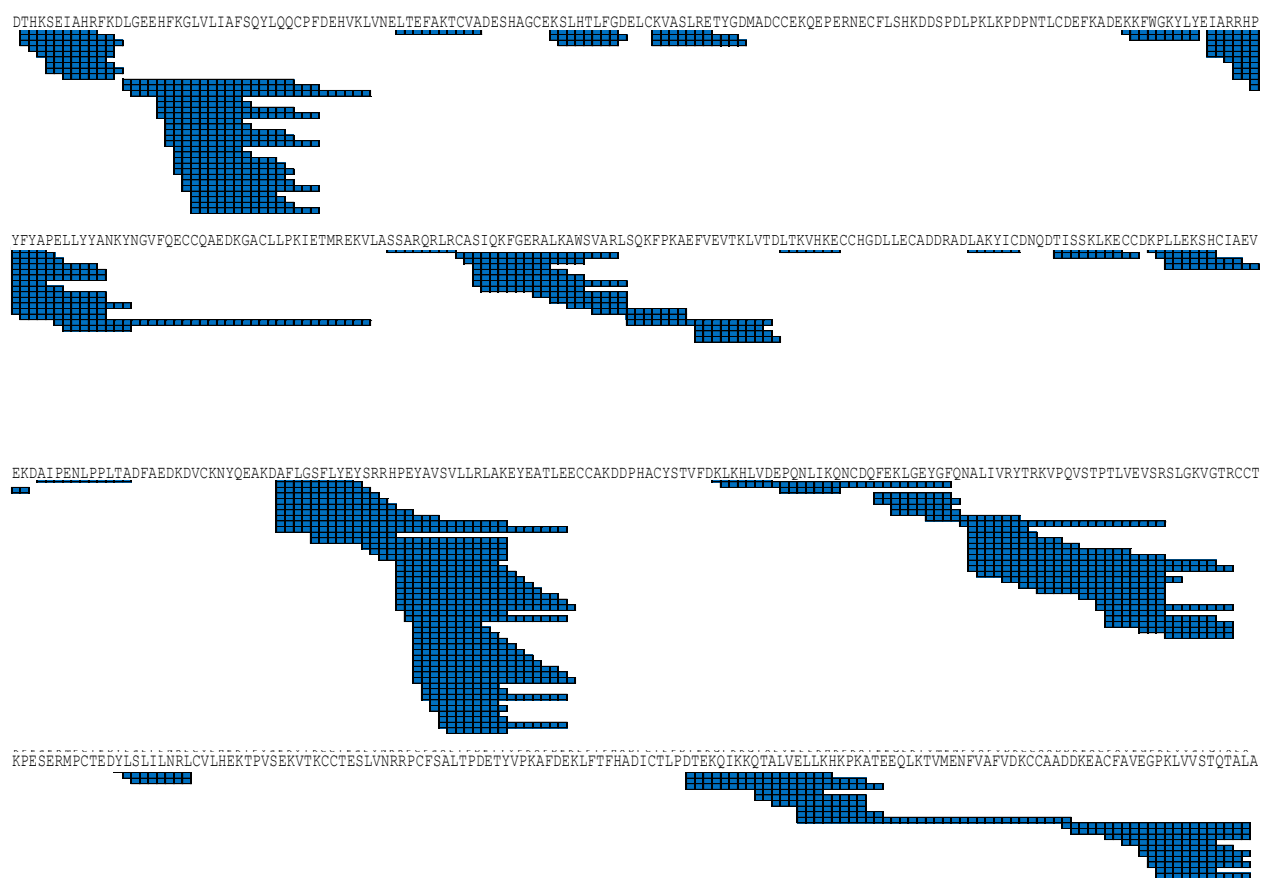
Appendix Figure 3.1 c) BSA reduction pre- SCW hydrolysis at 300⁰C for 20 minutes.



Appendix Figure 3.1 c) BSA reduction post- SCW hydrolysis at 160⁰C for 0 minutes.



Appendix Figure 3.1 c) BSA reduction post- SCW hydrolysis at 160⁰C for 20 minutes.



Appendix Figure 3.1 c) BSA reduction post- SCW hydrolysis at 207⁰C for 20 minutes.

DTHKSEIAHRFKDLGEEHFKGLVLIAFSQYLQQCPFDEHVKLVLNELTEFAKTCVADESHAGCEKSLHTLFGDELCKVASLRETYGDMADCEKQEPERNECFLSHKDDSPDLFKLPDPNTLCDEFKADEKFKFWGKYLEIARRHP

YFYAPELLYYANKYNGVFQEQCAEDKGACLLPKIETMREKVLASSARQRLRCASIQKFGERALKAWSVARLSQKFPKAEFVEVTKLVTDLTQVHKECCHGDLLECADDRADLAKYICDNQDTISSKLECCDKPLLEKSHCIAEV

EKDAIPENLPPLTADFAEDKDVCKNYQEAKDAFLGSFLYEYSRRHPYAVSVLLRLAKEYEATLEECCAKDDPHACYSTVFDKHLVDEPNLIKQNCDFEKLGEYGFQNALIVRYTRKVPQVSTPTLVEVSRLGKVGTRCCT

KPESERMPC TEDYLSLILNRLCVLHEKTPVSEKVKCTESLVNRRPCFSALTPDETYVPKAFDEKLFTFHADICTLPDTEKQIKKQ TALVELLKHKPKATEEQLKTVMENFVAFVDKCAADKKEACFAVEGPKLVVSTQTALA

Appendix Figure 3.1 c) BSA reduction post- SCW hydrolysis at 253⁰C for 20 minutes.

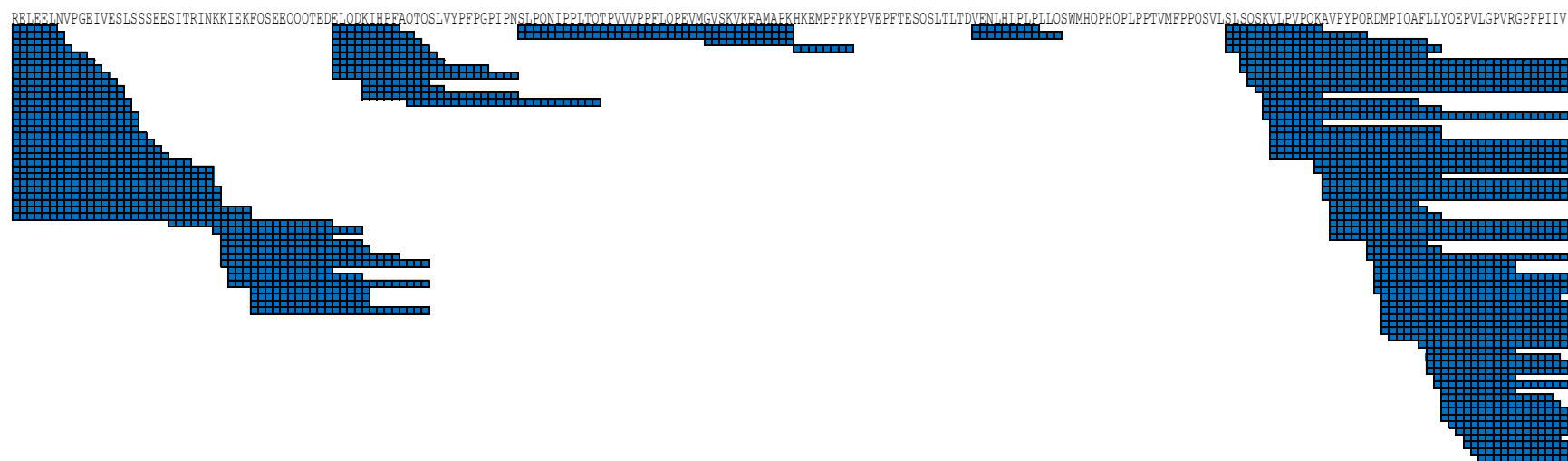
DTHKSEIAHRFKDLGEEHFKGLVLIAFSQYLQQCPFDEHVKLVNELTEFAKTCVADESHAGCEKSLHTLFGDELCKVASLRETYGDMADCEKQEPERNECFLSHKDDSPDLPKLKPDNPNTLCDEFKADEKKFWGKYLVEIARRHP

YFYAPELLYYANKYNGVFQECQQAEDKGACLLPKIETMREKVLASSARQRLRCASIQKFGERALKAWSVARLSQKFPKAEFVEVTKLVTDLTQVHKECCHGDLLECADDRADLAKYICDNQDTISSKLECCDKPILLEKSHCIAEV

EKDAIPENLPPLTADFAEDKDVCKNYOEAKDAFLGSFLYEYSRRHPEYAVSVLLRLAKEYEATLEECCAADDPHACYSTVFDKLLKHLVDEPONLIKONCDQFEKLGEYGFONALIVRYTRKVPPOVSTPTLVEVSRLGKVGTRCCT

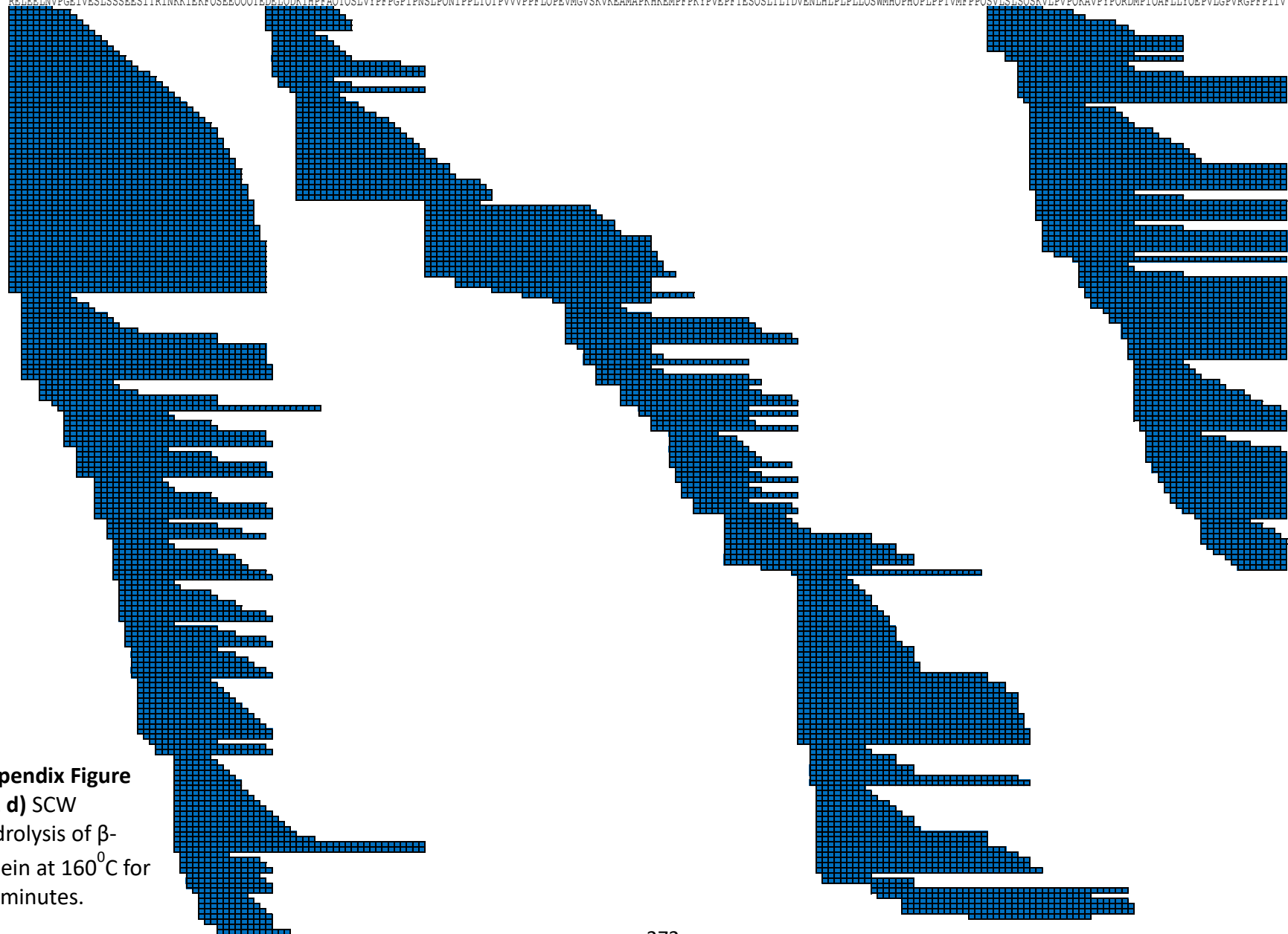
KPESERMPCTEDYLSLIILNRLCVLHEKTPVSEKVTKCCTESLVNRRPCFSALTPDETYVPKAFDEKLTFFHADICTLPDTEKQIKKQ TALVELLKHKPKATEEQKKTVMENFVAFVDKCCAADDKEACFAVEGPKLVVSTQTALA

Appendix Figure 3.1 c) BSA reduction post- SCW hydrolysis at 300⁰C for 20 minutes.



Appendix Figure 3.1 d) SCW hydrolysis of β - casein at 160⁰C for 0 minutes.

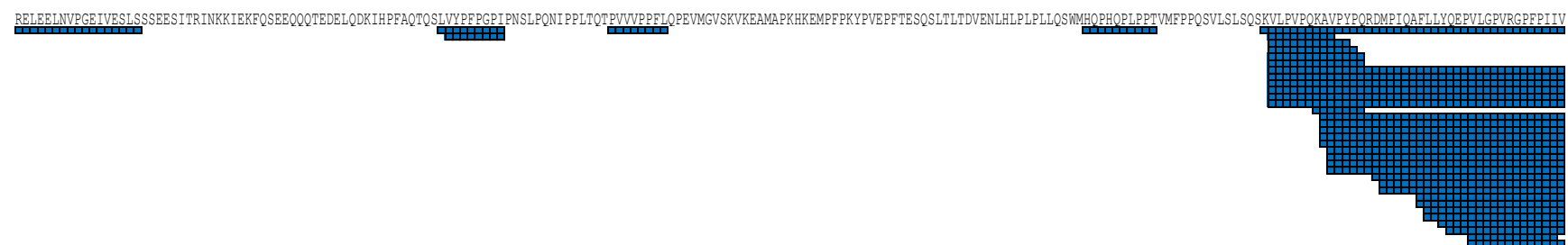
RELEEINVPGEIVESLSSEESITRINKIEKFOSEEOOTEDELQDKIHFFAOTOSLVYFFPGPIPNLTONIPPLTOTPVVVVPPFLOPEVMGVSKVKEAMAPKHKEMPFPKYPVEPTTESOSITLTDVENLHLPLLOSWMHOPHPLPPTVMFPPOSVLSLSOSKVLFPVPOKAVPYVORDMPIOAFLLYOEVLGPVRGPFPIIV



Appendix Figure 3.1 d) SCW hydrolysis of β -casein at 160°C for 20 minutes.



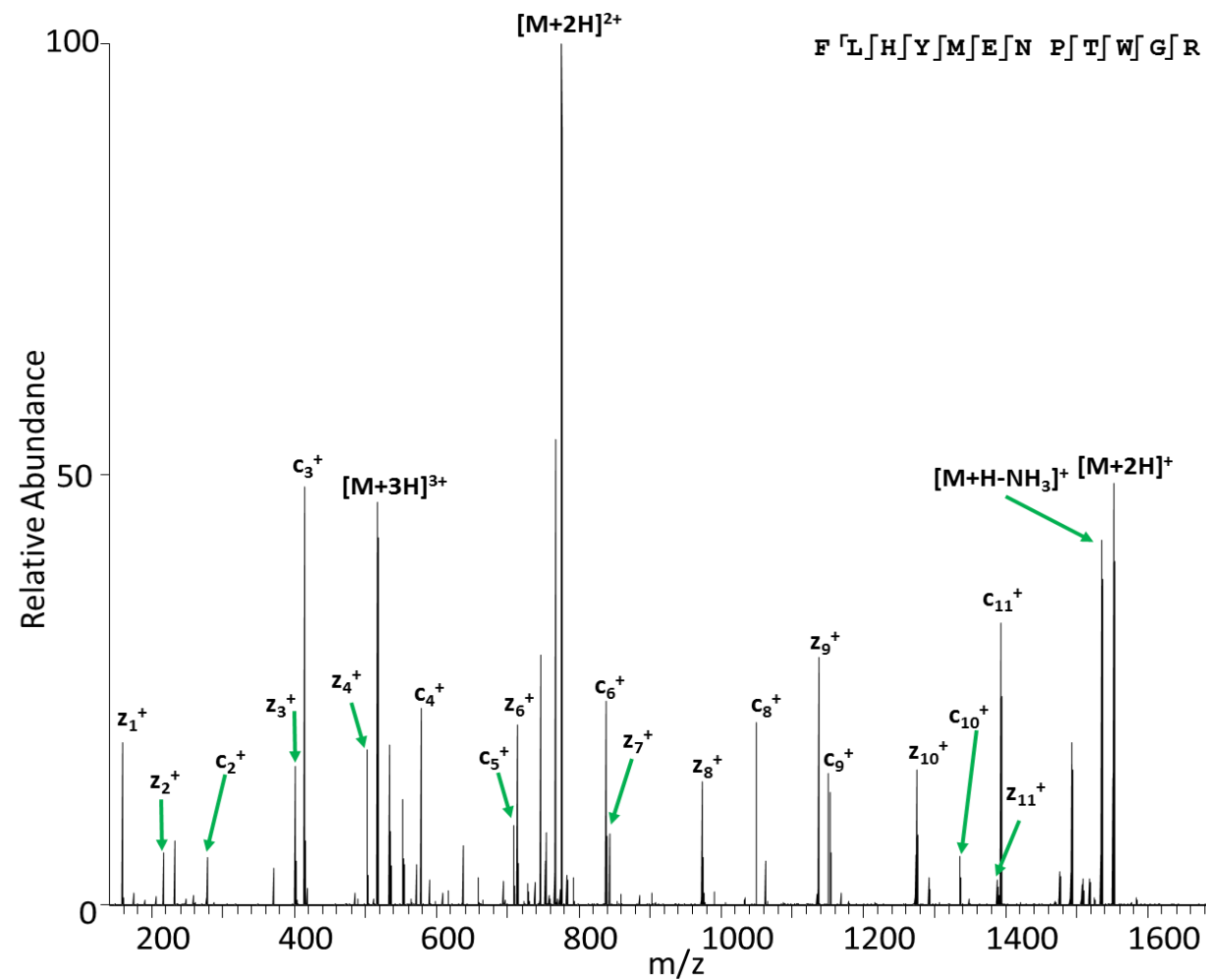
Appendix Figure 3.1 d) SCW hydrolysis of β -casein at 207°C for 20 minutes.



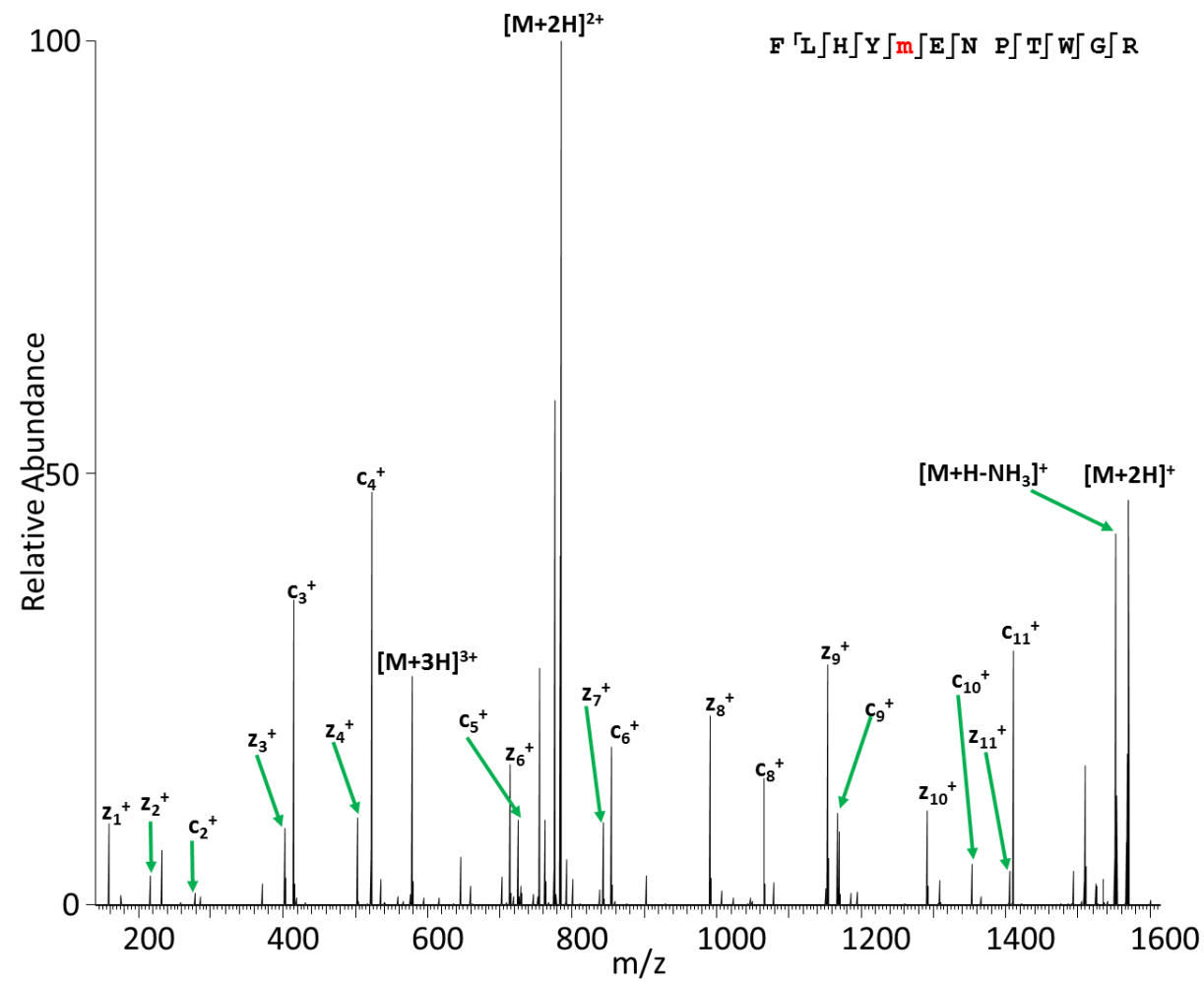
Appendix Figure 3.1 d) SCW hydrolysis of β - casein at 253⁰C for 20 minutes.

RELEELNVPGEIVESLSSEESI TRINKKIEKFOSEE OOTELODKIH PFAOTOSLVYFFPGPI P NSLPONIPPLTOTPVVPPFLOPEVMGVSKVKEAMAPKHKEMPPPKYPVEPFTESOSLTITDVENLHLPPLLOSWMHOPHOPLPPTVMFPPOSVLSLSOSKVLFPVPOKAVPY PORDMPIOAFLLYOEPVLGPVRGPPPIIV

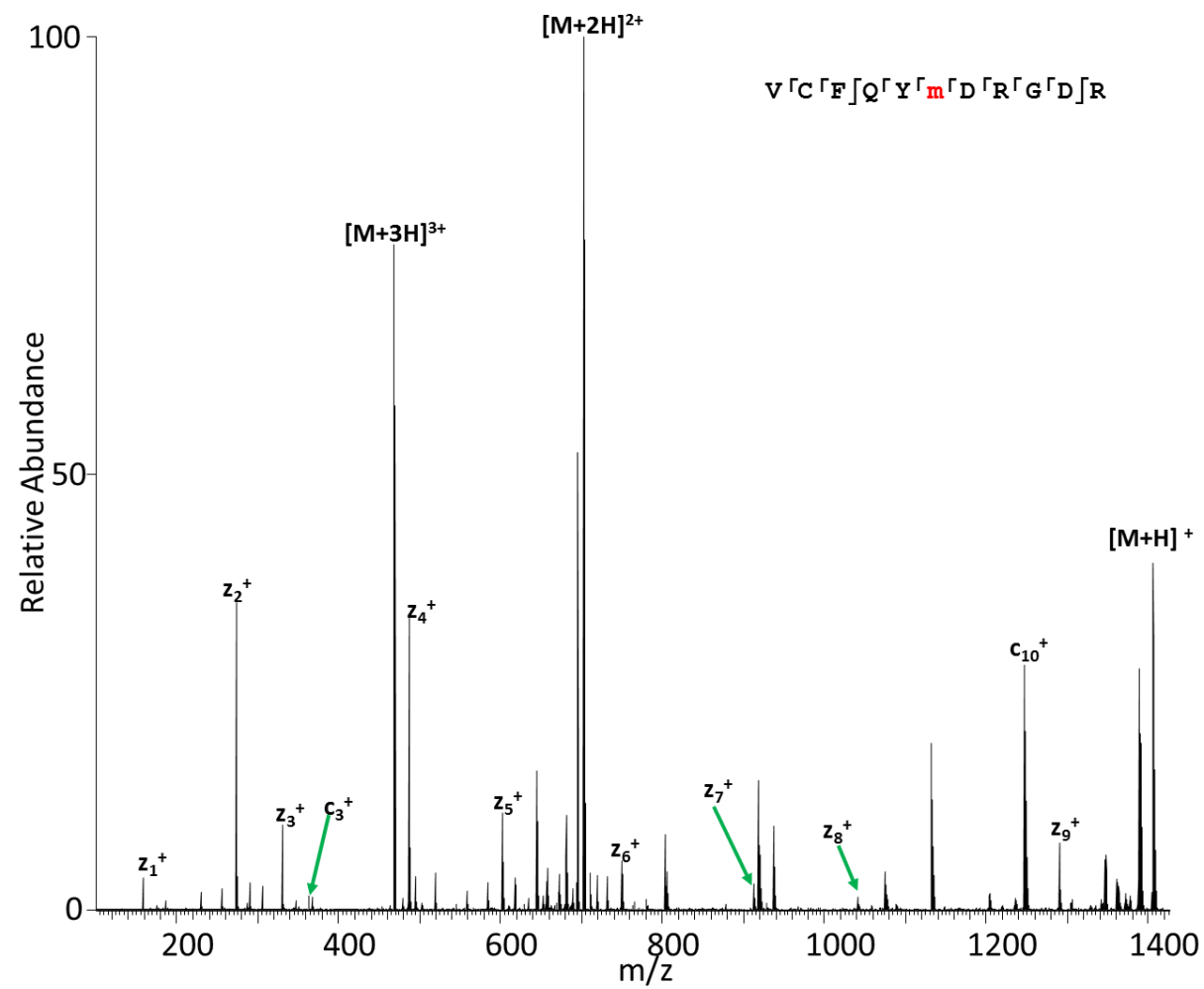
Appendix Figure 3.1 d) SCW hydrolysis of β - casein at 300⁰C for 20 minutes.



Appendix Figure 4. 1 - ETD MS/MS spectrum of 4+ ions of [VQSIKADFLHYENPTWGR +O].

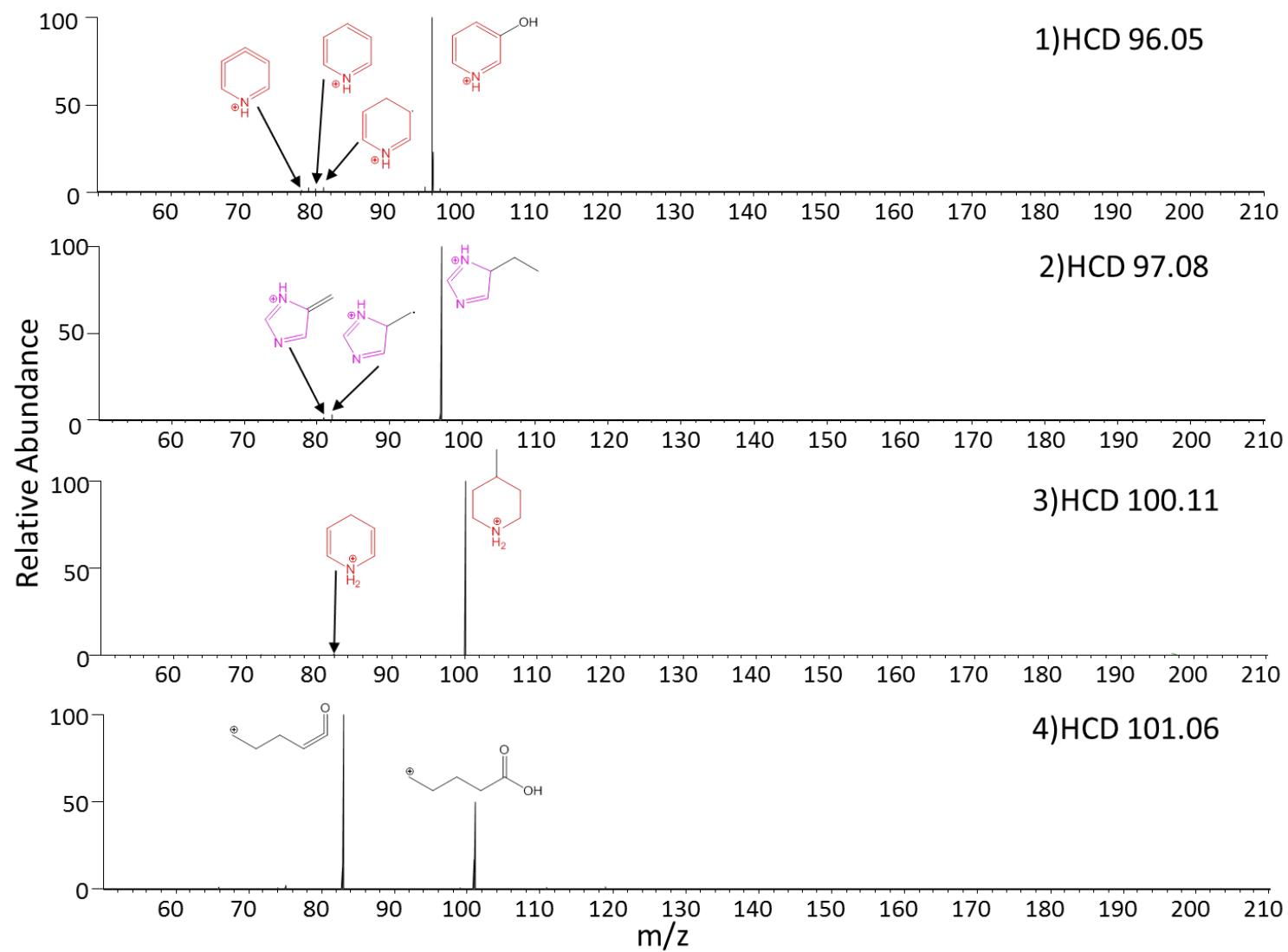


Appendix Figure 4. 2 - ETD MS/MS spectrum of 4+ ions of [VQSIKADFLHYENPTWGR +O]

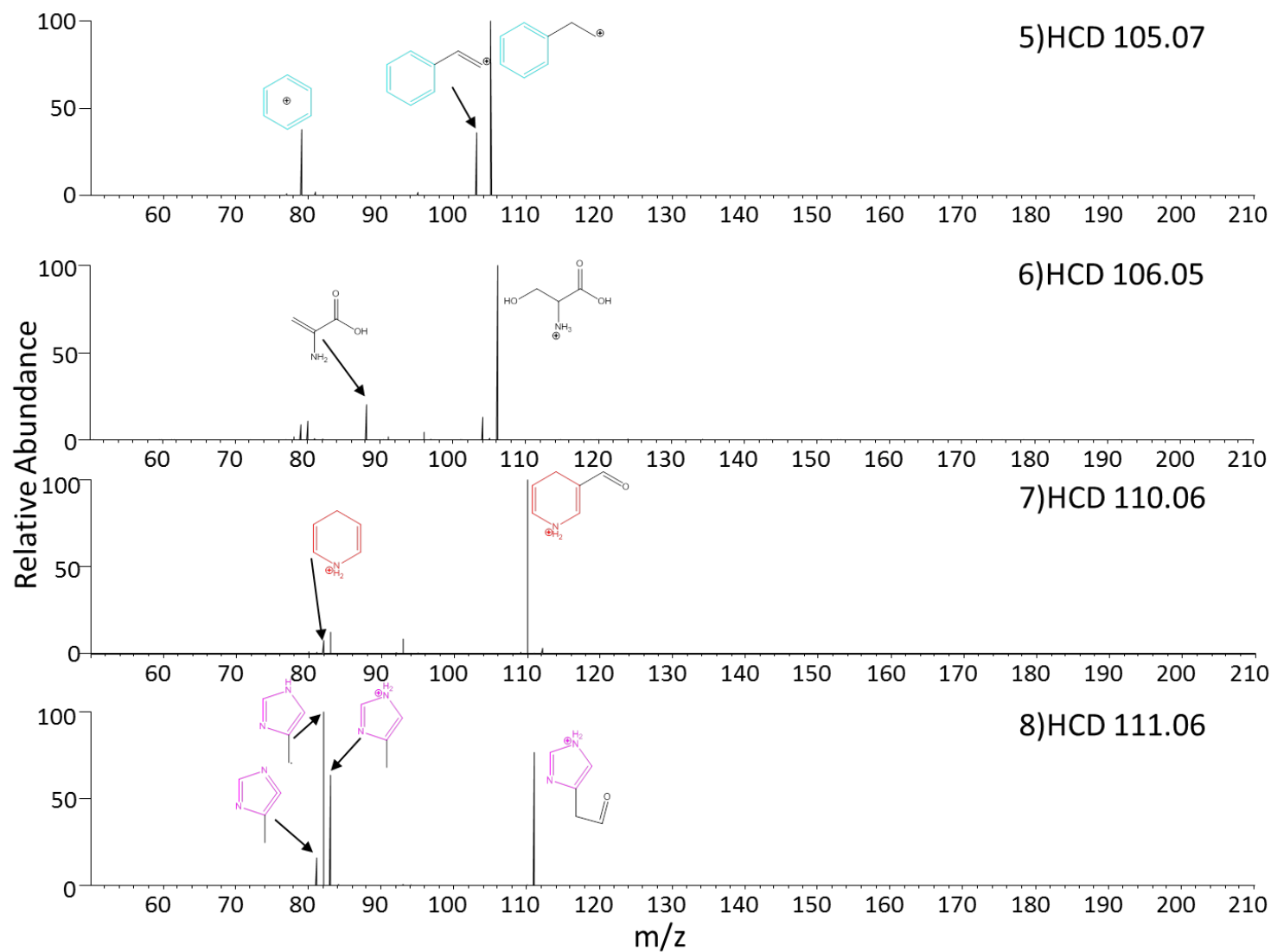


Appendix Figure 4. 3 - ETD MS/MS spectrum of 3+ ions of [VCFQYMDRGDR +O]

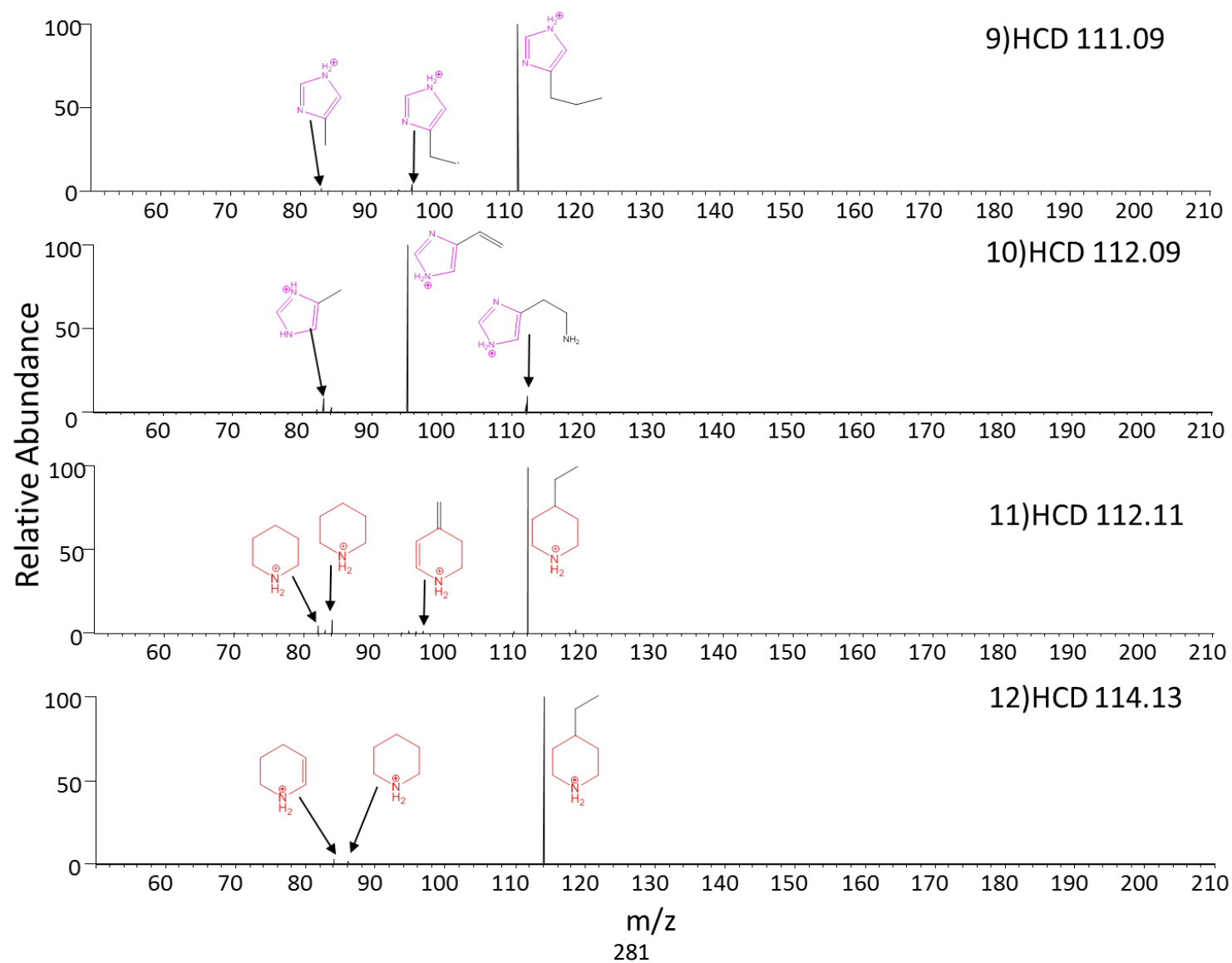
Appendix Figures 5.1 - 5.4.



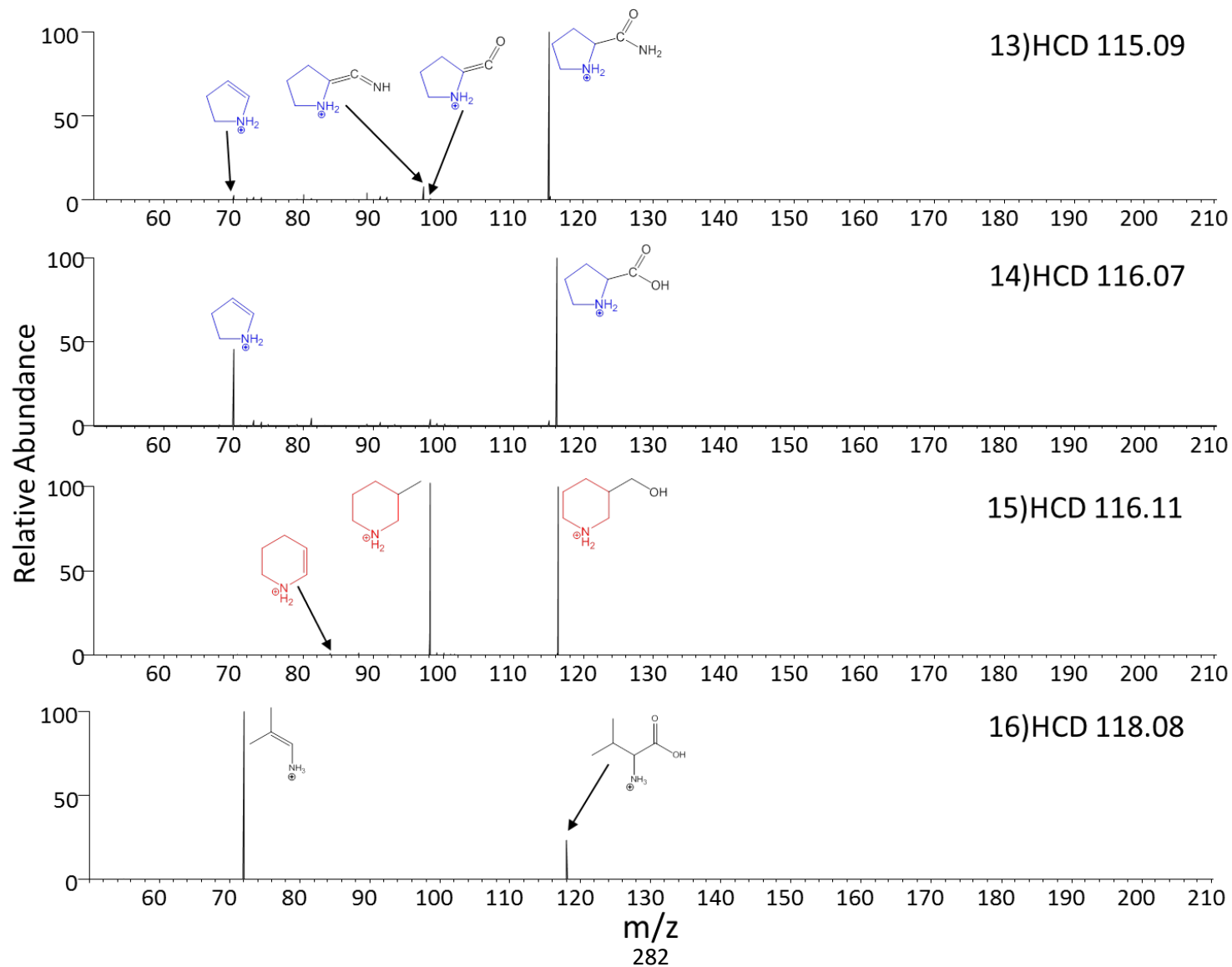
Appendix Figures 5.5 - 5.8.



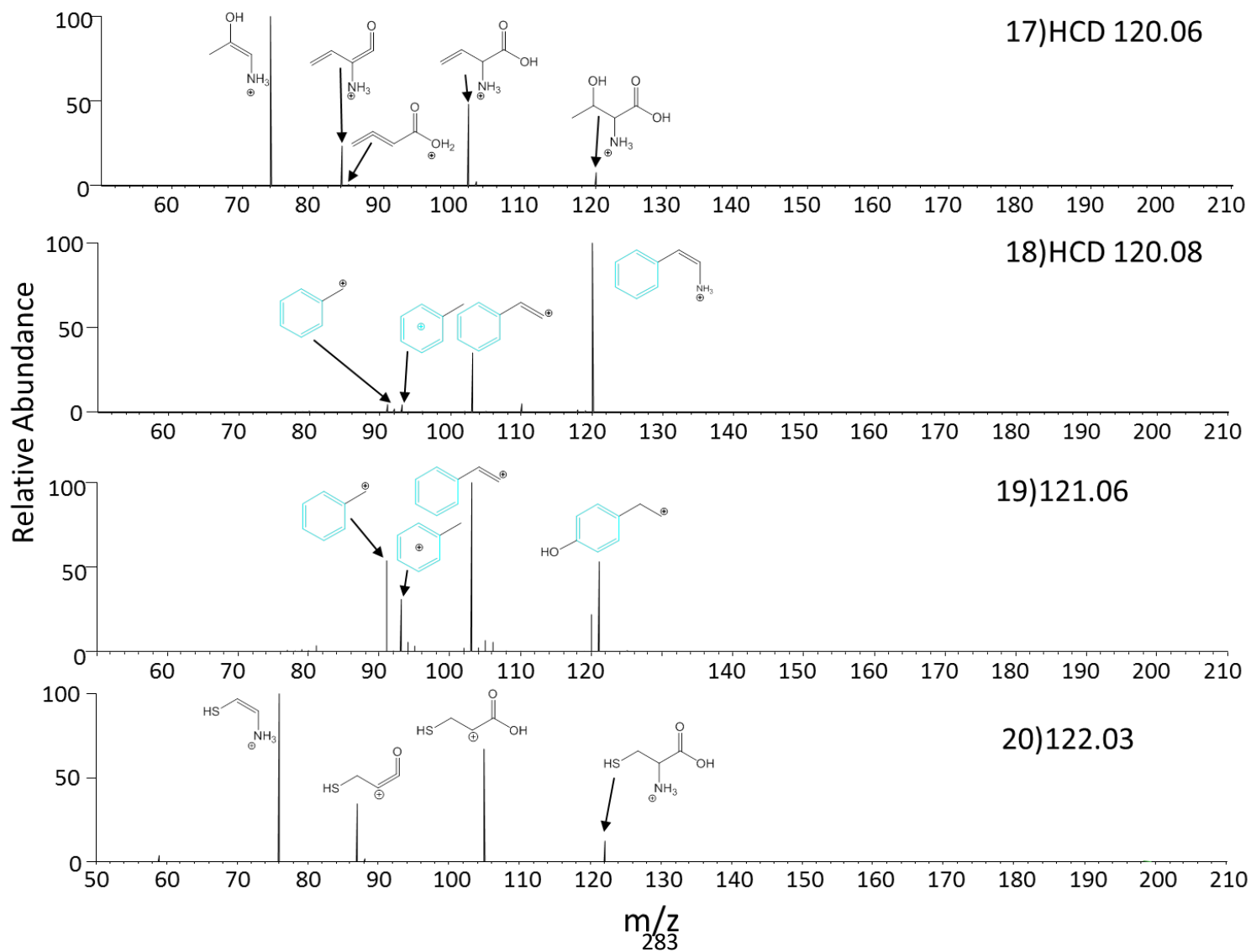
Appendix Figures 5.9 - 5.12.



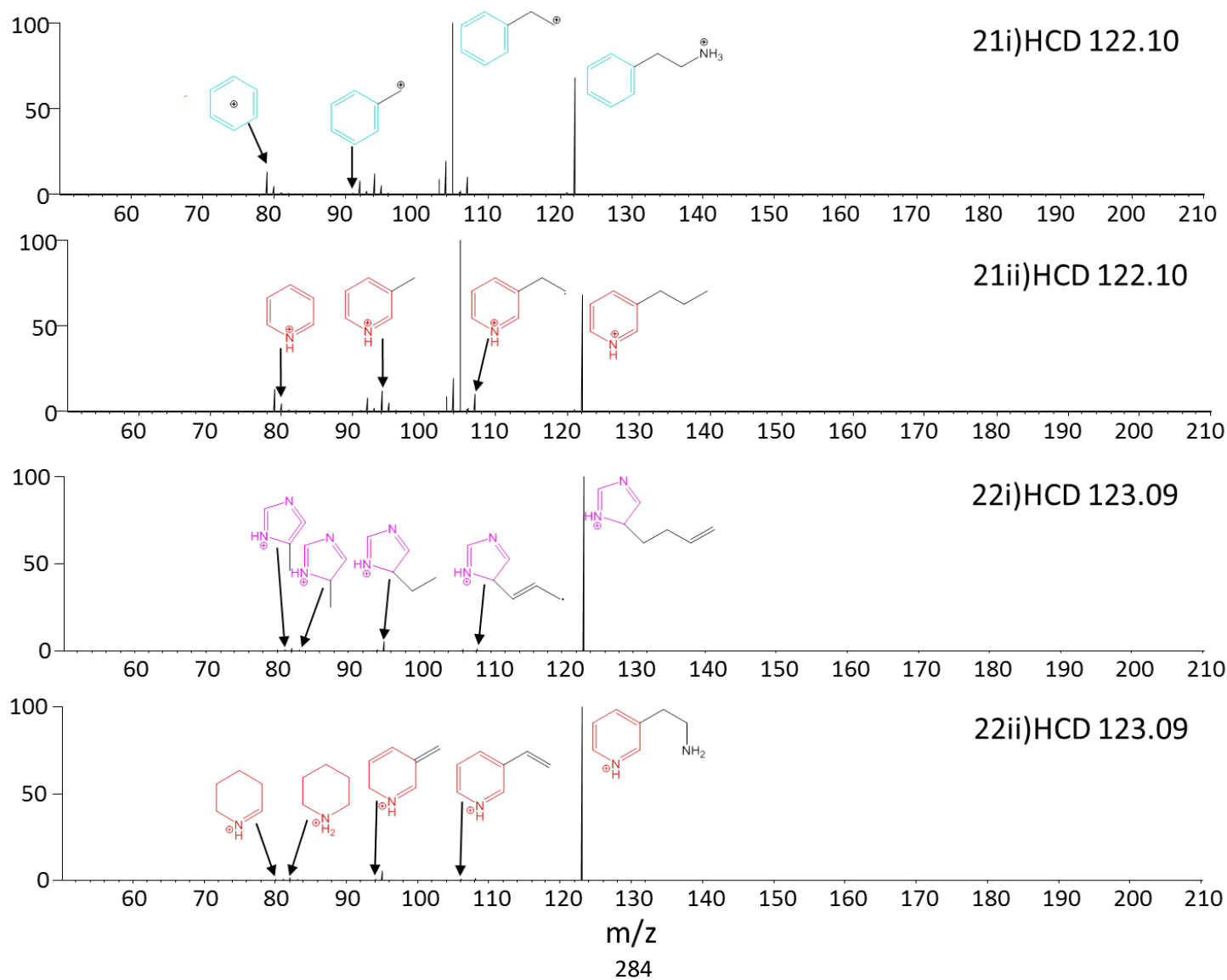
Appendix Figures 5.13 - 5.16.



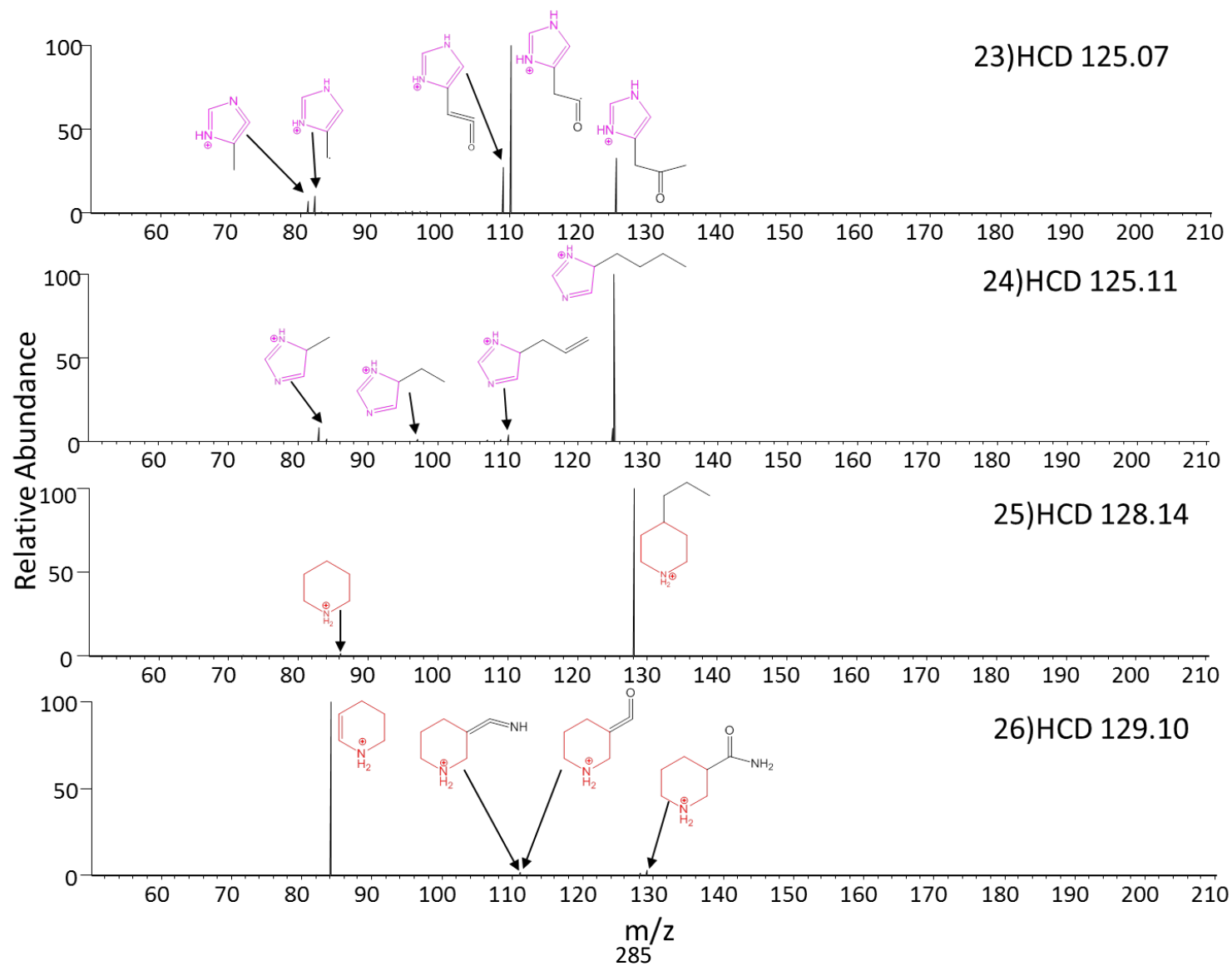
Appendix Figures 5.17 - 5.20.



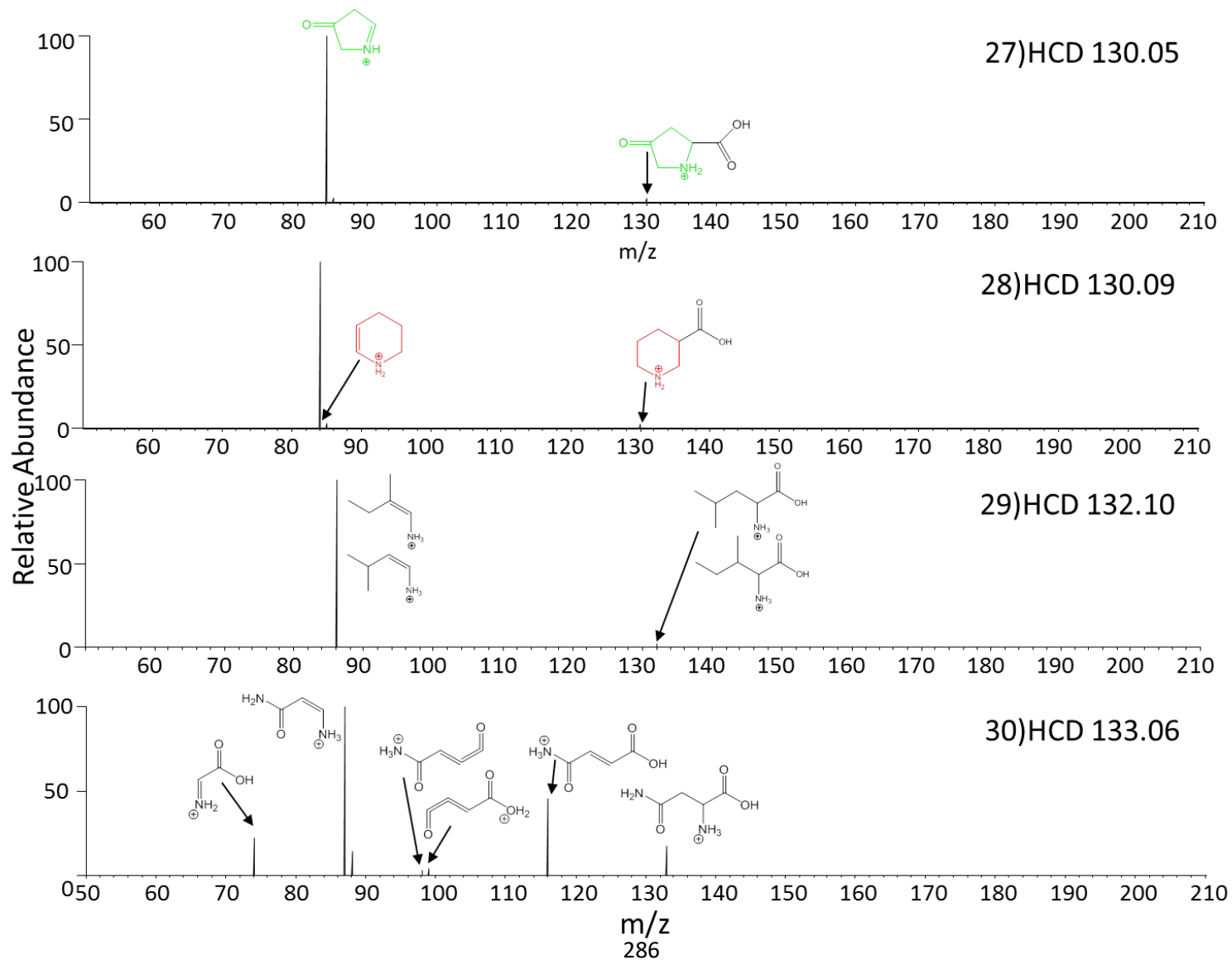
Appendix Figures 5.21 - 5.22.



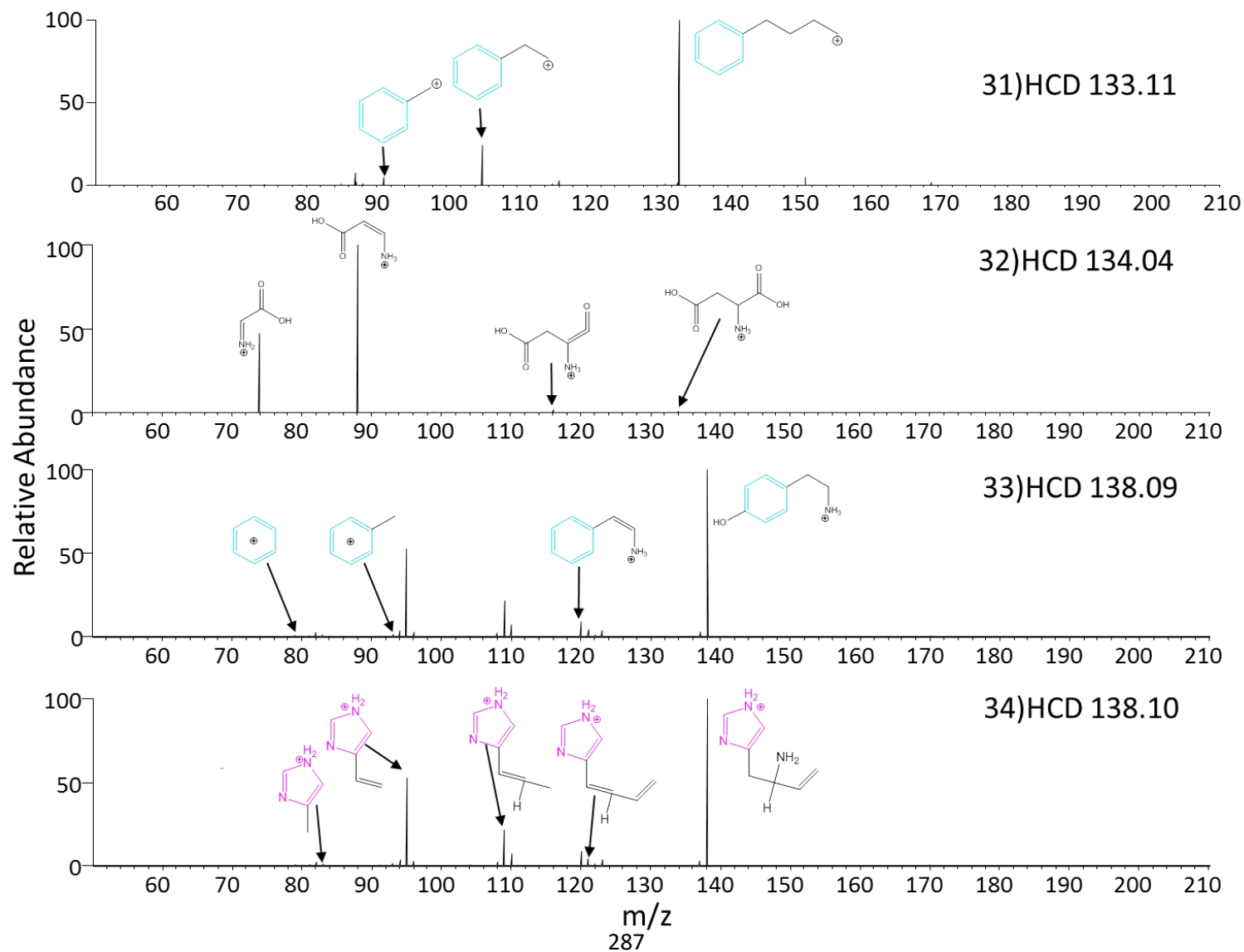
Appendix Figures 5.23 - 5.26.



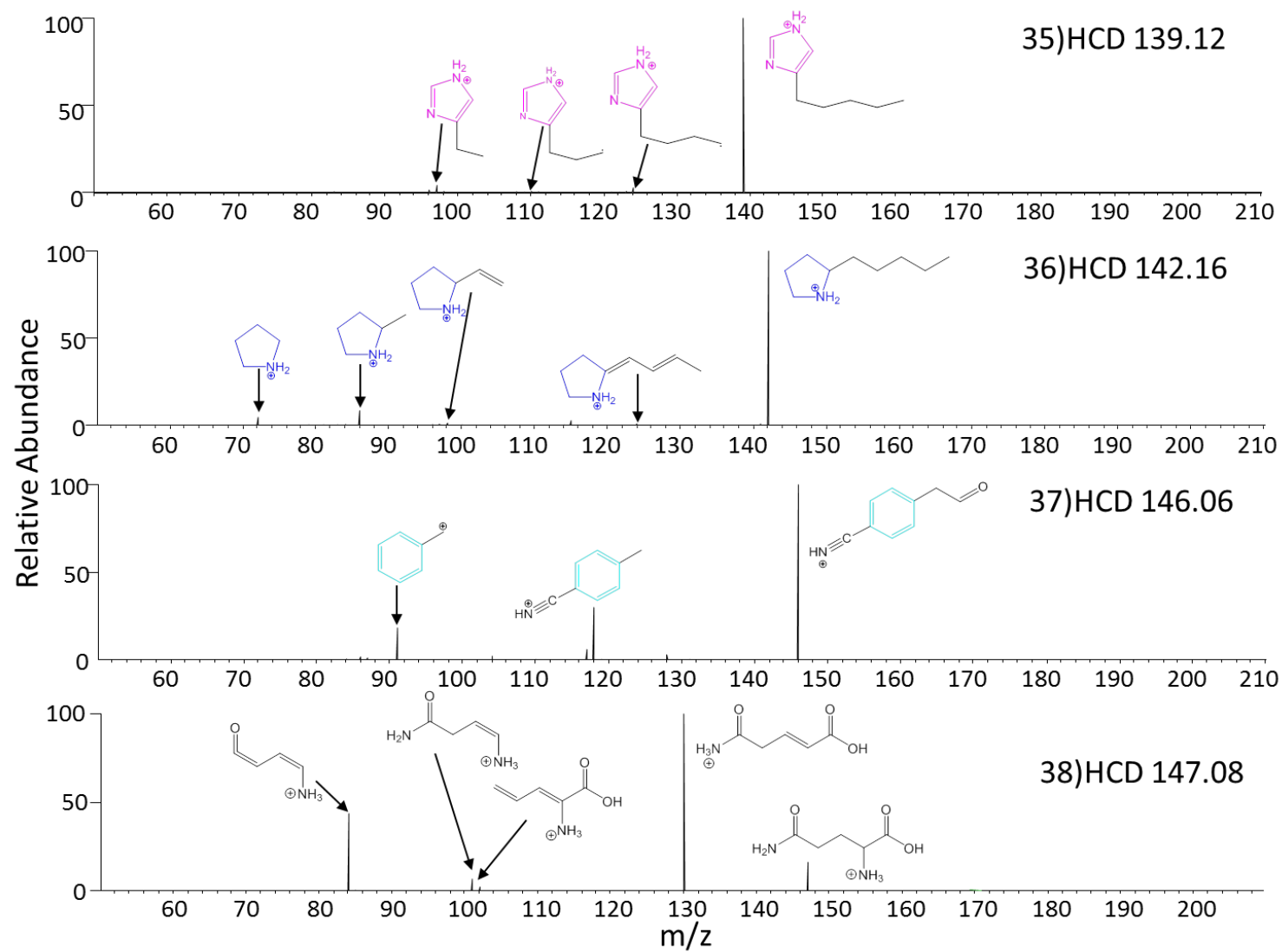
Appendix Figures 5.27 - 5.30.



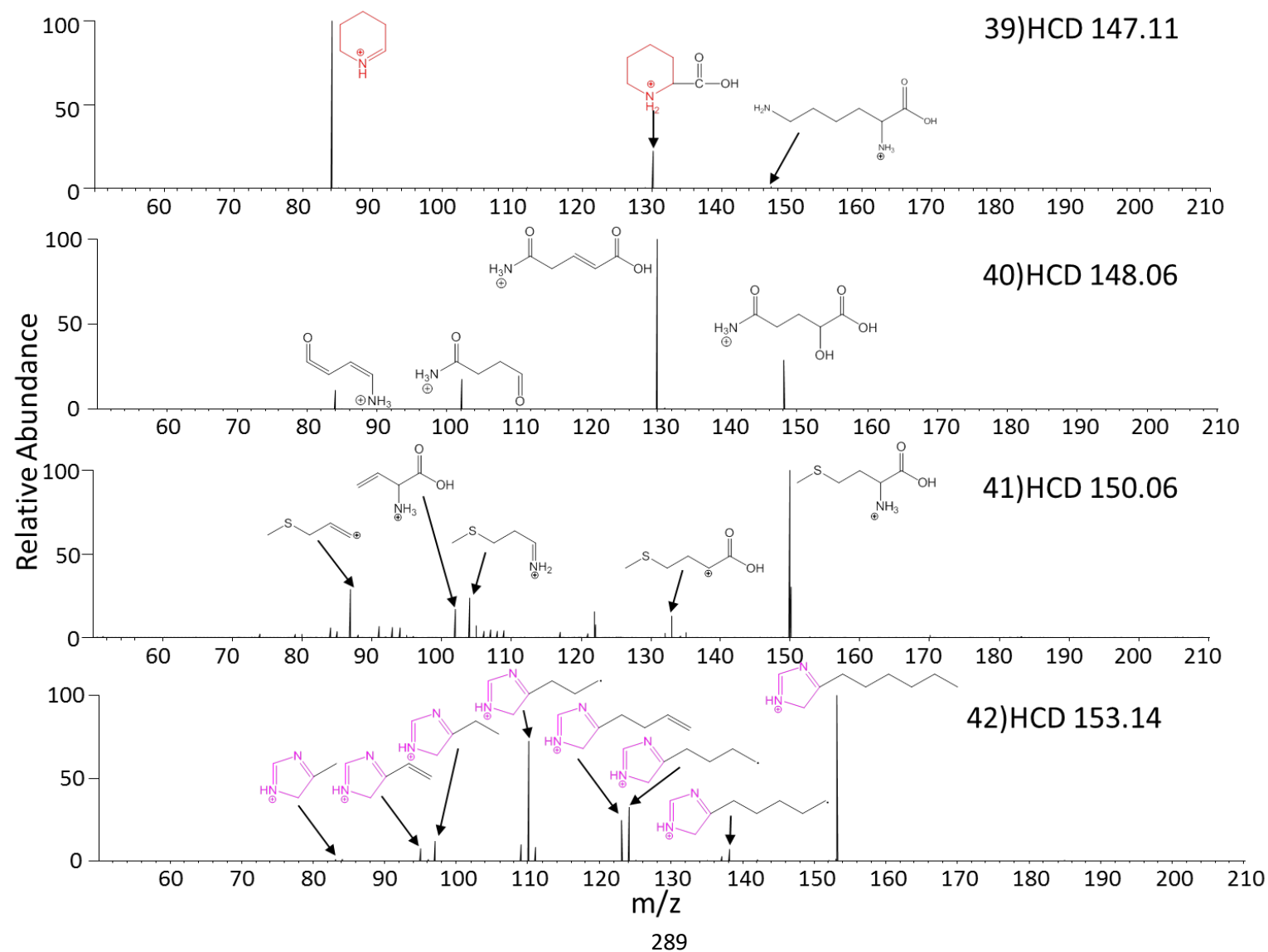
Appendix Figures 5.31 - 5.34.



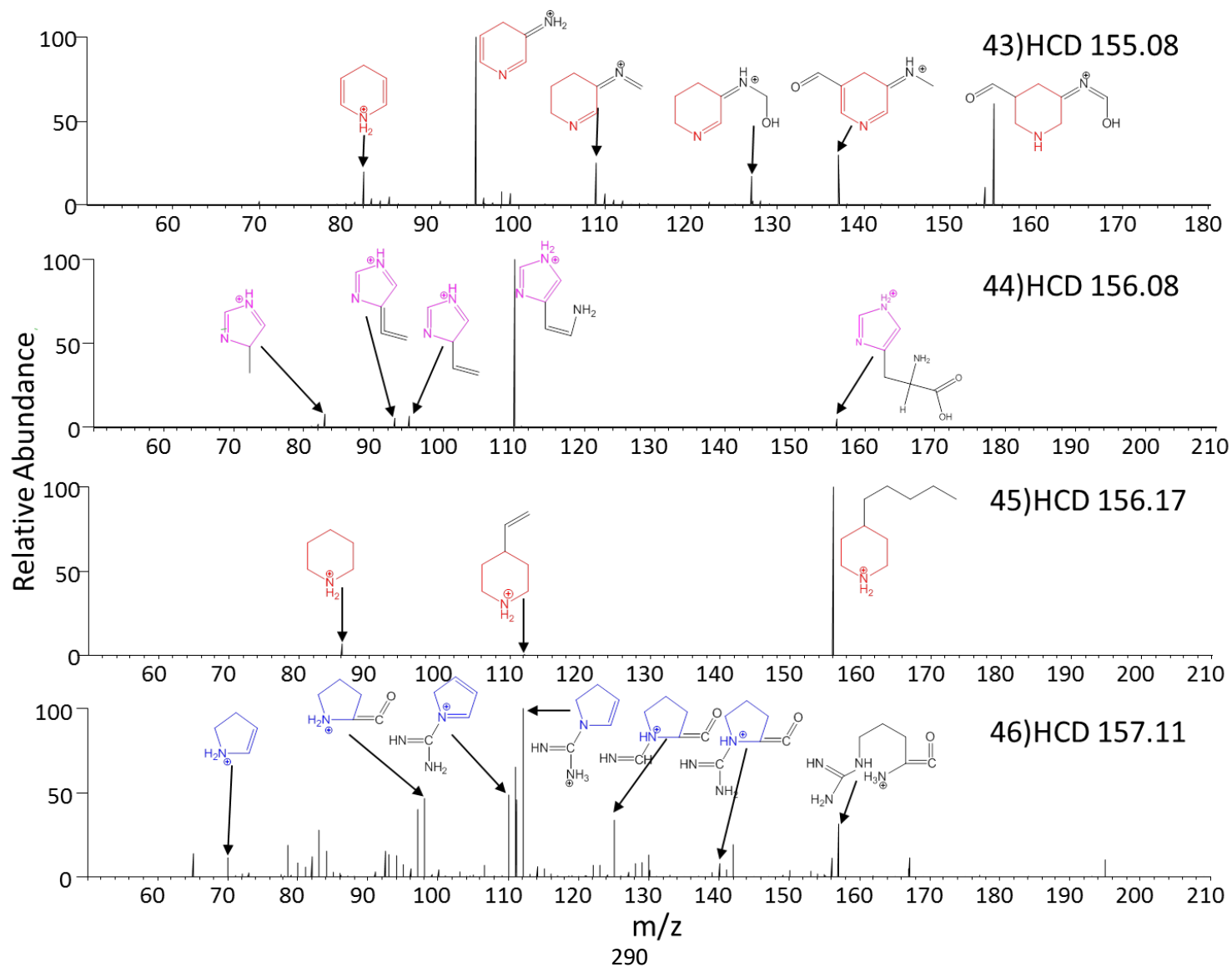
Appendix Figures 5.35 - 5.38.



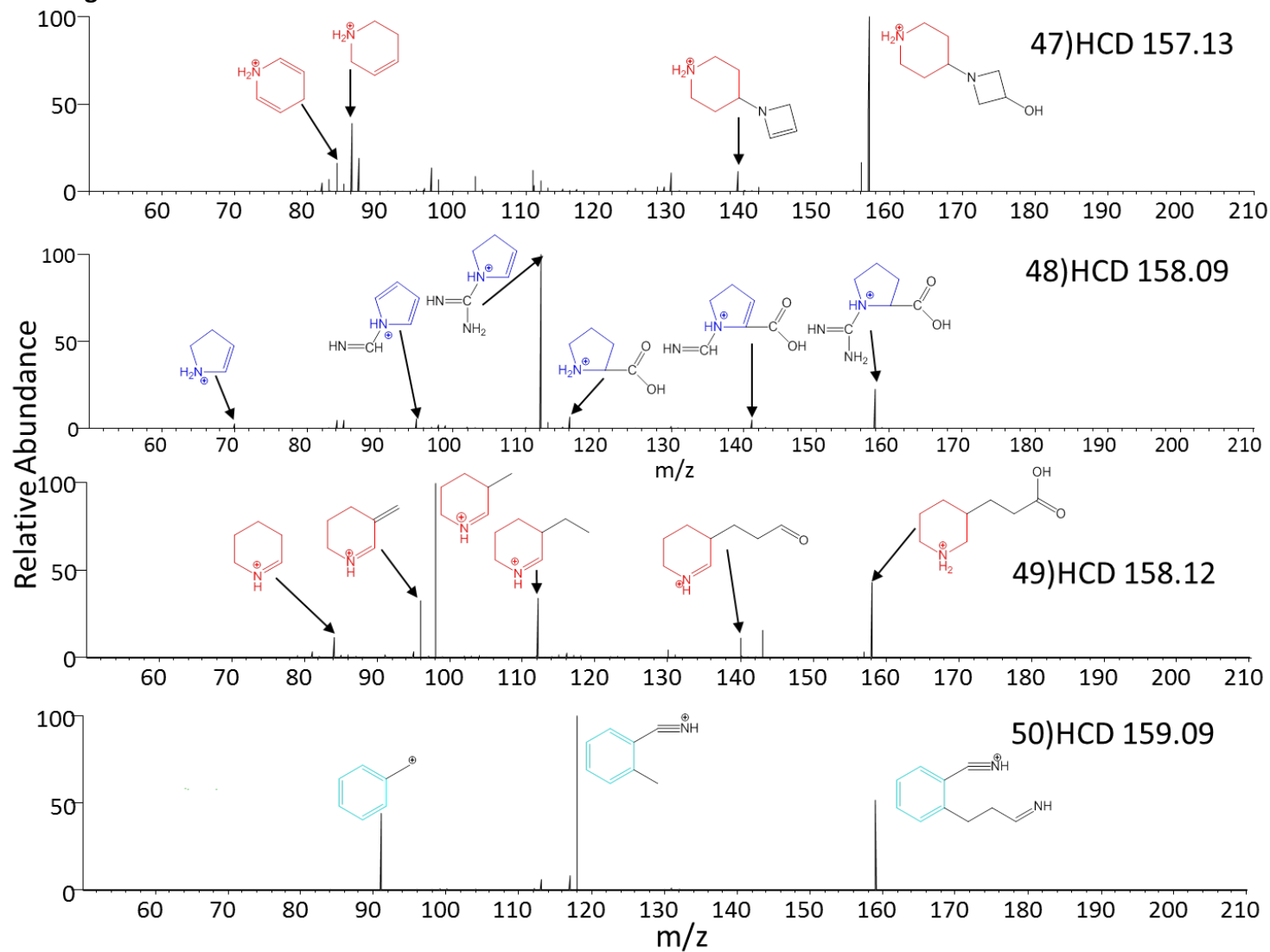
Appendix Figures 5.39 - 5.42.



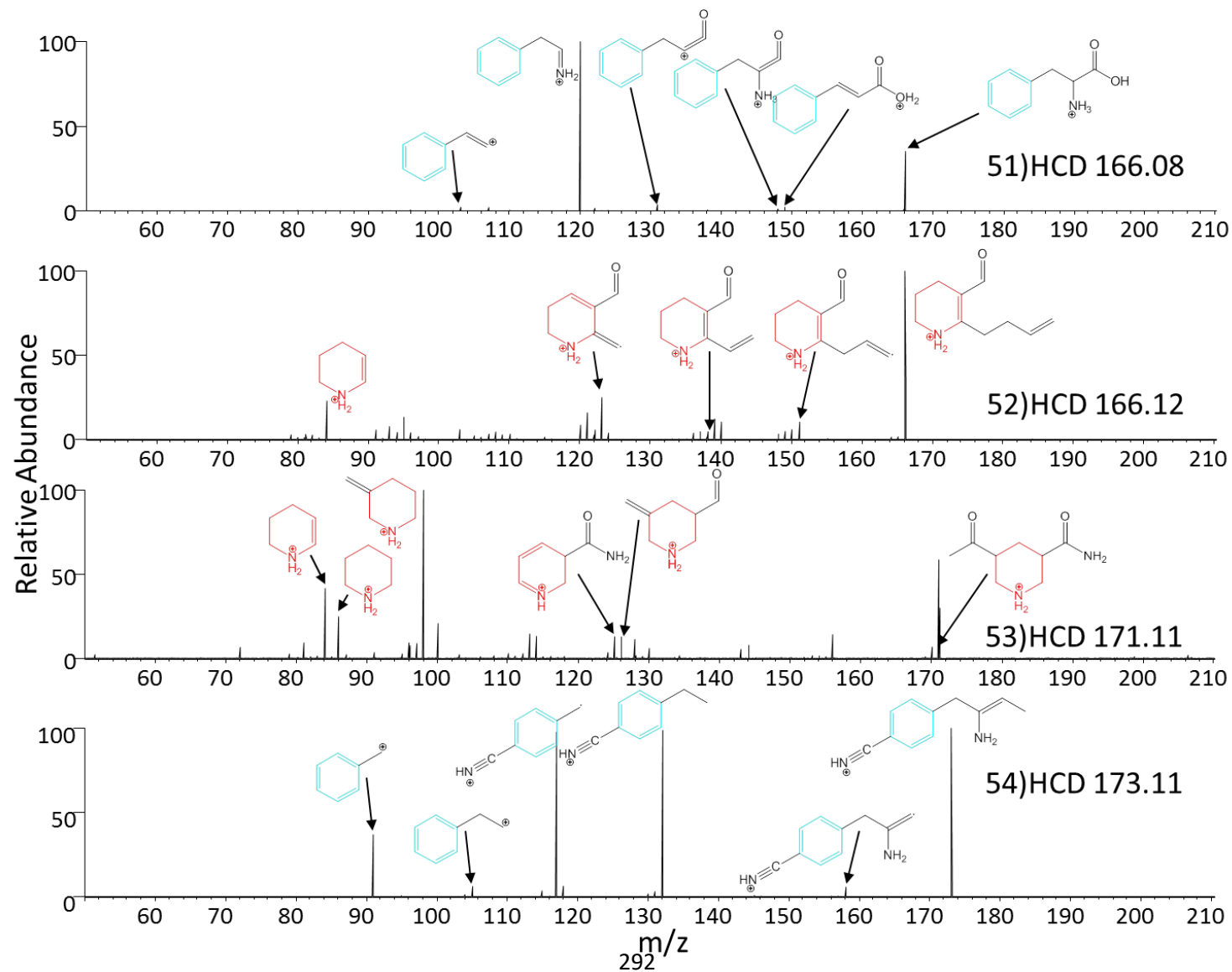
Appendix Figures 5.43 - 5.46.



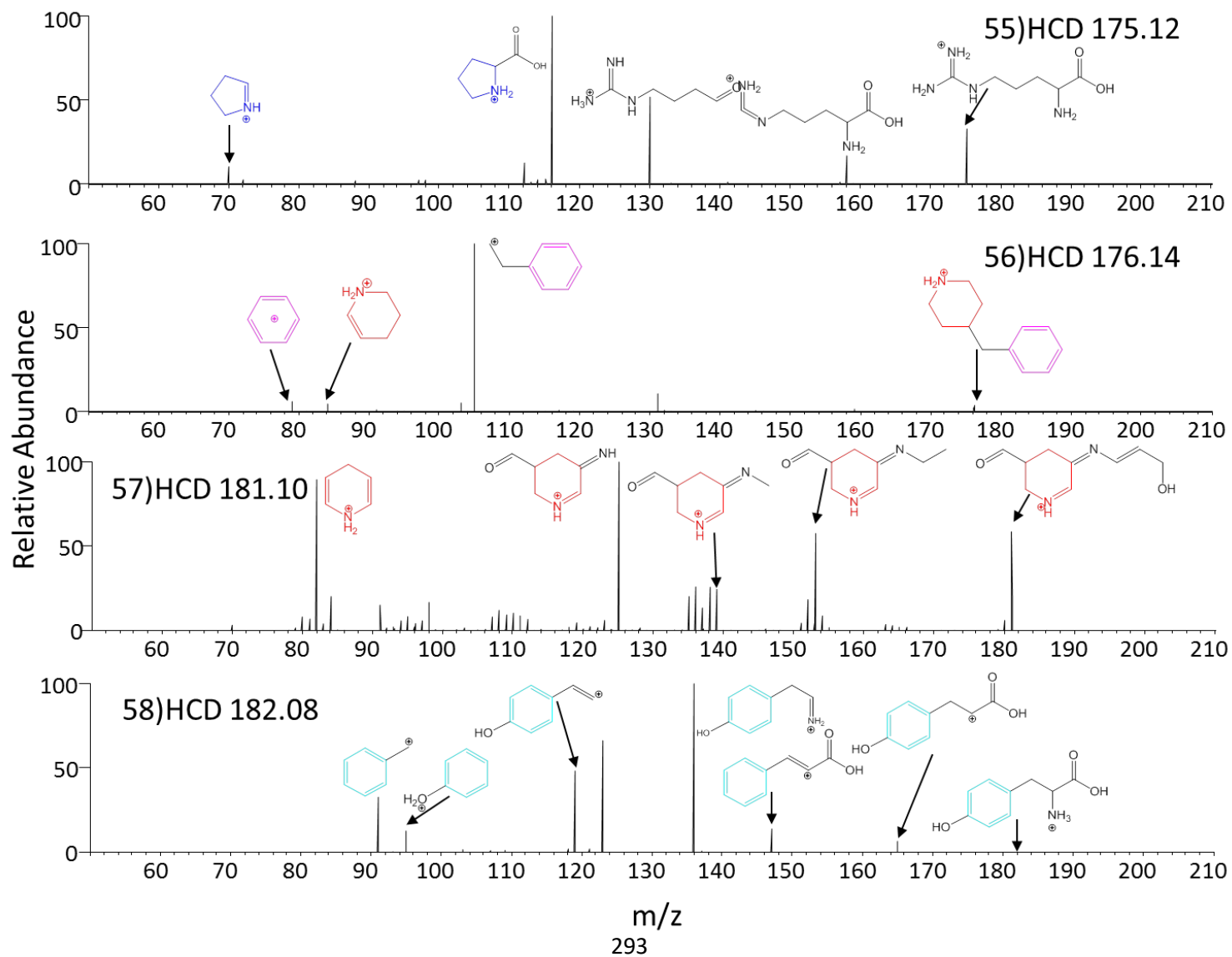
Appendix Figures 5.47 - 5.50.

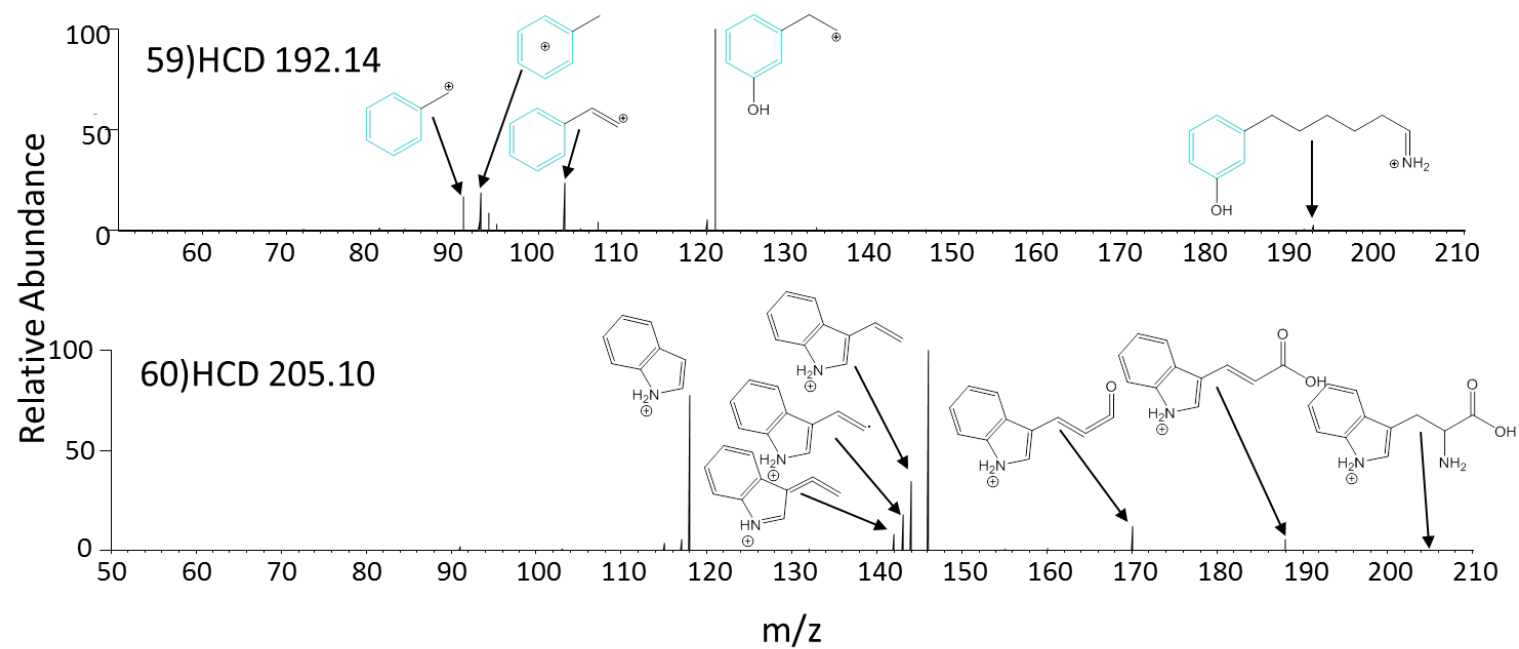


Appendix Figures 5.51 - 5.54.



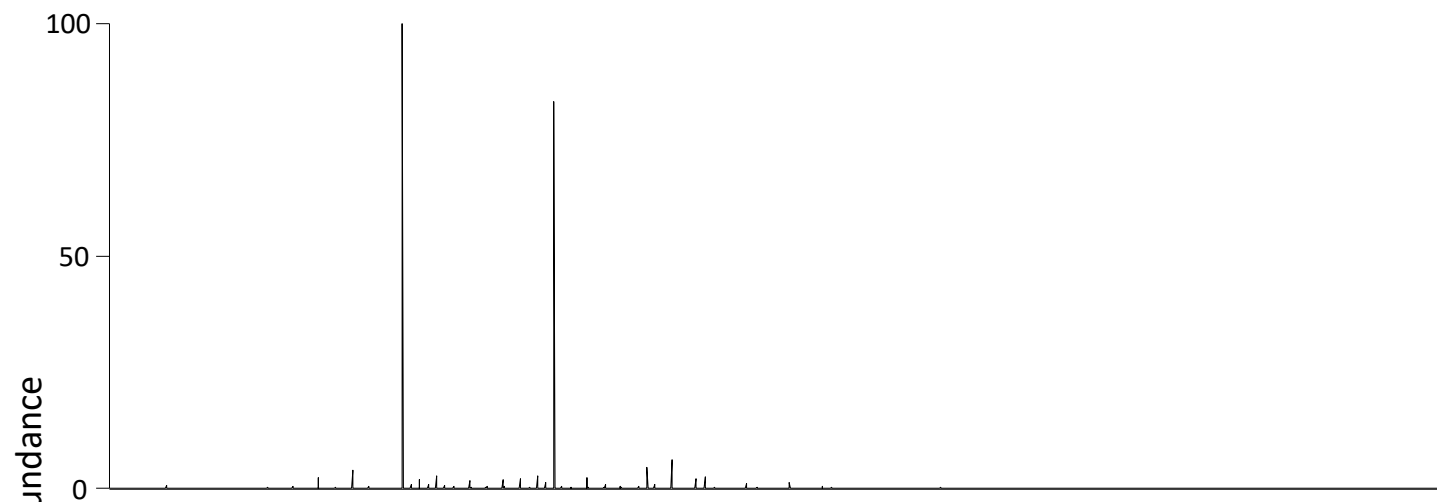
Appendix Figures 5.55 - 5.58.



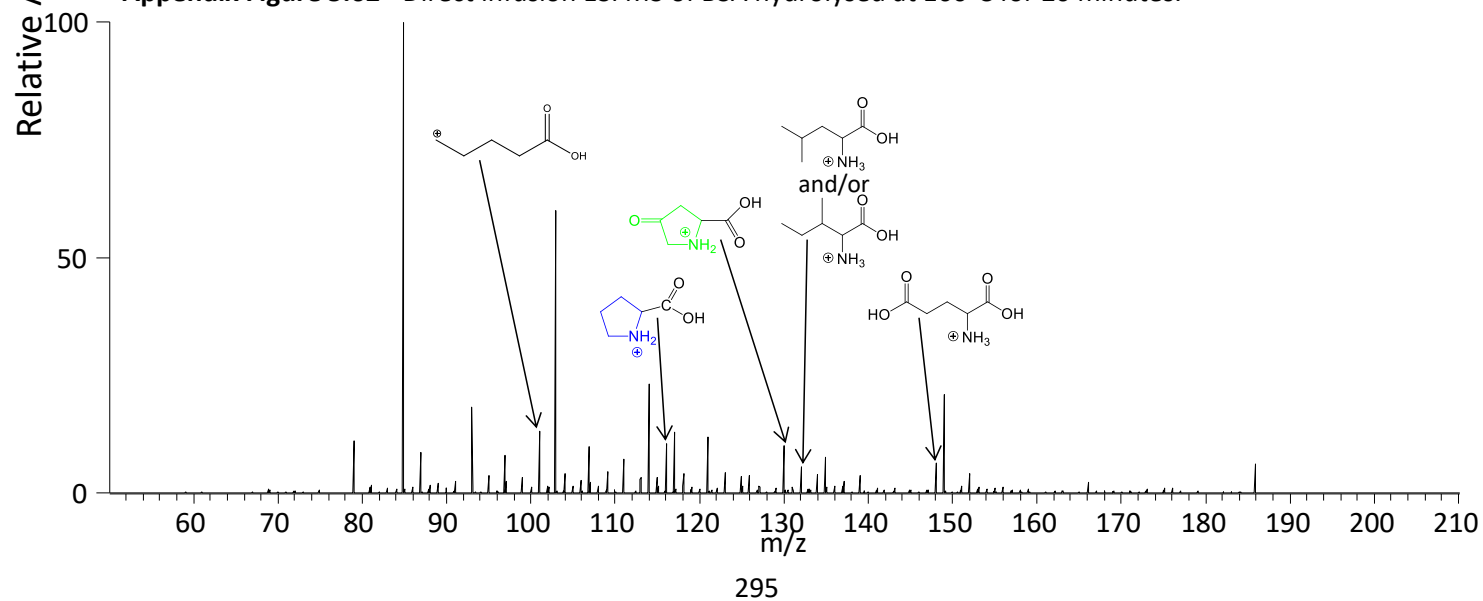


Appendix Figures 5.59 - 5.60.

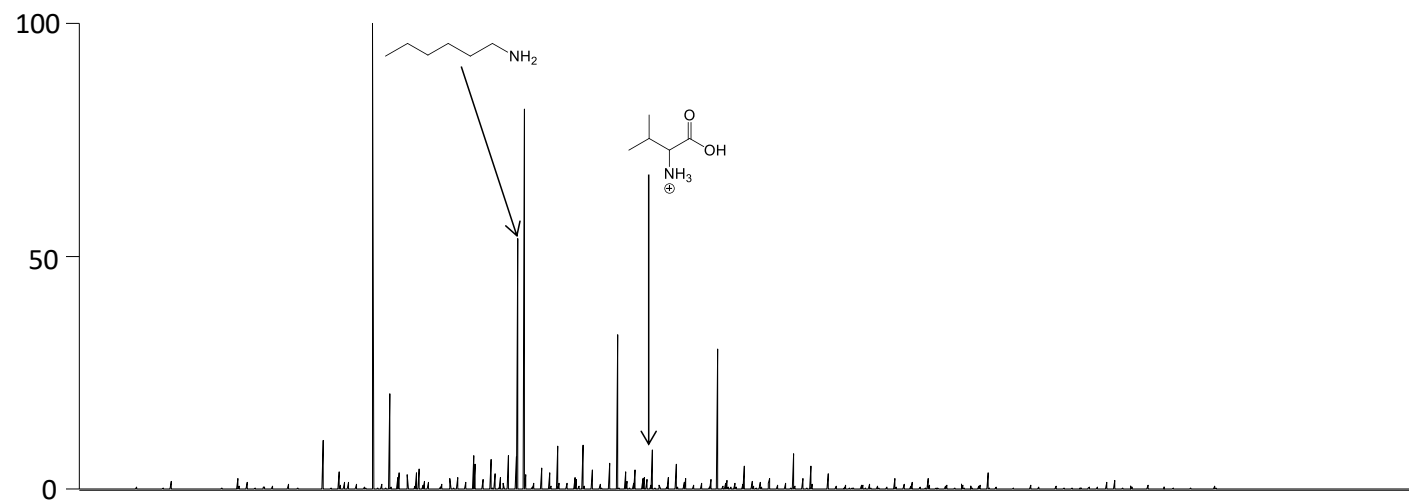
Appendix Figure 5.61 - Direct infusion ESI MS of BSA hydrolysed at 160°C for 0 minutes.



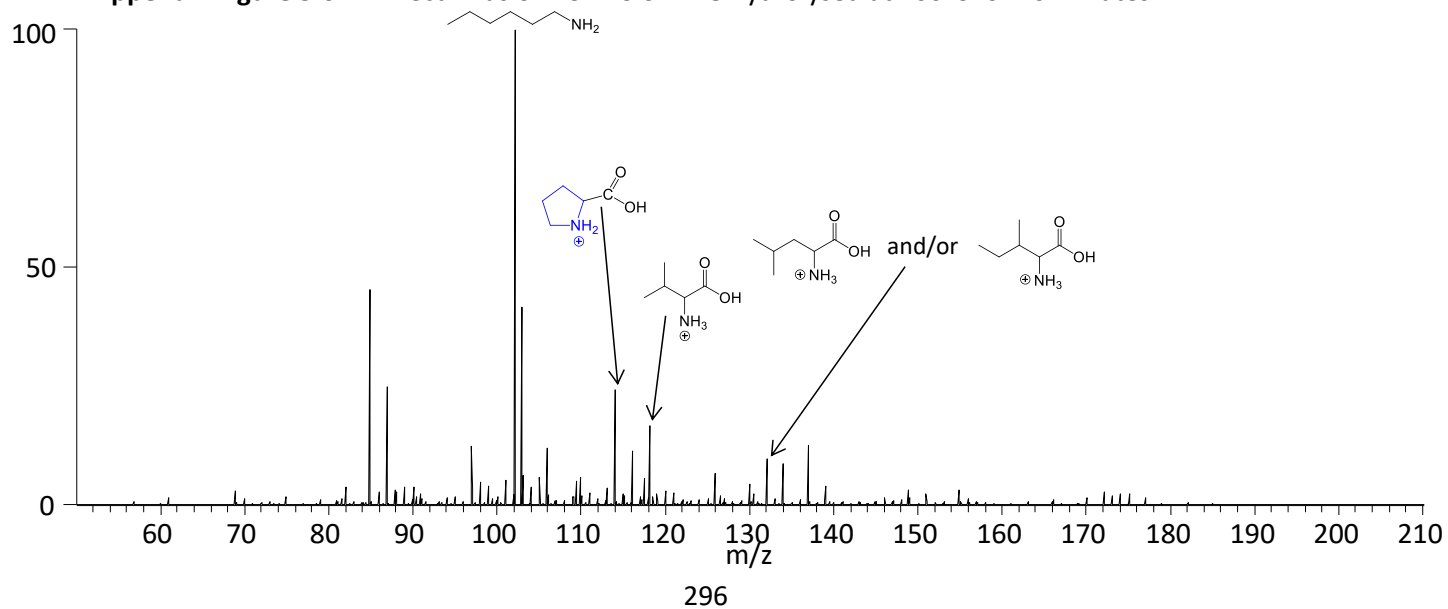
Appendix Figure 5.62 - Direct infusion ESI MS of BSA hydrolysed at 160°C for 20 minutes.



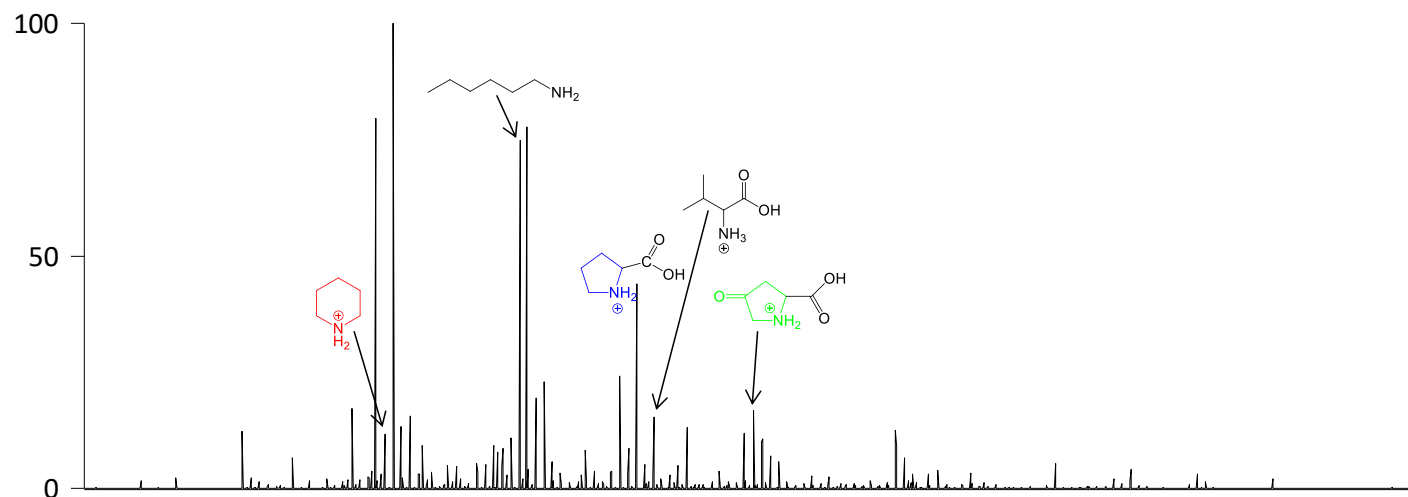
Appendix Figure 5.63 - Direct infusion ESI MS of NTG hydrolysed at 160°C for 0 minutes.



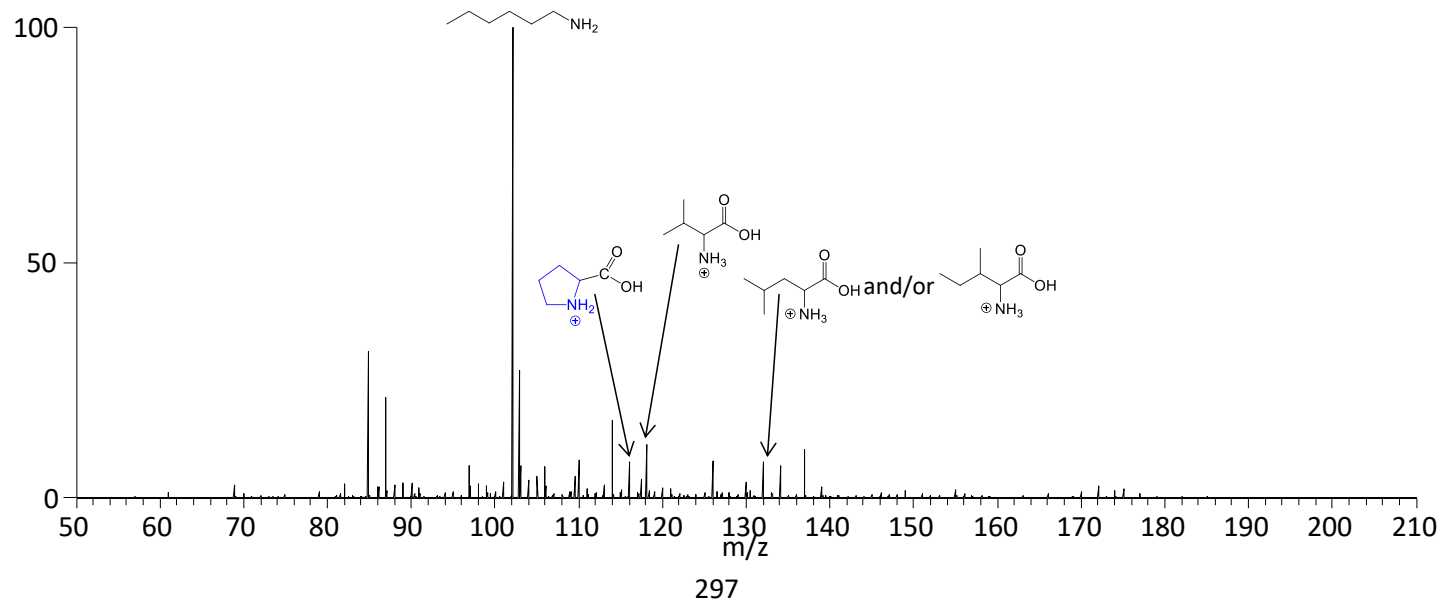
Appendix Figure 5.64 - Direct infusion ESI MS of NTG hydrolysed at 160°C for 20 minutes.

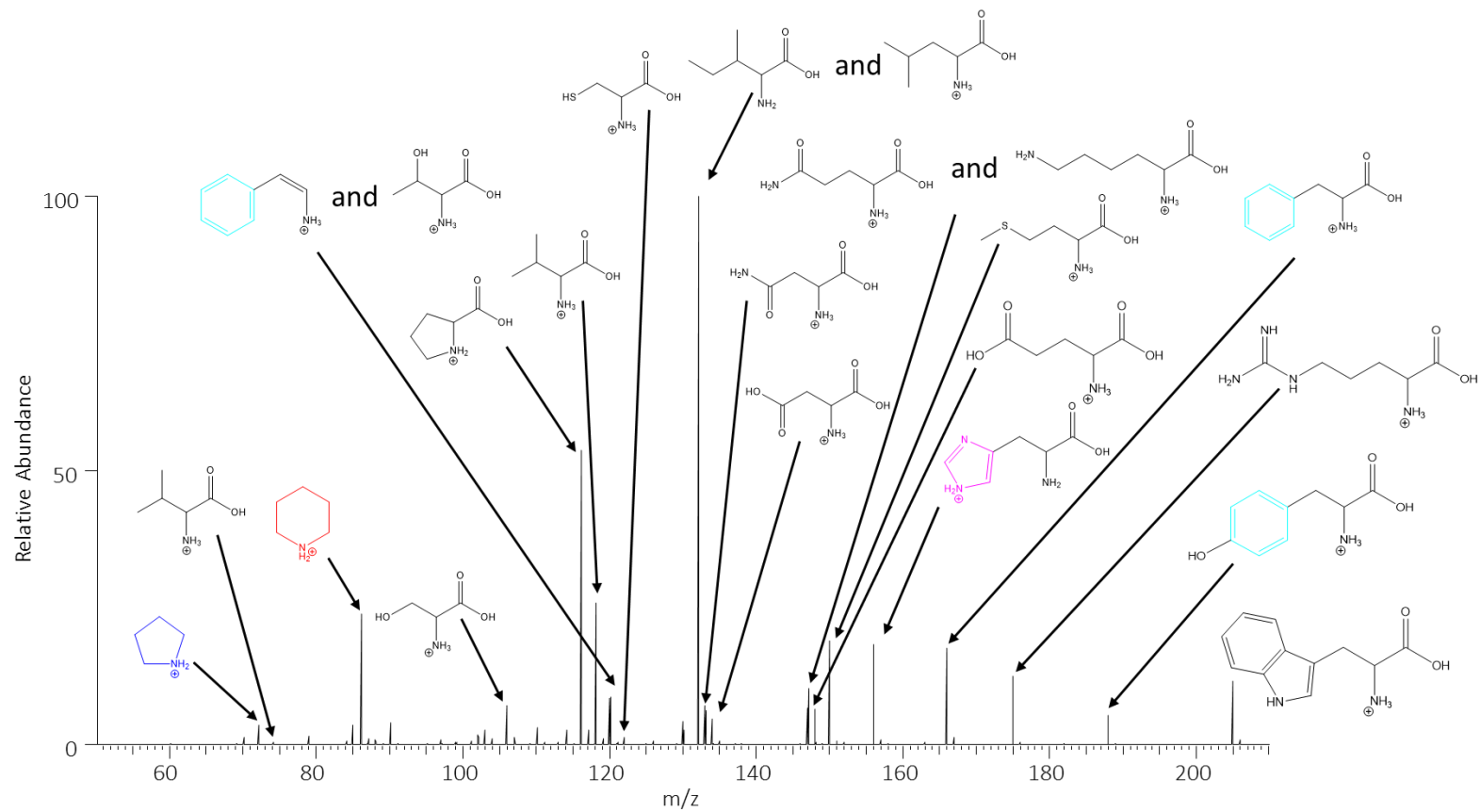


Appendix Figure 5.65 - Direct infusion ESI MS of BSG hydrolysed at 160°C for 0 minutes.



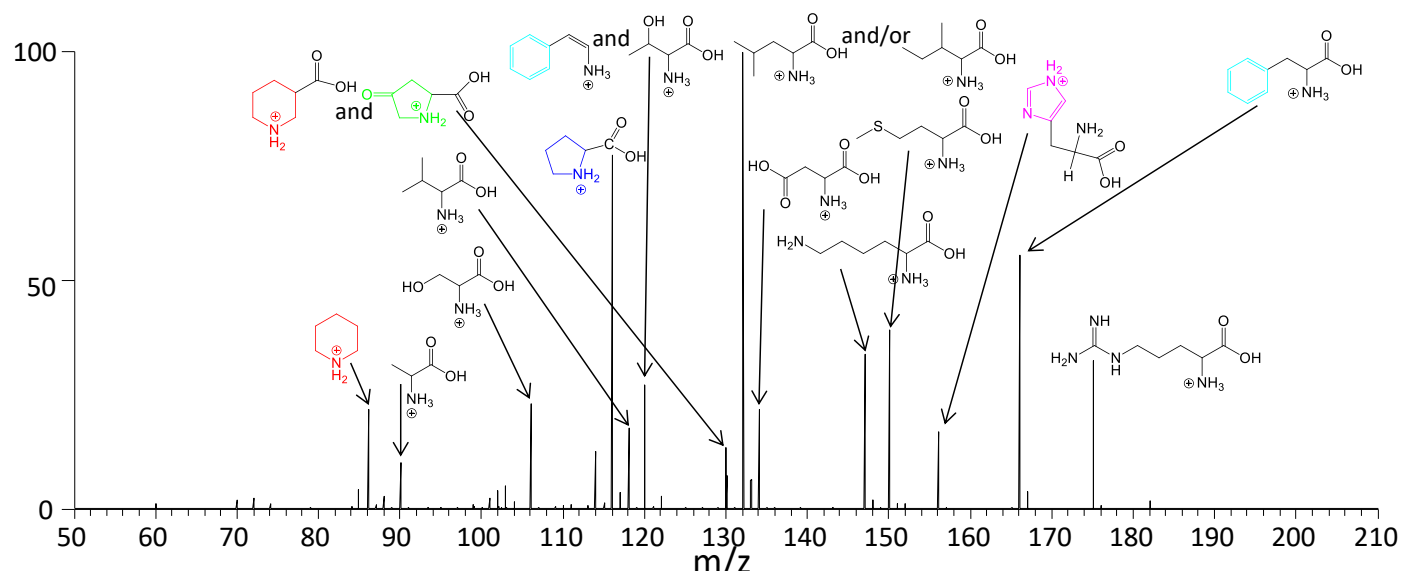
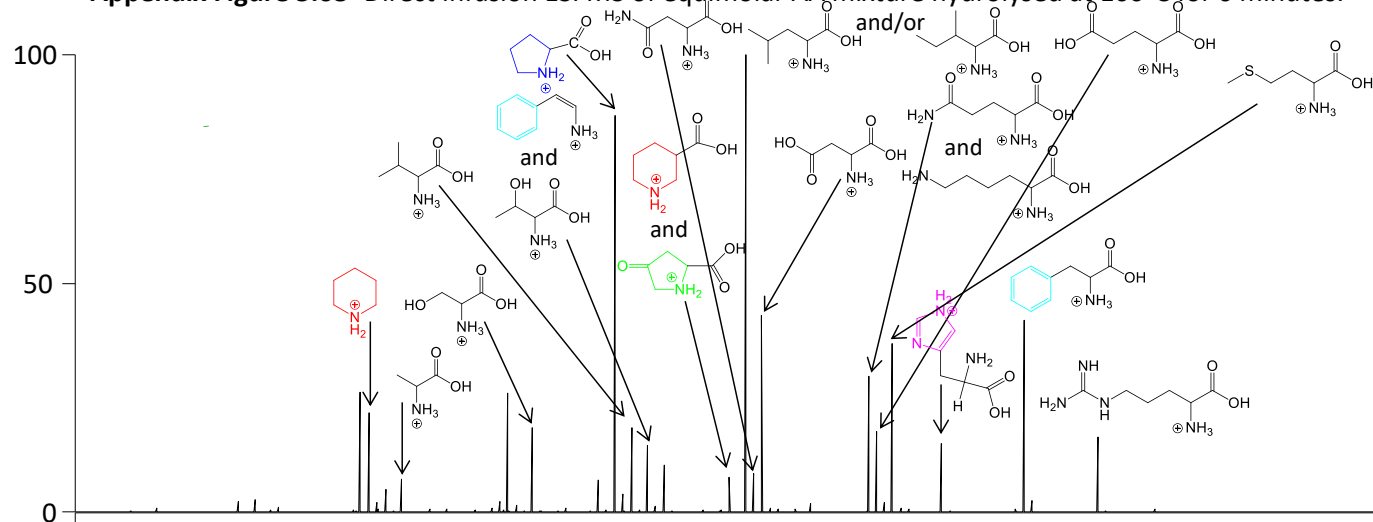
Appendix Figure 5.66 - Direct infusion ESI MS of BSG hydrolysed at 160°C for 20 minutes.





Appendix Figure 5.67- Direct infusion ESI MS of equimolar AA mixture.

Appendix Figure 5.68- Direct infusion ESI MS of equimolar AA mixture hydrolysed at 160°C for 0 minutes.



Appendix Figure 5.69- Direct infusion ESI MS equimolar aa mixture hydrolysed at 160°C for 20 minutes.

<i>m/z</i>	<i>z</i>	Calculated mass (Da)	Measured mass (Da)	Peptide	Δ PPM
599.538	4	2394.1249	2394.1213	VQSIKCADFLHYMENPTWGR	-1.5
609.024	4	2432.0803	2432.0673	VQSIKCADFLHYMENPTWGR (+K)	-5.3
799.047	3	2394.1249	2394.1204	VQSIKCADFLHYMENPTWGR	-1.9
806.375	3	2416.1063	2416.102	VQSIKCADFLHYMENPTWGR (+Na)	-1.8
811.696	3	2432.0803	2432.0668	VQSIKCADFLHYMENPTWGR (+K)	-5.5
1198.07	2	2394.1249	2394.1186	VQSIKCADFLHYMENPTWGR	-2.6
1209.06	2	2416.1063	2416.1008	VQSIKCADFLHYMENPTWGR (+Na)	-2.3

Appendix Table 4. 1 - Ions identified from the direct infusion electrospray MS of untreated VQSIKCADFLHYMENPTWGR.

c						y			z+1		
Calculated <i>m/z</i>	Measured <i>m/z</i>	Δ PPM				Calculated <i>m/z</i>	Measured <i>m/z</i>	Δ PPM	Calculated <i>m/z</i>	Measured <i>m/z</i>	Δ PPM
117.1022			1	V	20	---					
245.1608			2	Q	19	2328.0487			2313.0378	2313.0305	-3.1
332.1928			3	S	18	2199.9901			2184.9792	2184.9718	-3.4
445.2769	445.2767	-0.5	4	I	17	2112.9581			2097.9472	2097.9435	-1.7
573.3719	573.3716	-0.5	5	K	16	1999.8740			1984.8631	1984.8591	-2
708.3660	708.3708	6.9	6	c (2O)	15	1871.7790	1871.7778	-0.6	1856.7681		
779.4031	779.4075	5.7	7	A	14	1736.7850	1736.7795	-3.2	1721.7741	1721.7668	-4.2
894.4350	894.4342	-4.8	8	D	13	1665.7478			1650.7369	1650.7325	-2.7
1041.4984	1041.5027	4.2	9	F	12	1550.7209			1535.7100	1535.7070	-2
1154.5825			10	L	11	1403.6525			1388.6416	1388.6401	-1.1
1291.6414	1291.6453	3.1	11	H	10	1290.5684			1275.5575	1275.5565	-0.8
1454.7047	1454.7082	2.4	12	Y	9	1153.5095			1138.4986	1138.4974	-1.1
1585.7452	1585.7483	2.0	13	M	8	990.4462			975.4353	975.4345	-0.8
1714.7878	1714.7876	-0.1	14	E	7	859.4057			844.3948	844.3942	-0.7
---			15	N	6	730.3631			715.3522	715.3521	-0.1
1925.8835	1925.8799	-1.8	16	P	5	616.3202			---	---	---
2026.9312	2026.9268	-2.1	17	T	4	519.2674			504.2565	504.2562	-0.6
2213.0105			18	W	3	418.2197			403.2088	403.2086	-0.5
2270.0320	2270.0223	-4.3	19	G	2	232.1404			217.1295		
---			20	R	1	175.1190			160.1081		

Appendix Table 4. 2 - Peak assignments following ETD MS/MS of *m/z* 809.7136.

c			c+2O			c+3O				
Calculated <i>m/z</i>	Measured <i>m/z</i>	Δ PPM	Calculated <i>m/z</i>	Measured <i>m/z</i>	Δ PPM	Calculated <i>m/z</i>	Measured <i>m/z</i>	Δ PPM		
117.1022			149.0920			165.0869			1	V
245.1608			277.1506			293.1455			2	Q
332.1928			364.1826			380.1775			3	S
445.2769	445.2766	-0.7	477.2667			493.2616			4	I
573.3719	573.3715	-0.7	605.3617			621.3566			5	K
676.3811			708.3709	708.3704	-0.7	724.3658	724.3653	-0.7	6	C
747.4182			779.4080	779.4075	-0.6	795.4029	795.4026	-0.4	7	A
862.4451			894.4349	894.4342	-0.8	910.4298	910.4292	-0.7	8	D
1009.5135			1041.5033	1041.5026	-0.7	1057.4982			9	F
1122.5976			1154.5874			1170.5823	1170.5810	-1.1	10	L
1259.6565			1291.6463	1291.6455	-0.6	1307.6412	1307.6399	-1.0	11	H
1422.7198			1454.7096			1470.7045	1470.7012	-2.2	12	Y
1553.7603			1585.7501			1601.7450	1601.7409	-2.6	13	M
1682.8029			1714.7927			1730.7876	1730.7818	-3.4	14	E
---									15	N
1893.8986			1925.8884			1941.8833	1941.8758	-3.9	16	P
1994.9463			2026.9361			2042.9310	2042.9211	-4.8	17	T
2181.0256			2213.0154			2229.0103	2228.9990	-5.1	18	W
2238.0471			2270.0369			2286.0318	2286.0160	-6.9	19	G
---									20	R

Appendix Table 4. 3 - Peak assignments following ETD MS/MS of *m/z* 815.0426.

		z			z+O			z+3O		
		Calculated <i>m/z</i>	Measured <i>m/z</i>	Δ PPM	Calculated <i>m/z</i>	Measured <i>m/z</i>	Δ PPM	Calculated <i>m/z</i>	Measured <i>m/z</i>	Δ PPM
V	20	---			---			---		
Q	19	2281.0529			2297.0478			2329.0376	2329.0229	-6.3
S	18	2152.9943			2168.9892			2200.9790	2200.9640	-6.8
I	17	2065.9623			2081.9572			2113.9470	2113.9398	-3.4
K	16	1952.8782			1968.8731			2000.8629	2000.8530	-4.9
C	15	1824.7832			1840.7781			1872.7679	1872.7579	-5.3
A	14	1721.7741	1721.7679	-3.6	1737.7690	1737.7628	-3.6	1769.7588		
D	13	1650.7369	1650.7322	-2.8	1666.7318	1666.7266	-3.1	1698.7216		
F	12	1535.7100	1535.7068	-2.1	1551.7049	1551.7005	-2.8	1583.6947		
L	11	1388.6416	1388.6401	-1.1	1404.6365	1404.6346	-1.4	1436.6263		
H	10	1275.5575	1275.5562	-1.0	1291.5524	1291.5512	-0.9	1323.5422		
Y	9	1138.4986	1138.4972	-1.2	1154.4935	1154.4918	-1.5	1186.4833		
M	8	975.4353	975.4345	-0.8	991.4302	991.4295	-0.7	1023.4200		
E	7	844.3948	844.3943	-0.6	860.3897			892.3795		
N	6	715.3522	715.3521	-0.1	731.3471			763.3369		
P	5	---			---			---		
T	4	504.2565	504.2562	-0.6	520.2514			552.2412		
W	3	403.2088	403.2085	-0.7	419.2037			451.1935		
G	2	217.1295			233.1244			265.1142		
R	1	160.1081			176.1030			208.0928		

Appendix Table 4. 3 (continued) - Peak assignments following ETD MS/MS of *m/z* 815.0426.

b						y			y ⁺²		
Calculated m/z	Measured m/z	ΔPPM				Calculated m/z	Measured m/z	ΔPPM	Calculated m/z	Measured m/z	ΔPPM
---			1	V	20	---			---		
228.1343			2	Q	19	2344.0515			1172.5297		
315.1663	315.1671	2.5	3	S	18	2215.9929			1108.5004		
428.2504	428.2509	1.2	4	I	17	2128.9609			1064.9844		
556.3453	556.3457	0.7	5	K	16	2015.8768			1008.4423		
691.3443	691.3447	2.3	6	c (2o)	15	1887.7818			944.3948		
762.3814			7	A	14	1752.7809			876.8944	876.8939	-0.5
877.4084			8	D	13	1681.7437			841.3758		
1024.4768			9	F	12	1566.7168			783.8623	783.8618	-0.7
1137.5608			10	L	11	1419.6484			710.3281	710.3271	-1.4
1274.6198			11	H	10	1306.5643	1306.5649	0.5	653.7861	653.7853	-1.2
1437.6831			12	Y	9	1169.5054	1169.5048	-0.5	585.2566		
1568.7236			13	m(o)	8	1006.4421	1006.4405	-1.6	503.7250		
1697.7662			14	E	7	859.4057	859.4059	0.2	430.2065		
1811.8091			15	N	6	730.3631	730.3633	0.3	365.6852		
1908.8619			16	P	5	616.3202	616.3208	1.0	308.6637		
2009.9095			17	T	4	519.2674			260.1373		
2195.9888			18	W	3	418.2197	418.2205	2.0	209.6135		
2253.0103			19	G	2	232.1404			116.5738		
---			20	R	1	175.1190			88.06310		

Appendix Table 4. 4 a - Peak assignments following LC CID MS/MS of *m/z* 815.0457 at RT ~16 min 45 s.

b						y			y ⁺²		
Calculated <i>m/z</i>	Measured <i>m/z</i>	ΔPPM				Calculated <i>m/z</i>	Measured <i>m/z</i>	ΔPPM	Calculated <i>m/z</i>	Measured <i>m/z</i>	ΔPPM
---			1	V	20	---			---		
228.1343			2	Q	19	2344.0515			1172.5297		
315.1663	315.1671	2.5	3	S	18	2215.9929			1108.5004	1108.4980	-2.2
428.2504	428.2513	2.1	4	I	17	2128.9609			1064.9844	1064.9830	-1.7
556.3453	556.3456	0.5	5	K	16	2015.8768			1008.4423	1008.4410	-1.8
707.3422	707.3392	-4.2	6	c (3o)	15	1887.7818			944.3948	944.3935	-1.4
778.3793	778.3765	-3.6	7	A	14	1736.7860			868.8970	868.8963	-0.7
893.4063	893.4036	-3	8	D	13	1665.7488			833.3784	833.3782	-0.2
1040.4747	1040.4715	-3.1	9	F	12	1550.7219			775.8649	775.8642	-0.8
1153.5587			10	L	11	1403.6535	1403.6520	-0.1	702.3307	702.3304	-0.4
1290.6177			11	H	10	1290.5694	1290.5660	-2.2	645.7887	645.7882	-0.7
1453.6810			12	Y	9	1153.5105	1153.5080	-1.2	577.2592		
1584.7215			13	M	8	990.4472	990.4465	-0.3	495.7276		
1713.7641			14	E	7	859.4057	859.4061	0.5	422.2091		
1827.8070			15	N	6	730.3631	730.3635	0.5	365.6852		
1924.8598			16	P	5	616.3202	616.3204	0.3	308.6637		
2025.9074			17	T	4	519.2674	519.2682	1.5	260.1373		
2211.9867			18	W	3	418.2197	418.2202	1.2	209.6135		
2269.0082			19	G	2	232.1404			116.5738		
---			20	R	1	175.1190			88.06310		

Appendix Table 4. 4 b - Peak assignments following LC CID MS/MS of *m/z* 815.0457 at RT ~19 min.

c						z+1		
Calculated <i>m/z</i>	Measured <i>m/z</i>	Δ PPM				Calculated <i>m/z</i>	Measured <i>m/z</i>	Δ PPM
117.1022			1	V	20	---		
245.1608			2	Q	19	2345.0316	2345.0199	-5.0
332.1928			3	S	18	2216.9730	2216.9590	-6.3
445.2769	445.2758	-2.5	4	I	17	2129.9410		
573.3719	573.3761	7.3	5	K	16	2016.8569	2016.8495	-3.7
724.3658	724.3642	-2.2	6	c (3o)	15	1888.7619	1888.7554	-3.4
795.4029	795.4012	-2.1	7	A	14	1737.7690	1737.7621	-4.0
910.4298	910.4278	-2.2	8	D	13	1666.7318	1666.7242	-4.6
1057.4982	1057.496	-2.1	9	F	12	1551.7049	1551.6987	-4.0
1170.5823			10	L	11	1404.6365	1404.6420	3.9
1307.6412	1307.6377	-2.7	11	H	10	1291.5524	1291.5487	-2.9
1470.7045	1470.7001	-3.0	12	Y	9	1154.4935	1154.4901	-2.9
1617.7399	1617.7358	-2.5	13	m (o)	8	991.4302	991.4276	-2.6
1746.7825	1746.7744	-4.6	14	E	7	844.3948	844.3929	-2.3
---			15	N	6	715.3522	715.3509	-1.8
1957.8782	1957.8691	-4.6	16	P	5	---		
2058.9259	2058.9164	-4.6	17	T	4	504.2565	504.2555	-2.0
2245.0052			18	W	3	403.2088	403.2082	-1.5
2302.0267	2302.0086	-7.9	19	G	2	217.1295		
---			20	R	1	160.1081		

Appendix Table 4. 5 - Peak assignments following ETD MS/MS of *m/z* 820.3787.

c						z		
Calculated <i>m/z</i>	Measured <i>m/z</i>	Δ PPM				Calculated <i>m/z</i>	Measured <i>m/z</i>	Δ PPM
165.1022			1	F	12	---		
278.1863	278.1864	0.4	2	L	11	1387.6338	1387.6311	-2.0
415.2452	415.2454	0.5	3	H	10	1274.5497	1274.5485	-0.9
578.3085	578.3086	0.2	4	Y	9	1137.4908	1137.4904	-0.4
709.3490	709.3490	0.0	5	M	8	974.4275	974.4273	-0.2
838.3916	838.3917	0.1	6	E	7	843.3870	843.3871	0.1
---			7	N	6	714.3444	714.3455	1.5
1049.4873	1049.4873	0.0	8	P	5	---		
1150.5350	1150.5343	-0.6	9	T	4	503.2487	503.2488	0.2
1336.6143	1336.6129	-1.1	10	W	3	402.2010	402.2011	0.3
1393.6358	1393.6341	-1.2	11	G	2	216.1217	216.1218	0.5
---			12	R	1	159.1002	159.1005	1.9

Appendix Table 4. 6 - Peak assignments following ETD MS/MS of *m/z* 517.5779.

c						z		
Calculated <i>m/z</i>	Measured <i>m/z</i>	Δ PPM				Calculated <i>m/z</i>	Measured <i>m/z</i>	Δ PPM
165.1022			1	F	12	---		
278.1863	278.1865	0.7	2	L	11	1403.6287	1403.6267	-1.4
415.2452	415.2453	0.2	3	H	10	1290.5446	1290.5453	0.5
578.3085	578.3086	0.2	4	Y	9	1153.4857	1153.4853	-0.4
725.3439	725.3440	0.1	5	m(O)	8	990.4224	990.4222	-0.2
854.3865	854.3865	0.0	6	E	7	843.3870	843.3870	0.0
---			7	N	6	714.3444	714.3444	0.00
1065.4822	1065.4819	-0.3	8	P	5	---		
1166.5299	1166.5295	-0.3	9	T	4	503.2487	503.2487	0.0
1352.6092	1352.6077	-1.1	10	W	3	402.2010	402.2011	0.3
1409.6307	1409.6290	-1.2	11	G	2	216.1217	216.1219	0.9
---			12	R	1	159.1002	159.1005	1.9

Appendix Table 4. 7 - Peak assignments following ETD MS/MS of *m/z* 522.9105.

b			b ⁺ ₂						y		
Calculated <i>m/z</i>	Measured <i>m/z</i>	ΔPPM	Calculated <i>m/z</i>	Measured <i>m/z</i>	ΔPPM				Calculated <i>m/z</i>	Measured <i>m/z</i>	ΔPPM
---			---			1	F	9	---		
261.1598			---			2	L	8	1019.4615		
398.2187	398.2208	5.3	199.6133			3	H	7	906.3774	906.3836	6.9
561.2820			281.1449			4	Y	6	769.3185	769.3230	5.9
708.3174	708.3216	5.9	354.6626			5	M	5	606.2552		
837.3600	837.3647	5.6	419.1839			6	E	4	459.2198		
951.4029	951.4080	5.4	476.2054			7	N	3	330.1772	330.1789	5.2
1048.4557			524.7318	524.7348	5.8	8	P	2	216.1343	216.1354	5.2
---			---			9	t(Am)	1	119.0815		

Appendix Table 4. 8 - Peak assignments following CID MS/MS of *m/z* 583.7703.

<i>m/z</i>	<i>z</i>	Calculated mass (Da)	Measured mass (Da)	Peptide	Δ PPM
463.8725	3	1388.5965	1388.5957	VCFQYMDRGDR	-0.6
469.2041	3	1404.5914	1404.5905	VCFQYMDRGDR (+O)	-0.7
695.3052	2	1388.5965	1388.5958	VCFQYMDRGDR	-0.5
703.3028	2	1404.5914	1404.5910	VCFQYMDRGDR (+O)	-0.3
706.2962	2	1410.5779	1410.5778	VCFQYMDRGDR (+ Na)	0
717.2872	2	1432.5593	1432.5598	VCFQYMDRGDR (+2Na)	0.4
728.2781	2	1454.5407	1454.5416	VCFQYMDRGDR (+3Na)	0.6

Appendix Table 4. 9 - Ions identified from the direct infusion electrospray MS of iodoacetamide treated VQSIKCADFHYPENPTWGR.

c						z		
Calculated <i>m/z</i>	Measured <i>m/z</i>	Δ PPM				Calculated <i>m/z</i>	Measured <i>m/z</i>	Δ PPM
117.1022			1	V	11	---		
220.1114			2	C	10	1290.5116	1290.5073	-3.3
367.1798	367.1792	-1.6	3	F	9	1187.5024		
495.2384			4	Q	8	1040.4340	1040.4337	-0.3
658.3017			5	Y	7	912.3754	912.3750	-0.4
805.3371			6	m (O)	6	749.3121	749.3128	0.9
920.3641			7	D	5	602.2767	602.2766	-0.2
1076.4652			8	R	4	487.2497	487.2501	0.8
1133.4867			9	G	3	331.1486	331.1486	0.0
1248.5136	1248.5167	2.5	10	D	2	274.1272	274.1274	0.7
---			11	R	1	159.1002	159.1003	0.6

Appendix Table 4. 10 - Peak assignments following ETD MS/MS of *m/z* 469.2041.

b						y			y ⁺²		
Calculated m/z	Measured m/z	ΔPPM				Calculated m/z	Measured m/z	ΔPPM	Calculated m/z	Measured m/z	ΔPPM
---			1	V	11	---			---		
235.0747	235.0747	0.0	2	c (2o)	10	1322.5252			661.7662	661.7665	0.4
382.1431			3	F	9	1187.5262			594.2667	594.2665	-0.4
510.2017			4	Q	8	1040.4578			520.7325	520.7313	-2.4
673.2650			5	Y	7	912.3992			456.7032	456.7030	-0.5
804.3055			6	M	6	749.3359			375.1716	375.1713	-0.8
919.3324			7	D	5	618.2954			309.6513	309.6512	-0.4
1075.4335			8	R	4	503.2685	503.2682	-0.6	252.1379		
1132.4550			9	G	3	347.1674	347.1671	-0.9	174.0873		
1247.4819			10	D	2	290.1459			145.5766		
---			11	R	1	175.1190	175.1189	-0.6	88.0631		

Appendix Table 4. 11 - Peak assignments following CID MS/MS of *m/z* 474.5359.

c-1						z			z+1		
Calculated <i>m/z</i>	Measured <i>m/z</i>	Δ PPM				Calculated <i>m/z</i>	Measured <i>m/z</i>	Δ PPM	Calculated <i>m/z</i>	Measured <i>m/z</i>	Δ PPM
116.0944			1	V	11	---			---		
251.0934			2	c (2o)	10	1322.5014			1323.5092		
398.1618			3	F	9	1187.5024	1187.5022	-0.2	1188.5102		
526.2204			4	Q	8	1040.4340	1040.4336	-0.4	1041.4418		
689.2837			5	Y	7	912.3754			913.3832	913.3820	-1.3
836.3191			6	m(o)	6	749.3121			750.3199	750.3195	-0.5
951.3460			7	D	5	602.2767			603.2845	603.2840	-0.8
1107.4472	1107.4457	-1.4	8	R	4	487.2497			488.2576	488.2571	-1.0
1164.4686	1164.4673	-1.1	9	G	3	331.1486			332.1565		
1279.4956	1279.4950	-0.5	10	D	2	274.1272			275.1350		
---			11	R	1	159.1002			160.1081		

Appendix Table 4. 12 a - Peak assignments following LC ETD MS/MS of *m/z* 719.2973 at RT ~9min 30s.

c			c-1						z+1		
Calculated m/z	Measured m/z	Δ PPM	Calculated m/z	Measured m/z	Δ PPM				Calculated m/z	Measured m/z	Δ PPM
117.1022			116.0944			1	V	11	---		
268.0961			267.0883			2	c (3o)	10	1323.5092	1323.5084	-0.6
415.1645			414.1567			3	F	9	1172.5153	1172.5138	-1.3
543.2231			542.2153			4	Q	8	1025.4469	1025.4462	-0.7
706.2864			705.2786			5	Y	7	897.3883	897.3876	-0.8
837.3269			836.3191			6	M	6	734.3250	734.3245	-0.7
952.3539			951.3460			7	D	5	603.2845	603.2841	-0.7
1108.4550			1107.4472			8	R	4	488.2576	488.2571	-1.0
1165.4764	1165.4745	-1.6	1164.4686			9	G	3	332.1565	332.1561	-1.2
1280.5034			1279.4956	1279.4957	0.1	10	D	2	275.1350	275.1349	-0.4
---			---			11	R	1	160.1081		

Appendix Table 4.12 a – Peak assignments following LC ETD MS/MS of *m/z* 719.2973 at RT ~11 min 30s.

c-1						z			z+1		
Calculated m/z	Measured m/z	Δ PPM				Calculated m/z	Measured m/z	Δ PPM	Calculated m/z	Measured m/z	Δ PPM
116.0944			1	V	11	---			---		
267.0883			2	c (3o)	10	1338.4963	1338.4951	-0.9	1339.5041		
414.1567			3	F	9	1187.5024			1188.5102	1188.5094	-0.7
542.2153			4	Q	8	1040.4340			1041.4418	1041.4414	-0.4
705.2786			5	Y	7	912.3754			913.3832	913.3829	-0.3
852.3140			6	m (o)	6	749.3121			750.3199	750.3195	-0.5
967.3409			7	D	5	602.2767			603.2845	603.2841	-0.7
1123.4421	1123.4415	-0.5	8	R	4	487.2497			488.2576	488.2572	-0.8
1180.4635	1180.4629	-0.5	9	G	3	331.1486			332.1565	332.1562	-0.9
1295.4905	1295.4895	-0.8	10	D	2	274.1272			275.1350	275.1349	-0.4
---			11	R	1	159.1002			160.1081		

Appendix Table 4. 13 - Peak assignments following ETD MS/MS of *m/z* 727.2950.

c			c + 20				
Calculated <i>m/z</i>	Measured <i>m/z</i>	Δ PPM	Calculated <i>m/z</i>	Measured <i>m/z</i>	Δ PPM		
117.1022			149.0920			1	V
220.1114			252.1012			2	C
367.1798			399.1696	399.1695	-0.3	3	F
495.2384			527.2282	527.2279	-0.6	4	Q
658.3017			690.2915	690.2917	0.3	5	Y
789.3422			821.3320	821.3313	-0.9	6	M
904.3692			936.3590	936.3583	-0.7	7	D
1060.4703			1092.4601	1092.4593	-0.7	8	R
1117.4917			1149.4815	1149.4808	-0.6	9	G
1232.5187			1264.5085			10	D
---						11	R

Appendix Table 4. 14 - Peak assignments following ETD MS/MS of *m/z* 468.2838.

c + 2O - H ₂ O			c + 2O - 2H ₂ O				
Calculated <i>m/z</i>	Measured <i>m/z</i>	ΔPPM	Calculated <i>m/z</i>	Measured <i>m/z</i>	ΔPPM		
131.0815			113.0709			1	V
234.0907			216.0801			2	C
381.1591			363.1485			3	F
509.2177			491.2071			4	Q
672.2810			654.2704			5	Y
803.3215			785.3109			6	M
918.3485	918.3475	-1.0	900.3379			7	D
1074.4496	1074.4486	-0.9	1056.4390			8	R
1131.4710	1131.4702	-0.7	1113.4604			9	G
1246.4980	1246.4977	-0.2	1228.4874			10	D
						11	R

Appendix Table 4.14 (continued) - Peak assignments following ETD MS/MS of *m/z* 468.2838.

		z			z - H ₂ O			z - 2H ₂ O		
		Calculated <i>m/z</i>	Measured <i>m/z</i>	ΔPPM	Calculated <i>m/z</i>	Measured <i>m/z</i>	ΔPPM	Calculated <i>m/z</i>	Measured <i>m/z</i>	ΔPPM
V	11	---								
C	10	1274.5167			1256.5062			1238.4956		
F	9	1171.5075			1153.4970	1153.4960	-0.8	1135.4864		
Q	8	1024.4391			1006.4286	1006.4269	-1.6	988.4180		
Y	7	896.3805			878.3700	878.3697	-0.3	860.3594		
M	6	733.3172			715.3067			697.2961	697.2958	-0.4
D	5	602.2767			584.2662	584.2657	-0.8	566.2556		
R	4	487.2497	487.2493	-0.8	469.2392	469.2387	-1.0	451.2286		
G	3	331.1486	331.1486	0.0	313.1381	313.1380	-0.2	295.1275		
D	2	274.1272	274.1269	-1.1	256.1167	256.1164	-1.0	238.1061		
R	1	159.1002	159.1001	-0.6	141.0897			123.0791		

Appendix Table 4.14 (continued) - Peak assignments following ETD MS/MS of *m/z* 468.2838.

		z- H ₂ O+ 20			z - 2H ₂ O + 20		
		Calculated <i>m/z</i>	Measured <i>m/z</i>	ΔPPM	Calculated <i>m/z</i>	Measured <i>m/z</i>	ΔPPM
V	11	---			---		
C	10	1288.49595			1270.4854		
F	9	1185.48675			1167.4762		
Q	8	1038.41835			1020.4078		
Y	7	910.35975			892.3492		
M	6	747.29645			729.2859		
D	5	616.25595			598.2454		
R	4	501.22895			483.2184		
G	3	345.12785			327.1173		
D	2	288.10645			270.0959		
R	1	173.07945			155.0689		

Appendix Table 4.14 (continued) - Peak assignments following ETD MS/MS of *m/z* 468.2838.

c			c + 20			c + 30				
Calculated <i>m/z</i>	Measured <i>m/z</i>	Δ PPM	Calculated <i>m/z</i>	Measured <i>m/z</i>	Δ PPM	Calculated <i>m/z</i>	Measured <i>m/z</i>	Δ PPM		
117.1022			149.0920			165.0869			1	V
220.1114			252.1012			268.0961			2	C
367.1798			399.1696			415.1645			3	F
495.2384			527.2282			543.2231			4	Q
658.3017			690.2915			706.2864			5	Y
789.3422			821.3320			837.3269			6	M
904.3692			936.3590			952.3539			7	D
1060.4703			1092.4601			1108.4550	1108.4525	-2.3	8	R
1117.4917			1149.4815			1165.4764	1165.4710	-4.6	9	G
1232.5187			1264.5085			1280.5034			10	D
---			---			---			11	R

Appendix Table 4. 15 - Peak assignments following ETD MS/MS of *m/z* 710.2924.

c + 2O - H ₂ O			c + 2O - 2H ₂ O				
Calculated <i>m/z</i>	Measured <i>m/z</i>	ΔPPM	Calculated <i>m/z</i>	Measured <i>m/z</i>	ΔPPM		
131.0815			113.0709			1	V
234.0907			216.0801			2	C
381.1591			363.1485			3	F
509.2177			491.2071			4	Q
672.2810			654.2704			5	Y
803.3215			785.3109			6	M
918.3485			900.3379			7	D
1074.4496			1056.4390			8	R
1131.4710			1113.4604			9	G
1246.4980			1228.4874			10	D
---			---			11	R

Appendix Table 4.15 (continued) - Peak assignments following ETD MS/MS of *m/z* 710.2924.

c + 3O - H ₂ O			c + 3O - 2H ₂ O				
Calculated <i>m/z</i>	Measured <i>m/z</i>	ΔPPM	Calculated <i>m/z</i>	Measured <i>m/z</i>	ΔPPM		
147.0764			129.0658			1	V
250.0856			232.0750			2	C
397.1540			379.1434			3	F
525.2126			507.2020			4	Q
688.2759			670.2653			5	Y
819.3164			801.3058			6	M
934.3434			916.3328			7	D
1090.4445			1072.4339			8	R
1147.4659	1147.4635		1129.4553			9	G
1262.4929	1262.4875		1244.4823			10	D
---						11	R

Appendix Table 4.15 (continued) - Peak assignments following ETD MS/MS of *m/z* 710.2924.

		z			z+1 - H ₂ O			z+1 - 2H ₂ O		
		Calculated <i>m/z</i>	Measured <i>m/z</i>	ΔPPM	Calculated <i>m/z</i>	Measured <i>m/z</i>	ΔPPM	Calculated <i>m/z</i>	Measured <i>m/z</i>	ΔPPM
V	11	---			---			---		
C	10	1274.5167			1257.5140			1239.5034		
F	9	1171.5075			1154.5048	1154.5024	-2.1	1136.4942		
Q	8	1024.4391			1007.4364	1007.4356		989.4258		
Y	7	896.3805			879.3778	879.3772		861.3672		
M	6	733.3172			716.3145	716.3141		698.3039		
D	5	602.2767			585.2740	585.2730		567.2634	567.2625	-1.6
R	4	487.2497			470.2470	470.2465		452.2364		
G	3	331.1486			314.1459	314.1456		296.1353		
D	2	274.1272			257.1245	257.1242		239.1139		
R	1	159.1002			142.0975			124.0869		

Appendix Table 4.15 (continued) - Peak assignments following ETD MS/MS of *m/z* 710.2924.

		z+1- H ₂ O+ O			z+1 - 2H ₂ O + O		
		Calculated <i>m/z</i>	Measured <i>m/z</i>	ΔPPM	Calculated <i>m/z</i>	Measured <i>m/z</i>	ΔPPM
V	11	---			---		
C	10	1273.5089			1255.4983		
F	9	1170.4997			1152.4891	1152.4871	-1.8
Q	8	1023.4313	1023.4287	-2.5	1005.4207	1005.4189	-1.8
Y	7	895.3727	895.3702	-2.8	877.3621	877.3592	-3.3
M	6	732.3094	732.3079	-2.0	714.2988		
D	5	601.2689			583.2583		
R	4	486.2419			468.2313		
G	3	330.1408			312.1302		
D	2	273.1194			255.1088		
R	1	158.0924			140.0818		

Appendix Table 4.15 (continued) - Peak assignments following ETD MS/MS of *m/z* 710.2924.

		z+1 - H ₂ O + 3O			z+1 - H ₂ O + 3O		
		Calculated <i>m/z</i>	Measured <i>m/z</i>	ΔPPM	Calculated <i>m/z</i>	Measured <i>m/z</i>	ΔPPM
V	11	---			---		
C	10	1305.4987	1305.4911	-5.8	1287.4881		
F	9	1202.4895			1184.4789		
Q	8	1055.4211			1037.4105		
Y	7	927.3625			909.3519		
M	6	764.2992			746.2886		
D	5	633.2587			615.2481		
R	4	518.2317			500.2211		
G	3	362.1306			344.1200		
D	2	305.1092			287.0986		
R	1	190.0822			172.0716		

Appendix Table 4.15 (continued) - Peak assignments following ETD MS/MS of *m/z* 710.2924.

<i>m/z</i>	<i>z</i>	Calculated mass (Da)	Measured mass (Da)	Peptide	Δ PPM
541.0273	4	2160.0752	2160.0801	VQSIKADFLHYENPTWGR	2.3
550.5151	4	2198.0306	2198.0313	VQSIKADFLHYENPTWGR (+K)	0.3
721.0335	3	2160.0752	2160.0787	VQSIKADFLHYENPTWGR	1.6
728.3627	3	2182.0566	2182.0663	VQSIKADFLHYENPTWGR (+Na)	4.4
733.6844	3	2198.0306	2198.0314	VQSIKADFLHYENPTWGR (+K)	0.4
1081.0487	2	2160.0752	2160.0828	VQSIKADFLHYENPTWGR	3.5

Appendix Table 4. 16 - Ions identified from the direct infusion electrospray MS of untreated VQSIKADFLHYENPTWGR.

c						z			z+1		
Calculated <i>m/z</i>	Measured <i>m/z</i>	Δ PPM				Calculated <i>m/z</i>	Measured <i>m/z</i>	Δ PPM	Calculated <i>m/z</i>	Measured <i>m/z</i>	Δ PPM
117.1022			1	V	18	---			---		
245.1608	245.1598	-4.1	2	Q	17	2061.9903			2062.9981	2062.9825	-7.6
332.1928	332.1914	-4.2	3	S	16	1933.9317			1934.9395	1934.9273	-6.3
445.2769	445.2750	-4.3	4	I	15	1846.8997			1847.9075	1847.8981	-5.1
573.3719	573.3694	-4.4	5	K	14	1733.8156			1734.8234	1734.8144	-5.2
644.4090	644.4062	-4.3	6	A	13	1605.7206			1606.7285	1606.7207	-4.9
759.4359	759.4362	0.4	7	D	12	1534.6835			1535.6914	1535.6844	-4.6
906.5043	906.5003	-4.4	8	F	11	1419.6566			1420.6644	1420.6578	-4.6
1019.5884	1019.5839	-4.4	9	L	10	1272.5882			1273.5960	1273.5907	-4.2
1156.6473	1156.6420	-4.6	10	H	9	1159.5041			1160.5119	1160.5063	-4.8
1319.7106	1319.7063	-3.3	11	Y	8	1022.4452	1022.4407	-4.4	1023.4530		
1448.7532	1448.7477	-3.8	12	E	7	859.3819	859.3781	-4.4	860.3897		
---			13	N	6	730.3393	730.3362	-4.2	731.3471		
1659.8489	1659.8420	-4.2	14	P	5	---			---		
1760.8966	1760.8907	-3.4	15	T	4	519.2436	519.2412	-4.6	520.2514		
1962.9708	1962.9630	-4	16	w(O)	3	418.1959	418.1940	-4.5	419.2037		
2019.9878	2019.9820	-2.9	17	G	2	232.1166			233.1244		
---			18	R	1	175.0951			176.1030		

Appendix Table 4. 17 - Peak assignments following ETD MS/MS of *m/z* 545.0272

b			b ⁺²			b ⁺³				
Calculated <i>m/z</i>	Measured <i>m/z</i>	ΔPPM	Calculated <i>m/z</i>	Measured <i>m/z</i>	ΔPPM	Calculated <i>m/z</i>	Measured <i>m/z</i>	ΔPPM		
---			---			---			1	V
228.1343	228.1333	-4.4	---			---			2	Q
315.1663	315.1659	-1.3	---			---			3	S
428.2504			---			---			4	I
556.3453			278.6766			---			5	K
627.3824			314.1951			---			6	A
742.4094	742.4059	-4.7	371.7086	371.7065	-5.7	---			7	D
889.4778	889.4733	-5.1	445.2428			---			8	F
1002.5619			501.7849			---			9	L
1139.6208			570.3143	570.3113	-5.3	380.5455			10	H
1302.6841			651.8460			434.8999			11	Y
1431.7267			716.3673	716.3679	0.9	477.9141			12	E
1545.7696			773.3887	773.385	-4.8	515.9284			13	N
1642.8224			821.9151			548.2794			14	P
1743.8701			872.4390			581.9619	581.9588	-5.4	15	T
1961.9392			981.4735			654.6516			16	w(2O)
2018.9606			1009.9842			673.6588			17	G
---			---			---			18	R

Appendix Table 4. 18 - Peak assignments following CID MS/MS of *m/z* 549.0260

		y			y^{+2}			y^{+3}		
		Calculated m/z	Measured m/z	ΔPPM	Calculated m/z	Measured m/z	ΔPPM	Calculated m/z	Measured m/z	ΔPPM
V	18	---			---			---		
Q	17	2094.0039			1047.5059			698.6732	698.6695	-5.3
S	16	1965.9453			983.4766			655.9870	655.9839	-4.7
I	15	1878.9133			939.9606			626.9763		
K	14	1765.8292			883.4185			589.2816		
A	13	1637.7343			819.3711			546.5833		
D	12	1566.6972			783.8525			522.9043		
F	11	1451.6702			726.3390	726.3356	-4.7	484.5620		
L	10	1304.6018			652.8048			435.5392		
H	9	1191.5177			596.2628			397.8445		
Y	8	1054.4588			527.7333			---		
E	7	891.3955			446.2017			---		
N	6	762.3529	762.3492	-4.9	381.6804			---		
P	5	648.3100	648.3071	-4.5	324.6589			---		
T	4	551.2572			276.1325			---		
w(2O)	3	450.2095	450.2075	-4.4	225.6087			---		
G	2	232.1404	232.1394	-4.3	116.5741			---		
R	1	175.1190			88.0634			---		

Appendix Table 4. 18 (continued) - Peak assignments following CID MS/MS of m/z 549.0260

c						z+1		
Calculated <i>m/z</i>	Measured <i>m/z</i>	ΔPPM				Calculated <i>m/z</i>	Measured <i>m/z</i>	ΔPPM
117.1022			1	V	18	---		
245.1608			2	Q	17	2028.9927	2028.9880	-2.3
332.1928			3	S	16	1900.9341	1900.9305	-1.9
445.2769	445.2779	2.3	4	I	15	1813.9021	1813.8998	-1.2
573.3719	573.3730	1.9	5	K	14	1700.8180	1700.8164	-0.9
644.4090	644.4102	1.9	6	A	13	1572.7231	1572.7200	-1.9
741.4254	741.4268	2.0	7	d (- H ₂ O)	12	1501.6860	1501.6835	-1.6
888.4938	888.4952	1.6	8	F	11	1386.6590		
1001.5779	1001.5794	1.5	9	L	10	1257.6011	1257.6013	0.2
1138.6368	1138.6382	1.3	10	H	9	1144.5170	1144.5128	-3.7
1301.7001	1301.7009	0.7	11	Y	8	1007.4581	1007.4598	1.7
1430.7427	1430.7432	0.4	12	E	7	844.3948	844.3971	2.7
---			13	N	6	715.3522		
1641.8384	1641.8367	-1.0	14	P	5	---		
1742.8861	1742.8847	-0.8	15	T	4	504.2565	504.2575	2.0
1928.9654	1928.9595	-3.0	16	W	3	403.2088	403.2097	2.2
1985.9869	1985.9817	-2.6	17	G	2	217.1295	217.1303	3.7
---			18	R	1	160.1081		

Appendix Table 4. 19 - Peak assignments following CID MS/MS of *m/z* 715.0316

<i>m/z</i>	<i>z</i>	Calculated mass (Da)	Measured mass (Da)	Peptide	Δ PPM
613.7934	4	2451.1464	2451.1445	VQSIKCADFLHYMENPTWGR (+ C ₂ H ₅ ON)	-0.8
619.2887	4	2473.1278	2473.1257	VQSIKCADFLHYMENPTWGR (+ C ₂ H ₅ ON) + Na	-0.8
818.0553	3	2451.1464	2451.1441	VQSIKCADFLHYMENPTWGR (+ C ₂ H ₅ ON)	-0.9
825.3826	3	2473.1278	2473.126	VQSIKCADFLHYMENPTWGR (+ C ₂ H ₅ ON) + Na	-0.7
1226.579	2	2451.1464	2451.1434	VQSIKCADFLHYMENPTWGR (+ C ₂ H ₅ ON)	-1.2

Appendix Table 4. 20 - Ions identified from the direct infusion electrospray MS of iodoacetamide treated VQSIKCADFLHYMENPTWGR.

b						y			y ⁺ ₂		
Calculated <i>m/z</i>	Measured <i>m/z</i>	ΔPPM				Calculated <i>m/z</i>	Measured <i>m/z</i>	ΔPPM	Calculated <i>m/z</i>	Measured <i>m/z</i>	ΔPPM
---			1	V	20	---			---		
228.1343			2	Q	19	2353.0862			1177.0470		
315.1663			3	S	18	2225.0276			1113.0177	1113.0187	0.9
428.2504	428.2514	2.3	4	I	17	2137.9956			1069.5017	1069.5031	1.4
556.3453	556.3464	2.0	5	K	16	2024.9115			1012.9597	1012.9607	1.0
716.3541			6	^c (+C ₂ H ₅ ON)	15	1896.8165	1896.8167	0.1	948.9122		
787.4140	787.4146	0.7	7	A	14	1736.7850	1736.7866	0.9	868.8964		
902.4410	902.4417	0.7	8	D	13	1665.7478	1665.7499	1.3	833.3778		
1049.5094	1049.5104	0.9	9	F	12	1550.7209	1550.7223	0.9	775.8644		
1162.5934			10	L	11	1403.6525	1403.6550	1.8	702.3302		
1299.6524	1299.6535	0.8	11	H	10	1290.5684	1290.5706	1.7	645.7881		
1462.7157	1462.7175	1.2	12	Y	9	1153.5095	1153.5113	1.6	577.2587		
1593.7562	1593.7575	0.8	13	M	8	990.4462	990.4481	1.9	495.7270		
1722.7988	1722.7995	0.4	14	E	7	859.4057	859.4074	2.0	430.2068		
1836.8417	1836.8421	0.2	15	N	6	730.3631	730.3645	1.9	365.6855		
1933.8945	1933.8955	0.5	16	P	5	616.3202	616.3214	1.9	308.6640		
2034.9421			17	T	4	519.2674	519.2686	2.3	260.1376		
2221.0214			18	W	3	418.2197	418.2207	2.4	209.6138		
2278.0429			19	G	2	232.1404			116.5741		
---			20	R	1	175.1190			88.0634		

Appendix Table 4. 21 - Peak assignments following ETD MS/MS of *m/z* 818.0553.

c						z+1		
Calculated <i>m/z</i>	Measured <i>m/z</i>	Δ PPM				Calculated <i>m/z</i>	Measured <i>m/z</i>	Δ PPM
117.1022			1	V	20	---		
245.1608			2	Q	19	2354.0693	2354.0515	-7.5
332.1928			3	S	18	2226.0107	2225.9960	-6.6
445.2769			4	I	17	2138.9787	2138.9654	-6.3
573.3719	573.3694	-4.4	5	K	16	2025.8946	2025.8829	-5.8
733.4026	733.3995	-4.2	6	c (+C ₂ H ₅ ON)	15	1897.7996		
804.4397	804.4362	-4.3	7	A	14	1737.7690	1737.7594	-5.5
919.4666	919.4627	-4.2	8	D	13	1666.7318	1666.7228	-5.4
1066.5350	1066.5306	-4.1	9	F	12	1551.7049	1551.6972	-5.0
1179.6191	1179.6135	-4.7	10	L	11	1404.6365	1404.6304	-4.3
1316.6780	1316.6725	-4.1	11	H	10	1291.5524	1291.5471	-4.1
1479.7412	1479.7351	-4.2	12	Y	9	1154.4935	1154.4881	-4.7
1626.7767	1626.7691	-4.6	13	m(O)	8	991.4302	991.4259	-4.3
1755.8193	1755.8100	-5.3	14	E	7	844.3948	844.3914	-4.0
---			15	N	6	715.3522	715.3493	-4.1
1966.9150	1966.9036	-5.8	16	P	5	---		
2067.9627	2067.9499	-6.2	17	T	4	504.2565	504.2543	-4.4
2254.0420	2254.0235	-8.2	18	W	3	403.2088	403.2071	-4.2
2311.0635	2311.0470	-7.1	19	G	2	217.1295		
---			20	R	1	160.1081		

Appendix Table 4. 22 - Peak assignments following ETD MS/MS of *m/z* 823.3905.

b			b + C ₂ H ₃ ON			b + 2(C ₂ H ₃ ON)				
Calculated <i>m/z</i>	Measured <i>m/z</i>	ΔPPM	Calculated <i>m/z</i>	Measured <i>m/z</i>	ΔPPM	Calculated <i>m/z</i>	Measured <i>m/z</i>	ΔPPM		
---									1	V
228.1343			285.1557			342.1772			2	Q
315.1663	315.1649	-4.4	372.1877	372.1860	-4.7	429.2092			3	S
428.2504	428.2486	-4.2	485.2718	485.2696	-4.6	542.2933			4	I
556.3453	556.3430	-4.1	613.3667	613.3641	-4.3	670.3882			5	K
659.3545			716.3759	716.3728	-4.4	773.3974	773.3940	-4.4	6	C
730.3916			787.4130	787.4093	-4.8	844.4345	844.4309	-4.3	7	A
845.4186			902.4400	902.4359	-4.6	959.4615	959.4571	-4.6	8	D
992.4870			1049.5084	1049.5038	-4.4	1106.5299	1106.5247	-4.7	9	F
1105.5710			1162.5924	1162.5871	-4.6	1219.6139	1219.6088	-4.2	10	L
1242.6300			1299.6514			1356.6729			11	H
1405.6933			1462.7147			1519.7362	1519.7301	-4.0	12	Y
1536.7338			1593.7552			1650.7767			13	M
1665.7764			1722.7978			1779.8193			14	E
1779.8193			1836.8407			1893.8622			15	N
1876.8721			1933.8935			1990.9150			16	P
1977.9197			2034.9411			2091.9626			17	T
2163.9990			2221.0204			2278.0419			18	W
2221.0205			2278.0419			2335.0634			19	G
---									20	R

Appendix Table 4. 23 - Peak assignments following CID MS/MS of *m/z* 837.0585.

$(b + C_2H_3ON)^{+2}$			$(b + 2(C_2H_3ON))^{+2}$				
Calculated <i>m/z</i>	Measured <i>m/z</i>	Δ PPM	Calculated <i>m/z</i>	Measured <i>m/z</i>	Δ PPM		
---			---			1	V
---			---			2	Q
---			---			3	S
---			---			4	I
307.1873			335.6980			5	K
358.6919			387.2026			6	C
394.2104			422.7212			7	A
451.7239			480.2347	480.2342	-1.0	8	D
525.2581			553.7689	553.7661	-5.0	9	F
581.8001			610.3109	610.3080	-4.7	10	L
650.3296	650.3264	-5.0	678.8404	678.8370	-5.0	11	H
731.8613			760.3720	760.3682	-5.0	12	Y
797.3815			825.8923	825.8882	-4.9	13	M
861.9028			890.4136	890.4091	-5.0	14	E
918.9243			947.4350	947.4303	-5.0	15	N
967.4507			995.9614			16	P
1017.9745			1046.4852			17	T
1111.0141			1139.5249			18	W
1139.5249			1168.0356			19	G
---			---			20	R

Appendix Table 4. 23 (continued) - Peak assignments following ETD MS/MS of *m/z* 837.0585.

y			y + C ₂ H ₃ ON				
Calculated <i>m/z</i>	Measured <i>m/z</i>	ΔPPM	Calculated <i>m/z</i>	Measured <i>m/z</i>	ΔPPM		
---						V	20
2296.0638			2353.0852			Q	19
2168.0052			2225.0266			S	18
2080.9732			2137.9946			I	17
1967.8891			2024.9105			K	16
1839.7941			1896.8155			C	15
1736.7850			1793.8064			A	14
1665.7478	1665.7394	-5.0	1722.7692			D	13
1550.7209	1550.7136	-4.7	1607.7423	1607.7357	-4.1	F	12
1403.6525	1403.6462	-4.5	1460.6739	1460.6669	-4.8	L	11
1290.5684	1290.5629	-4.3	1347.5898	1347.5840	-4.3	H	10
1153.5095	1153.5041	-4.7	1210.5309	1210.5252	-4.7	Y	9
990.4462	990.4417	-4.5	1047.4676	1047.4628	-4.6	M	8
859.4057	859.4017	-4.7	916.4271	916.4230	-4.5	E	7
730.3631	730.3598	-4.5	787.3845			N	6
616.3202	616.3178	-3.9	673.3416			P	5
519.2674	519.2651	-4.4	576.2888			T	4
418.2197	418.2178	-4.5	475.2411			W	3
232.1404			289.1618			G	2
175.1190			232.1404			R	1

Appendix Table 4. 23 (continued) - Peak assignments following ETD MS/MS of *m/z* 837.0585.

y^{+2}			$(y + C_2H_3ON)^{+2}$			$(y + 2(C_2H_3ON))^{+2}$				
Calculated m/z	Measured m/z	ΔPPM	Calculated m/z	Measured m/z	ΔPPM	Calculated m/z	Measured m/z	ΔPPM		
---									V	20
1148.5355			1177.0465	1177.0399		1205.5572			Q	19
1084.5062			1113.0172	1113.0117		1141.5279	1141.5222	-5.0	S	18
1040.9902			1069.5012	1069.4957		1098.0119	1098.0066	-4.9	I	17
984.4482			1012.9592	1012.9543		1041.4699	1041.4647	-5.0	K	16
920.4007			948.9117	948.9071	-4.8	977.4224	977.4176	-4.9	C	15
868.8961	868.8919	-4.8	897.4071	897.4028	-4.8	925.91786			A	14
833.3776			861.8885	861.8843	-4.9	890.39926			D	13
775.8641	775.8604	-4.8	804.3751	804.3711	-5.0	832.8858			F	12
702.3299	702.3267	-4.6	730.8409			759.3516			L	11
645.7878	645.7849	-4.5	674.2988	674.2954	-5.1	702.8096			H	10
577.2584	577.256	-4.2	605.7694			634.2801			Y	9
495.7267			524.2377			552.7485			M	8
430.2065			458.7175			487.2282			E	7
365.6852			394.1962			422.7069			N	6
308.6637			337.1747			365.6855			P	5
260.1373			288.6483			317.1591			T	4
209.6135			238.1245			266.6352			W	3
116.5738			145.0848			173.5956			G	2
88.0631			116.5741			145.0849			R	1

Appendix Table 4. 23 (continued) - Peak assignments following ETD MS/MS of m/z 837.0585.

b			b+C ₇ H ₆				
Calculated <i>m/z</i>	Measured <i>m/z</i>	ΔPPM	Calculated <i>m/z</i>	Measured <i>m/z</i>	ΔPPM		
---						1	V
228.1343	228.1343		318.1813			2	Q
315.1663	315.1663	0.0	405.2133			3	S
428.2504	428.2503	0.2	518.2974			4	I
556.3453	5556.3453	0.0	646.3923			5	K
659.3545	659.3545	0.0	749.4015			6	C
730.3916	730.3917	-0.1	820.4386			7	A
845.4186	845.4186	0.0	935.4656			8	D
992.4870	992.4871	-0.1	1082.5340	1082.5349	-0.9	9	F
1105.5710	1105.5714	-0.4	1195.6180	1195.6184	-0.4	10	L
1242.6300	1242.6299	0.1	1332.6770			11	H
1405.6933			1495.7403			12	Y
1536.7338			1626.7808			13	M
1665.7764			1755.8234			14	E
1779.8193			1869.8663			15	N
1876.8721			1966.9191			16	P
1977.9197			2067.9667			17	T
2163.9990			2254.0460			18	W
2221.0205			2311.0675			19	G
---			---			20	R

Appendix Table 4. 24 - Peak assignments following CID MS/MS of *m/z* 622.0462.

b⁺²			(b+C7H6)⁺²				
Calculated <i>m/z</i>	Measured <i>m/z</i>	ΔPPM	Calculated <i>m/z</i>	Measured <i>m/z</i>	ΔPPM		
---			---			1	V
---			---			2	Q
---			---			3	S
---			---			4	I
278.6763			323.6998			5	K
330.1809			375.2044			6	C
365.6994			410.7229			7	A
423.2129			468.2364			8	D
496.7471			541.7706			9	F
553.2891	553.2893	-0.3	598.3126	598.3098	4.7	10	L
621.8186			666.8421	666.8420	0.2	11	H
703.3503	703.3522	-2.7	748.3738	748.3747	-1.3	12	Y
768.8705	768.8712	-0.9	813.8940	813.8939	0.1	13	M
833.3918	833.3913	0.6	878.4153	878.4149	0.5	14	E
890.4133	890.4133	0.0	935.4368	935.4365	0.3	15	N
938.9397			983.9632			16	P
989.4635	989.4637	-0.2	1034.4870			17	T
1082.5031	1082.5039	-0.7	1127.5266			18	W
1111.0139			1156.0374			19	G
---			---			20	R

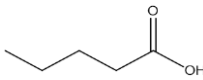
Appendix Table 4. 24 (continued) - Peak assignments following CID MS/MS of *m/z* 622.0462.

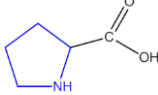
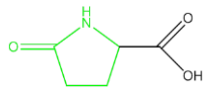
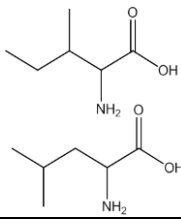
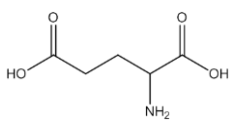
		y			y+C ₇ H ₆		
		Calculated <i>m/z</i>	Measured <i>m/z</i>	ΔPPM	Calculated <i>m/z</i>	Measured <i>m/z</i>	ΔPPM
V	20	---					
Q	19	2296.0638			2386.1108		
S	18	2168.0052			2258.0522		
I	17	2080.9732			2171.0202		
K	16	1967.8891			2057.9361		
C	15	1839.7941			1929.8411		
A	14	1736.7850			1826.8320		
D	13	1665.7478			1755.7948		
F	12	1550.7209			1640.7679		
L	11	1403.6525			1493.6995		
H	10	1290.5684	1290.5675	0.7	1380.6154		
Y	9	1153.5095	1153.5090	0.4	1243.5565		
M	8	990.4462	990.4462	0.0	1080.4932		
E	7	859.4057	859.4061	-0.5	949.4527	949.4535	-0.9
N	6	730.3631	730.3635	-0.5	820.4101	820.4110	-1.2
P	5	616.3202	616.3203	-0.2	706.3672	706.3676	-0.6
T	4	519.2674	519.2676	-0.4	609.3144	609.3146	-0.4
W	3	418.2197	418.2197	0.0	508.2667	508.2667	-0.1
G	2	232.1404	232.1404		322.1874		
R	1	175.1190			---		

Appendix Table 4. 24 (continued) - Peak assignments following CID MS/MS of *m/z* 622.0462.

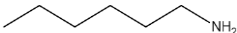
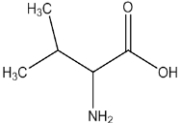
<u>m/z</u>	<u>Calculated mass (Da)</u>	<u>Measured mass (Da)</u>	<u>Formula</u>	<u>Structure</u>	<u>ΔPPM</u>	<u>Relative abundance</u>
84.96	n/a	n/a	solvent	n/a	n/a	100
102.97	n/a	n/a	solvent	n/a	n/a	81.55
116.99	n/a	n/a	solvent	n/a	n/a	6.3

Appendix Table 5.15 - Ions observed following SCW hydrolysis of BSA at 160 °C for 0 min.

<u>m/z</u>	<u>Calculated mass (Da)</u>	<u>Measured mass (Da)</u>	<u>Formula</u>	<u>Structure</u>	<u>ΔPPM</u>	<u>Relative abundance</u>
78.9968	n/a	n/a	solvent	n/a	n/a	11.37
84.9595	n/a	n/a	solvent	n/a	n/a	100
86.9925	n/a	n/a	solvent	n/a	n/a	8.59
93.0125	unassigned	n/a	n/a	n/a	n/a	18.88
97.0074	n/a	n/a	solvent	n/a	n/a	8.03
101.0595	102.0681	102.0679	C ₅ H ₁₀ O ₂		-2.2	13.18
102.9701	n/a	n/a	solvent	n/a	n/a	61.51
106.9918	n/a	n/a	solvent	n/a	n/a	9.98
111.0231	unassigned	n/a	n/a	n/a	n/a	7.16
114.0912	n/a	n/a	solvent	n/a	n/a	23.02

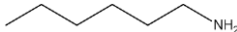
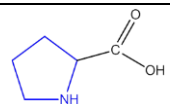
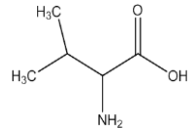
116.0704	115.0633	115.0631	C ₅ H ₉ O ₂ N		-1.5	10.57
116.9858	n/a	n/a	solvent	n/a	n/a	13.11
121.0075	n/a	n/a	solvent	n/a	n/a	12.02
130.0497	129.0426	129.0424	C ₅ H ₇ O ₃ N		-1.4	10.47
132.1018	131.0946	131.0945	C ₄ H ₉ O ₂ N ₃		-0.6	5.56
134.9868	n/a	n/a	solvent	n/a	n/a	7.55
148.0603	147.0532	147.0530	C ₅ H ₉ O ₄ N		-1.2	6.39
149.0024	unassigned	n/a	n/a	n/a	n/a	21.18

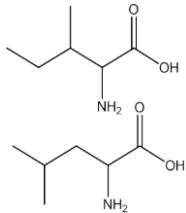
Appendix Table 5.16 - Ions observed following SCW hydrolysis of BSA at 160 °C for 20 min.

<u>m/z</u>	<u>Calculated mass (Da)</u>	<u>Measured mass (Da)</u>	<u>Formula</u>	<u>Structure</u>	<u>ΔPPM</u>	<u>Relative abundance</u>
78.9971	n/a	n/a	solvent	n/a	n/a	8.13
84.9597	n/a	n/a	solvent	n/a	n/a	100
86.9928	n/a	n/a	solvent	n/a	n/a	18.06
97.0077	n/a	n/a	solvent	n/a	n/a	5.32
102.1279	101.1205	101.1206	C ₆ H ₁₅ N		1.2	39.33
102.9704	n/a	n/a	solvent	n/a	n/a	81.9
106.9921	n/a	n/a	solvent	n/a	n/a	7.93
110.0089	n/a	n/a	solvent	n/a	n/a	9.05
114.0915	n/a	n/a	solvent	n/a	n/a	23.64
118.0865	117.0790	117.0792	C ₅ H ₁₁ O ₂ N		1.9	6.17

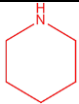
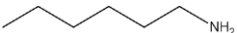
125.9865	n/a	n/a	solvent	n/a	n/a	32.12
134.9872	n/a	n/a	solvent	n/a	n/a	6.35

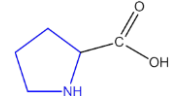
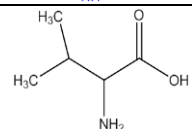
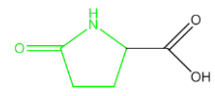
Appendix Table 5.17 - Ions observed following SCW hydrolysis of NTG at 160 °C for 0 min.

<u>m/z</u>	<u>Calculated mass (Da)</u>	<u>Measured mass (Da)</u>	<u>Formula</u>	<u>Structure</u>	<u>ΔPPM</u>	<u>Relative abundance</u>
84.9598	n/a	n/a	Solvent	n/a	n/a	46.32
86.9928	n/a	n/a	Solvent	n/a	n/a	25.41
96.9870	n/a	n/a	Solvent	n/a	n/a	12.37
101.0599	n/a	n/a	Solvent	n/a	n/a	5.36
102.1279	101.1205	101.1206	C ₆ H ₁₅ N		1.2	100
102.9704	n/a	n/a	Solvent	n/a	n/a	42.36
105.9923	n/a	n/a	Solvent	n/a	n/a	12.16
114.0916	n/a	n/a	Solvent	n/a	n/a	24.05
116.0708	115.0633	115.0635	C ₅ H ₉ O ₂ N		1.9	11.49
118.0865	117.0790	117.0792	C ₅ H ₁₁ O ₂ N		1.9	16.94

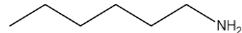
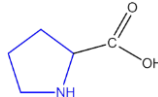
125.9865	n/a	n/a	Solvent	n/a	n/a	6.69
132.1022	131.0946	131.0949	C ₆ H ₁₃ O ₂ N		2.3	9.65
134.0451	n/a	n/a	Solvent	n/a	n/a	8.76

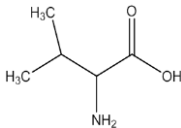
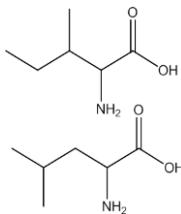
Appendix Table 5.18 - Ions observed following SCW hydrolysis of NTG at 160 °C for 20 min.

<u>m/z</u>	<u>Calculated mass (Da)</u>	<u>Measured mass (Da)</u>	<u>Formula</u>	<u>Structure</u>	<u>ΔPPM</u>	<u>Relative abundance</u>
68.9826	n/a	n/a	solvent	n/a	n/a	11.57
82.0144	n/a	n/a	solvent	n/a	n/a	22.31
84.9603	n/a	n/a	solvent	n/a	n/a	74.39
86.0971	85.0892	85.0898	C ₅ H ₁₁ N		7.3	11.6
86.9934	n/a	n/a	solvent	n/a	n/a	100
87.9942	n/a	n/a	solvent	n/a	n/a	13.12
88.9909	n/a	n/a	solvent	n/a	n/a	15.57
90.5076	n/a	n/a	solvent	n/a	n/a	11.72
102.1285	101.1205	101.1212	C ₆ H ₁₅ N		7.2	73.96
102.9711	n/a	n/a	solvent	n/a	n/a	74.11
104.1078	103.0997	103.1005	C ₅ H ₁₃ ON	Unassigned		19.5

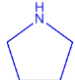
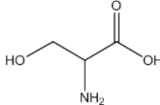
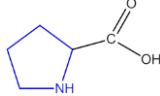
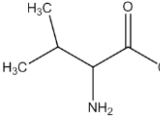
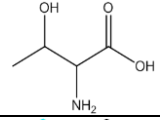
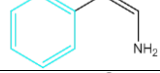
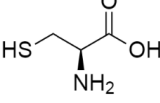
105.0041	n/a	n/a	solvent	n/a	n/a	23.16
114.0923	n/a	n/a	solvent	n/a	n/a	31.01
116.0716	115.0633	115.0643	C ₅ H ₉ O ₂ N		8.9	50.56
118.0872	117.0790	117.0799	C ₅ H ₁₁ O ₂ N		7.9	16.65
122.0822	Unassigned	n/a	n/a	n/a	n/a	15.23
128.987	n/a	n/a	solvent	n/a	n/a	11.66
130.051	129.0426	129.0437	C ₅ H ₇ O ₃ N		8.7	19.79
131.1303	130.1226	130.1230	C ₇ H ₁₆ ON	Unassigned		11.09
146.9978	n/a	n/a	solvent	n/a	n/a	11.62

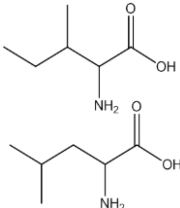
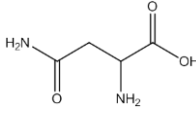
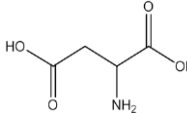
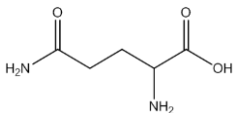
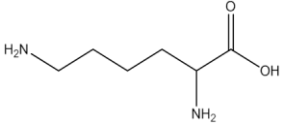
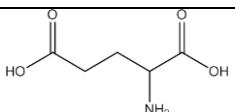
Appendix Table 5.19 - Ions observed following SCW hydrolysis of BSG at 160 °C for 0 min.

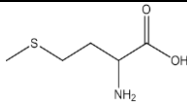
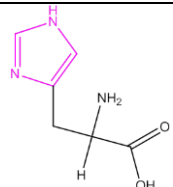
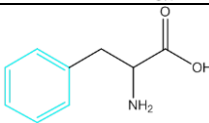
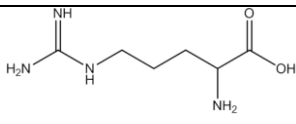
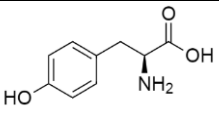
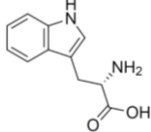
<u>m/z</u>	<u>Calculated mass (Da)</u>	<u>Measured mass (Da)</u>	<u>Formula</u>	<u>Structure</u>	<u>ΔPPM</u>	<u>Relative abundance</u>
84.9598	n/a	n/a	Solvent	n/a	n/a	46.32
86.9928	n/a	n/a	Solvent	n/a	n/a	25.41
96.9870	n/a	n/a	Solvent	n/a	n/a	12.37
101.0599	n/a	n/a	Solvent	n/a	n/a	5.36
102.1279	101.1205	101.1206	C ₆ H ₁₅ N		1.2	100
102.9704	n/a	n/a	Solvent	n/a	n/a	42.36
105.9923	n/a	n/a	Solvent	n/a	n/a	12.16
114.0916	n/a	n/a	Solvent	n/a	n/a	24.05
116.0708	115.0633	115.0635	C ₅ H ₉ O ₂ N		1.9	11.49

118.0865	117.079	117.0792	C ₅ H ₁₁ O ₂ N		1.9	16.94
125.9865	n/a	n/a	Solvent	n/a	n/a	6.69
132.1022	131.0946	131.0949	C ₆ H ₁₃ O ₂ N		2.3	9.65
134.0451	n/a	n/a	Solvent	n/a	n/a	8.76
137.0093	n/a	n/a	Solvent	n/a	n/a	12.59

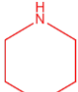
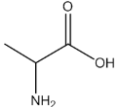
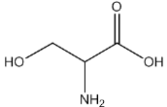
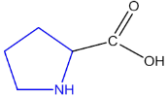
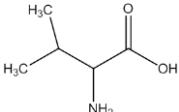
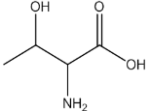
Appendix Table 5.20 - Ions observed following SCW hydrolysis of BSG at 160 °C for 20 min.

<u>m/z</u>	<u>Calculated mass (Da)</u>	<u>Measured mass (Da)</u>	<u>Formula</u>	<u>Structure</u>	<u>PPM</u>	<u>Relative abundance</u>
86.0965	85.0892	85.0892	C ₅ H ₁₁ N		0.3	25.22
106.0500	105.0426	105.0427	C ₅ H ₁₁ N		1.2	7.24
116.0708	115.0633	115.0635	C ₅ H ₉ O ₂ N		2.0	49.69
118.0864	117.0790	117.0791	C ₅ H ₁₁ O ₂ N		1.1	25.77
120.0657	119.0582	119.0584	C ₄ H ₉ O ₃ N		1.9	7.92
120.0809	119.0735	119.0736	C ₈ H ₉ N		1.1	8.73
122.0272	121.0197	121.0199	C ₃ H ₇ O ₂ NS		1.5	1.4

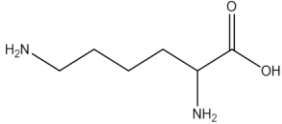
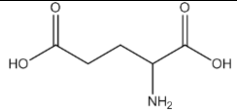
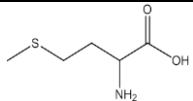
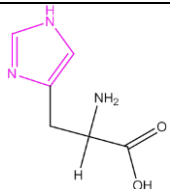
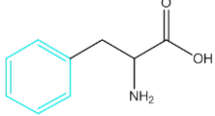
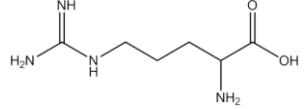
132.1021	131.0946	131.0948	C ₆ H ₁₄ ON ₂		1.7	100
133.0610	132.0535	132.0537	C ₄ H ₈ O ₃ N ₂		1.7	7.26
134.0450	133.0375	133.0377	C ₇ H ₇ O ₄ N		1.7	4.53
147.0767	146.0691	146.0694	C ₅ H ₁₀ O ₃ N ₂		2.2	7.31
147.1131	146.1055	146.1058	C ₆ H ₁₄ O ₂ N ₂		2.2	9.27
148.0607	147.0532	147.0534	C ₅ H ₉ O ₄ N		1.5	6.58

150.0586	149.0511	149.0513	C ₅ H ₁₁ O ₂ NS		1.5	17.56
156.0770	155.0695	155.0697	C ₆ H ₉ O ₂ N ₃		1.5	17.41
166.0866	165.0790	165.0793	C ₉ H ₁₁ O ₂ N		2.0	17.22
175.1193	174.1118	174.1120	C ₆ H ₁₄ O ₄ N ₂		1.3	10.16
182.0816	181.0739	181.0743	C ₉ H ₁₁ O ₃ N		2.4	0.326
205.0976	204.089874	204.0903	C ₁₁ H ₁₂ O ₂ N ₂		2.1	9.71

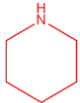
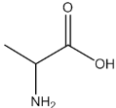
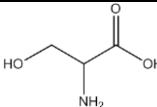
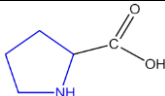
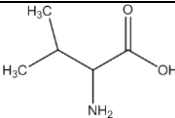
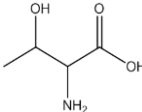
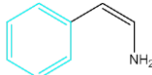
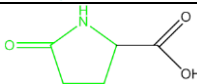
Appendix Table 5.21 - Ions observed from an equimolar AA mixture incubated at room temperature.

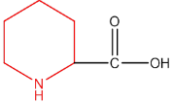
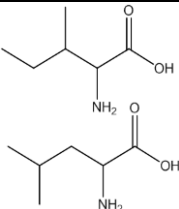
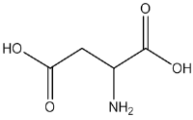
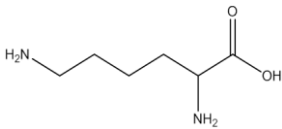
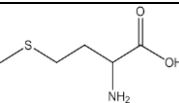
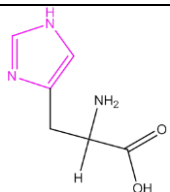
<u>m/z</u>	<u>Calculated mass (Da)</u>	<u>Measured mass (Da)</u>	<u>Formula</u>	<u>Structure</u>	<u>ΔPPM</u>	<u>Relative abundance</u>
84.9598	n/a	n/a	Solvent	n/a	n/a	26.23
86.0965	85.0892	85.0892	C ₅ H ₁₁ N		0.3	22.74
90.0551	89.0477	89.0478	C ₃ H ₇ NO ₂		1.4	7.53
102.9705	n/a	n/a	Solvent	n/a	n/a	26.26
106.0501	105.0426	105.0428	C ₃ H ₇ NO ₃		2.1	18.68
114.0916	n/a	n/a	Solvent	n/a	n/a	7.20
116.0708	115.0633	115.0635	C ₅ H ₉ O ₂ N		2.0	88.56
118.0865	117.0790	117.0792	C ₅ H ₁₁ O ₂ N		1.9	19.24
120.0658	119.0582	119.0585	C ₄ H ₉ O ₃ N		2.7	14.67

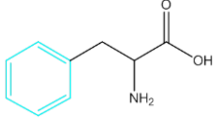
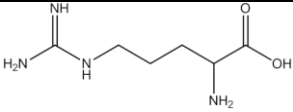
120.0810	119.0735	119.0737	C ₈ H ₉ N		1.9	12.34
122.0814	Unassigned	n/a	n/a	n/a	n/a	10.79
130.0503	129.0426	129.0430	C ₅ H ₇ O ₃ N		3.3	8.01
130.0866	129.0790	129.0793	C ₆ H ₁₁ O ₂ N		2.5	6.92
132.1022	131.0946	131.0949	C ₆ H ₁₄ ON ₂		2.5	100.00
134.0451	133.0375	133.0378	C ₇ H ₇ O ₄ N		2.5	43.58
147.0768	146.0691	146.0695	C ₅ H ₁₀ O ₃ N ₂		2.7	7.92

147.1132	146.1055	146.1059	C ₆ H ₁₄ O ₂ N ₂		2.9	30.28
148.0608	147.0532	147.0535	C ₅ H ₉ O ₄ N		2.2	17.97
150.0587	149.0511	149.0514	C ₅ H ₁₁ O ₂ NS		2.2	36.74
156.0771	155.0695	155.0698	C ₆ H ₉ O ₂ N ₃		2.1	15.24
166.0866	165.0790	165.0793	C ₉ H ₁₁ O ₂ N		2.0	42.09
175.1193	174.1118	174.1120	C ₆ H ₁₄ O ₄ N ₂		1.3	16.05

Appendix Table 5.22 - Ions Observed following SCW hydrolysis of an equimolar amino acid mixture at 160 °C for 0 minutes.

<u>m/z</u>	<u>Calculated mass (Da)</u>	<u>Measured mass (Da)</u>	<u>Formula</u>	<u>Structure</u>	<u>ΔPPM</u>	<u>Relative abundance</u>
86.0966	85.0892	85.0893	C ₅ H ₁₁ N		1.5	20.72
90.0551	89.0477	89.0478	C ₃ H ₇ NO ₂		1.4	9.64
106.0501	105.0426	105.0428	C ₃ H ₇ NO ₃		2.1	22.13
114.0916	n/a	n/a	Solvent	n/a	n/a	12.04
116.0709	115.0633	115.0636	C ₅ H ₉ O ₂ N		2.8	77.79
118.0865	117.0790	117.0792	C ₅ H ₁₁ O ₂ N		1.9	17.68
120.0658	119.0582	119.0585	C ₄ H ₉ O ₃ N		2.7	26.17
120.081	119.0735	119.0737	C ₈ H ₉ N		1.9	12.92
130.0503	129.0426	129.0430	C ₅ H ₇ O ₃ N		3.3	13.63

130.0866	129.0790	129.0793	C ₆ H ₁₁ O ₂ N		2.5	7.14
132.1022	131.0946	131.0949	C ₆ H ₁₄ ON ₂		2.5	100
134.0451	133.0375	133.0378	C ₇ H ₇ O ₄ N		2.5	22.07
147.1132	146.1055	146.1059	C ₆ H ₁₄ O ₂ N ₂		2.9	32.97
150.0587	149.0511	149.0514	C ₅ H ₁₁ O ₂ NS		2.2	38.84
156.0771	155.0695	155.0698	C ₆ H ₉ O ₂ N ₃		2.1	16.68

166.0866	165.0790	165.0793	C ₉ H ₁₁ O ₂ N		2.0	53.66
175.1193	174.1118	174.1120	C ₆ H ₁₄ O ₄ N ₂		1.3	31.16

Appendix Table 5.23 - Ions Observed following SCW hydrolysis of an equimolar amino acid mixture at 160 °C for 20 minutes.

